

Time-Resolved Spectroscopic Analysis of Fucoxanthin-Chlorophyll Proteins and Isolated Carotenoids

Dissertation
zur Erlangung des Doktorgrades
der Naturwissenschaften

vorgelegt beim Fachbereich
Biochemie, Chemie und Pharmazie
der Johann Wolfgang Goethe-Universität
in Frankfurt am Main

von
Nina Gildenhoff
aus Offenbach

Frankfurt am Main 2011
D30

Vom Fachbereich Biochemie, Chemie und Pharmazie der
Johann Wolfgang Goethe-Universität als Dissertation angenommen.

Dekan: Prof. Dr. Dieter Steinhilber

1. Gutachter: Prof. Dr. Josef Wachtveitl

2. Gutachter: Prof. Dr. Claudia Büchel

Datum der Disputation:

Für meine Familie

"Das Leben ist nichts anderes, als die endlose Probe
einer Vorstellung, die niemals stattfindet."

(aus *Die fabelhafte Welt der Amelie*)

Contents

1	Motivation	1
2	Fucoxanthin Chlorophyll Proteins and Isolated Carotenoids	5
2.1	Photosynthesis	5
2.2	Photosynthetic Pigments	7
2.2.1	Chlorophylls	7
2.2.2	Carotenoids	9
2.3	Fucoxanthin-Chlorophyll Proteins	15
2.3.1	Pigment Composition	17
2.3.2	Oligomeric State - FCPa and FCPb	17
2.3.3	Growth Conditions - High Light and Low Light Cultures	18
2.3.4	Sample Preparation - Isolation of FCPs and Carotenoids	19
3	Experimental Methods - Theoretical Background	21
3.1	Absorption and Fluorescence	21
3.1.1	Fluorescence Anisotropy	24
3.1.2	Fluorescence Quantum Yields	25
3.2	Principles of Ultrafast Spectroscopy	26
3.2.1	Pump-Probe Spectroscopy	26
3.2.2	Nonlinear Optics	27
3.2.3	Generation of Ultrashort Pulses	30
3.2.4	Methods for Wavelength Conversion	32
3.2.5	Time-Resolved Fluorescence Techniques	33
4	Experimental Setups	39
4.1	Time-Resolved Fluorescence Spectroscopy	39
4.1.1	The <i>Tsunami-Spitfire</i> Laser System	40
4.1.2	The Kerr-Shutter Setup	41
4.1.3	The TCSPC-Upconversion Setup	50
4.1.4	Data Analysis	53

4.2	Transient Absorption Spectroscopy	53
4.2.1	The <i>CPA 2001</i> Laser System	54
4.2.2	fs-Pump-Probe Setup	54
4.2.3	Data Analysis	56
4.3	Autocorrelator	59
5	Characterization of Isolated Carotenoids	61
5.1	Steady State Characterization	61
5.2	Transient Absorption Measurements	65
5.3	Fluorescence Lifetimes	75
6	Excitation Energy Transfer in FCPs	81
6.1	Steady State Characterization	81
6.2	Fluorescence Lifetimes	84
6.3	Transient Absorption Dynamics in FCPs	84
6.3.1	Comparison of HL and LL Cultures	88
6.3.2	Comparison of FCPa and FCPb	88
6.3.3	Excitation Wavelength Dependence	92
6.3.4	Influence of Diadinoxanthin and Diatoxanthin on the Excitation Energy Transfer	96
6.3.5	Excitation of Chl c_2	98
6.3.6	Energy Transfer Model	100
6.4	Transient Anisotropy Measurements	101
7	Coherent Effects	109
7.1	Carotenoids in Solution	109
7.2	FCP Complexes	117
7.3	The Origin of the Coherent Effects	118
8	Concluding Remarks	123
9	Zusammenfassung	127
	Publikationen	157
	Danksagung	159
	Lebenslauf	161

List of Figures

2.1	Photosynthetic electron transport	6
2.2	Structures of different chlorophylls	7
2.3	Absorption spectrum of a Chl <i>a/b</i> mixture	8
2.4	Simplified energy level scheme of chlorophyll <i>a</i>	9
2.5	Chemical structures of β -carotene and fucoxanthin	10
2.6	Simplified energy level scheme of carotenoids	11
2.7	Schematic model of the energy transfer pathways in LHCII	13
2.8	Xanthophyll cycle pigments	15
2.9	FCP model including the pigments	16
2.10	Model of the two different assemblies of FCPs	18
2.11	Pigment stoichiometries of FCPa and FCPb	19
3.1	Jablonski diagram	23
3.2	Scheme for pump-probe experiments	26
3.3	Principle of the TCSPC technique	34
3.4	Principle of optical gating	36
4.1	Scheme of the <i>Tsunami-Spitfire</i> laser system	40
4.2	Experimental setup of the Kerr gating experiment	41
4.3	Wavelength dependent reflection of blazed gratings	42
4.4	Spectral sensitivity of the CCD camera	43
4.5	Noncollinear optical parametric amplifier	44
4.6	Optical parametric amplifier	46
4.7	Prism compressor	47
4.8	Cross correlation signals measured with the Kerr shutter	49
4.9	TCSPC and fluorescence upconversion	51
4.10	Instrument response of the TCSPC experiment	52
4.11	Experimental setup of the transient absorption spectrometer	55
4.12	Pulse sequence	56
4.13	Transient absorption signals from pure ethanol	57

4.14	Main signals in transient absorption spectra	58
4.15	Autocorrelator	59
5.1	Steady state absorption spectra for fucoxanthin	62
5.2	FWHM of the $S_0 \rightarrow S_2$ absorption band	63
5.3	Transient absorbance changes of diadinoxanthin and diatoxanthin	66
5.4	Individual kinetic traces of diadinoxanthin and diatoxanthin	67
5.5	Transient absorption spectra of fucoxanthin	68
5.6	Transient absorbance changes of fucoxanthin	69
5.7	Individual kinetic traces of fucoxanthin	71
5.8	Individual kinetic traces of fucoxanthin	72
5.9	Lifetimes of the lowest excited state of fucoxanthin	72
5.10	Potential energy surface scheme of fucoxanthin	74
5.11	Solvent dependence of the cross correlation width	76
5.12	Upconversion measurements of β -carotene	77
5.13	Upconversion measurements of fucoxanthin	78
5.14	Upconversion measurements of diadinoxanthin and diatoxanthin	79
6.1	Steady state absorption spectra of FCPs	82
6.2	Fluorescence quantum yield of Chl <i>a</i>	83
6.3	Chl <i>a</i> fluorescence lifetimes of HL-FCPs	85
6.4	Transient absorption changes of HL-FCPa excited at 500 nm	86
6.5	Individual kinetic traces of FCPs after excitation at 500 nm	87
6.6	Decay associated spectra of FCPa and FCPb	89
6.7	Individual transients of FCPa and FCPb	90
6.8	DAS of FCPa and FCPb excited at 500 nm and 550 nm	91
6.9	Transient absorption changes of FCPs upon excitation of fx_{blue} and fx_{red}	93
6.10	Individual transients for HL-FCPa and HL-FCPb	94
6.11	Transient absorption spectra of FCPa for 500 nm and 550 nm excitation	95
6.12	DAS of HL-FCPa and HL-FCPb excited at 500 nm and 550 nm	95
6.13	Steady state absorbance spectra of FCPs without diadinoxanthin	97
6.14	Transient absorbance spectra of FCPs without diadinoxanthin	97
6.15	Comparison of the transient spectra	98
6.16	2D-plots of the results obtained from Chl c_2 excitation	99
6.17	Schematic model describing the excitation energy transfer in HL-FCPa	100
6.18	Anisotropy data of HL-FCPa	102
6.19	DAS for HL-FCPa with fixed time constants for all polarizations	103
6.20	Time dependent anisotropy decay and corresponding fit curves	104
6.21	Simplified FCP model including possible energy transfer channels	106

6.22	Modified schematic model of the excitation energy transfer in FCPa . . .	107
7.1	2D-plot focusing on the oscillations	110
7.2	Individual transients of fucoxanthin with coherent oscillations	110
7.3	Coherent artifact obtained for pure ethanol	111
7.4	Oscillatory features in the transient absorbance data of fucoxanthin . . .	113
7.5	FFT spectra calculated for fucoxanthin	114
7.6	Oscillations in the transient absorption data of β -carotene	116
7.7	Oscillatory features in transient absorbance data of FCPs	117
7.8	Excited state dynamics of carotenoids including the dark $1B_u^+$ state . . .	120

List of Tables

5.1	Time constants obtained for diadinoxanthin and diatoxanthin	65
5.2	Time constants obtained for fucoxanthin	70
5.3	Solvent dependence of the S_1 lifetime of isolated carotenoids	73
5.4	Fluorescence lifetimes in fs of carotenoids	76
6.1	Time constants obtained for HL-FCPa and HL-FCPa	91
6.2	Pigment content in FCPa samples	96
7.1	Frequencies and corresponding periods of oscillation for fucoxanthin . . .	115
7.2	Frequencies and periods of oscillation for FCPs and fucoxanthin	118

Chapter 1

Motivation

*The answer is out there, Neo, and it's looking for you,
and it will find you if you want it to.*

(Trinity in *Matrix*)

Nature has created amazingly efficient systems for the use of sunlight as an energy source: the photosynthetic complexes. Plants and other photosynthetic organisms are perfectly adapted to use the resources available in their environments. The various organisms capable of oxygenic photosynthesis have developed a variety of light-harvesting complexes, which collect sunlight and transfer the energy to the reaction centers. With an estimated energy conversion of $2\text{-}4\cdot 10^{18}$ kJ, photosynthetic organisms synthesize about $2\cdot 10^{11}$ tons global biomass annually [1,2]. Extensive knowledge of these specific and highly efficient energy conversion processes is of fundamental interest. Today, the use of sunlight as a clean and abundant energy source is of particular importance. Therefore, current research deals with the development of an artificial photosynthetic process with an efficient photochemical conversion of solar energy [3]. Because of their immobility plants have developed a diversity of strategies to cope with changing environmental conditions. Fluctuations in the intensity of the incident light pose a major challenge. In case of low solar radiation, the light energy available is harvested completely and efficiently. Increasing light intensity, however, can damage the photosynthetic apparatus. Therefore, photosynthetic organisms need a protection mechanism which can respond depending on the intensity of the incident sunlight and dissipate excess energy in order to prevent damage. Carotenoids play an essential role in the light harvesting processes as well as in the protection against excessive irradiation. Along with chlorophylls, they are the most common pigments found on earth. This large group of pigments has a multitude of biological functions [4]. Carotenoids act as accessory pigments in the photosynthetic apparatus, because they reduce the so-called "green gap" in the absorption

spectrum of chlorophylls and enable the absorption of a larger amount of sunlight. Furthermore, they are involved in photoprotective mechanisms by quenching triplet states of chlorophylls, preventing the formation of dangerous singlet oxygen. This turns them into effective antioxidants not only in plants but also in animals and humans. Besides their chromophoric properties they have stabilizing structural functions in proteins and membranes. For the understanding of the structure-function-relationship a detailed knowledge of the excited state dynamics and the arrangement of the electronic states is crucial [5]. Since the excited state properties of carotenoids are very complicated they are still under discussion. For example, the role of carotenoid radical cations in the nonphotochemical quenching mechanism [6, 7] and the role of dark electronic states in the relaxation dynamics are controversial [8].

The present thesis deals with the ultrafast energy transfer dynamics in the fucoxanthin-chlorophyll proteins from the centric diatom *Cyclotella meneghiniana* and the excited state dynamics of the contained carotenoids fucoxanthin, diadinoxanthin, and diatoxanthin. Diatoms are eukaryotic, unicellular algae embedded in a silica shell made of two asymmetrical sides [9, 10]. With over 100,000 species they play a major global role in the biochemical cycles of carbon, nitrogen, phosphorus, and silicon and thus are of considerable ecological importance [11, 12]. Though their light harvesting complexes (LHCs) show high homology with LHCII of higher plants, they contain different pigments with an unusual stoichiometry. Besides a small amount of the xanthophyll cycle pigments diadinoxanthin and diatoxanthin they possess the carbonyl containing carotenoid fucoxanthin in an unusual high carotenoid-to-chlorophyll ratio of about one. Fucoxanthin enhances the absorption of the green light available in the sea and transfers it to the chlorophylls with high efficiency.

To investigate the properties of fucoxanthin and its role for the energy transfer pathways in fucoxanthin-chlorophyll proteins both isolated carotenoids as well as protein complexes were characterized by means of time-resolved spectroscopic methods. The experiments focused on the excited state dynamics of carotenoids in solution and the dependence of the energy transfer within the protein complexes on the pigmentation, the oligomeric state, and the excitation wavelength.

Modern laser spectroscopy allows the study of photophysical and photochemical processes on different time scales [13]. Time-resolved optical spectroscopy with time resolutions down to tens of femtoseconds enables the study of e.g. the electronic structure, dissipation pathways and conformational dynamics within biological molecules and larger systems. After excitation of the photosynthetic pigments the energy transfer within the light harvesting complexes and electron transfer within the reaction centers can be studied as summarized in [5, 14, 15]. Within the scope of this thesis a number of experiments were performed and the already existing transient absorption setup was complemented by two setups based on ultrafast time-resolved fluorescence techniques, namely fluorescence upconversion and Kerr-gating. The well-established time-resolved absorption technique based on the pump-probe principle enables the measuring of transient broadband absorption spectra. These consist of several contributions such as excited state

absorption, stimulated emission, vibrational relaxation of the ground state, and ground state bleaching. Both fluorescence techniques, upconversion and Kerr-gating, allow directly monitoring the depopulation of electronically excited states without additional overlapping contributions. With the complementary techniques of transient absorption and time-resolved fluorescence, excited state dynamics and fluorescence lifetimes in the femtosecond and picosecond range can be determined.

In the following an overview about the scope and content of the present thesis is given. *Chapter 2* provides a short introduction into photosynthesis, especially light harvesting and the involved pigments chlorophylls and carotenoids, with a focus on the excited states and the properties of carbonyl containing carotenoids. Furthermore, it includes an overview of the investigated fucoxanthin-chlorophyll proteins, their pigment composition and oligomeric states, as well as the sample preparation.

Chapter 3 deals with the theoretical background of the applied spectroscopic techniques. It includes a short introduction to nonlinear optics and basic principles of ultrafast time-resolved spectroscopy such as the pump-probe principle. In addition, the time-resolved fluorescence techniques implemented during this thesis are explained: Kerr-gating and fluorescence upconversion.

A detailed description of the Kerr-gating experiment is given in *Chapter 4*. The laser system used, specifically single parts of the setup such as the two-stage OPA, the NOPA, and the prism compressor are explained. A first characterization of the setup is given by cross correlation measurements. The other setups used for transient absorption, time correlated single photon counting and fluorescence upconversion experiments performed within the scope of this work are also described.

Chapters 5 to 7 include the results and discussion of the different experiments performed. In *Chapter 5* the results on isolated carotenoids are presented including time-resolved absorption and fluorescence spectroscopy. *Chapter 6* addresses the investigation of the fucoxanthin-chlorophyll proteins. Transient absorption measurements to study the excitation energy transfer within the light-harvesting proteins were complemented by steady state characterizations and time-resolved anisotropy experiments. The coherent effects observed in several of the time-resolved absorption spectra are described and discussed in *Chapter 7*. Additional investigations of the oscillatory features promise to give further insight in the excited state dynamics and the dark states involved.

Chapter 2

Fucoxanthin Chlorophyll Proteins and Isolated Carotenoids

This is called farming! You kids are gonna grow all kinds of plants! Vegetable plants, pizza plants...

(Captain B. McCrea in *WALL-E*)

2.1 Photosynthesis

All life on this planet ultimately depends on the energy conversion of the sunlight to chemical energy by organisms capable of oxygenic photosynthesis. Plants, algae and photosynthetic bacteria harvest light from the sun to synthesize carbohydrates from carbon dioxide and water. Specialized pigment-protein complexes absorb solar energy and efficiently transfer it to photochemical reaction centers where the charge separation takes place to induce a transmembrane electrochemical potential difference. This membrane potential is then used by the ATP synthase to produce the energy carrier ATP (adenosine triphosphate). In oxygenic organisms (plants, algae, and cyanobacteria) two photosystems working in series are involved in the light dependent reactions of photosynthesis (Figure 2.1). High resolution studies discovered the structure of these core complexes, photosystem (PS) I and II [18–21]. Both photosystems contain a chlorophyll *a* dimer called special pair. They are ionized either upon direct light absorption or excitation energy transfer from surrounding pigments and thus release the electrons to the respective electron transport chain. In PSII the electrons are transferred via plastoquinone to the cytochrome b_6/f complex. Water is split into molecular oxygen and protons and the electrons are used to neutralize the pair of chlorophyll *a* molecules in PSII. The special pair in PSI receives the electrons from the carriers connecting PSII

2.1. Photosynthesis

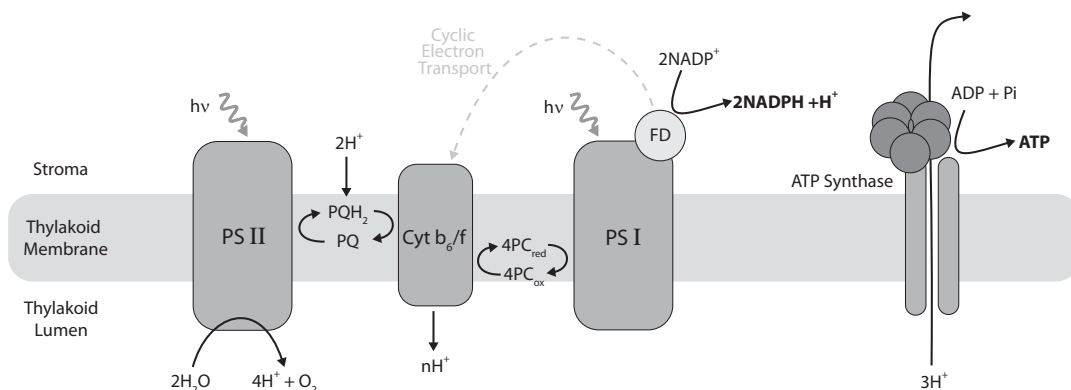


Figure 2.1: Schematic model of components involved in the photosynthetic electron transport and adenosine triphosphate (ATP) synthesis, adopted from [16,17]. The cytochrome b_6/f complex connects PSI and PSII via plastoquinones (PQ) and plastocyanines (PC). Ferredoxin (FD) mediates the electron transport to NADP^+ . The enzyme ATP synthase catalyzes the formation of ATP using the potential difference.

and PSI. Via ferredoxin PSI transfers the electrons to a final electron acceptor NADP^+ (nicotinamide adenine dinucleotide phosphate) and reduces it to the reducing equivalent NADPH. The described electron transfer processes in photosynthetic reaction centers occur on the picosecond and subpicosecond time scales. Thus, time-resolved optical spectroscopy is most suitable to analyze these ultrafast reactions [14,15]. ATP and NADPH formed in the so called ‘light reactions’ in turn catalyze the ‘dark reactions’ in which carbon dioxide is fixed and reduced (Calvin cycle) to build up carbohydrates and all other biomolecules [16,22].

For the success of photosynthesis efficient light-harvesting as well as rapid excitation energy transfer (EET) are essential. The large variety of photosynthetic organisms developed different light-harvesting antennas to ensure efficient transfer of the absorbed light energy to the reaction centers. These membrane associated complexes contain chlorophylls (Chl) or bacteriochlorophylls (BChl) as main light harvesting pigments arranged with accessory pigments, carotenoids and phycobilins [17,23]. Today the structures of various light-harvesting complexes (LHCs) are resolved in atomic detail like the complexes LH2 [24–26] and LH1 [27,28] from purple bacteria and LHCII [29–31] from higher plants. The excited pigments transfer the energy resulting in an ultrafast cascade from higher to lower states and deliver it to the reaction center. LH1 and LH2 from purple bacteria build up rings of antenna proteins with peripheral mobile LH2 antenna complexes and large LH1 rings enclosing the reaction center [32]. LHC I and II from green algae and higher plants are structured differently. LHCI functions as an antenna only for PSI forming a PSI supercomplex with four LHCI proteins [33]. In contrast, LHCII is mainly associated to PSII [34–36]. It can protect the photosynthetic apparatus

against a surplus of light [37,38] and regulates the distribution of the incident sunlight between PSII and PSI [39]. The antenna systems of cyanobacteria and red algae are called phycobilisomes since they contain phycobilins instead of carotenoids as accessory pigments [40].

2.2 Photosynthetic Pigments

As mentioned before, there are three basic classes of photosynthetic pigments – chlorophylls, carotenoids, and phycobilins. In nature chlorophylls and carotenoids are abundant. Chl *a* is the most abundant pigment on earth. Besides the coloring these pigments have multiple important functions such as absorption of light, efficient energy transfer to the reaction centers, stabilization of the photosynthetic apparatus as well as the protection against excessive light.

2.2.1 Chlorophylls

The greenish chlorophylls consist of a porphyrin ring with a central metal ion (Mg^{2+}) and most of them possess a long phytol chain (Figure 2.2). The most important one, Chl *a*, is contained in all plants, algae and cyanobacteria which photosynthesize. As mentioned before, the Chl *a* dimers in the reaction centers act as primary electron donors in the electron transport chain. While this function is unique for Chl *a*, all chlorophylls can act as light harvesting pigments in the photosynthetic apparatus. In the case of diatoms,

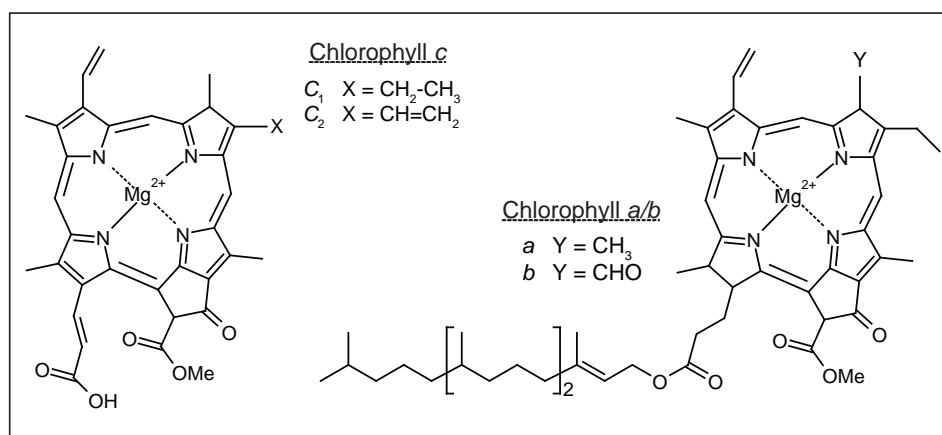


Figure 2.2: Structures of different chlorophylls. Chl *a* is found in all organisms capable of oxygenic photosynthesis. In diatoms the light-harvesting pigment Chl *b* is replaced by Chl *c*₂, which lacks the phytol chain.

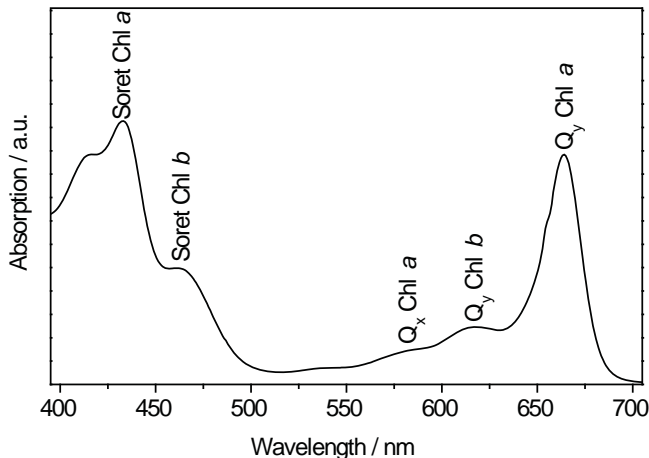


Figure 2.3: Absorption spectrum of a Chl *a/b* mixture in ethanol. The Q_x band of Chl *b* is very weak located around 549 nm [41].

i.e. algae with a silica shell, the second chlorophyll species present is Chl c_2 instead of Chl *b* found in higher plants. The structure of Chl c_2 is shown in Figure 2.2: it lacks the phytol chain. Its absorption spectrum is shifted like Chl *b* when compared to Chl *a* [42]. Like porphyrins chlorophylls show two main characteristic absorption bands in the visible spectral region which are called Soret (B) and Q band (Figure 2.3). However, the structural asymmetry in chlorophylls causes a splitting of these two bands into x and y components [43]. The Q_x transition dipole moment is oriented perpendicular to the Q_y dipole moment and the former has a lower oscillator strength. The Soret band with higher energy has the strongest transition in the visible. Absorption and emission properties strongly depend on the substitutions on the porphyrin ring influencing the π -electron system. The electronic structure, the energy levels, and the transition probabilities for different porphyrin structures can be calculated [44, 45]. A simplified energy level scheme of Chl *a* is shown in Figure 2.4.

Excitation is only possible into excited singlet states since the transition between singlet and triplet states is spin-forbidden (see also chapter 3.1). By internal conversion fast deexcitation ($\approx 10^{-12}$ s) to the first excited singlet state (S_1) takes place with subsequent fluorescence to the ground state ($\approx 10^{-9}$ s). Due to intersystem crossing population of the triplet state is possible resulting in long-lived phosphorescence [46].

Under excess light conditions more excitation energy is absorbed than can be utilized for photosynthesis. This leads to an accumulation of excited states of chlorophyll ($^1\text{Chl}^*$) and thus an increased probability for the formation of triplet excited states ($^3\text{Chl}^*$). Chlorophyll triplet states in turn are responsible for the generation of highly reactive singlet oxygen ($^1\text{O}_2^*$). This toxic oxygen species can destroy the photosynthetic appa-

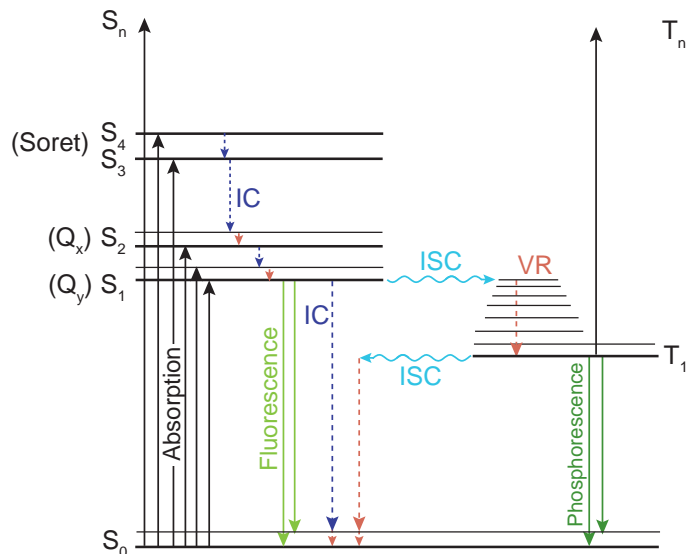


Figure 2.4: Simplified energy level scheme of chlorophyll *a*. IC: internal conversion, ISC: intersystem crossing, VR: vibrational relaxation. Adopted from [46].

ratus by oxidizing proteins and lipids of the membrane as well as pigments [47]. Hence efficient protection mechanisms are required either to quench or to prevent the formation of toxic oxygen species in photosynthetic organisms [17,48]. Due to their ability to quench chlorophyll triplet states as well as singlet oxygen, carotenoids can protect the photosynthetic apparatus. The formed carotenoid triplet states decay harmlessly, since they are lower in energy compared to the singlet oxygen and emit the energy as heat. Non-photochemical quenching is an additional protection mechanism with participation of specific xanthophylls (for details see chapter 2.2.2).

2.2.2 Carotenoids

Though they can only be synthesized by plants and microorganisms, carotenoids are found in almost all organisms. They serve as accessory pigments in the light harvesting process since carotenoids absorb in a visible spectral region not accessible by chlorophylls. More than 65 years ago the first study reporting on efficient energy transfer of carotenoids to chlorophylls was based on fluorescence spectroscopy of a diatom suspension [49]. As stated above, these unique pigments also act as quenchers of reactive chlorophyll and oxygen species and thus protect the photosynthetic apparatus against a surplus of light [50]. Besides photosynthesis carotenoids are required to stabilize the structure of protein complexes and have antioxidative functions [51,52]. There is evidence that they can inhibit certain types of cancer [53,54] and protect against other diseases e.g. macular

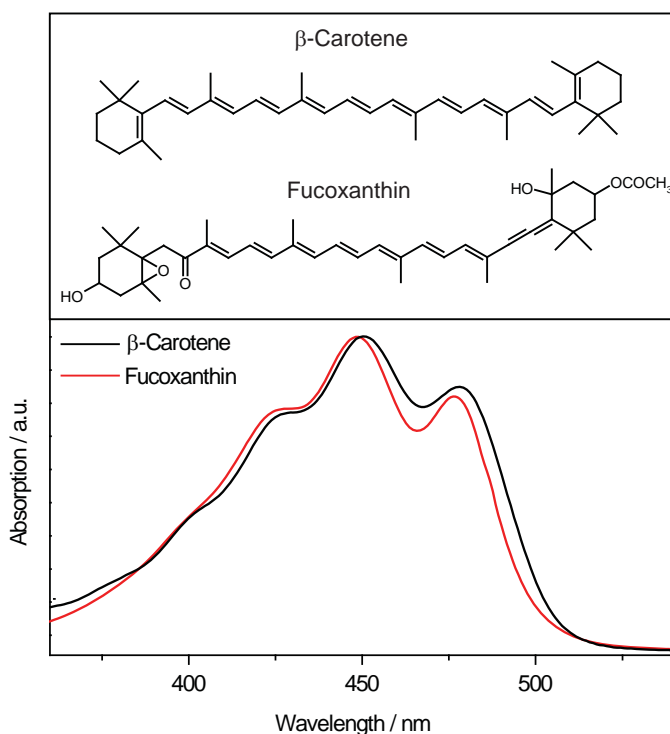


Figure 2.5: Chemical structures of β -carotene and fucoxanthin and ground state absorption (S_0 - S_2 transition) of β -carotene and fucoxanthin in n-hexane.

degeneration and atherosclerosis [55,56]. In addition, carotenoids are responsible for many yellow to red coloring in photosynthetic organisms. If ingested by animals they can also color e.g. skin, feathers, and fish scales [57].

The variety of their special functions is related to the structural features of the carotenoid molecules and the corresponding spectroscopic properties. With their conjugated π -electron system all-*trans* carotenoids belong to the same idealized C_{2h} point symmetry group as polyenes (Figure 2.5). Like these, carotenoids have a low-lying, symmetry forbidden $2A_g^-$ (according to its symmetry in pure polyenes) or S_1 state and a high-lying, absorbing state labeled $1B_u^+$ or S_2 [58]. A and B classify the electronic state according to the elements of the symmetry of its electronic distribution. States with a rotational symmetry are labeled with A. B states do not show rotational symmetry. The parity is even (g) or odd (u) depending on the behavior of the wavefunction under inversion through the center of symmetry. Transitions are allowed if the symmetry $A \leftrightarrow B$ and the symmetry designation $g \leftrightarrow u$ change [59,60]. In addition to the group theoretical designations, carotenoids and other polyenes must satisfy pseudoparity selection rules [61,62]. The pseudo-parity signs $+\leftrightarrow-$ are derived from the π -electron molecular

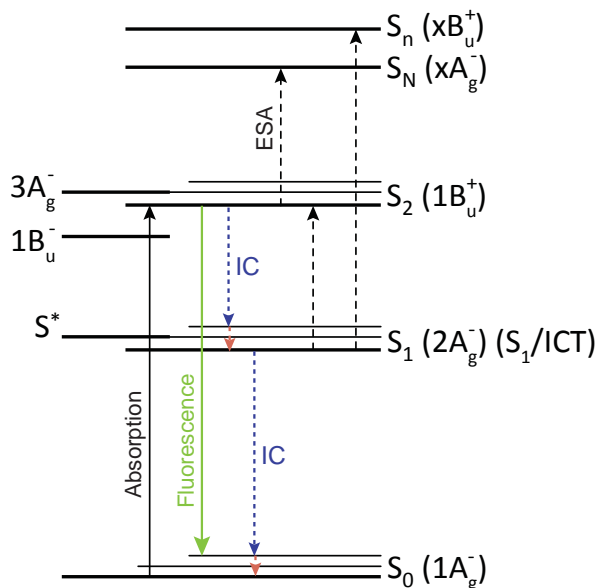


Figure 2.6: Simplified energy level scheme of carotenoids. $3A_g^-$, $1B_u^-$ and S^* are dark excited states predicted by theoretical studies and experimental results (see text for details) [8]. IC: internal conversion, ESA: excited state absorption. An intramolecular charge transfer (ICT) state is only observed for carotenoids containing a carbonyl group.

orbital pairing relationships when configuration interaction among singly excited configurations are included [60]. Thus, the transition to the S_2 state is strongly allowed and responsible for the characteristic absorption band in the visible spectral region between 400 - 550 nm. Upon binding to proteins the absorption of specific carotenoids can shift significantly due to the interactions with the respective protein binding pocket [17,63,64].

The existence of the 'dark' S_1 state and its location between the ground state and the absorbing (S_2) state was first demonstrated in 1972 [58,65] and further theoretical studies of polyenes revealed the existence of other dark states [66,67]. After the first measurement of the S_1 lifetime of β -carotene in 1986 by Wasielewski and Kispert [68] a large number of experiments concerning carotenoids excited state dynamics in both solution and light harvesting complexes followed [50,69]. Further time-resolved spectroscopic data revealed the existence of other dark states [70,71] and their roles in excited state processes and energy transfer pathways are still under discussion [8]. In Figure 2.6 a simplified energy level scheme is displayed including these dark states and excited state transitions.

$1B_u^-$ and S^* are the most discussed dark excited states of carotenoids because it is assumed that they play a role in the relaxation pathways [8]. By means of theoretical

calculations the $1B_u^-$ state was predicted to be located between the S_2 and S_1 state for carotenoids with $N > 9$ [67], which was further confirmed by recent theoretical [72, 73] and spectroscopic results [74–76]. It is hypothesized that coherent excitation of the S_2 and the $1B_u^-$ state is possible and there is already experimental evidence supporting this assumption [77–79]. In contrast, results from four-wave mixing experiments could explain the anomalous relationship between the S_2 lifetime and the conjugation length with a conical intersection between the S_2 and S_1 state without the involvement of a dark intermediate state [80–82]. In case of the S^* state there is clear experimental evidence for its existence though its origin is still discussed. It could be either a hot ground state [83] or an excited state of a twisted carotenoid conformation [84]. However, to be able to explain their origins and participations in the relaxation processes further investigations are necessary for both dark states.

Typically, for the S_0 – S_2 transition characteristic bands are observed which are assigned to the lowest vibrational levels of the S_2 excited state (Figure 2.5). Changes in the intensity of the vibrational peaks reflect structural properties of the carotenoid molecules. In case of linear carotenoids (e.g. lycopene or spheroidene) the vibrational structure is pronounced and vanishes if the π -electron conjugation is extended to an end group. The conjugation length itself hardly influences the vibrational structure but it affects the energy of the S_0 – S_2 transition which decreases with increasing conjugation length [85–87]. In addition, changes of the polarizability and refractive index of the solvent also lead to a shift of the absorption spectra of carotenoids. However, the solvent polarity hardly shows an effect on the resolution of the vibrational structure except for carotenoids with a conjugated carbonyl group such as fucoxanthin (see below) [88, 89].

Usually emission occurs from the lowest excited electronic state following a radiationless decay from higher excited states (see chapter 3.1). However, longer carotenoids ($N \geq 8$ conjugated double bonds) exhibit fluorescence mainly from their S_2 state violating Kasha’s rule [85–87, 90]. With increasing conjugated chain length the energy gap between the S_1 and S_2 excited state increases and thus the probability of internal conversion between the two states is reduced. Hence, radiative decay from the S_2 state is enhanced and usually emission from the S_1 state is negligible ($\phi_{fl} < 10^{-5}$) in carotenoids. Phosphorescence from the lowest triplet state is not observed [59].

Excited state lifetimes of carotenoids are in the range of femtoseconds in case of the S_2 state and picoseconds in case of the S_1 state. For the first excited triplet state T_1 lifetimes in the microsecond range are obtained. With increasing conjugation length a concomitant decrease of the S_1 lifetime from several hundred picoseconds down to ≈ 1 picosecond is observed [5]. This can be explained by the energy gap law with regard to the S_0 – S_1 energy gap [85, 91]. The polarity of the solvent shows almost no effect on the S_1 lifetime with the exception of carbonyl containing carotenoids [88, 92, 93]. The S_2 lifetime is in the range of 50–300 fs depending on both the carotenoid structure and the environment [89, 94–96]. For carotenoids in solution an increasing polarizability of the solvent reduces the S_2 – S_1 energy gap and facilitates the internal conversion between the two states. This results in shorter S_2 fluorescence lifetimes for carotenoids in polar

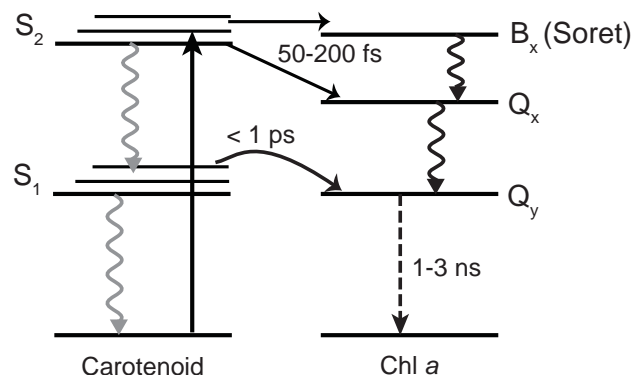


Figure 2.7: Schematic model of the energy transfer pathways in LHCII including energy levels of carotenoids and Chl *a*. Wavy arrows represent intramolecular relaxation processes and the dashed arrow denotes the Chl *a* fluorescence. Adopted from [5].

solvents.

In photosynthesis the fast internal conversion processes and short singlet lifetimes compete with the excitation energy transfer to chlorophylls. A basic requirement for efficient energy transfer is a defined distance between donor and acceptor molecules [59]. The rate of energy transfer depends on the orientation of the carotenoids relative to the chlorophylls and the mechanism (Förster or Dexter mechanism) controlling the transfer process [97,98]. A general, simplified scheme of the energy transfer pathways between carotenoids and chlorophylls in LHCII is represented in Figure 2.7 [5]. Upon excitation of the carotenoid S_2 state besides fast internal conversion a rapid energy transfer to chlorophyll takes place with time constants below 200 fs. After relaxation to the first excited state of the carotenoid efficient energy transfer is possible in less than 1 ps.

Carbonyl Containing Carotenoids – Fucoxanthin

Carotenoids with a conjugated carbonyl group – like fucoxanthin, peridinin, and siphonaxanthin – show unique excited state properties depending strongly on the solvent. The conjugated carbonyl group with its electron-withdrawing property induces a charge transfer character to the ground as well as the excited states and thus affects the energetics and the dynamics of the respective carotenoids [88,99,100]. The vibrational bands of the S_0 – S_2 transition are obtained for carbonyl carotenoids in nonpolar solvents. The vibrational structure vanishes with increasing polarity of the solvent accompanied by a broadening towards longer wavelengths [101,102]. In polar solvents the charge transfer character of the ground state is stabilized leading to several ground state conformations and thus to the loss of vibrational structure [88,101,102].

In contrast to non-carbonyl carotenoids one characteristic of carbonyl containing carotenoids is their S_1 fluorescence [103,104]. In addition, the S_1 lifetime depends on the polarity of the solvent. With increasing solvent polarity the S_1 lifetime decreases significantly [88,99,100,105]. The presence of an excited state with charge transfer character was used to explain these results. The electron density shifts from the terminal ring with the epoxy group to the polyene chain and the conjugated carbonyl group [106]. In polar solvents the stabilized intramolecular charge transfer (ICT) state lies below the S_1 state and thus is able to quench the S_1 state leading to shorter lifetimes. The transient absorption spectra of carbonyl containing carotenoids are also influenced by the formation of the ICT state. Whereas transient spectra of those carotenoids in nonpolar solvents are very similar to non-carbonyl carotenoids, transient spectra recorded in polar solvents reveal an additional excited state absorption band red shifted compared to the S_1 - S_n excited state absorption. Again, this can be explained with the stabilization of the ICT state in polar solvents [88,99,105]. Additionally, in polar solvents a negative band appears in the near infrared spectral region of the transient absorption spectra not observed in nonpolar solvents and for noncarbonyl carotenoids. Thus, this signal was assigned to the stimulated emission from the ICT state [105].

To date it is still a matter of debate if the ICT state is coupled to the S_1 state or if the two states are separated. There are several suggestions concerning the molecular nature of the ICT state [107]. Different experimental results confirmed the assumption that the ICT state is an electronic separated state [106,108–110]. However, other studies suggest quantum mechanically mixed ICT and S_1 states, therefore they should be considered as a single S_1 /ICT electronic state [101,111]. Recent experimental results combined with theoretical calculations led to the conclusion that the formation of the ICT state requires a mixing of the low lying S_1 ($2A_g$ -like) and S_2 ($1B_u$ -like) excited states [107].

Mechanisms of Photoprotection - Diadinoxanthin and Diatoxanthin

High light conditions can cause damage in the photosynthetic apparatus known as photoinhibition [112,113]. Increasing light absorption leads to the accumulation of excited chlorophyll molecules with a higher probability to form chlorophyll triplet states compared to low light conditions. As mentioned before, carotenoids can protect the photosynthetic apparatus by quenching these triplet states to prevent the generation of toxic oxygen species, in particular superoxide and hydroxyl radicals. They can also directly scavenge 1O_2 if it is formed [47]. The energy levels of the generated carotenoid triplet states are below that of singlet oxygen and they decay to the ground state by releasing heat [114].

In addition, non-photochemical quenching (NPQ) is another very important protection mechanism to regulate the dissipation of excess excitation energy. A surplus of excitation energy is quenched and released harmlessly as heat by specific xanthophylls. The NPQ mechanism is directly correlated with the pH gradient across the thylakoid membrane. Measurements of the chlorophyll fluorescence make it possible to quantify

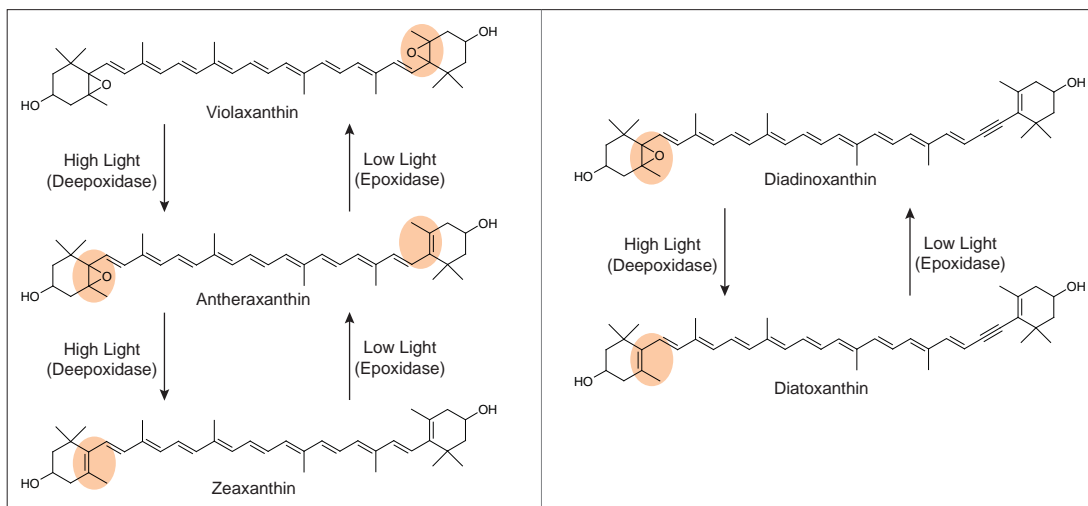


Figure 2.8: Xanthophyll cycle pigments in higher plants (left) and algae (right). Upon excess energy the epoxide groups on the β -rings are removed by the enzyme deepoxidase to lower the energy of the S_1 state. The back reaction is catalyzed by epoxidase under low light conditions.

NPQ [115]. In higher plants NPQ is associated with the xanthophyll cycle depicted in Figure 2.8. Under high light conditions violaxanthin is deepoxidated to zeaxanthin in two steps via antheraxanthin. The epoxide group on each β -ring is removed by the enzyme deepoxidase which is activated by a low pH value in the thylakoid lumen. Epoxidase catalyzes the reverse reaction to convert zeaxanthin back to violaxanthin [116]. The quenching can take place either through a lowered energy of the carotenoid S_1 state or by a carotenoid cation [6,7,117,118]. Besides Chlorophyta, diatoms and brown algae appear to be the only algae which possess a xanthophyll cycle comparable to the one in higher plants. Under high light conditions the monoepoxide diadinoxanthin is converted into diatoxanthin (Figure 2.8) [119–121].

2.3 Fucoxanthin-Chlorophyll Proteins

Fucoxanthin-chlorophyll proteins (FCPs) are found in algae belonging to the group of Cryptophyceae, Haptophyta, and Stramenopiles, for example diatoms (Bacillariophyta) and brown algae (Phaeophyceae) [10,122]. The FCPs analyzed in this work were isolated from the centric diatom *Cyclotella (C.) meneghiniana* in the group of Prof. Dr. Claudia Büchel [12]. Diatoms are unicellular, eukaryotic algae surrounded by a silica shell (valves and girdle bands) [9] and capable of oxygenic photosynthesis. With over 10,000 described species found in oceans and freshwater environment they are one of the major players

2.3. Fucoxanthin-Chlorophyll Proteins

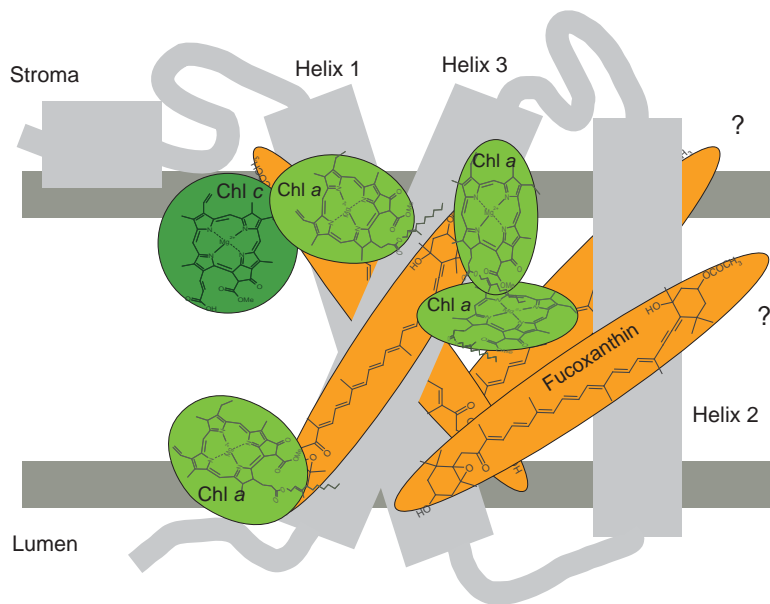


Figure 2.9: FCP model including the pigments Chl *a* (green), Chl *c*₂ (dark green) and fucoxanthin (orange) adopted from Wilhelm et al. [11]. Two fucoxanthin molecules are placed parallel to helix 1 and 3 taking conserved binding sites into account. The question marks label the fucoxanthins arranged randomly due to insufficient structural information in the region of helix 2. Diadinoxanthin and diatoxanthin are not displayed since they are contained in substoichiometric amounts.

in the biochemical cycles of carbon, nitrogen, phosphorus, and silica [9, 11].

FCPs are membrane intrinsic antenna proteins with three transmembrane helices with a size in the range of 17-22 kDa [123–125]. Like LHCII they function as light harvesting complexes and can dissipate excess energy as heat [126]. Belonging to the chlorophyll *a/b*-binding proteins (*cab*-family) FCPs show high sequence homology to other light harvesting complexes [127]. In contrast to other LHCs, where thylakoid membranes are arranged in grana and stroma, in diatoms thylakoids are arranged in groups of three. Thus, the two photosystems are not segregated and have no special antennas (like LHCI and LHCII) [128, 129]. Until now a molecular structure for the FCPs is not available, but a preliminary model (Figure 2.9) has been developed by Wilhelm et al. [11]. It is based on the sequence analysis of the diatoms *Phaeodactylum tricornutum* and *C. cryptica* and comparison to LHC proteins [123, 124] as well as ultrafast transient absorption measurements [130]. Three transmembrane α -helices are predicted from sequence analysis, whereby the homology to LHC is significant, especially in the helices 1 and 3 [131].

2.3.1 Pigment Composition

Despite these similarities there are big differences in the pigmentation (Figure 2.2 and 2.5) and pigment ratio of FCPs compared to LHCs. Like all *cab*-proteins they contain Chl *a* but the accessory Chl *b* is replaced by Chl *c*₂ which has no phytol chain. The main carotenoid is the carbonyl containing fucoxanthin. The xanthophyll cycle pigments diadinoxanthin and diatoxanthin are bound in substoichiometric amounts [126, 132]. Fucoxanthin is responsible for the brown color of the cells and isolated antennas, since upon binding to the protein its absorbance shifts bathochromic and occurs between 460 nm and 570 nm [64]. Usually LHCs bind much more chlorophyll than carotenoid molecules, e.g. 14 chlorophylls and 4 carotenoids in LHCII complexes [30, 31, 133]. However, in FCPs the chlorophyll to carotenoid ratio is almost one with four chlorophyll and four fucoxanthin molecules per monomer [129, 130, 134].

In the preliminary model (Figure 2.9) the pigments are included (except the xanthophyll cycle pigments) and arranged considering conserved binding sites and spectroscopic results [11, 130] with respect to LHCII. The Chl *c*₂ molecule has to be located close to one of the Chl *a* molecules because energy is transferred very fast to Chl *a* upon Chl *c*₂ excitation [130]. Similar to the luteins in LHCII two of the four fucoxanthin molecules are arranged parallel to helix 1 and helix 3. However, the other two fucoxanthin molecules are placed randomly since no structural informations concerning the binding sites are available and the sequence of helix 2 is much less similar to LHCII than helix 1 and 3 [11].

Similar to the solvent polarity dependence the absorption spectrum of fucoxanthin shifts as a result of its specific environment within the binding pocket. Due to their location and associated function in the protein individual fucoxanthin molecules have different absorption maxima. Thus, they are classified as red and blue absorbing fucoxanthins, respectively [42, 64, 135]. Recent results obtained from resonance Raman spectroscopy even identified green absorbing fucoxanthin molecules and suggested a pigment stoichiometry of actually 5-6 fucoxanthins per monomer [136]. Nevertheless, within the scope of this work only red (*fx_{red}*) and blue fucoxanthins (*fx_{blue}*) will be distinguished.

2.3.2 Oligomeric State - FCPa and FCPb

Two different FCP complexes (FCPa and FCPb, see Figure 2.10) were isolated from *C. meneghiniana* which differ in their polypeptide composition and oligomeric states [125]. From the related diatom *C. cryptica* the genes encoding FCPs were analyzed by Eppard and Rhiel [124, 137]. The genes *fcp1*, *fcp2*, *fcp3*, and *fcp4* encode FCPs of about 18 kDa and *fcp5*, *fcp6*, and *fcp7* encode 19 kDa proteins. It is difficult to separate the different FCP complexes since they are very similar in size, sequence, and pigmentation. However, by means of gel filtration two fractions of FCPs with different oligomeric states were obtained from *C. meneghiniana* by Beer et al. [12]. The trimeric FCPa consists of mainly 18 kDa proteins (Fcp2 polypeptides) and only small amounts of 19 kDa subunits (Fcp6

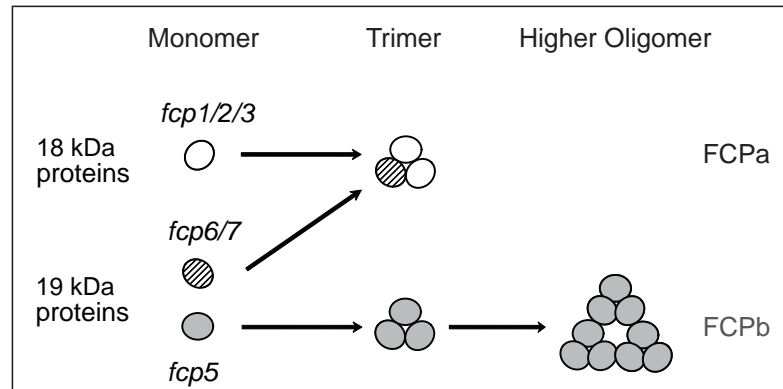


Figure 2.10: Model of the two different assemblies of FCPs adopted from Büchel [125]. The trimeric FCPa is composed of 18 kDa and 19 kDa proteins and FCPb consists of 19 kDa proteins associated into higher oligomers.

polypeptides) whereas in case of FCPb exclusively 19 kDa proteins (Fcp5 polypeptides) assemble into higher oligomers [12, 125].

To date there is no hard evidence for distinct functions of the two FCP complexes, i.e. it is unclear if they function as a specific antenna for either PSI or PSII. Biochemical studies complemented with spectroscopic methods by Veith et al. suggested that the trimeric FCPa is associated with PSII whereas FCPb might be weakly bound to PSI [138]. In addition, two quenching sites located in two different FCP complexes were proposed based on time-resolved spectroscopic studies on intact cells of *C. meneghiniana* and *P. tricornutum* [139]. According to the authors' interpretation, one antenna (most likely FCPa) stays attached to PSII. The other subpopulation is detached and forms aggregates comparable to FCPb. However, this assignment still needs to be validated by means of additional studies performed on the isolated complexes.

2.3.3 Growth Conditions - High Light and Low Light Cultures

To analyze the influence of the growth conditions on the polypeptide composition and the pigment content *C. meneghiniana* was grown under high light (HL) and low light (LL) conditions. As shown for *C. cryptica* by Oeltjen et al. [140] the mRNA levels of Fcp polypeptides depend on the light intensity during the growth. In case of *C. meneghiniana* the amount of other polypeptides relative to FCPs was higher in HL than in LL cultures. Furthermore, under LL conditions the 18 kDa polypeptides are clearly dominant whereas under HL conditions there is a slight shift in the 18 to 19 kDa ratio [12]. In addition, HL and LL FCPs differ in their pigmentation (Figure 2.11). Under both light conditions FCPa binds slightly more fucoxanthin than FCPb. The xanthophyll content is higher in FCPa compared to FCPb. The amount of diadinoxanthin (ddx) and diatoxanthin (dtx)

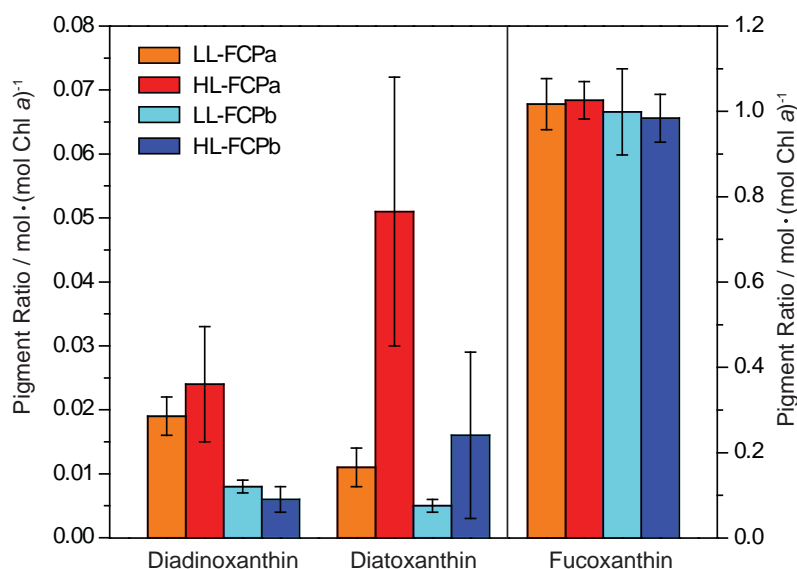


Figure 2.11: Pigment stoichiometries of FCPa (HL: red, LL: orange) and FCPb (HL: blue, LL: cyan). Pigment ratios are given in mol/(mol Chl *a*) as mean value \pm standard deviation of 3-6 measurements, adopted from Beer et al. [12].

increases in the HL cells, which means that the deepoxidation ratio ($\text{dtx}/(\text{ddx}+\text{dtx})$) is influenced significant by the varying light conditions. The amount of diatoxanthin increases by a factor of more than two in both FCPs accompanied with a growth of the pool of xanthophyll cycle pigments only in FCPa [12, 141].

2.3.4 Sample Preparation - Isolation of FCPs and Carotenoids

All investigated FCP samples were prepared in the group of Prof. C. Büchel. *Cyclotella meneghiniana* was grown under either HL ($145 \mu\text{E m}^{-2} \text{s}^{-1}$ of white light) or LL ($40 \mu\text{E m}^{-2} \text{s}^{-1}$) conditions in a 16 h light / 8 h dark cycle for two weeks [12]. For preparation of the FCPs the cells were harvested by centrifugation and the thylakoid membranes were isolated as described in Beer et al. [12, 125, 142]. In brief, cells were disrupted and the membrane fraction was washed and then resuspended in a buffer containing EDTA (ethylenediaminetetraacetic acid) to reduce chlorophyllase activity. The thylakoids were solubilized and the proteins were separated with an ion exchange column attached to a FPLC (fast protein liquid chromatography) system. The fractions were harvested and concentrated by means of Amicon filtration devices with a cutoff at 30 kDa. To analyze the oligomeric state of the different FCPs analytical gel filtration was used. By means of analytical HPLC (high-performance liquid chromatography) the

2.3. Fucoxanthin-Chlorophyll Proteins

extracted pigments were separated and quantified to obtain their stoichiometries.

All measurements were carried out at room temperature. The FCPs were diluted in a buffer with 25 mM Tris (tris(hydroxymethyl)aminomethane), 2 mM KCl, 0.03 % β -DDM (n-Dodecyl-beta-D-maltoside) at pH 7.4 and adjusted to an optical density of $\approx 0.9/\text{mm}$ at 671 nm with a concentration of $0.13 \text{ mg Chl } a \text{ mL}^{-1}$. The investigated carotenoids fucoxanthin, diadinoxanthin and diatoxanthin were either extracted from the isolated FCP complexes in the group of Prof. Claudia Büchel or bought from *DHI LAB products*, Denmark. β -carotene was purchased from *Sigma-Aldrich*. All samples including FCPs and carotenoids were closed airtight and stored at -20°C or -70°C . The isolated carotenoids were diluted in various solvents with analytical purity and adjusted to an optical density between 0.5-1.0/mm at the respective absorption maximum.

Chapter 3

Experimental Methods - Theoretical Background

A neutron walks into a bar and asks how much for a drink. The bartender replies: "For you, no charge."

(Dr. Dr. Sheldon Lee Cooper in
The Big Bang Theory)

To investigate biological processes such as the light reaction of photosynthesis or the early steps in protein folding, which occur on time scales from femtoseconds up to seconds, the use of several time-resolved methods is required. Time-resolved optical spectroscopy as applied in this work enables the observation of dynamics in biological molecules and larger systems, for example electron and energy transfer, excited state lifetimes, and internal conversion. The pump-probe experiment is a common technique to investigate absorbance changes upon excitation with time resolutions down to several 10 fs. To investigate fluorescence decays in the fs and ps time regime optical gating techniques are widely used. In our group two methods, fluorescence upconversion and Kerr-gating, are available.

3.1 Absorption and Fluorescence

Absorption spectroscopy investigates the interaction of the sample with electromagnetic radiation. The energy of a photon taken up by matter is measured as a function of frequency or wavelength. While absorption of infrared (IR) light (0.75 μm - 1000 μm) leads to the excitation of molecular rotations and vibrations, absorption of light in the visible (VIS, 400 nm - 750 nm) and ultraviolet (UV, 10 nm - 400 nm) spectral range

3.1. Absorption and Fluorescence

induces the transition of valence electrons. If the photon energy of the incident radiation is in resonance with a permitted transition of two molecular states, absorption is possible. The energy of the photons is expressed by:

$$E = h \cdot \nu = \frac{h \cdot c}{\lambda} = h \cdot c \cdot \tilde{\nu} \quad (3.1)$$

where h is the Planck constant and c the speed of light.

The Lambert-Beer law describes the intensity of absorption as the ratio of incident (I_0) and transmitted light (I), that depends on the length of the sample d and the molar concentration c of the absorbing species. The absorbance A is defined as:

$$A(\lambda) = \log \frac{I_0}{I} = \epsilon(\lambda) \cdot c \cdot d \quad (3.2)$$

The quantity ϵ is called the molar absorption coefficient or extinction coefficient. It is an intrinsic property of the investigated molecule and depends on the frequency of the incident photons. The product $\epsilon(\lambda) \cdot c \cdot d$ is called optical density OD and the ratio $\frac{I}{I_0}$ is named transmittance T .

As mentioned before there are different types of transitions with specific selection rules. A transition takes place if the transition dipole moment μ_{fi} given by

$$\mu_{fi} = \int \psi_f^* \hat{\mu} \psi_i d\tau \quad (3.3)$$

is nonzero. $\hat{\mu}$ is the electric dipole moment operator and ψ_i and ψ_f the wave functions of the initial and final state. According to the Franck-Condon principle, the excitation of an electron into an electronic excited state occurs without changes of the nuclei positions. In addition, transitions between states of different multiplicity $M = 2S + 1$ (S : angular spin momentum) are spin-forbidden since the total spin is not conserved. Transitions between two singlet states are allowed whereas transitions between singlet and triplet states are forbidden. Furthermore, transitions are only allowed if they are accompanied by a change of parity. Thus, for centrosymmetric molecules such as carotenoids $u \rightarrow g$ (g : even symmetry, u : odd symmetry) and $g \rightarrow u$ transitions are allowed, but $g \rightarrow g$ and $u \rightarrow u$ transitions are forbidden (symmetry-forbidden) [143–145].

Molecular processes which can occur in excited states are usually described in a Jablonski diagram as shown in Figure 3.1. Following light absorption, several deactivation processes can occur. Besides radiative and radiationless decays photochemical processes, energy transfer, and electron transfer reactions are possible. The most common deactivation in condensed phase is a nonradiative decay as a combination of internal conversion (IC), internal vibrational relaxation (IVR), and external conversion, in which the excitation energy is converted to rotational, vibrational, and translational energy of the surrounding molecules.

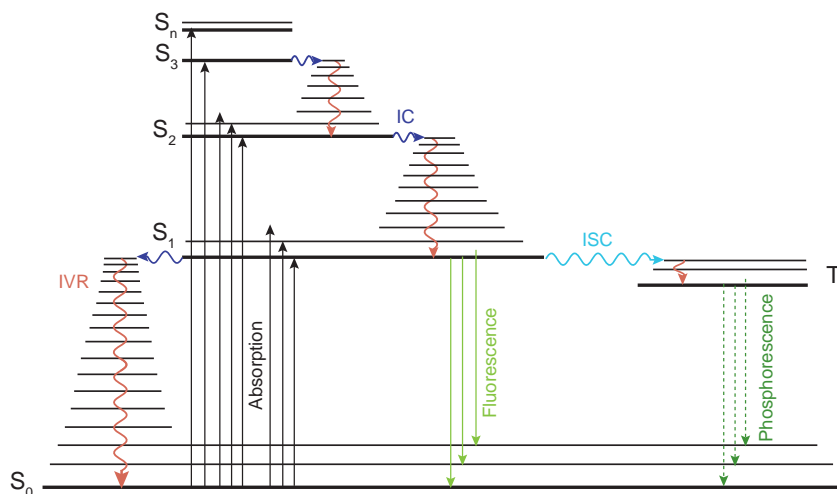


Figure 3.1: Jablonski diagram illustrating processes that can occur after absorption. IC: internal conversion, ISC: intersystem crossing, IVR: internal vibrational relaxation.

Excess energy can also be ejected as an emitted photon. Two types of emission can be distinguished depending on the nature of the emitting excited state – fluorescence from singlet states (S) and phosphorescence from triplet states (T). The return from the lowest singlet excited state (S_1) to the ground state (S_0) is spin allowed, thus emission occurs rapidly and typical fluorescence lifetimes are on the nanosecond time regime. For molecules in condensed phase the energy of the emitted photon is typically lower than that of the absorbed photon (Stokes shift) due to the rapid nonradiative decay to the lowest vibrational level of the S_1 state and solvation processes. Hence the emission occurs from the S_1 vibrational ground state to higher vibrational levels of the S_0 state.

Upon excitation into higher excited states the energy is dissipated radiationless in about 10^{-12} s leading to the population of the lowest vibrational level of the S_1 state. Therefore emission spectra are typically independent of the excitation wavelength. This is known as Kasha’s rule [146] or mirror image rule since the emission spectrum usually is a red shifted mirror image of the $S_0 \rightarrow S_1$ absorption. However, there are many exceptions to this rule. For example, molecules such as polyenes emit from their S_2 state, since the $S_1 \rightarrow S_0$ transition is symmetry forbidden whereas the $S_2 \rightarrow S_0$ transition is strongly allowed.

Nonradiative transitions between states of different multiplicity enabled by spin-orbit coupling (intersystem crossing) lead to the population of triplet states. Transition to the singlet ground state is again only possible via spin-orbit coupling and therefore the emission rates are much lower compared to fluorescence lifetimes resulting in phosphorescence lifetimes of milliseconds to seconds or even longer.

3.1.1 Fluorescence Anisotropy

Regarding polarized fluorescence spectroscopy the anisotropy r is defined as:

$$r = \frac{I_{\parallel} - I_{\perp}}{I_{\parallel} + 2I_{\perp}} \quad (3.4)$$

with I being the intensity of the emission detected with parallel (\parallel) polarization and perpendicular (\perp) polarization with respect to the polarization of the excitation light. Measurements with an angle of 54.7° between the polarizations of fluorescence and the excitation light lead to an isotropic signal (see below) and is called the magic angle.

In unoriented samples (e.g. in solution) absorption of the polarized light is most likely if the electric field vector of the incident beam and the molecular transition dipole moment are oriented parallel and zero if they are oriented perpendicular to each other. The probability for angles in between follows a \cos^2 -distribution. Therefore fluorophores with their transition dipole moment oriented along the vector of the incident light are preferentially excited. In solution this photoselection decreases due to rotational diffusion which depends on the size and shape of the rotating molecule (e.g. rotational time constant ≈ 14 ns for a 50 kDa protein) as well as on the viscosity of the solvent [147–149].

The average angular displacement between the absorption and emission transition dipole moment can be determined by means of anisotropy measurements and calculated with the following equation:

$$r = \frac{2}{5} \left(\frac{3\langle \cos^2 \beta \rangle - 1}{2} \right) \quad (3.5)$$

where β is the angle between absorption and emission transition dipole [149]. As mentioned before, measurements with magic angle conditions result in an isotropic signal, since the term $(3 \cos^2 \beta_{ma} - 1)$ becomes zero.

The loss of fluorescence polarization by relaxation processes faster than the rotational diffusion can be investigated by time-resolved anisotropy measurements. After initial population of the excited states of fluorophores in parallel orientation, the anisotropy value decays due to internal conversion and/or energy transfer processes. In case of large molecules such as protein systems rotational diffusion is slow compared to the investigated dynamics and can be neglected. To calculate the time dependent anisotropy $r(t)$ the fluorescence intensity I in equation 3.4 has to be exchanged with the time dependent fluorescence intensity $I(t)$. Time-resolved anisotropy experiments can be used e.g. to study energy and electron transfer processes [150–152].

The analysis of this time-dependent anisotropy decay is not only possible for time-resolved fluorescence but also for transient absorption spectroscopy [153,154]. The time dependent anisotropy value $r(t)$ can be calculated analogous to equation 3.4 by exchanging

ing the fluorescence intensity I by the time dependent absorption changes $\Delta A(t)$:

$$r(t) = \frac{\Delta A_{\parallel}(t) - \Delta A_{\perp}(t)}{\Delta A_{\parallel}(t) + 2\Delta A_{\perp}(t)} \quad (3.6)$$

One has to consider that several contributions of a transient absorption spectra such as excited state absorption and ground state bleach (see chapter 4.2.3) all have their own anisotropy. Thus, analysis of the anisotropy decay of an investigated transition is only possible if it contributes in an isolated part of the transient spectrum. In congested areas, where the different bands are overlapping an analysis is not possible [147].

3.1.2 Fluorescence Quantum Yields

Besides the fluorescence lifetime the quantum yield is probably the most important property of a fluorophore. The fluorescence quantum yield ϕ_{fl} is defined as the ratio of emitted photons to absorbed photons.

$$\phi_{fl} = \frac{N_{em}}{N_{abs}} \quad (3.7)$$

To determine the fluorescence quantum yield a comparative method is usually employed. Determination of absolute quantum yields is much more complicated and needs a great experimental effort [155–157]. Both, emission and absorption rates have to be determined very accurately and this requires the knowledge of specific instrumental parameters. However, for the comparative method the emission of the sample is compared to the emission of a reference fluorophore with known quantum yield [149, 158, 159]. For this purpose the absorption and emission spectra of the reference and of the investigated sample should be in the same spectral range. All spectra have to be recorded with identical spectrometer adjustment. The fluorescence quantum yields can be calculated as:

$$\phi_{fl} = \phi_{ref} \frac{I_{fl}}{I_{ref}} \frac{n_{fl}^2}{n_{ref}^2} \quad (3.8)$$

with I being the integrated fluorescence spectrum and n the refractive index of the respective solvent. In this work absorption and emission spectra were recorded for the sample and reference at different concentrations in a range where re-absorption can be excluded ($OD < 0.1$ in a 1 cm cuvette). The integrated fluorescence was plotted against the absorbance and the resulting slopes were used to calculate the fluorescence quantum yield analogous to equation 3.8.

3.2 Principles of Ultrafast Spectroscopy

In optical spectroscopy time resolutions down to picoseconds are possible using electronic devices. The resolution is restricted mainly by the response time of the respective detector. To observe time dependent absorbance changes in the order of nanoseconds laser flash-photolysis can be used [160,161]. Time correlated single photon counting (TCSPC) is applied to determine fluorescence lifetimes with a time resolution down to a few 10 ps [149,162]. However, for a time resolution in the order of femtoseconds optical techniques applying ultrashort laser pulses are required [13].

3.2.1 Pump-Probe Spectroscopy

Spectroscopic methods with high time resolution beyond the capability of electronic detectors are usually achieved by means of the pump-probe technique (see Figure 3.2). In short, an ultrashort laser pulse is split into a pump and a probe beam. The pump pulse excites the sample into an electronic or vibronic excited state and triggers the process of interest. The second beam monitors the initiated modification of an optical property. To perform time dependent measurements the time delay between the two pulses is modified by a variable delay line (see chapter 4.2.2).

The time resolution in such experiments is provided by the optical delay and mainly depends on the pulse duration, hence ultrashort pulses in the fs time domain are required. In many cases the spectral characteristics of the laser output is not suitable for both the

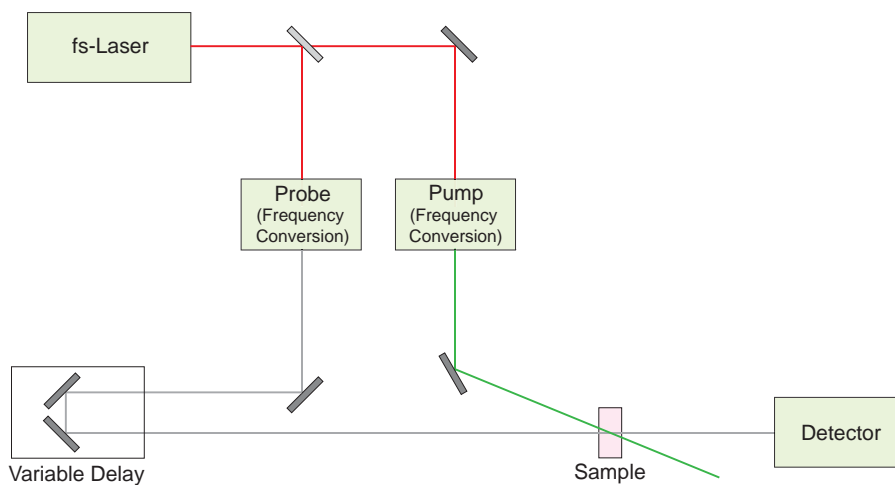


Figure 3.2: Scheme for pump-probe experiments.

excitation of the sample and the probing of the respective process, so the laser frequency has to be adjusted using nonlinear optical effects. Thus, the following sections address the basic principles of nonlinear optics, the generation of ultrashort laser pulses, and techniques for wavelength conversion used within this work. It is a short summary of the comprehensive information found in the cited books [163–167].

3.2.2 Nonlinear Optics

Polarization and Electric Field

In linear optics light propagating through a given material is delayed compared to speed of light in vacuum but its frequency remains unchanged. The dielectric polarization $\vec{P}(\vec{E})$ depends linearly on the electric field \vec{E} :

$$\vec{P} = \epsilon_0 \chi^{(1)} \cdot \vec{E} \quad (3.9)$$

where $\chi^{(1)}$ is the linear susceptibility and ϵ_0 the permittivity of free space. However, sufficiently intense light modifies the optical properties of a material, i.e. the response of the material to a high electric field depends in a nonlinear manner on the strength of the field and quadratic and cubic terms of the susceptibility χ can no longer be neglected. This nonlinear response can be described by a Taylor expansion of the polarization:

$$\vec{P}(\vec{E}) = \epsilon_0 \left[\chi^{(1)} \vec{E} + \left(\chi^{(2)} \vec{E} \right) \vec{E} + \left(\left(\chi^{(3)} \vec{E} \right) \vec{E} \right) \vec{E} \right] \quad (3.10)$$

with the nonlinear susceptibilities $\chi^{(n)}$ in the order of $\chi^{(1)} \approx 1$, $\chi^{(2)} \approx 10^{-10} \text{cm} \cdot \text{V}^{-1}$, $\chi^{(3)} \approx 10^{-17} \text{cm}^2 \cdot \text{V}^{-2}$. Because $\chi^{(n)} \ll \chi^{(n+1)}$ higher-order terms only play a role in case of extremely high field strength, as for example obtained for ultrashort laser pulses. The contributions of the higher-order terms give rise to interactions of light beams in a medium resulting in new frequencies. The oscillating, induced atomic dipole moments affected by the incident light $\vec{E}(\omega)$ are the origin of new electromagnetic waves whose frequency spectrum is determined by that of $\vec{P}(\vec{E})$. As an example one can consider the incident light as a superposition of two electromagnetic waves with the frequencies ω_1 and ω_2 propagating in \vec{z} -direction:

$$\vec{E} = \vec{E}_1 \cos(\omega_1 t + \vec{k}_1 \vec{z}) + \vec{E}_2 \cos(\omega_2 t + \vec{k}_2 \vec{z}) \quad (3.11)$$

Due to $\cos^2 x = \frac{1}{2}(1 + \cos(2x))$ the quadratic term in equation 3.10 then contains the following frequencies:

$$\begin{aligned}
 \vec{P}^{(2)}(\omega) &= \epsilon_0 \chi^{(2)} E_1^2 E_2^2 & (3.12) \\
 &+ \epsilon_0 \chi^{(2)} \left[E_1^2 \cos(2\omega_1 t + 2\vec{k}_1 \vec{z}) + E_2^2 \cos(2\omega_2 t + 2\vec{k}_2 \vec{z}) \right] \\
 &+ \epsilon_0 \chi^{(2)} \left[E_1 E_2 \cos \left((\omega_1 + \omega_2) t + (\vec{k}_1 + \vec{k}_2) \vec{z} \right) \right] \\
 &+ \epsilon_0 \chi^{(2)} \left[E_1 E_2 \cos \left((\omega_1 - \omega_2) t + (\vec{k}_1 - \vec{k}_2) \vec{z} \right) \right]
 \end{aligned}$$

assuming that only the first nonlinear term in equation 3.10 contributes. The nonlinear polarization $P^{(2)}(\omega)$ contains a constant term independent of frequency (optical rectification), terms with $2\omega_1$ and $2\omega_2$ describing the second harmonic generation (SHG) of each input frequency, and terms corresponding to the sum frequency generation (SFG, $\omega_1 + \omega_2$) and the difference frequency generation (DFG, $\omega_1 - \omega_2$), respectively. Depending on the experimental conditions certain processes can be very efficient. Phenomena such as the quadratic electro-optic effect (Kerr-effect) and third harmonic generation (THG) are third-order interactions. The light intensity, the choice of the nonlinear medium, and the polarization of the incident light are crucial to enable the described processes.

Phase matching in anisotropic media

Isotropic media have no preferred direction, thus the susceptibility is a scalar quantity and the speed of light is independent of its polarization. In anisotropic media such as birefringent crystals the propagation speed of light depends on its polarization and the orientation of the crystal. Commonly used nonlinear media are e.g. β -bariumborat (β -BBO) or lithium triborate (LBO) crystals which have high damage thresholds.

To be efficient most nonlinear processes such as frequency doubling and parametric amplification require phase matching of the waves, i.e. a constant phase relationship along the propagation direction. This means conservation of momentum ($\vec{k}_3 = \vec{k}_1 + \vec{k}_2$) and energy ($\hbar\omega_3 = \hbar\omega_1 + \hbar\omega_2$). The phase mismatch is given by

$$\Delta\vec{k} = \vec{k}_3(\omega_3) - \vec{k}_1(\omega_1) - \vec{k}_2(\omega_2) = \frac{n_3}{\lambda_3} - \frac{n_1}{\lambda_1} - \frac{n_2}{\lambda_2} \quad (3.13)$$

Anisotropic materials can be applied to avoid phase mismatch by modulation of the phase velocity based on the polarization dependence of the refractive index. Biaxial crystals with three different refractive indices (n_x, n_y, n_z) are distinguished from uniaxial crystals with only two different refractive indices ($n_x = n_y \neq n_z$). In praxis the latter are more important. They contain a symmetry axis called the optical axis. Incident beams with their polarization oriented perpendicular with respect to the optical axis are termed ordinary beams with the refractive index n_o . The refractive index n_e of an

extraordinary beam depends on the angle θ between the optical axis and the propagation direction of the beam. Due to the different refractive indices n_o and n_e of the ordinary and the extraordinary beam phase matching can be achieved by varying the angle θ .

In principle, type I and type II phase matching are distinguished. Type I phase matching means that the two beams with lower frequency have the same polarization. In case of type II phase matching the polarization of the two beams is oriented perpendicular to each other. The type of crystal determines whether the involved waves are ordinary or extraordinary beams. One can differentiate between positive uniaxial crystals ($n_e > n_o$) and negative uniaxial crystals ($n_e < n_o$) such as β -BBO used in this work. Phase matching can be achieved for both collinear and noncollinear geometries of the incident beams. If the phase matching angle is adjusted correctly, all waves are exposed to the same refractive index resulting in positive interference and fulfilled phase matching conditions. However, dispersion leading to a group velocity dispersion mismatch (see below) limits the process to a certain bandwidth.

Group-Velocity Dispersion

Group-velocity dispersion (GVD) is defined as the frequency dependence of the group velocity in a medium. This phenomenon is responsible for a dispersive broadening of pulses propagating through a medium causing a temporal stretching of the pulse. In case of ordinary dispersion this effect is named *positive chirp*, i.e. long-wavelength components propagate faster compared to the short-wavelength components. The opposite process is called *negative chirp* and occurs in case of anomalous dispersion.

If the pulses propagate through optical elements GVD occurs, which can be compensated by a composition of prisms or gratings causing a negative chirp. In case of the utilized setups a prism compressor was used to compress the excitation pulses as well as the gate pulses down to several 10 fs (see chapter 4.1.2). In addition, this principle is used in the chirped pulse amplification (see chapter 3.2.3).

Quadratic Electro-Optic Effect

The modification of the refractive index n of a medium caused by a strong electric field is called Kerr-effect or quadratic electro-optic effect [167]. Along the polarization direction of the applied electric field birefringence is induced and the refractive index change is proportional to the square of the electric field strength. For this third order nonlinear process the applied materials usually are isotropic, whereby the second order susceptibility and resulting processes such as SHG are eliminated due to destructive interference. Assuming a temporally variable electric field (e.g. an ultrashort pulse), the nonlinear, intensity dependent refractive index is given by:

$$n(I, r, t) = n_0 + n_2 I(r, t) = n_0 + \Delta n(r, t, I) \quad (3.14)$$

where $I(t)$ is the intensity of the electric field, n_0 is the refractive index in the absence of the electric field, and $\Delta n = n_{\perp} - n_{\parallel}$ is the difference between the ordinary and the extraordinary refractive index with respect to the polarization of the so called gate pulse. Intense laser pulses can cause an instantaneous response of the Kerr medium. Ultrashort pulses open the gating medium only a very short time period and thus make it a powerful technique for time-resolved spectroscopic experiments in the femtosecond time regime (see chapter 3.2.5 and 4.1.2).

3.2.3 Generation of Ultrashort Pulses

Ultrashort pulses are a basic requirement for time-resolved spectroscopic techniques in the femtosecond time domain. Methods for the generation of ultrashort pulses are described in detail in several review articles and textbooks [164, 165, 168–170]. In the following section important terms and definitions are described.

The Heisenberg uncertainty principle states that the pulse duration is connected with the band width:

$$\Delta\omega\Delta t \geq 1 \quad (3.15)$$

The lower limit of the pulse duration depends on the optical spectrum of the pulse. A pulse at this limit with the minimal spectral width is called Fourier transform or bandwidth limited. Therefore, for short pulse generation, laser media with a sufficient bandwidth are required, e.g. a titanium-doped sapphire (Ti:Sa) with a broadband fluorescence between 690 nm and 1080 nm. With its broad absorption band (450-600 nm) it can be pumped by several lasers such as Argon-lasers and frequency doubled Nd:YAG lasers. Q-switching, cavity-dumping, and mode-locking are techniques to reduce the duration of the laser emission compared to the excitation [169]. Active and in particular passive mode locking enables the generation of ultrashort pulses.

Mode Locking

In a ‘free-running’ laser all modes are oscillating independently with random phases. This results in a laser output with no regular temporal structure. If all or some of the modes are in phase they will interfere constructively and produce a short intense laser output (‘coherent spike’). Oscillation of all laser modes in phase, i.e. locking them together, can be achieved by the so called mode locking. Phase mismatching has to be disabled so that all modes interfere constructively every round-trip in the resonator. Thus, the laser output becomes temporally well defined due to a fixed phase relationship

between all modes. As mentioned before, the larger the number of frequencies involved, the shorter the emitted pulse can be [169].

In mode-locked lasers the resonator contains either an active component (an optical modulator) or a passive element (e.g. saturable absorber, Kerr-lens). Active mode locking uses external signals e.g. from an acousto-optic or electro-optic modulator modulating the optical properties of the laser resonator. If the periodic modulation is synchronized with the resonator round trips all modes can be locked. While the reproducibility of the pulses formed by active mode locking is better compared to passive mode locking the latter enables the generation of even shorter pulses.

The laser emission itself modulates the optical properties of a nonlinear material within the laser resonator in case of passive mode-locking. In principle, short pulses with high intensity are amplified and weaker pulses are suppressed by the passive medium. For example absorbers with a nonlinear saturation behavior are more transparent with increasing pulse intensity. Fluctuations with higher intensities are less absorbed whereby locked modes are amplified every round-trip [171–173]. Kerr-lens mode locking is another passive technique which enables the generation of pulses down to 5 fs in Ti:Sa lasers. The application of a medium with a nonlinear intensity dependent refractive index results in self-phase modulation as well as self-focusing [174,175].

Chirped Pulse Amplification

Due to the damage threshold of the resonator materials the intensity of the outcoupled pulses is restricted. However, in many cases amplifiers are needed to increase the intensity of the weak ultrashort pulses. In an amplifier the peak intensities of ultrashort pulses can become very high resulting in distortion or destruction of the gain medium or other optical components. This can be prevented by means of chirped pulse amplification (CPA), which is a common technique to amplify ultrashort laser pulses [176,177]. To avoid damage, the pulses are chirped and therefore temporally stretched by means of a stretcher, e.g. a prism pair, a grating pair, or a long fiber. Thus, the peak power is reduced and the stretched pulses can be amplified in another laser resonator. After the amplification process the compressor with opposite dispersion removes the chirp and compresses the pulses.

Characterization of Ultrashort Pulses

Typically, short events are characterized by means of a shorter event. Unfortunately, there are usually no shorter events available than the femtosecond laser pulse itself. Hence nonlinear autocorrelation techniques are applied to characterize ultrashort pulses, where the short pulse measures itself [169,178]. A widely used technique is the second harmonic autocorrelation to measure the time dependent intensity profile of an ultrashort pulse. Therefore the pulse is split into two sub-pulses and one part is then delayed with

respect to the other. A nonlinear optical effect, e.g. SHG, is used to generate an optical signal which is proportional to the product of the two incoming electric fields. The intensity of the detected signal depends on the temporal overlap of the two sub-pulses. The power of the mixing product is recorded as a function of the varied path length of one sub-pulse. From the width (Gaussian FWHM) of the autocorrelation signal the actual pulse duration can be calculated assuming a Gaussian pulse shape for the input signals as well as the output signal (see chapter 4.3).

3.2.4 Methods for Wavelength Conversion

Second Harmonic Generation, Sum and Difference Frequency Generation

Second harmonic generation (SHG) is a second order nonlinear process (see chapter 3.2.2) which occurs only in crystals without inversion center. Two incident photons with the same frequency ω create a photon of doubled frequency 2ω under conservation of momentum and energy.

Just as SHG sum and difference frequency generation are second order nonlinear optical processes. Two incident photons of the frequencies ω_1 and ω_2 interact in a nonlinear medium to generate a third photon with either the sum ($\omega_3 = \omega_1 + \omega_2$) or difference ($\omega_3 = \omega_1 - \omega_2$) frequency. At least one of the beams has to be intense and because the process requires efficient phase matching, usually there is no simultaneous SFG and DFG. SFG is utilized in the upconversion technique to achieve femtosecond time resolution of fluorescence decay measurements (see chapter 4.1.3).

Optical Parametric Amplification

Parametric conversion enables the generation of light with tunable wavelengths by means of second order nonlinear processes. Photons of the intense pump beam ($\hbar\omega_p$) are split into signal ($\hbar\omega_s$) and idler ($\hbar\omega_i$) photons with lower energy in accordance with the energy conservation $\hbar\omega_p = \hbar\omega_s + \hbar\omega_i$. Underlying process is the DFG, i.e. the photon energy of the signal is the difference between the energies of pump and idler wave.

Optical parametric amplification can be achieved if a weak seed photon is superimposed with a pump photon of much higher intensity and frequency within the nonlinear crystal. The latter can cause parametric fluorescence due to the generation of several pairs of signal and idler with sufficient phase matching conditions. The frequency of the amplified signal is determined by the frequency of the seed pulse and as mentioned before the idler frequency corresponds to the difference between the frequencies of the seed and the pump. Usually, the seed photons are obtained from a supercontinuum generated in a suitable medium (see below).

The propagation direction of all waves is determined by phase matching conditions and conservation of momentum. In case of collinear alignment of all involved beams the

corresponding setup is called optical parametric amplifier (OPA) [179, 180] whereas in noncollinear optical parametric amplifiers (NOPAs) pump and seed wave arrive at the crystal with a certain angle to each other [181–183]. With the same phase matching angle several wavelengths can be amplified by simultaneous phase matching in a large frequency range. To be able to obtain variable excitation pulses in the visible spectral range usually a NOPA is used which is described in detail in chapter 4.1.2. A two stage OPA was built to generate gate pulses in the NIR spectral range for the Kerr gating technique (see also chapter 4.1.2).

White-Light Generation

To convert the fundamental laser wavelength to pulses with a broad spectral bandwidth white-light generation (or supercontinuum generation) in different media (e.g. sapphire and CaF_2) can be used. The mechanism of this nonlinear process is not completely understood yet. A short laser pulse is focused on the transparent solid and self-focusing as well as self-phase modulation are part of the complex processes broadening the spectrum [184–186]. The high electric field distorts the charge distribution in the nonlinear medium that affects phase, amplitude, and frequency of the incident wave (self-phase modulation). Self-focusing due to the intensity dependent refractive index gives rise to further nonlinear processes [187–189]. Recent results from Dachraoui et al. confirmed that phenomena such as Kerr nonlinearity, plasma generation, group-velocity dispersion, diffraction, and self-steepening of the pulse front spatiotemporally modify the pulse shape [190]. The spectral properties of the generated white-light continuum are influenced by four-wave mixing, stimulated Raman or Brillouin scattering, and the band gap of the applied material [191, 192]. In this work white-light generated in solid media was used as seed wave for optical parametric amplification (chapter 4.1.2) as well as for spectrally broad probe light in the transient absorption experiments (chapter 4.2.2).

3.2.5 Time-Resolved Fluorescence Techniques

Time Correlated Single Photon Counting

The time correlated single photon counting (TCSPC) principle relies on the determination of the time delay between excitation of the sample and subsequent emission of a photon (Figure 3.3). It is based on the repeated detection of single photons, the measurement of their detection time, and the reconstruction of the time dependent fluorescence signal [149, 193–195].

A short laser pulse excites the sample and triggers the photon counter via a photodiode simultaneously. The emitted photons are collected and guided to the detector whereas the excitation beam is blocked. Usually in front of the detector a monochromator is used to spectrally separate scattered excitation light from the fluorescence. The

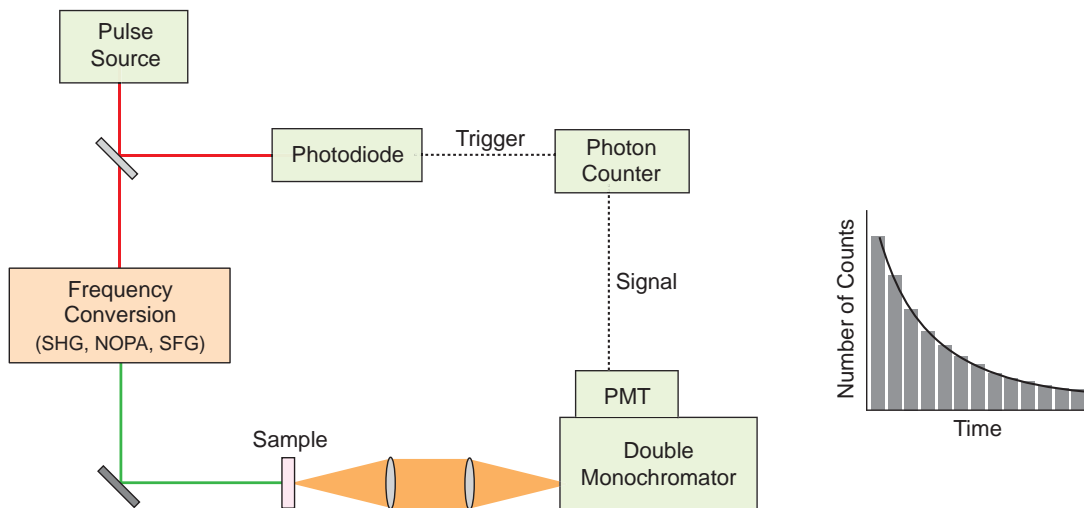


Figure 3.3: Principle of the TCSPC technique. A short laser pulse excites the sample and simultaneously triggers a photon counter. The collected fluorescence photons are detected as single events by a photomultiplier tube (PMT), which sends a stop signal to the photon counter. The detected photons are then displayed correlated to their detection time resulting in a histogram.

most common detectors for signals with low intensity are photomultiplier tubes (PMT). Upon the arrival of a single photon the produced current is multiplied and a halt signal is sent to the photon counting card. Here the photons are collected as an event in a memory location correlated to the time difference between trigger signal and detection time. After repeating this process numerous times a histogram of the number of detected photons versus detection time can be generated which represents the temporal fluorescence behavior of the excited sample.

It is important to have a low fluorescence signal, since the PMT does not distinguish between the arrival of one or more photons and also needs a recovery time before it is able to detect the next photon. Thus, the probability to detect one photon after each excitation pulse should be very low. For a probability of 1 % or less the chance to detect two photons as one event is negligible (<0.01 %). In case of higher counting rates the obtained histogram is distorted to shorter times. Most TCSPC setups are performed in 'reverse-mode' where the fluorescence photon triggers the photon counter and the subsequent excitation pulse serves as the halt signal.

The duration of the excitation pulse and the dead time range of the detection system limit the time resolution of TCSPC experiments. In case of fs laser pulses the latter limitation is crucial. Time resolutions of several 10 ps are possible with high demands

for the electronic devices and the stability of the measurement conditions. It is important to keep in mind that the measured intensity decay is convoluted with the instrument response function (IRF). The IRF contains information about the time characteristics of the whole measurement system including the rise time of the detector. Before analysis of the actual kinetics deconvolution with the IRF has to be performed.

Optical Gating

Optical gating techniques are implied to improve the time resolution restricted by the electronic detection systems. In contrast to transient absorption spectroscopy in transient fluorescence techniques the probe pulse does not pass the sample but is required for an additional procedure called optical gating [196–198]. Thus, the probe pulse is called 'gate' pulse. The emitted fluorescence photons are collected and focused on a suitable gating medium. The optical gating device only gains its functionality if the gate pulse is present, which alters the optical properties of the gating medium. In case of absence of the gate pulse the fluorescence can not pass the gating device. The latter is opened by temporal and spatial overlap of fluorescence light with the ultrashort gate pulse. So the gated fluorescence photons can be detected as a function of the delayed gate pulse. A scheme of the optical gating process is shown in Figure 3.4. As shown in the inset, the intensity of the gated light depends on the intensity of the fluorescence. Hence the time dependent signal intensity of the gated light resembles the temporal behavior of the collected fluorescence. Within the scope of this work two optical gating techniques were used – fluorescence upconversion and Kerr gating.

In case of fluorescence upconversion the gating medium is a nonlinear crystal [198–200], e.g. a BBO crystal with a cutting angle depending on the fluorescence wavelength. The high intensity of the gate pulse enables frequency conversion via SFG. Photons with sum frequency (ω_{SFG}) are generated only if gate pulse (ω_{gate}) and fluorescence photons (ω_{fl}) overlap temporally and spatially in the crystal with phase matching condition:

$$\omega_{SFG} = \omega_{gate} + \omega_{fl} \quad (3.16)$$

$$\vec{k}_{SFG} = \vec{k}_{gate} + \vec{k}_{fl} \quad (3.17)$$

By means of a delay stage the gate pulse is delayed with respect to the excitation beam. Due to the SFG a temporally selected part of the fluorescence is separated spectrally from the rest of the fluorescence. A monochromator is adjusted for the sum frequency hence fluorescence photons are not detected if they are not upconverted.

Only a very small part of the spectral range of the fluorescence light can be gated simultaneously since phase matching conditions are required for the SFG. The frequency range is restricted by the cutting angle and thickness l of the crystal [201]:

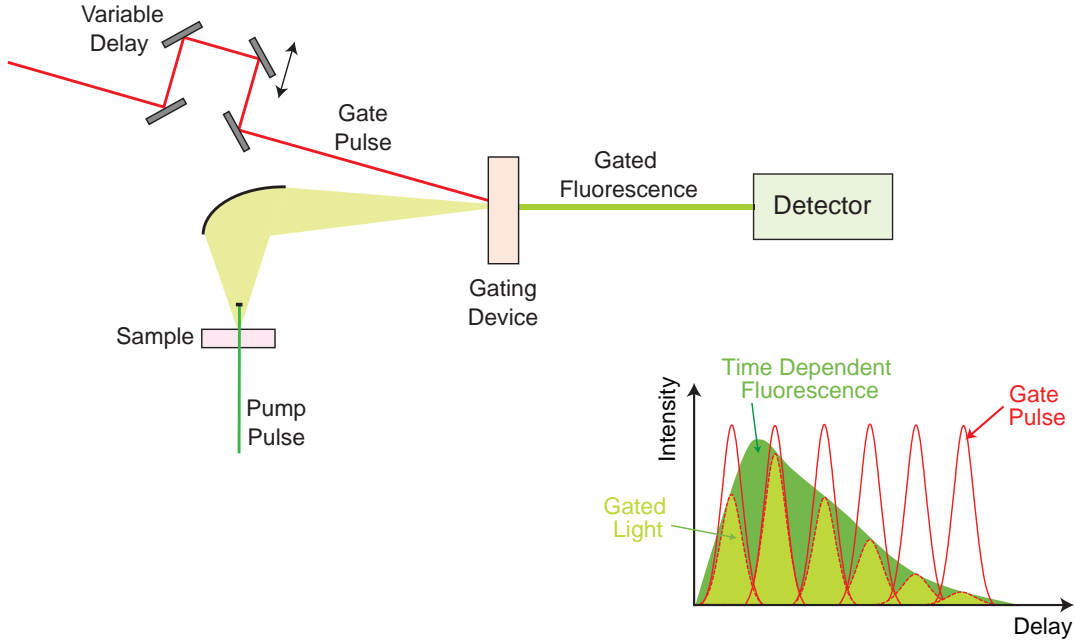


Figure 3.4: Principle of optical gating. An ultrashort laser pulse is used to change the properties of the gating medium. Fluorescence can only propagate through the gating device if it is superimposed spatially and temporally with the gate pulse in the gate medium. The detected gated fluorescence photons resemble the temporal behavior of the fluorescence when displayed with respect to the delay of the gate pulse.

$$\Delta\omega \propto \frac{1}{l} \cdot \left(\frac{c}{v(\omega_{SFG})} - \frac{c}{v(\omega_{fl})} \right) \quad (3.18)$$

with $v(\omega)$ the group velocity of light in the medium. The use of very thin crystals ($l \leq 0.1$ mm) with low dispersion and gate pulses converted to the NIR spectral region allows upconversion of fluorescence in a wide frequency range [201–203]. However, the quantum efficiency of the upconversion process depends on the interaction length of the light pulses in the crystal. With decreasing pathlength in the crystal the efficiency also decreases. The time resolution basically depends on the pulse duration of the excitation and the gate pulses and the dispersive elements in the setup.

In the Kerr gating technique the BBO crystal is replaced by an isotropic Kerr medium that can be a gas, a liquid, or a solid [204–206]. It is placed between two crossed polarizers. The fluorescence is collected and after passing through the first polarizer

propagates through the Kerr medium. If the gate pulse is absent the fluorescence is blocked by the second polarizer. Focusing the gate pulse into the Kerr medium induces strong anisotropy and it becomes birefringent. Due to the modulation of the refractive index the linearly polarized fluorescence alters to an elliptical polarization in case of spatial and temporal overlap with the gate pulse. Maximal elliptical polarization can be achieved for an angle of $\Theta = 45^\circ$ between the polarization of the fluorescence and the polarization of the gate pulse [206,207]. A part of the elliptical polarized light can pass the second polarizer and can be detected.

In contrast to the upconversion technique ($\chi^{(2)}$ process) the Kerr effect is based on a third order nonlinear process. The nonlinear susceptibility $\chi^{(3)}$ is proportional to the nonlinear part of the refractive index n_2 . Upon interaction with a short laser pulse with the intensity $I(r, t)$ the second order susceptibility $\chi^{(2)}$ is correlated to the temporal modification of the refractive index $n(I, r, t)$ (see equation 3.14). The external field induces a difference between the ordinary and the extraordinary refractive index relative to the polarization of the gate pulse [208].

Like in the upconversion process the time resolution depends on the pulse duration of both excitation and gate pulse and the dispersive elements in the setup. In addition, the angle between the polarizations of the gate pulse and the fluorescence light and the characteristics of the Kerr medium influence the time resolution. The gating efficiency T is defined as the ratio of gated fluorescence per time unit to the total fluorescence arriving at the Kerr medium:

$$T = \sin^2(2\Theta) \cdot \sin^2\left(\frac{1}{2}\varphi(r, t)\right) \quad (3.19)$$

where $\varphi(r, t) = 2\pi\Delta n(r, t, I)l/\lambda_{fl}$ is the induced phase shift between the ordinary and the extraordinary part of the fluorescence light with the wavelength λ_{fl} induced in the Kerr medium with pathlength l . For $\Theta = 45^\circ$ and a small phase shift $\varphi(r, t)$ the gating efficiency can be approximated by:

$$T \approx \pi^2 n_2^2 l^2 I_{gate}^2 / \lambda_{fl}^2 \quad (3.20)$$

Thus, the efficiency of the Kerr gating process is proportional to the square of the product of the intensity of the gate pulse I_{gate} , the nonlinear refractive index n_2 , and the pathlength l of the Kerr medium as well as inversely proportional to the square of the wavelength λ_{fl} . In contrast to the upconversion the Kerr process enables to gate the whole frequency range of the fluorescence simultaneously. It is just delimited by the transmission properties of the applied optical elements and the characteristics of the detection unit.

There are different requirements for the characteristics of the Kerr medium. The

induced anisotropy should follow the electric field of the gate pulse instantaneously. The GVD as well as the background induced by the gate pulse should be as low as possible. A high gating efficiency and transparency from the UV to the NIR spectral region is required. These parameters are important for a high temporal resolution and a good signal-to-noise ratio. In liquids and gases orientation and relaxation of the molecules upon interaction with the gate pulse lasts picoseconds resulting in a poor time resolution [209]. In solids the induced anisotropy mainly generates a displacement of the electrons. A contribution of the nucleus is negligible [210]. This instantaneous response of the electrons permits time resolutions < 100 fs. Glasses with a nonlinear refractive index n_2 seem to be a good choice. However, they also have a high dispersion in the VIS spectral range [210]. Hence, fused silica is a suitable Kerr medium in spite of its low nonlinear refractive index n_2 . The gating efficiency lies between 1-4 % depending on the pathlength of the medium [208].

Chapter 4

Experimental Setups

Marty McFly: *Wait a minute, Doc. Ah... Are you telling me that you built a time machine... out of a DeLorean?* Dr. Emmett Brown: *The way I see it, if you're gonna build a time machine into a car, why not do it with some style?*

(Back to the Future)

In the following chapter all setups are depicted used for time-resolved spectroscopic measurements of FCPs and isolated carotenoids during this thesis. The first part focuses on time-resolved fluorescence techniques. The Kerr-gating setup for broad band time-resolved fluorescence spectra is described. It was designed and built within the scope of this work, hence single parts e.g. NOPA, OPA, and prism compressors are depicted in detail. The following section considers the combined TCSPC/upconversion setup designed by Ute Förster which was implemented during this thesis. A short summary of the transient absorption experiment and the data analysis is given next. Most of the depicted data in the chapters 5, 6, and 7 resulted from these pump-probe measurements. Finally, the home-made autocorrelator to characterize ultrashort pulses is described.

4.1 Time-Resolved Fluorescence Spectroscopy

The inherent sensitivity of fluorescence signals provides a useful alternative for probing excited state dynamics. In case of carotenoids there are difficulties including the low quantum yields and fluorescent impurities of the samples. However, with sufficiently pure samples e.g. obtained by HPLC (high-performance liquid chromatography) upon excitation with laser pulses for efficient pumping the weak emission from carotenoids can be detected by sensitive detectors [211,212].

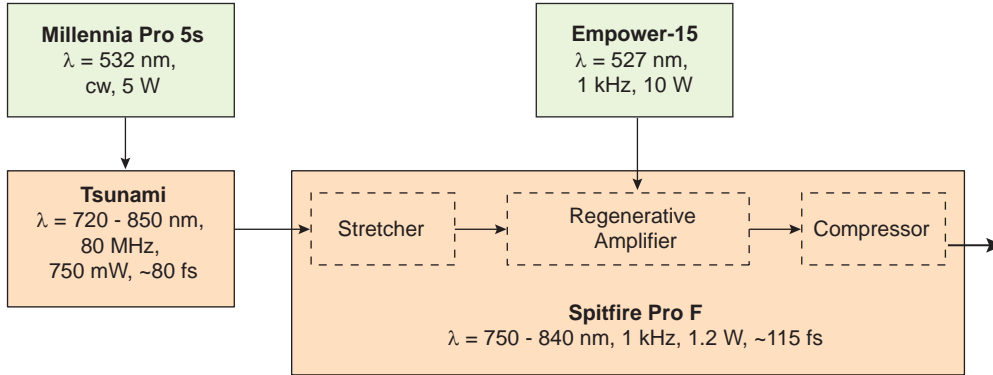


Figure 4.1: Scheme of the *Tsunami-Spitfire* laser system.

As mentioned before, for time-resolved fluorescence measurements in principle two techniques are widely used: time correlated single photon counting for a time resolution from a few 10 ps up to μ s, and optical gating which enables time resolutions down to the sub 100 fs time domain. The latter includes the upconversion and the Kerr gating technique which were both implemented during this work.

4.1.1 The *Tsunami-Spitfire* Laser System

All time-resolved fluorescence measurements were performed with a *Tsunami-Spitfire* system from Spectra-Physics [213–216]. Short pulses from the oscillator are amplified by means of chirped pulse amplification. A scheme is shown in Figure 4.1.

The *Millennia* laser medium is a Nd^{3+} -doped yttrium vanadate crystal (Nd:YVO_4) pumped by a diode laser. The *Millennia* output (cw, 532 nm, 5 W) pumps the Ti:Sa laser oscillator *Tsunami* which emits pulses with a pulse length of about 80 fs at a repetition rate of 80 MHz by combination of active and passive mode locking and compensation of the GVD. Using a prism sequence and a variable slit the *Tsunami* wavelength can be tuned between 720 nm and 850 nm. The *Spitfire Pro* system amplifies the output of the oscillator by means of CPA (see chapter 3.2.3). The pulses are coupled into the *Spitfire* where first of all they are temporally stretched. The energy of these pulses is then increased by passing them through the amplifier. The Q-switched pulsed *Empower* laser (Nd:YLF, 527 nm, 1 kHz, 10 W) pumps the Ti:Sa amplifier which is then able to amplify the pulses. By means of Pockels cells the timing of in- and outcoupling of the pulses is achieved. The repetition of Pockels cell switching is synchronized on the repetition rate of the pump pulse (from the *Empower*). Hence the amplified pulses with

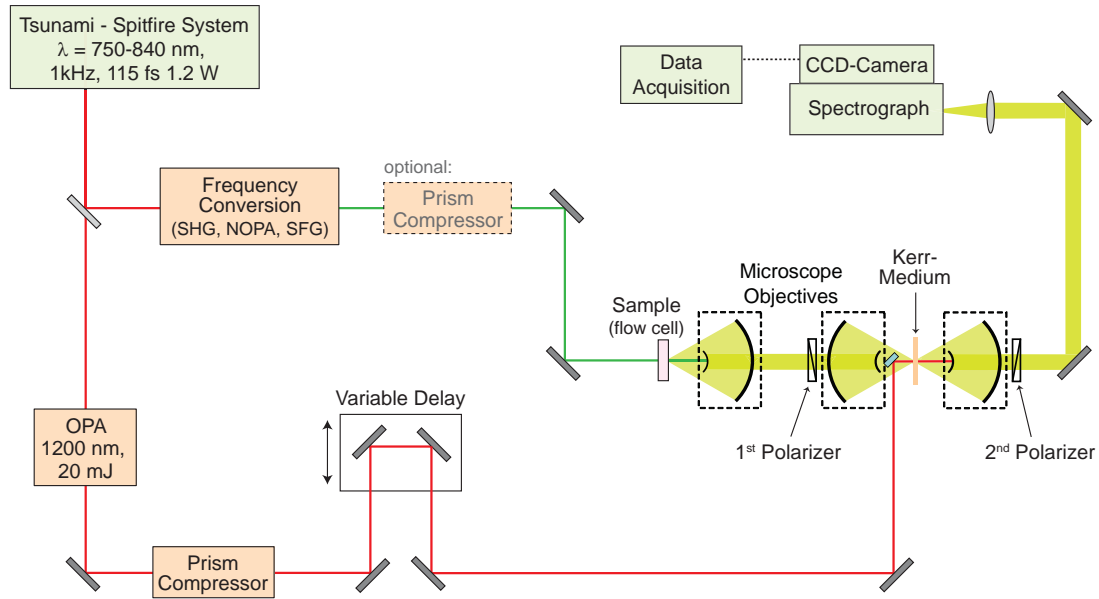


Figure 4.2: Experimental setup of the Kerr gating experiment (see text for details).

energies of ≈ 1.2 mJ have a repetition rate of 1 kHz. Afterwards they are compressed again and can be characterized by an autocorrelation measurement (see chapter 4.3).

4.1.2 The Kerr-Shutter Setup

A scheme of the complete Kerr gating experiment is shown in Figure 4.2. The design is based on the work of Bernhard Schmidt and Björn Heinz [208,217]. A beam splitter is used to split the laser fundamental into the excitation and gate pulse. In principle, excitation of different samples is possible with the laser fundamental or the second harmonic generated in a BBO. To be able to examine a variety of samples additional wavelength regions have to be accessible. This is realized by means of the noncollinear optical parametric amplifier (NOPA) described in detail below.

In case of the upconversion experiment the laser fundamental directly serves as the gate pulse. In the Kerr gating technique applying the laser fundamental as the gate pulse would lead to a high background signal since the CCD camera is sensitive for wavelengths up to 1000 nm. Scattered gate light collected from the third microscope objective and guided to the detection system would disturb the fluorescence measurements. Thus, the gate pulse is converted to the NIR spectral region by means of a two stage optical parametric amplifier (OPA, see below). The use of a prism compressor for the NOPA and the OPA output, respectively, allows to considerably reduce the pulse durations and thus to improve the temporal resolution of the experiment.

4.1. Time-Resolved Fluorescence Spectroscopy

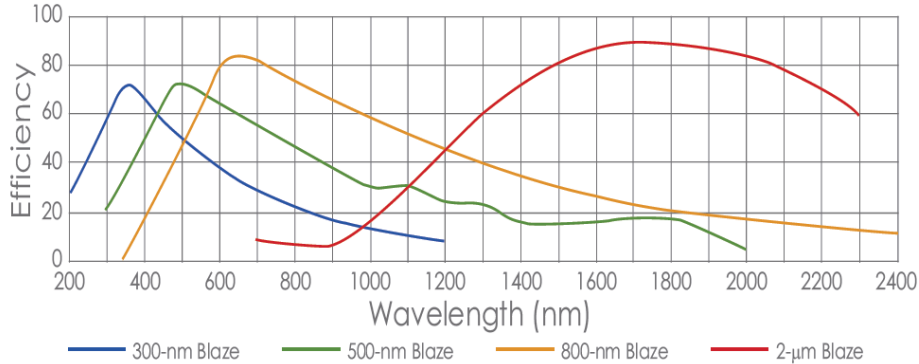


Figure 4.3: Wavelength dependent reflection of the blazed gratings for nonpolarized light, taken from [218]. In the described setup the spectrograph model *SpektraPro 2358* includes a 300 nm, 500 nm, and 800 nm blazed grating.

For the Kerr gating experiment a flow cell is used and a minimal sample volume of $\approx 500 \mu\text{L}$ is required. The sample thickness is 0.5 mm and the flow rate is regulated in order to exchange the sample volume for each excitation pulse. After excitation of the sample the fluorescence is collected by means of a reflecting Cassegrain microscope objective (*Modell 5002-000*, Davin Optonics) with a numerical aperture of 0.5, 13.41 mm focal length, and 23.2 mm working distance. Due to the Cassegrain reflector dispersion of the emitted light can be avoided and the excitation beam is blocked automatically at the front of the microscope body. The collimated fluorescence propagates through a first wire grid polarizer (*PPL04*, Moxtek) on fused silica with a substrate thickness of 0.7 mm and 1:1000 extinction for $\lambda > 350 \text{ nm}$. The linearly polarized fluorescence is then focused into the Kerr medium with a second identical microscope objective. As Kerr medium fused silica (*Suprasil*, Heraeus, $l = 0.2\text{-}1.0 \text{ mm}$) was chosen. The instantaneous response of the electrons in solid Kerr-media permits time resolutions $< 100 \text{ fs}$. In spite of its low nonlinear refractive index n_2 , fused silica is a suitable Kerr medium due to the low dispersion in the visible spectral region and the very weak background signal compared to glasses with a higher nonlinear refractive index. The gating efficiency lies between 1-4 % depending on the pathlength of the medium [208].

The compressed gate pulse first passes a optical delay stage (*M-531.DD*, Physik Instrumente, $0.1 \mu\text{m}$ min. incremental motion, 306 mm travel range) that allows to delay the gate pulse with respect to the excitation pulse. Then it propagates through a half wave plate (Laser Components, 1100-1300 nm) turning its polarization. As mentioned before, an angle of 45° between the polarization of the gate pulse and the polarization of the fluorescence yields the highest gating efficiency. A telescope system ($f_1 = 100 \text{ cm}$, $f_2 = -50 \text{ cm}$) is used to focus the gate pulse into the Kerr medium.

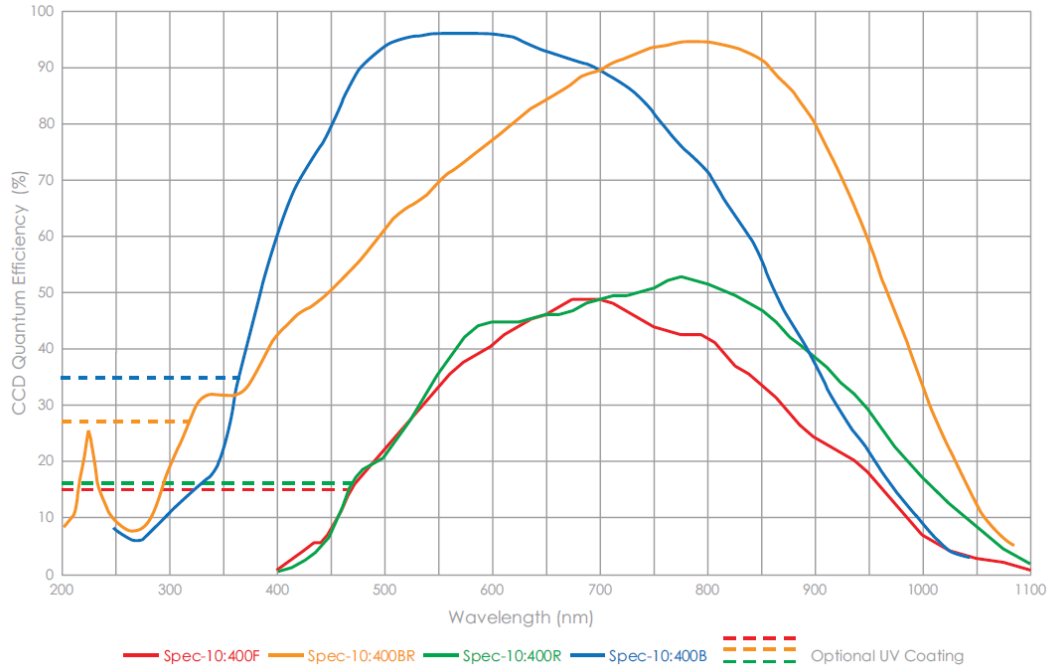


Figure 4.4: Spectral sensitivity of the liquid nitrogen cooled CCD camera, taken from [219]. The applied model *Spec-10:400B* (blue line) is back illuminated and has an additional UV coating.

The gate pulse is lead to the Kerr medium collinearly with respect to the fluorescence by placing a small silver coated mirror (Photonics, $d = 4$ mm) right behind the second microscope body. A pinhole and a camera are used to adjust the spatial overlap of the fluorescence with the gate pulse. A third identical microscope objective collects and collimates the fluorescence again after propagating through the Kerr medium. Here the gate pulse is blocked automatically by the microscope body. Right behind this objective a second wire grid polarizer orientated perpendicular with respect the first one blocks the linearly polarized fluorescence. However, gated fluorescence with elliptical polarization due to the interaction of the gate pulse with the medium can pass the second polarizer. Two silver coated mirrors and a lens ($f = 40$ mm) are used to guide the gated fluorescence into the spectrograph (*SpektraPro 2358*, Acton Research, $f = 300$ mm). It is equipped with three gratings with maximum reflection at a wavelength (blaze) of 300 nm, 500 nm and 800 nm, respectively (see Figure 4.3). The dispersed light is then detected by means of a CCD camera (*Spec-10:400B/LN*, Princeton Instruments) which is cooled with liquid nitrogen. The quantum efficiency curves, i.e. the spectral sensitivity of the detector is shown in Figure 4.4. With this setup fluorescence spectra in a wavelength range from

4.1. Time-Resolved Fluorescence Spectroscopy

about 200 nm to 1080 nm can be analyzed with a time resolution of ≈ 100 fs.

The Kerr gating experiment can be controlled by a program based on LabVIEW. The program was written by Peter Trojanowski during his diploma thesis [220]. Here the synchronization and control of the delay stage and the CCD camera is realized. The steps of the delay stage can be either linear or logarithmic and the observed temporal range can be adjusted. Usually the software *WinSpec* from Roper Scientific is used to adjust the parameters of the CCD camera. *Active-X* enables the access to this software via the LabVIEW program. Thus, the exposure time, the number of spectra and accumulations, the wavelength range, and the binning of single channels can be adjusted. Only the blazed gratings have to be adjusted with an external program provided by the manufacturer.

NOPA – Generation of Excitation Pulses

The application of a NOPA provides excitation pulses in the VIS (470-700 nm, signal) and NIR (900-1200 nm, idler) spectral region. In combination with SFG of the NOPA signal and the laser fundamental the generation of excitation pulses in the UV (290-365 nm) is also possible. The NOPA built for the Kerr gating experiment (Figure 4.5) is very similar to those in the upconversion and transient absorption setup [181,221–224].

By means of a beam splitter (BS) the fundamental light with an energy of $\approx 200 \mu\text{J}$ is split into pump and seed pulse. The bulk of the incident light ($\approx 99 \%$) is used

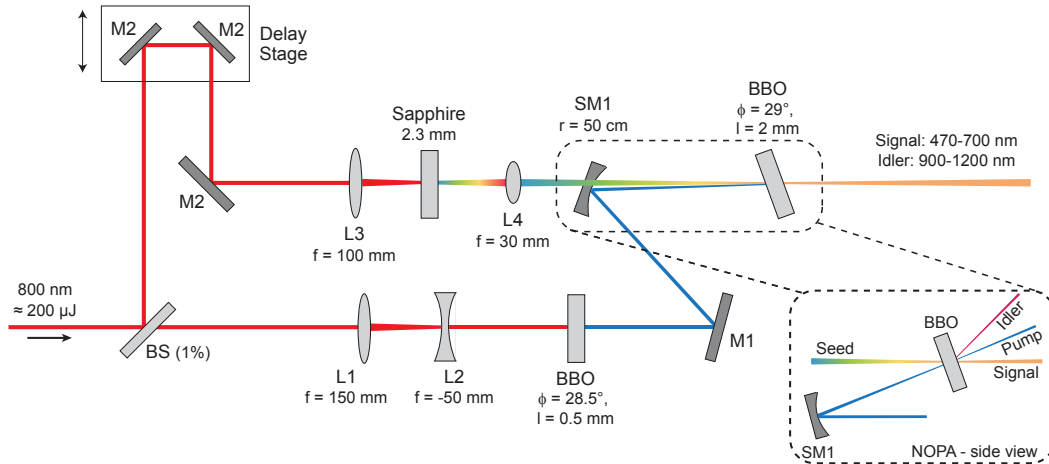


Figure 4.5: Experimental arrangement of a noncollinear optical parametric amplifier. BS: beam splitter; M1: HR 400 nm; M2: HR 800 nm, SM1: spheric mirror, HR 400 nm, $r = 50$ cm; L1-4: lenses.

for the SHG process. After passing a telescope system ($f = 150$ mm, $f = -50$ mm) to reduce the beam diameter the second harmonic was generated by means of a BBO crystal ($\phi = 28.5^\circ$, $l = 0.5$ mm, type I). Residual fundamental light was cut off by using mirrors high reflecting (HR) for 400 nm after the SFG-BBO crystal. A spherical mirror (HR 400 nm, $r = 50$ cm) placed below the usual beam height (14.5 cm) was used to guide the second harmonic to the NOPA-BBO crystal ($\phi = 29^\circ$, $l = 2$ mm, type I) with its focus right before the crystal. From the crystal parametric fluorescence is emitted.

The seed pulse is generated from the reflection of the beam splitter (≈ 2 μ J). After passing a manually controlled delay stage and a gradient neutral density filter, a lens ($f = 100$ mm) focuses the beam into a sapphire plate ($l = 2.3$ mm) for supercontinuum generation [184, 191, 225]. Due to this process the laser fundamental is spectrally and temporally broadened and white light with a positive chirp is generated. A second lens ($f = 30$ mm) focuses the seed pulse right before the NOPA-BBO crystal for amplification. Here it has to be spatially and temporally overlapped with the pump pulse. Pump and seed arrive at the BBO crystal noncollinearly with an angle of 3.7° between the two beams. Hence phase matching conditions can be achieved for all wavelengths (signal and idler) with the same BBO crystal. That allows easy tuning of the NOPA over a wide spectral region. Figure 4.5 shows a scheme of the NOPA as applied in the various setups. Due to the much longer pulse duration of the seed pulse the desired NOPA wavelength can be chosen by varying the delay time between seed and pump pulse. Another lens ($f = 100$ mm) is used to collimate the NOPA output. The pulse duration of the NOPA output can be reduced by means of a prism compressor to ≈ 30 -50 fs (see 4.1.2).

Two Stage OPA – Generation of the Gate Pulse

About 250 μ J of the laser output are used to generate the gate pulses by means of optical parametric amplification (see chapter 3.2.4) [226, 227]. The experimental arrangement of the two stage OPA is shown in Figure 4.6. Like in the NOPA only a small fraction of ≈ 1 % is separated for the seed pulse generation. A half wave plate turns the polarization by 90° . To generate a supercontinuum, a lens ($f = 100$ mm) focuses the beam into a sapphire plate ($l = 3$ mm). Subsequently a second lens ($f = 30$ mm) focuses or collimates the white light which needs to be overlapped spatially and temporally with the pump pulse in the upper part of the OPA-BBO crystal ($\theta = 27^\circ$, $\phi = 30^\circ$, type II).

The bulk of the incident light is used as the pump pulse for both amplifier stages. After passing a manually controlled delay stage a second beam splitter separates the first pump pulse (≈ 20 μ J) and a lens ($f = 500$ mm) focuses it in the OPA crystal. A neutral density filter is used to reduce the pump power to avoid parametric fluorescence. By a dichroitic mirror (HR 800 nm, HT 1050-1600 nm, DM1 in Figure 4.6) the pump pulse is lead to the crystal collinearly with the seed pulse, which passes through the dichroitic mirror. In case of type II phase matching optical parametric amplification results in vertically polarized signal pulses variable in a spectral region from 1.1 μ m

4.1. Time-Resolved Fluorescence Spectroscopy

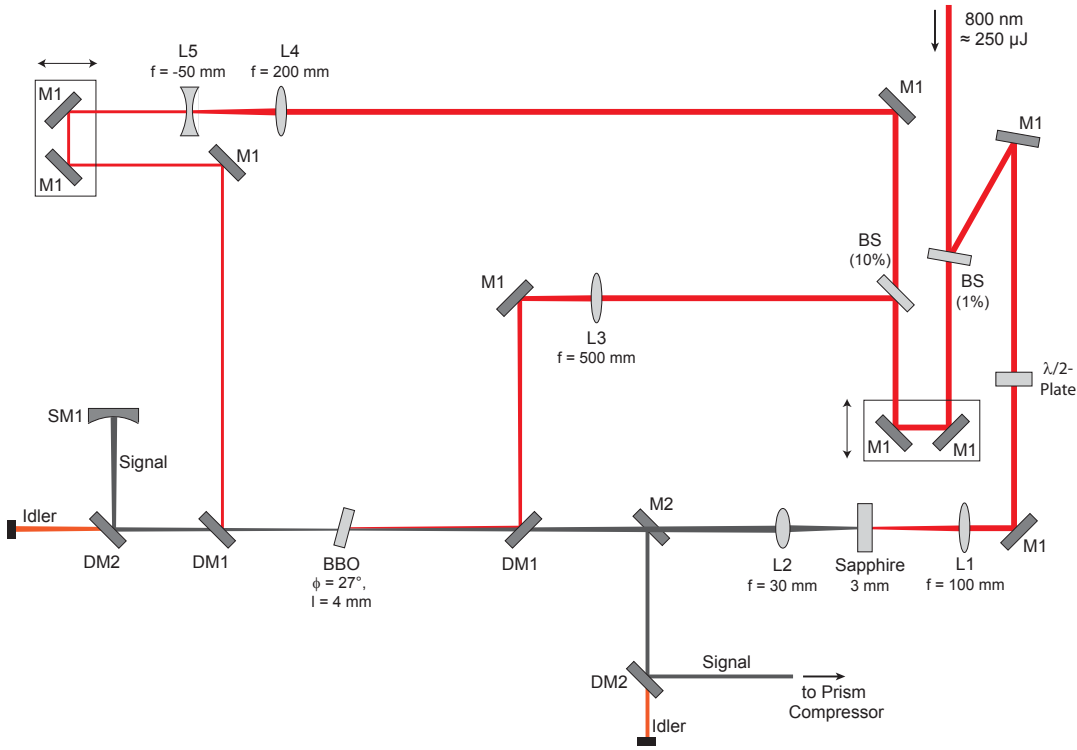


Figure 4.6: Schematic representation of the optical parametric amplifier to generate a gate pulse in the NIR spectral region. BS: beam splitter; M1: HR 800 nm; L1-5: lenses; DM1: dichroic mirror, HR 800 nm, HT 1050-1600 nm; DM2: HR 1100-1300 nm, R 1800-3000 nm < 3 %; SM1: spheric mirror, silver coated, $r = 50$ cm; M2: silver coated mirror.

to $1.45 \mu\text{m}$. Collinearly with the signal pulse the idler pulse is generated ($1.68 \mu\text{m}$ to $2.2 \mu\text{m}$). It is polarized perpendicular with respect to the polarization of the signal and can be separated by using a second dichroic mirror (HR 1120-1280 nm, R 1800-3000 nm < 3 %, DM2) reflecting the signal and transmitting the idler pulse. The latter is blocked since it is not needed in the experiment.

The signal pulse is reflected back to the lower part of the OPA crystal by a gold coated spherical mirror ($r = 50$ cm) and serves as seed pulse for the second amplifier stage. The residual fundamental light transmitted through the second beam splitter with a pulse energy $> 200 \mu\text{J}$ serves as the second pump pulse. Its beam diameter is reduced to $1/4$ by means of a telescope system ($f = 200$ mm, $f = -50$ mm). After passing a manually controlled delay stage it is superimposed with the NIR seed pulse from the first amplification process. Again the pump pulse power is reduced by means of a neutral density filter to avoid parametric fluorescence in the BBO crystal. The amplified signal

and idler beams of the second amplification stage are guided below the seed pulse of the first stage to be able to uncouple it with a silver coated mirror. Signal and idler pulse together have energies up to $40 \mu\text{J}$. However, for the gate pulse only the signal is required, hence again a dichroitic mirror (HR 1120-1280 nm, R 1800-3000 nm < 3 %) is used to separate the idler pulse.

The signal pulse is adjusted to wavelengths between 1150 nm and 1200 nm by rotating the OPA crystal around its vertical axis. The OPA signal output has pulse energies of $\approx 20 \mu\text{J}$ when it arrives at the Kerr medium. Its initial energy of $> 30 \mu\text{J}$ is reduced mainly due to power losses in the prism compressor. As mentioned before, the signal output is temporally broadened and its duration has to be reduced (70-80 fs) to improve the time resolution of the experiment.

Prism Compressor

The converted pulses, i.e. the NOPA and OPA output, have passed several optical media and thus they are temporally broadened due to positive GVD. To improve the time resolution with a preferably short excitation and gate pulse negative GVD can be applied to reduce the pulse duration [186, 228–230].

In every setup used the pulse duration of the NOPA output was reduced by a prism compression stage with fused silica prisms. Pulse durations of a few 10 fs (Gaussian FWHM) are achievable due to the spectrally broad output pulses. The experimental setup is displayed in Figure 4.7. The incident beam is refracted by the first prism. After passing a manually controlled delay stage the light passes a second prism. Here negative group velocity dispersion is induced since the distance in the medium varies for different spectral components due to their spatial arrangement. The delay stage was used to vary the distance between the two prisms to align it for the respective output wavelength of the NOPA. The distance between the two prisms determines the extent of negative

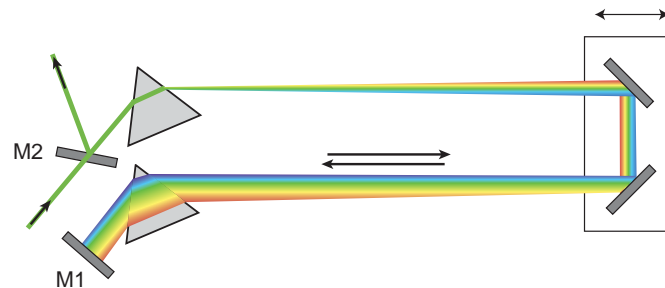


Figure 4.7: Scheme of a double pass prism compressor using a pair of prisms and a mirror.

dispersion. After reflection at the end mirror (M1) the beam again passes through the same optical path. The dispersive effect is thus duplicated and the spectral components are spatially overlapped. The end mirror is slightly tilted down so that it is possible to uncouple the compressed pulses beneath the beam height of the incident beam by means of a mirror (M2). The prism compression stage for the OPA output was similar. However, the fused silica prisms are exchanged by SF10 prisms and a pulse duration of 70-80 fs can be achieved for the gate pulse.

A home-built autocorrelator (see chapter 4.3) is used to adjust the prism compressor in order to achieve pulse duration as short as possible. It allows real-time observation of the pulse duration while varying the alignment of the prism compressor. As mentioned before, the pulse duration was adjusted by changing the distance between the prisms with the delay stage.

Characterization of the Kerr-Shutter

Unfortunately, it was not possible to record a gated fluorescence spectrum with the described Kerr-shutter setup so far. Anyhow, it was possible to demonstrate that the setup works in principle by measuring the cross correlation signal from the gate and the excitation pulse. Some difficulties which occurred during the search of the temporal and spacial overlap of the two pulses indicate that various improvements are still necessary.

To find the temporal overlap, in a first attempt a BBO crystal was used to generate the sum frequency between pump and gate pulse. This signal stems from a second order nonlinear process and is supposed to be much higher compared to a gated signal using a third order nonlinear process, i.e. the Kerr process. By means of the two stage OPA the gate pulse was adjusted to a wavelength of ≈ 1200 nm. After the OPA, the gate pulse passes a long pass filter (*FGL850*, Thorlabs) to get rid of the visible spectral components including the laser fundamental. With an energy of $\approx 30 \mu\text{J}$ and a pulse duration of ≈ 90 fs the gate pulse arrives at the Kerr medium. The pump pulse was adjusted by means of the NOPA with $\lambda_{\text{max}} = 670$ nm and a pulse energy of 25 nJ after passing the prism compressor. The generation of the sum frequency with $\lambda_{\text{SF}} = 432$ nm requires a crystal angle of 28.6° for collinear alignment. The results are shown in Figure 4.8 a. The 2D-spectrum (left panel) demonstrates the spectral and temporal behavior of the sum frequency signal. Due to the spectral width of the NOPA pulse of ≈ 50 nm a chirp is observed. The single transients in the right panel were fit with a Gaussian function resulting in a FWHM from 80 fs to 100 fs and varying delay time zero depending on the wavelength.

First it was managed to gate a NOPA pulse with $\lambda_{\text{max}} = 485$ nm. The NOPA pulse was focused on a cuvette with a scattering sample. The scattered excitation light was collected with the first microscope objective and focused on the Kerr medium with a second one. In the Kerr medium it was overlapped spatially and temporally with the gate pulse (≈ 1200 nm). The gated light was collected with the third microscope objective

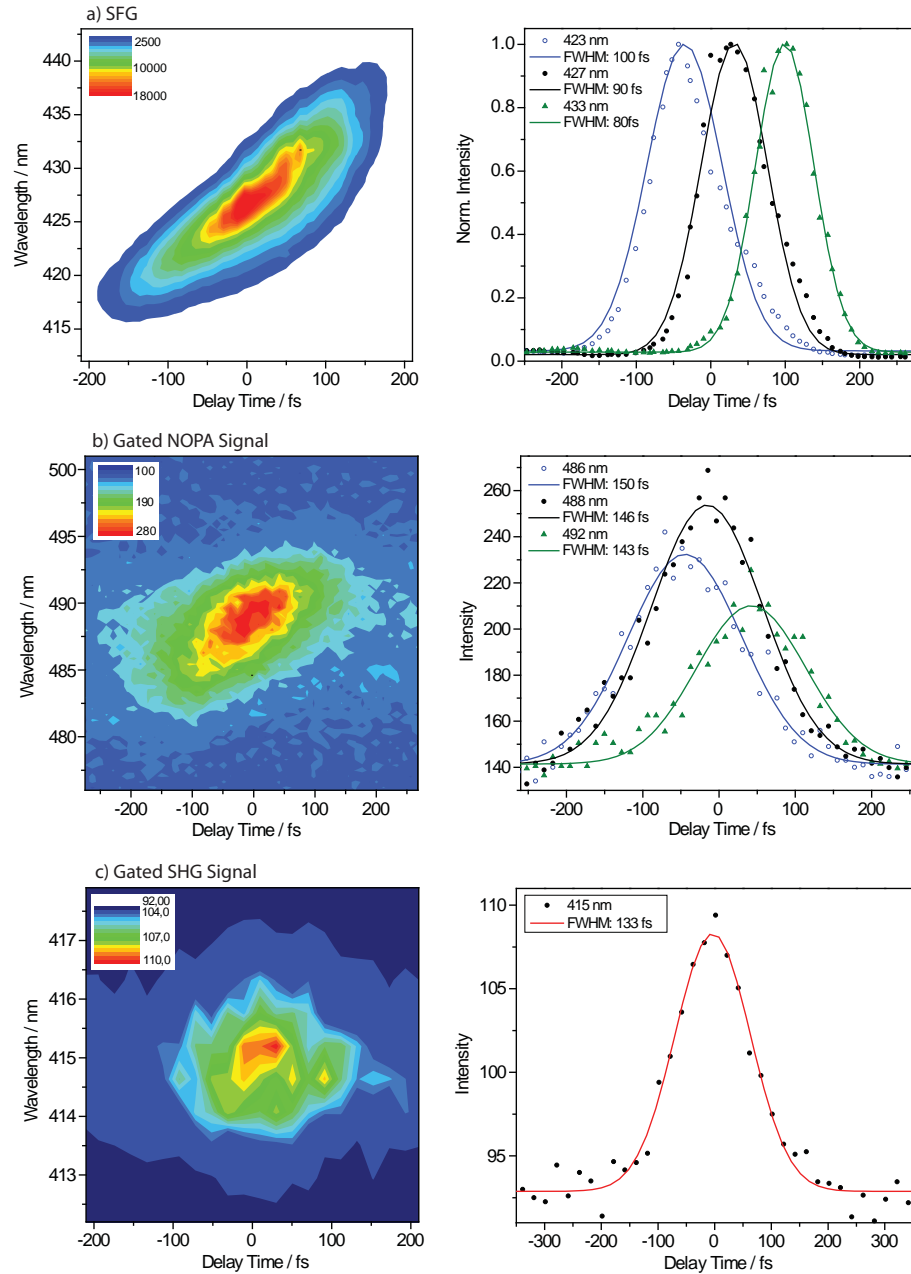


Figure 4.8: Comparison of different cross correlation signals between pump and gate pulse measured with the Kerr shutter setup. a) Sum frequency of gate and NOPA pulse generated in BBO crystal to find the temporal overlap of the two pulses. b) Gated NOPA pulse with $\lambda_{max} = 485$ nm. c) Gated second harmonic of the laser fundamental. The 2D-plots of the cross correlation signal (left panels) as well as individual cross correlation curves (symbols, right panels) and corresponding fit curves (solid lines) are shown. See text for details.

and guided to the detector. The results are shown in Figure 4.8 b. The chirp visible in the 2D-spectra is much smaller compared to the one obtained from the SFG (Figure 4.8 a) since the spectral width of the NOPA pulse at 485 nm was smaller. The single transients in the left panel (Figure 4.8 b) were analyzed with a Gaussian fit resulting in a FWHM of ≈ 150 fs. It can be assumed that the NOPA pulse was longer compared to the one used for the SFG due to a suboptimal adjustment of the prism compressor. As expected, the intensity of the gated light is orders of magnitude smaller compared to the sum frequency signal. With these adjustments the gating of β -carotene fluorescence was attempted. Since this was not possible it was concluded that the fluorescence is too weak upon excitation at 485 nm. Thus, the experiment was repeated with the second harmonic of the laser fundamental resulting in an excitation wavelength of 415 nm.

Up to now it was only possible to detect a very low signal of the gated second harmonic serving as excitation pulse. The beam path was the same as for the NOPA pulse with the exception of passing the prism compressor. The results are shown in Figure 4.8 c. Due to the narrow spectral width of the excitation pulse no chirp appears. The FWHM of this cross correlation signal was 133 fs. So far it was neither possible to increase this signal nor to gate a fluorescence. Further improvements of the setup will be necessary to enhance the efficiency of the gating process. It is very sensitive to the quality of the focuses in the Kerr medium and to the intensity of the gate pulse and its polarization with respect to the gated light. Furthermore it is difficult to align the three microscope objectives to achieve an optimal path of the fluorescence light from the sample to the detector. The Kerr medium itself plays an important role since already small impurities can cause a high background signal which superimposes the gated signal.

4.1.3 The TCSPC-Upconversion Setup

With the setup designed by Ute Förster [224, 231] fluorescence decay times can be determined from fs up to μ s due to the combination of the TCSPC and the fluorescence upconversion technique (chapter 4.1). A scheme of the combined setup is displayed in Figure 4.9.

The described *Tsunami-Spitfire* System from Spectra-Physics (see chapter 4.1.1) was used to generate the excitation pulse as well as the gate pulse. The repetition rate of 1 kHz is rather low for TCSPC experiments where usually light sources with repetition rates of several MHz are applied. Depending on the absorption characteristics of the sample the excitation wavelength can be adjusted by means of the NOPA, SHG or SFG (see chapter 3.2.4). Both, the NOPA and the prism compressor are almost identical to the one in the Kerr shutter setup (see chapter 4.1.2). The excitation beam is focused into the laterally moved cuvette (1 mm thick) with a focus of ≈ 200 μ m diameter. After passing the cuvette the excitation beam is blocked by means of a very small beam blocker. If necessary, scattered light can be attenuated by a long pass, colored glass filter. The emitted fluorescence light is collected and parallelized by an off-axis

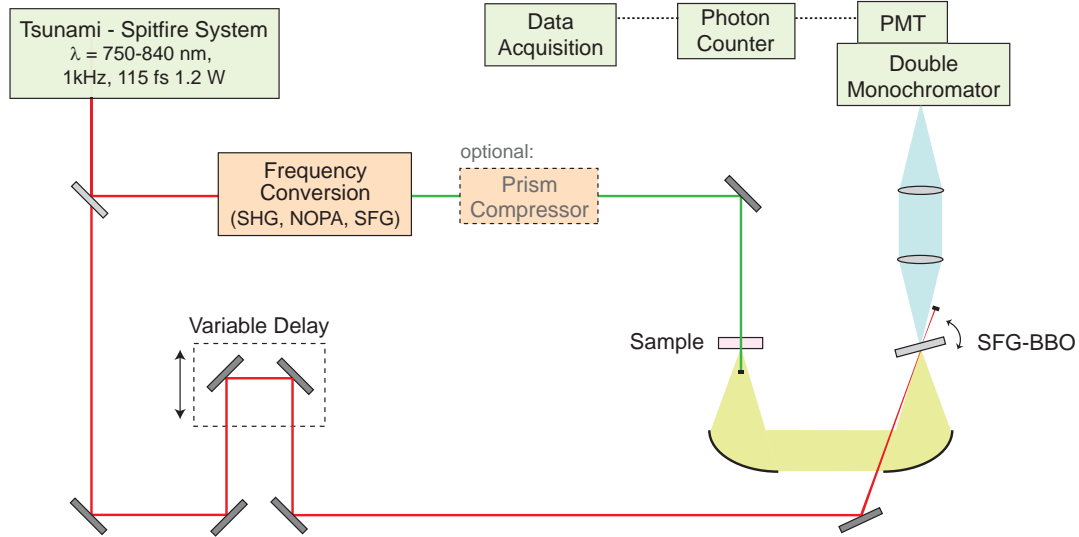


Figure 4.9: Experimental setup of the combined TCSPC and fluorescence upconversion experiment. The scheme shows the adjustment for the upconversion mode. In case of TCSPC measurements neither the gate pulse nor the BBO crystal are needed and the fluorescence wavelength is selected by the monochromator.

parabolic mirror (aluminium coated, 76.2 mm focal length, 90° reflection angle, Janos Technologies) and then focused into the upconversion crystal by a second, identical parabolic mirror. Behind the crystal the fluorescence in case of TCSPC and the gated fluorescence (SFG of fluorescence and gate pulse) in case of the upconversion technique is again parallelized by a lens ($f = 50$ mm, fused silica). A second lens ($f = 125$ mm, fused silica) focuses the light into a double monochromator (*D3-180 Gemini*, Jobin-Yvon, 180 mm focal length, 0.15 nm resolution) where the detection wavelength is selected and residual excitation light can be separated.

The single fluorescence photons are detected by a photomultiplier tube (PMT, *PMC 100-4*, Becker & Hickl GmbH) which passes the signal on to the TCSPC counting card (*MSA-100010*, Becker & Hickl GmbH, 1 ns time resolution). It is operated in the forward mode, i.e. the excitation beam triggers the counting card and the fluorescence photons stop it. It is possible to integrate several of the 1024 channels which leads to a maximum observation period of 131 μ s. For the TCSPC mode no BBO crystal needs to be added and the gate pulse should be blocked. To determine the IRF an instantaneous signal (here the fs laser pulse) is detected. The measured curve is much broader (≈ 1 ns) compared to the initial signal due to the rise time of the detector (Figure 4.10).

For the upconversion mode the laser fundamental is used as the gate pulse with an energy of ≈ 100 μ J. It passes an optical delay line (*M 531 DD15*, Physik Instrumente,

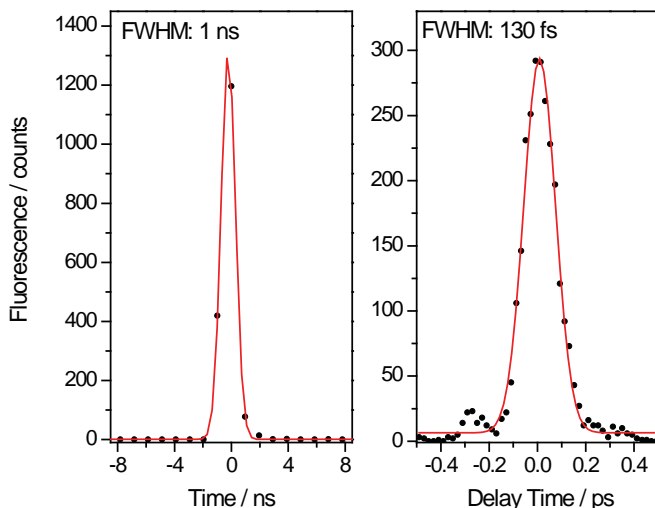


Figure 4.10: Instrument response of the TCSPC experiment (left): the excitation pulse is much shorter than the time resolution of the TCSPC card. Thus, this instantaneous signal can be used to determine the instrument response. A Gaussian fit results in a time resolution of 1 ns (FWHM) corresponding to the step width of the applied TCSPC-card. Cross correlation of the upconversion experiment (right): the detected sum frequency (304 nm) of the gate pulse (800 nm) and the NOPA pulse (490 nm) was fitted with a Gaussian curve resulting in a pulse width of 130 fs.

0.1 μm min. incremental motion, 306 mm travel range) that enables to delay the gate pulse with respect to the excitation pulse. By means of a telescope system ($f = 150$ mm, $f = -50$ mm) the gate pulse is focused with a long focal length into the BBO crystal (e.g. $\theta = 51^\circ$, $d = 0.1$ mm varying with the requirements of the specific experiment). In this noncollinear alignment the generation of the sum frequency of the fluorescence and the gate pulse is most efficient for an angle of 13.5° between the two beams [232]. To separate the upconverted fluorescence light from residuals of the excitation light, the gate pulse, and the SHG an iris is used behind the crystal. Additional scattered light passing through the iris can be separated by the monochromator. The upconverted fluorescence photons are also detected by the PMT. The integrated signal intensity is not correlated to the detection time determined by the photon counter but to the delay of the gate pulse. In case of the upconversion experiment the time resolution depends mainly on the duration of the excitation and the gate pulse. To determine the time resolution a solvent measurement is performed to obtain the cross correlation of the two pulses. The duration of the detected signal (Gaussian FWHM) corresponds to the time resolution of the respective experiment (Figure 4.10).

The whole setup including TCSPC as well as upconversion experiments can be controlled by a program based on LabVIEW which was written by Ute Förster [224]. Two

different modes with a corresponding user interface for TCSPC and upconversion measurements are available. They synchronize and control the different components: the monochromator to select the detection wavelength, the TCSPC card for data acquisition, a shutter to block the excitation beam between the measurements, and the optical delay line (only required for upconversion experiments). For the search of the temporal overlap of excitation pulse and gate pulse the control of the delay stage is also possible in the TCSPC mode. For both techniques a wavelength scan is possible. The upconversion mode enables linear and logarithmic steps for scanning the fluorescence. For every delay time the signal of the sum frequency is recorded and the corresponding integral is proportional to the intensity of the gated fluorescence. The x-axis represents either the detection time of the TCSPC card or the delay time calculated from the position of the delay stage. For the TCSPC mode the measurement time (*sweeps*), the time resolution (min. 1 ns), and the number of measurement points (64-1000) can be selected. The collected photons are saved as a single decay curve for every probe wavelength. In case of the upconversion experiment besides every single scan the averaged transient from multiple scans is saved. For both modes a second data file (*parameter.txt*) contains information of the measuring parameters. For detailed information see [224].

4.1.4 Data Analysis

Analysis of the TCSPC data was performed with the program TCSPCfit (based on Matlab) provided by Jörg Enderlein. The basic principles are explained in the work from Enderlein and Erdmann [233]. In short, a Nelder-Meade algorithm is used to fit the data with a sum of exponential decays convoluted with the instrument response function (IRF). This enables the determination of fluorescence lifetimes in the range of the IRF. It is also possible to fit decay curves obtained from the upconversion and Kerr gating experiments for a single detection wavelength. For this procedure the measured cross correlation curve is used as IRF.

To analyze the measured decay profiles of whole fluorescence spectra, the program *z20* based on IDL is used like for the transient absorption spectra (see chapter 4.2.3 for details). The same fit algorithm is used to fit the data with a sum of exponential decays as described in chapter 4.2.3.

4.2 Transient Absorption Spectroscopy

As mentioned before, to investigate ultrafast dynamics in the ps and fs time domains the pump-probe technique is applied (see chapter 3.2.1). It is a sensitive method to study the time evolution of excited states and the corresponding lifetimes. After excitation with an ultrashort pump pulse the sample is probed with a second pulse at a distinct delay time. Monitoring of the probe pulses as a function of the delay time reflects the dynamics triggered by the pump pulse. The following sections summarize the setup used

and how the collected data were analyzed.

4.2.1 The CPA 2001 Laser System

For the transient absorption experiments an amplified Ti:Sa laser system (CPA 2001 from Clark-MRX) was used. It is composed of a diode laser pumping a frequency doubled erbium fiber oscillator, a pulse stretcher, a regenerative Ti:Sa amplifier pumped by a frequency doubled Nd:YAG laser, and a compressor [234]. The laser output with a 1 kHz repetition rate and ≈ 150 fs pulse duration provides energies of $\approx 800 \mu\text{J}$ at a wavelength of 775 nm.

4.2.2 fs-Pump-Probe Setup

The time-resolved absorption measurements shown in this work were performed with a setup (see Figure 4.11) described in detail earlier [223,235]. The excitation wavelength was adjusted by a NOPA and subsequently these pulses were compressed with a prism compressor. After passing the delay stage the excitation pulses with a pulse energy of ≈ 20 nJ were focused in the sample with a focal diameter of $\approx 100 \mu\text{m}$. For generation of the probing white light a small fraction of the laser fundamental was focused on sapphire plates with different thickness depending on the spectral region of interest. For probing in the NIR spectral region from 850 nm to 1100 nm a thick sapphire plate with $d = 5.0$ mm was used and for the VIS spectral range from 450 nm to 730 nm the sapphire plate was thinner with $d = 2.3$ mm. The white light pulses were split into two beams serving as probe and reference. Pump and probe beam are focused on the sample by means of an off-axis parabolic mirror, the reference beam is sent directly to the reference-spectrometer. The cuvette with an optical path length of 1 mm was moved laterally to prevent degradation of the sample as well as multiple excitation. The optical density of the different samples varied between 0.5 and 1.5 at the respective excitation wavelength.

For detection, the transient absorption signal as well as the reference beam are dispersed and afterwards analyzed by two 42 segment diode arrays (Hamamatsu S4114-46Q, multi-channel detection), which are read out for every single shot. The detected signal is amplified and then digitized in an analog to digital converter (LeCroy model 1885F). To improve the signal-to-noise ratio choppers are integrated in the optical path of both pump and probe beam which block every third pulse. The choppers are coordinated resulting in the pulse sequence shown in Figure 4.12 so that scattered light and fluctuations in the white light can be subtracted from the signal. An absolute spectrum can not be measured due to the difference in intensity of probe and reference beam. However, it is possible to obtain a relative spectrum with the term:

$$\frac{N(t, \lambda)_{block,ref}}{N(t, \lambda)_{block,sig}} \quad (4.1)$$

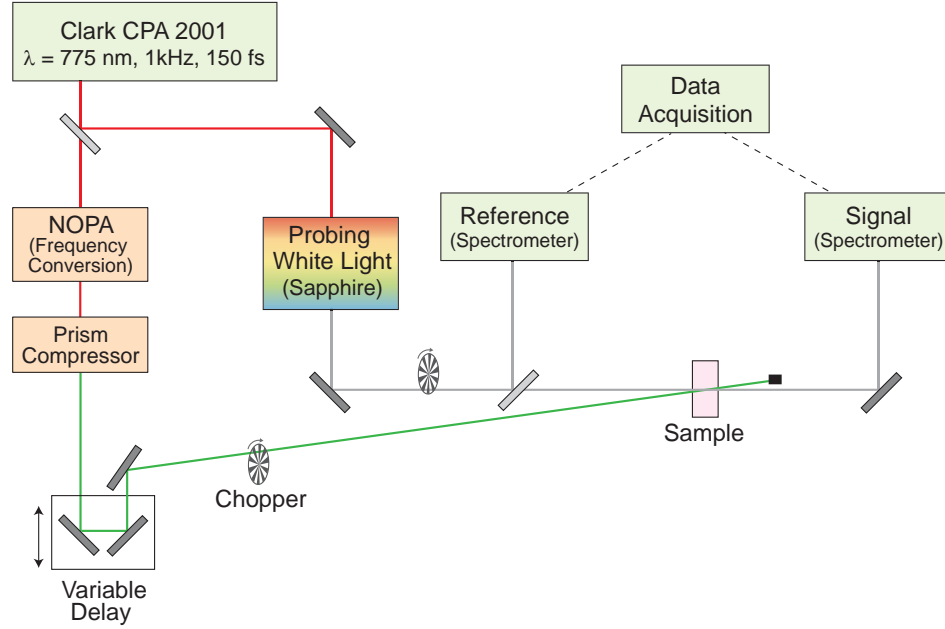


Figure 4.11: Experimental setup of the femtosecond transient absorption spectrometer. An ultrashort laser pulse is split into a pump and probe beam by means of a beam splitter. After excitation with a short narrowband pump pulse whose wavelength is adjusted by the NOPA the sample is probed with broadband white light at distinct delay times.

The absorption change ΔA can be calculated according to the following equation:

$$\Delta A(\lambda) = \log \left(\frac{N(t, \lambda)_{block,ref} - N(t, \lambda)_{therm,ref}}{N(t, \lambda)_{block,sig} - N(t, \lambda)_{therm,sig}} \right) \cdot \left(\frac{N(t, \lambda)_{sig} - N(t, \lambda)_{therm,sig} - N(t, \lambda)_{scat,sig}}{N(t, \lambda)_{ref} - N(t, \lambda)_{therm,ref} - N(t, \lambda)_{scat,ref}} \right) \quad (4.2)$$

with ref = reference, sig = signal, block = blocked, therm = thermal noise, scat = scattering. The thermal noise is recorded while both pump and probe beam are blocked.

In order to analyze the time dependent anisotropy the pump beam passed a zero-order half-wave plate that allowed adjustment to parallel, perpendicular, and magic angle polarization with respect to the probe beam. To control the success of the measurement the parallel (ΔA_{\parallel}) and the perpendicular (ΔA_{\perp}) data were used to calculate the isotropic data ($\Delta A_{ma} = (\Delta A_{\parallel} + 2\Delta A_{\perp})/3$) which then was compared with the measured magic angle signals.

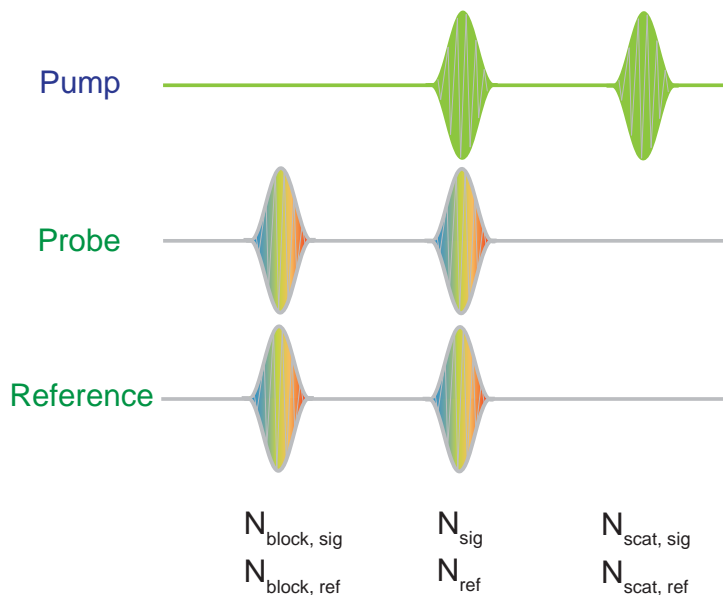


Figure 4.12: Pulse sequence obtained from the application of the choppers (block = blocked, sig = signal, ref = reference, scat = scattering).

4.2.3 Data Analysis

Nonlinear interactions between the pump and the probe pulse give rise to coherent artifacts around delay time zero. Contributing effects such as two quantum absorption, cross-phase modulation, and stimulated Raman processes occur in the sample as well as in the solvent [236–238]. If necessary, the solvent signal can be subtracted from the signal of the actual sample to get rid of distracting solvent contributions [238]. Upon passing through various optical components including cuvette and sample the spectral components of the probe pulse are dispersed, i.e. delay time zero varies depending on the wavelength (see Figure 4.13). By detection of the solvent signal this temporal shift is determined for each experiment to be able to correct the data accordingly. Delay time zero is identified by the temporal position of the coherent artifact and then plotted against the wavelength. The resulting curve can be fitted by the Sellmeier equation which describes the refractive index n of a media as a function of the wavelength λ [167]. Based on the resulting fit the displacement of the zero point due to GVD in the different media can be calculated and corrected accordingly for other measurements performed under identical conditions.

From the cross correlation measurement of pump and probe pulse the time resolution of the particular experiment can also be calculated. The temporal resolution is

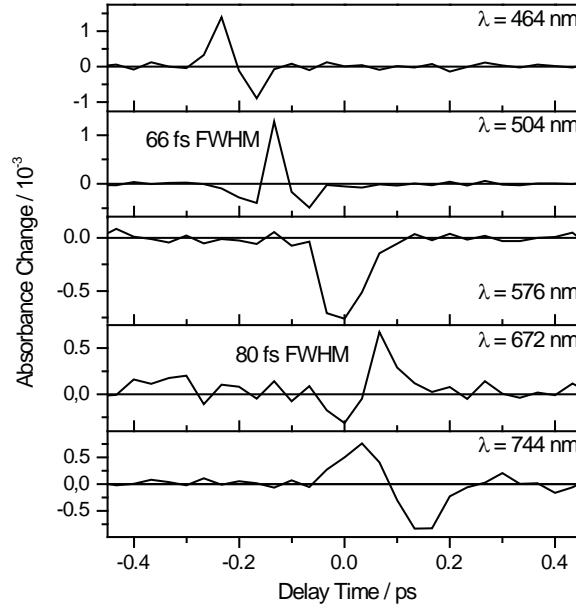


Figure 4.13: Transient absorption signals from pure ethanol upon excitation at $\lambda = 500$ nm at different probe wavelengths.

affected by the laser pulse duration, the shortest delay between pump and probe pulse, excitation geometry, sample thickness, and influence of the GVD [239]. Depending on the experimental conditions - especially the adjustment of the prism compressor - the time resolution in the performed measurements differed from 50 fs to 150 fs.

Correction of the raw data and subsequent data analysis were carried out with the software *z20* based on IDL 6.0. At first all single scans are compared and defective scans can be discarded. Then all remaining scans are averaged (subprogram *ikmittel*) and the resulting data are corrected for dispersion as well as coherent artifacts if necessary (subprogram *nkview*). In the subprogram *multiview* the data can be plotted as single transients, transient spectra, and 2D- or 3D-spectra and different measurements can be compared. In addition it allows a quantitative data analysis using a kinetic model that describes the data as a sum of exponential decays. A combination of simplex algorithm and Levenberg-Marquart downhill algorithm optimizes n global time constants τ_i for all probing wavelengths λ simultaneously. A simultaneous fit of all decay curves can be performed according to the following equation:

$$\Delta A(\lambda, t) = \sum_{i=1}^n a_i(\lambda) \exp\left(\frac{t_{cc}^2}{4\tau_i^2} - \frac{t - t_0}{\tau_i}\right) \cdot \frac{1 + \operatorname{erf}\left(\frac{t-t_0}{t_{cc}} - \frac{t_{cc}}{2\tau_i}\right)}{2} \quad (4.3)$$

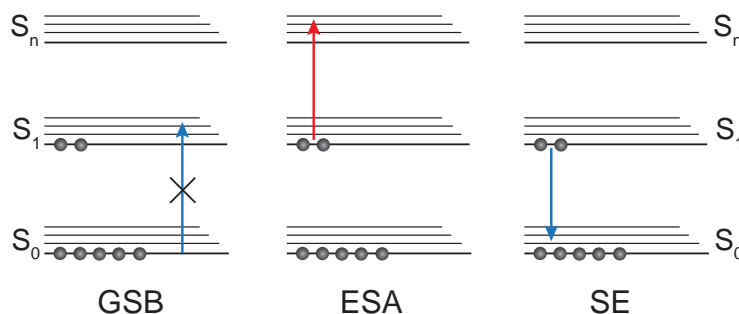


Figure 4.14: Main signals in transient absorption spectra: ground state bleach (GSB), excited state absorption (ESA), stimulated emission (SE).

with the cross correlation t_{cc} , delay time zero t_0 , and the instrument response function erf (error function). The n wavelength dependent fit amplitudes $a_i(\lambda)$ represent the decay associated spectra (DAS) for each decay time constant, which allow an assignment of the time constants to specific processes. An infinite time constant corresponds to transient signals that remain at the maximum delay time of the experiment (≈ 1.5 ns). Data obtained from anisotropy measurements can also be analyzed by calculating the time dependent anisotropy values $r(t)$ (see equation 3.6) and plotting the resulting anisotropy decay.

Transient absorption spectra (TAS) usually consist of three different contributions (Figure 4.14). First of all, due to transition of some molecules to their excited states upon excitation less molecules are in the ground state and the ground state absorption will be reduced (ground state bleach, GSB). This results in a negative difference signal, i.e. a negative absorption change ΔA depicted in blue in all following 2D-plots. Molecules in the excited state can absorb light since transitions to higher excited states are possible. This excited state absorption (ESA) leads to a positive difference signal and is color coded in red. Radiative deexcitation of molecules upon interacting with the probe pulse by stimulated emission leads to more photons on the detector. This is interpreted as reduced absorption in the transient absorption experiment, hence the stimulated emission (SE) signal is also depicted in blue. It is important to keep in mind that the different contributions can overlap and that additional effects such as dynamic band shifts, the formation of new species, and the population of new states not accessible by steady state absorption also appear in the TAS. For example, energy transfer between different chromophores can lead to additional contribution from chromophores not excited directly by the pump pulse. Thus, by excitation of a certain chromophore, e.g. a carotenoid, the energy transfer rate to another molecule, e.g. chlorophyll, can be monitored by analyzing the rise and decay of the different chromophore contributions.

4.3 Autocorrelator

As mentioned before, nonlinear autocorrelation techniques are used to characterize the temporal profiles of ultrashort pulses (see chapter 3.2.3). The autocorrelator built during this thesis together with Karsten Neumann was used to optimize the adjustment of the grating compressor in the CPA as well as the prism compressor after NOPA and OPA, respectively. The compact design is based on the work of Kozma et al. [178] and can easily be moved and repositioned in different experimental setups. A nondispersive optical arrangement as presented in Figure 4.15 is required for precise autocorrelation of ultrashort pulses.

After passing an iris the incident beam is split using a two-part mirror to create two identical pulse replicas. One part of the protected silver coated mirror is fixed on an adjustable mirror mounting and the other part on a piezoceramic translator (PZT, *PX 400*, Piezosystem Jena). The latter represents an optical delay line with 400 μm path length which allows to delay the two replicas with respect to each other. An off-axis parabolic mirror (aluminium coated, 51 mm focal length, 30° reflection angle) focuses both parts of the beam in a BBO crystal (25–100 μm thick). Besides SHG of the two individual beams, SFG between the two replicas occurs in case of spatial and temporal overlap of the two beams. By means of a second iris the SHG signal is separated from the SFG signal. After passing a color filter to get rid of the remaining scattered fundamental light, a mirror (UV-enhanced aluminium) directs the correlation signal to the detector diode (*PDI-400-1-P-UV*, Becker & Hickl GmbH). To avoid saturation of the nonlinear crystal and the detector and thus broadening of the correlation signal the input pulses should have energies of some 100 nJ.

Autocorrelation traces can be detected over a broad spectral range from the NIR down to about 420 nm. For this purpose BBO crystals with particular cutting angles

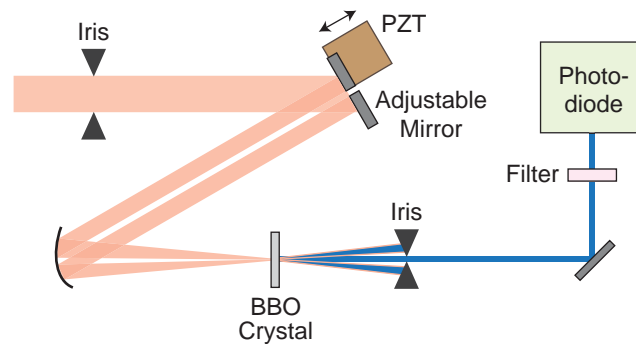


Figure 4.15: Experimental arrangement of the autocorrelator setup.

and several color glass filters are necessary. For example, a BBO crystal cut at 45° is applicable for characterizing the NOPA signal (480–680 nm). It is placed in a rotation stage which allows adjustment of the angle for type I phase matching conditions of the SFG in this wavelength range. Usually the combination with an appropriate filter is necessary transmitting the SFG signal and suppressing fundamental light at the same time (*UG 5*, Schott).

For data acquisition, evaluation, and real-time display a monitoring program based on *LabVIEW* (National Instruments) is used. By means of an analog to digital card (*DAQCard-6024E*, National Instruments) the diode signal and the drive voltage of the PZT converted into time delay are monitored continuously. If collecting of the data of a rising drive voltage is complete the detected SFG signal is plotted against the delay time. Furthermore, a Gaussian curve is fitted to the data using a Levenberg-Marquardt algorithm. Assuming a Gaussian or sech^2 pulse shape the final pulse duration (FWHM) can be calculated using the obtained fit parameters.

Chapter 5

Characterization of Isolated Carotenoids

We accept the reality of the world with which we are presented.

(Christof in *The Truman Show*)

The following chapter includes the results on the carotenoids contained in the FCP complexes: fucoxanthin, diadinoxanthin, and diatoxanthin. A detailed knowledge of the excited state dynamics of the free pigments is required to be able to analyze the complicated energy transfer processes within the protein complexes upon photoexcitation. Thus, in a first step the free pigments were studied by means of time-resolved absorption and fluorescence techniques combined with steady state absorption spectroscopy. The excited state dynamics and fluorescence lifetimes were investigated with regard to the carotenoids structure and the solvent environment. The pigments were extracted from the FCP complexes in the group of Prof. Claudia Büchel.

5.1 Steady State Characterization

The influence of the solvent environment on the spectroscopic characteristics of the carotenoids contained in the FCP complexes was investigated. In Figure 5.1 the carotenoid structures and steady state absorption spectra recorded at room temperature are shown for fucoxanthin (left upper panel) as well as diadinoxanthin and diatoxanthin (lower panels). All applied solvents are listed in table 5.3 with their polarity factor $P(\epsilon)$, where ϵ is the dielectric constant of the solvent.

The steady state absorption spectra are characterized by a broad absorption band

5.1. Steady State Characterization

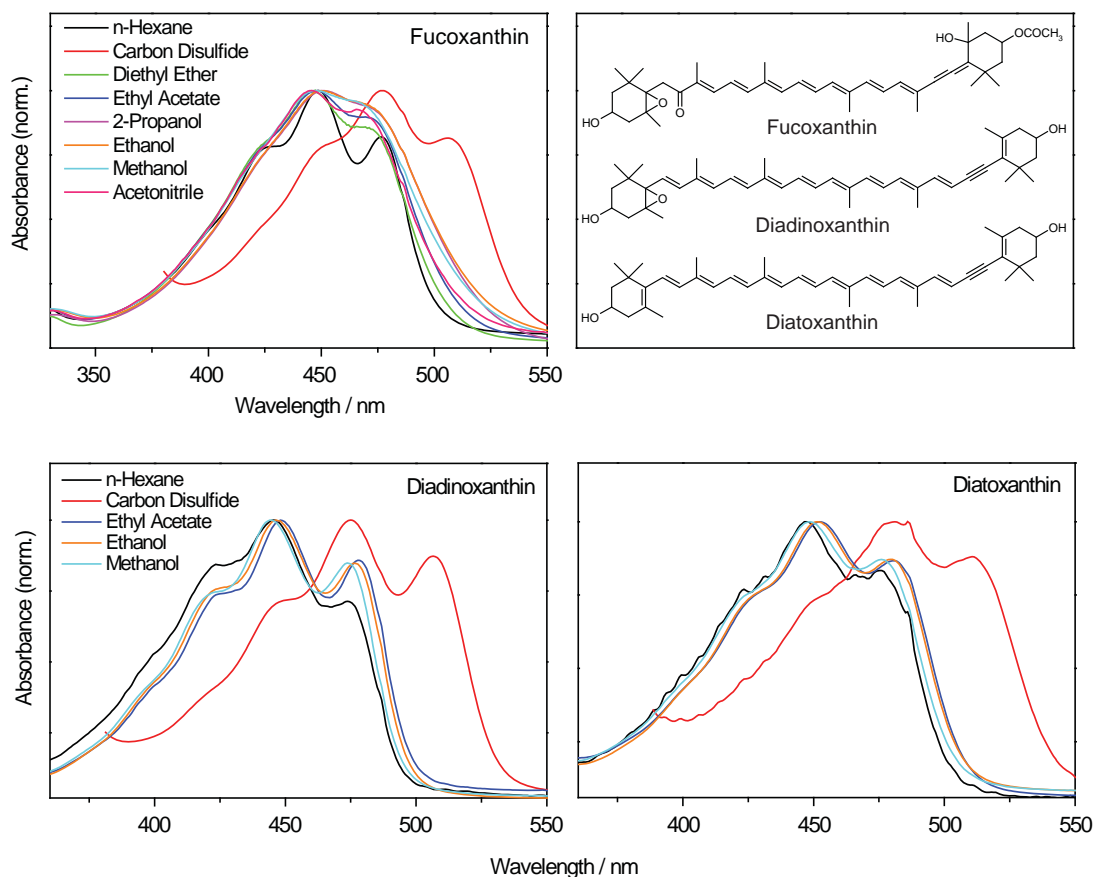


Figure 5.1: Steady state absorption spectra for fucoxanthin (left upper panel) as well as for diadinoxanthin and diatoxanthin (lower panels) in various solvents recorded at room temperature. The spectra were normalized to the maximum absorbance of the $S_0 \rightarrow S_2$ transition.

(FWHM $\approx 4000 - 5000 \text{ cm}^{-1}$) in the spectral region between 350 nm and 550 nm associated with the $S_0 \rightarrow S_2$ transition (Figure 5.1). The vibronic structure is resolved for all investigated carotenoids in nonpolar solvents. In case of fucoxanthin the resolution of the vibronic structure decreases considerably and finally disappears with increasing solvent polarity. In addition, the width of the $S_0 \rightarrow S_2$ absorption band increases with diminishing vibronic structure (Figure 5.2). This band broadening is restricted to the red edge of the absorption spectra. The peak positions are hardly affected with the only exception for carbon disulfide where a considerably red shift of the $S_0 \rightarrow S_2$ absorption band is observed. The resolution of the vibronic structure and the width of the absorption band are much less influenced in case of diadinoxanthin and diatoxanthin.

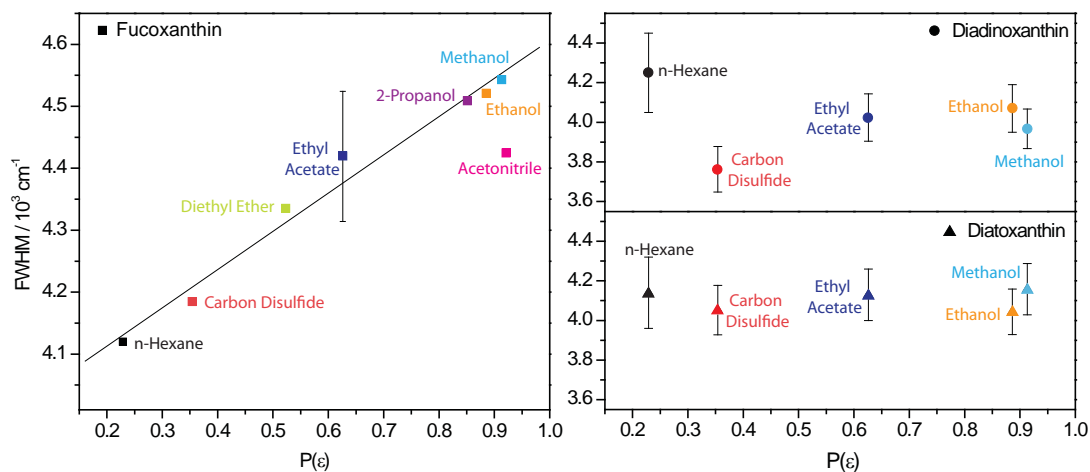


Figure 5.2: A plot of the bandwidth (FWHM) of the $S_0 \rightarrow S_2$ absorption band plotted against the solvent polarity for fucoxanthin (■), diadinoxanthin (●), and diatoxanthin (▲). The errors were derived from the uncertainty in assigning the FWHM and were approximately $\pm 100 \text{ cm}^{-1}$ for fucoxanthin and slightly higher ($120\text{-}200 \text{ cm}^{-1}$) for diadinoxanthin and diatoxanthin.

Here only small shifts of the peak positions are observed with varying solvent polarity except for carbon disulfide.

The shift of the peak position found for all carotenoids dissolved in carbon disulfide can be explained with the high polarizability of the solvent. The energy of the $S_0 \rightarrow S_2$ transition not only depends on the conjugation length but also on the refractive index and accordingly on the polarizability of the solvent. The polarizability factor $P(n)$ can be calculated from the refractive index of the respective solvent with $\tilde{P}(n) = (n^2 - 1)/(n^2 + 2)$. The polarizability factor of carbon disulfide with $\tilde{P}(n) = 0.356$ ($n = 1.63$) is much higher compared to the other applied solvents ($\tilde{P}(n) = 0.23\text{-}0.28$). This solvatochromic effect was explained by theoretical models and a linear dependence of the band position and the polarizability factor was found for many carotenoids [89,99].

The spectral broadening observed for fucoxanthin depending on the polarity of the solvent is demonstrated in the left plot of Figure 5.2. The bandwidth shows an almost linear dependence on the solvent polarity except for the polar solvent acetonitrile. Though its polarity is even higher than that of methanol the bandwidth is clearly smaller. Thus, it can be concluded that the bandwidth is largest in hydrogen bonding solvents and does not only depend on the solvent polarity. In case of diatoxanthin the bandwidth is nearly constant in nonpolar and polar solvents (Figure 5.2, right panel). For diadinoxanthin in n-hexane the bandwidth is higher compared to the bandwidth in polar solvents with a high error value ($\approx 200 \text{ cm}^{-1}$). One possible explanation is the poor solubility of

diadinoxanthin and diatoxanthin in n-hexane resulting in a scattering sample and a very weak absorption spectrum. Due to the small available amount of diadinoxanthin and diatoxanthin additional experiments in other nonpolar solvents could not be performed.

Since the solvent-induced broadening only occurs in carbonyl containing carotenoids, this effect must be traced back to the presence of the carbonyl group conjugated with the π -electron system [88]. Highly substituted carotenoids deviate from the idealized C_{2h} symmetry. Hence, the usually strongly forbidden $S_0 \rightarrow S_1$ transition becomes more allowed. The $S_0 \rightarrow S_1$ absorption band is predicted to be located red shifted but close to the $S_0 \rightarrow S_2$ absorption band. Thus, the $S_0 \rightarrow S_1$ transition could contribute to the spectral line shape leading to a broadening in the red edge of the absorption band. However, absorption experiments at 77 K to enhance the resolution of the vibronic structure showed no evidence for a contribution of a $S_0 \rightarrow S_1$ transition [88]. Other possible origins of spectral broadening were suggested by Christensen and Kohler based on experiments with retinal and polyene analogues [240]. According to their work, the coupling of the S_2 state to closely located dark states, the presence of a manifold of strongly coupled vibrational states, and/or a conformational disorder in consequence of interactions between the β -ionylidene ring and the methyl groups along the chain are possible reasons for the solvent dependent band broadening. A repulsion between methyl groups at the terminal rings and a neighboring hydrogen atom on the conjugated backbone could lead to a loss of the vibrational resolution [5, 88, 240]. A flat potential energy surface associated with the dihedral bond angle for the carbons can cause several conformational isomers with a broad range of effective π -electron conjugation. This ensemble of conformers would exhibit a distribution of transition energies resulting in a broad unstructured absorption spectrum.

In case of a carbonyl group located close to the β -ionylidene ring the distribution of isomers is enhanced compared to the steric repulsion only between the methyl groups on the β -ionylidene rings and hydrogens on the carbon chain [88]. Further spectral broadening can be explained by additional flattening of the S_0 potential energy surface due to interactions of the carbonyl group with polar solvent molecules. While the polarity of the solvent seems to hardly effect the properties of the S_2 state, the polar solvents can stabilize the negative charge on the carbonyl oxygen resulting in an enhanced charge transfer character of the ground state. Due to the presence of several ground state conformations the vibrational structure diminishes and the spectra is broadened [101, 102]. Protic solvents such as ethanol and methanol can form a hydrogen bond to the carbonyl oxygen and thus further stabilize the charge transfer character of the ground state. This might also account to the fact that for acetonitrile the spectral width is smaller compared to 2-propanol, ethanol, and methanol.

5.2 Transient Absorption Measurements

In a second step, the different carotenoids in the various solvents were characterized by means of transient absorption spectroscopy in order to investigate the influence of the solvent polarity on the excited state dynamics. The carotenoids were excited at the red edge of the $S_0 \rightarrow S_2$ absorption band with $\lambda_{\text{exc}} = 485$ nm. In Figures 5.3 and 5.6 the 2D spectra of diadinoxanthin, diatoxanthin, and fucoxanthin in various solvents are displayed. For fucoxanthin transient spectra at a delay time of 5 ps and individual decay traces recorded at $\lambda_{\text{pr}} = 530$ nm are shown in Figure 5.5 and Figure 5.8, respectively. Table 5.3 summarizes the S_1 lifetimes of the three carotenoids. The table is sorted by the polarity factor $P(\epsilon)$ of the solvents, which can be determined from their dielectric constants with $P(\epsilon) = (\epsilon - 1) / (\epsilon + 2)$ [88].

Diadinoxanthin and Diatoxanthin

In the 2D spectra of the xanthophyll cycle pigments diadinoxanthin and diatoxanthin shown in Figure 5.3 two bands are observed upon excitation at $\lambda_{\text{exc}} = 485$ nm. A GSB signal for $\lambda_{\text{pr}} < 500$ nm and a positive signal between $\lambda_{\text{pr}} = 500$ nm and 570 nm corresponding to the $S_1 \rightarrow S_n$ ESA. No additional ESA band appears as found for fucoxanthin in polar solvents (see Figure 5.6). The transient spectra are nearly identical in polar and nonpolar solvents without significant changes in the dynamics. This becomes even more obvious for the individual transients depicted in Figure 5.4. The kinetic traces were recorded at $\lambda_{\text{pr}} = 534$ nm in the maximum of the S_1 ESA band. In almost all 2D spectra (Figure 5.3 and 5.6) a really short lived negative signal is observed around delay time zero. It is located in the spectral probing region from $\lambda_{\text{pr}} \approx 490$ nm to ≈ 580 nm and is more pronounced in case of diadinoxanthin and diatoxanthin compared to fucoxanthin.

Pigment	Solvent	τ_1	τ_2	τ_3
Diadinoxanthin	n-Hexane	0.17	0.66	20
	Ethyl Acetate	0.13	0.67	21
	Ethanol	0.12	0.72	21
	Methanol	0.12	0.66	21
Diatoxanthin	n-Hexane	0.15	0.54	12
	Ethyl Acetate	0.12	0.48	13
	Ethanol	0.12	0.47	13
	Methanol	0.11	0.46	12

Table 5.1: Time constants in ps obtained in a global fit analysis of diadinoxanthin and diatoxanthin in different solvents.

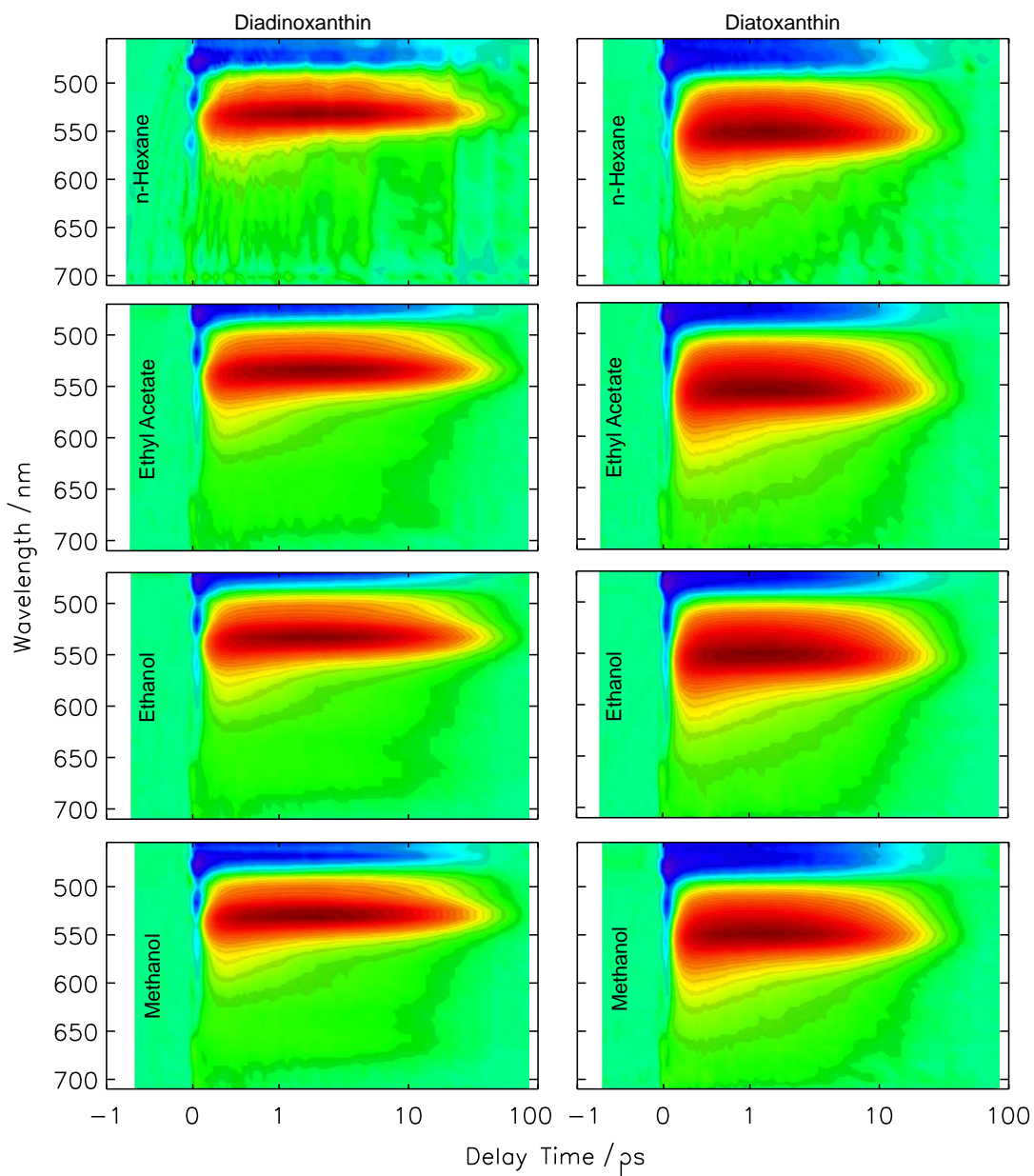


Figure 5.3: Transient absorbance changes of diadinoxanthin (left) and diatoxanthin (right) in n-hexane, ethyl acetate, ethanol, and methanol. The molecules were excited at $\lambda_{\text{exc}} = 485$ nm. Here and in all following 2D-plots the time axis is linear up to 1 ps and logarithmic for longer delay times. Negative absorbance changes are color coded in blue and positive absorbance changes are depicted in red.

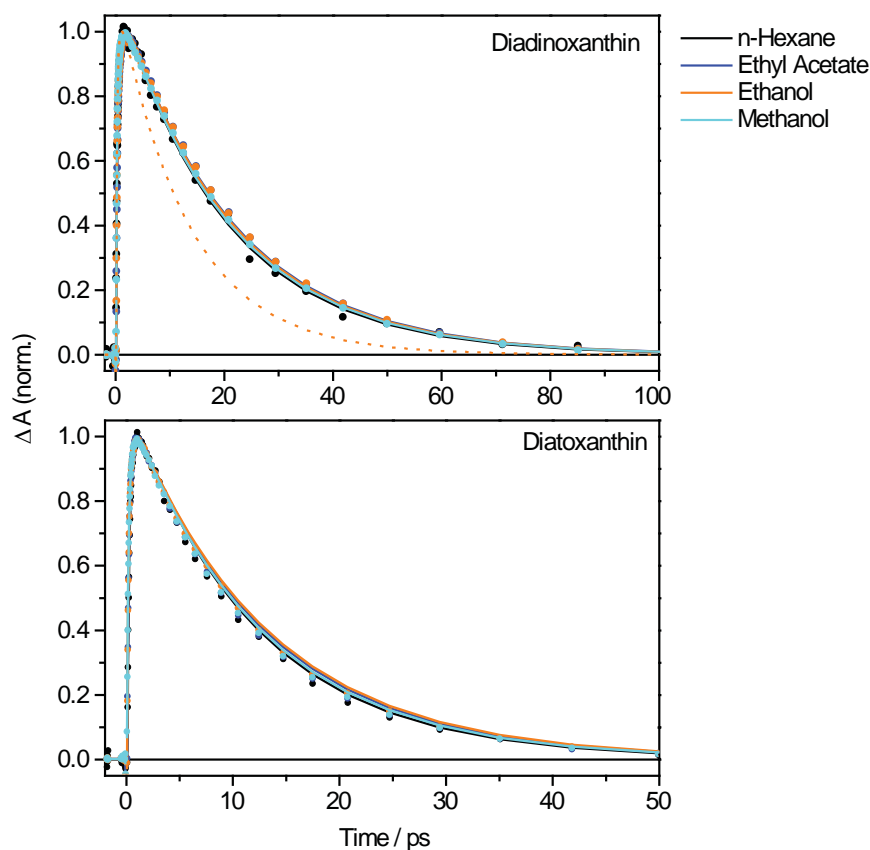


Figure 5.4: Individual kinetic traces of diadinoxanthin (top) and diatoxanthin (bottom) in different solvents recorded at $\lambda_{pr} = 534$ nm upon excitation at $\lambda_{exc} = 485$ nm. The transient data (\bullet) were fitted in a global fit analysis from which the fit curves (-) and the corresponding lifetimes (see table 5.3) were obtained. The dotted orange curve (upper panel) represents the kinetics of diatoxanthin in ethanol for better comparison between the two pigments.

It can be assigned to the $S_2 \rightarrow S_0$ stimulated emission.

The data was analyzed in a global fit analysis. The three time constants which are necessary to obtain a satisfactory fit are depicted in table 5.1. For all solvents τ_1 is slightly longer compared to the time resolution of the experiment (≈ 80 fs). Though it can be attributed to the S_2 lifetime the associated dynamics is a mixture of the coherent artifact and the S_2 SE signal. In order to obtain the values for the S_2 lifetime fluorescence upconversion experiments were performed (see chapter 5.3). τ_2 and τ_3 are both shorter in case of diatoxanthin compared to diadinoxanthin. The second time constant with $\tau_2 \approx 700$ fs and ≈ 500 fs for diadinoxanthin and diatoxanthin, respectively, can be attributed to vibrational cooling of the first excited singlet state. This cooling is also

visible in the 2D-spectra as a narrowing in the red edge of the ESA band. τ_3 with 13 ps for diatoxanthin and 21 ps for diadinoxanthin corresponds to the S_1 lifetimes. They are independent of the solvent conditions.

Fucoxanthin

The excited state dynamics of the carbonyl containing carotenoid fucoxanthin was investigated in a multitude of solvents with varying solvent polarity. The pigment was excited in the red edge of the $S_0 \rightarrow S_2$ absorption band at $\lambda_{exc} = 485$ nm. In contrast to diadinoxanthin and diatoxanthin the data obtained for fucoxanthin show a dramatic solvent effect on the excited state dynamics as can be seen in the 2D plots in Figure 5.6. For fucoxanthin in n-hexane two main transient features are observed, the GSB for $\lambda_{pr} < 500$ nm and an ESA band between $\lambda_{pr} = 500$ nm and 570 nm corresponding to the $S_1 \rightarrow S_n$ transition. There is only a very weak additional ESA contribution observed, which is red shifted and extended to $\lambda_{pr} \approx 700$ nm. With increasing solvent polarity this additional ESA band clearly arises between $\lambda_{pr} = 570$ nm and 700 nm. This feature is most pronounced in the polar solvents methanol and acetonitrile with two maxima at $\lambda_{pr} = 650$ nm and 605 nm. Furthermore, the observed dynamics are faster in polar solvents compared to the dynamics in nonpolar solvents (Figure 5.6 and 5.8).

Transient absorption spectra of fucoxanthin in the representative solvents n-hexane, ethyl acetate, and methanol are plotted in Figure 5.5. The spectra were taken at $\tau_D = 5$ ps. For fucoxanthin in n-hexane the ESA band between $\lambda_{pr} = 570$ nm and 700 nm is very weak. It increases dramatically with increasing solvent polarity and is

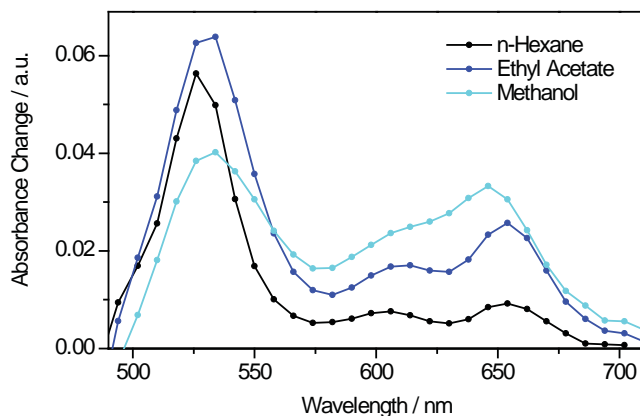


Figure 5.5: Transient absorption spectra of fucoxanthin in n-hexane, ethyl acetate, and methanol, representing environments with differing polarity. The molecules were excited at $\lambda_{exc} = 485$ nm and the depicted transient spectra were recorded after a delay time of 5 ps.

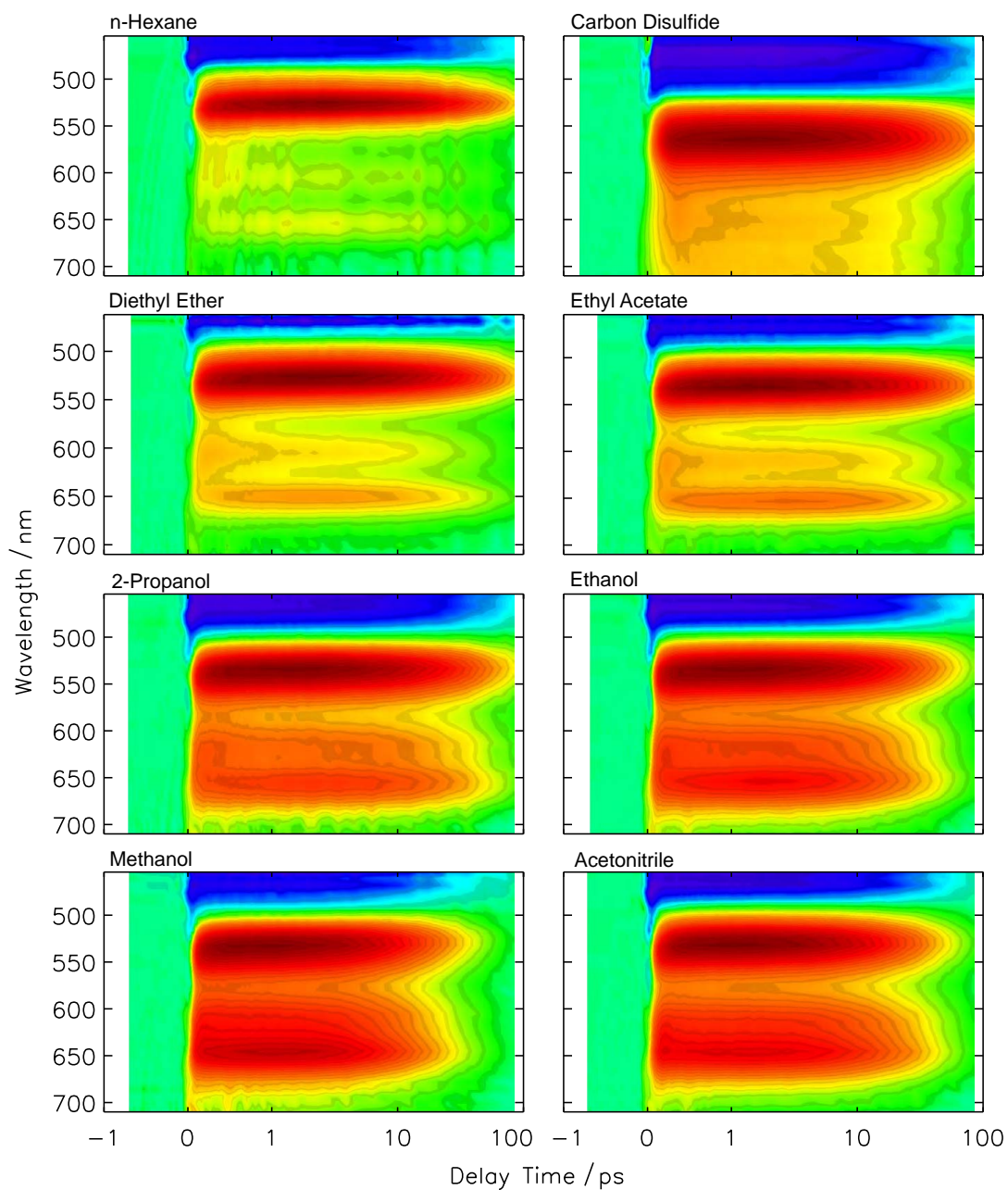


Figure 5.6: Transient absorbance changes of fucoxanthin in various solvents upon excitation at $\lambda_{\text{exc}} = 485$ nm. With increasing solvent polarity an additional ESA band arises between $\lambda_{\text{pr}} = 570$ nm and 700 nm.

characterized by two distinct bands. Here it can be seen that the rise of the second ESA band is accompanied by the decrease of the $S_1 \rightarrow S_n$ ESA band. The additional red shifted ESA band can be attributed to an intramolecular charge transfer (ICT) state. The ICT ESA shows two maxima which are most probably two vibrational bands. However, the two maxima could also result from an overlap with a negative signal. As mentioned before, for highly substituted carotenoids like fucoxanthin the $S_0 \rightarrow S_1$ transition becomes more allowed. Thus, for those pigments fluorescence from the S_1 state is observed between ≈ 550 nm and 800 nm [86]. The corresponding S_1 SE signal is thus expected to appear in the same spectral region as the ICT ESA and could be also responsible for the insetion.

The data for all solvents were analyzed in global fit analyses. As for the xanthophyll cycle pigments three time constants are sufficient for a good approximation of the data. The obtained lifetimes are summarized in table 5.2. τ_1 is nearly independent of the solvent. It is very short ($\tau_1 < 100$ fs), within the time resolution of the experiment (≈ 80 fs). Again, it can be assigned to the lifetime of the S_2 state. The second time constant τ_2 varies from 300 fs to 800 fs and is probably related to a vibrational cooling of the S_1 state. The expected accompanied narrowing of the ESA band is less pronounced than for diadinoxanthin and diatoxanthin due to the overlap with the red shifted second ESA band. The third time constant τ_3 is attributed to the lifetime of the first excited singlet state. Like τ_2 it varies in different solvent environments with lifetimes from 20 ps to 63 ps. An additional lifetime to describe the dynamics of the ICT state was not necessary. It can be concluded that the lifetimes of the S_1 state and the ICT state are correlated. This can be further confirmed when the individual transients of the respective maxima of the ESA bands are compared (see Figure 5.7). Exemplary the kinetic traces for fucoxanthin in 2-propanol and methanol are depicted for $\lambda_{pr} = 534$ nm, $\lambda_{pr} = 606$ nm, and $\lambda_{pr} = 646$ nm, respectively. The decay dynamics are almost identical with only very

Solvent	τ_1	τ_2	τ_3
n-Hexane	0.07	0.59	57
Carbon Disulfide	0.04	0.63	63
Diethyl Ether	0.07	0.57	61
Ethyl Acetate	0.06	0.38	62
2-Propanol	0.06	0.50	50
Ethanol	0.05	0.47	36
Methanol	0.06	0.81	20
Acetonitrile	0.05	0.33	30

Table 5.2: Time constants in ps obtained in a global fit analysis for fucoxanthin in various solvents.

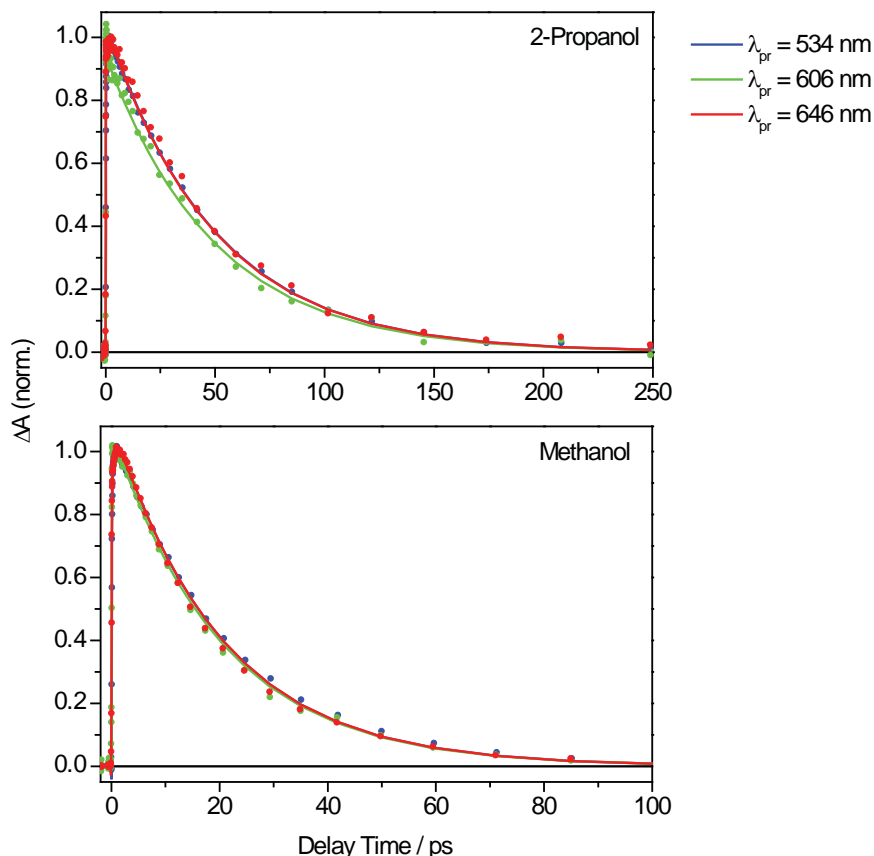


Figure 5.7: Individual kinetic traces of fucoxanthin in 2-propanol and methanol recorded at $\lambda_{\text{pr}} = 534$ nm, 606 nm, and 646 nm representing the maxima of the S_1 /ICT ESA bands.

small variance for $\lambda_{\text{pr}} = 606$ nm in case of 2-propanol. It can be assumed that the two states are coupled and not separated, though this assumption is still a matter of debate (see chapter 2.2.2) [101, 107, 108].

According to the time constants obtained in the global fit analysis not only the spectral characteristics change depending on the solvent environment but also the lifetimes of the excited states are influenced. τ_2 varies but shows no clear dependence on the solvent polarity. This is different in case of τ_3 . Individual kinetic traces for fucoxanthin in the different solvents are plotted in Figure 5.8. The transients were recorded at $\lambda_{\text{pr}} = 534$ nm representing the decay dynamics of the first excited singlet state. In table 5.3 the S_1 lifetimes are depicted related to the solvent polarity and compared to the S_1 lifetimes obtained for the xanthophyll cycle pigments. The S_1 lifetimes for all carotenoids are plotted against the solvent polarity in Figure 5.9. For solvent polarities

5.2. Transient Absorption Measurements

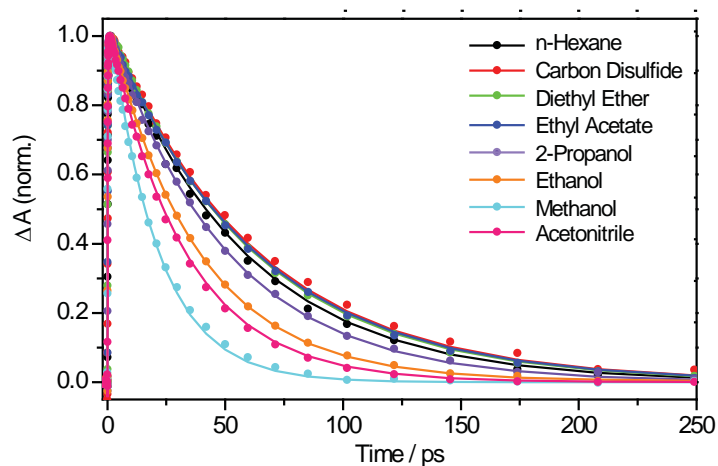


Figure 5.8: Individual kinetic traces of fucoxanthin in various solvents recorded at $\lambda_{pr} = 534$ nm upon excitation at $\lambda_{exc} = 485$ nm. The transient data (\bullet) were fitted in a global fit analysis from which the lifetimes (see table 5.3) and the fit curves ($-$) were derived.

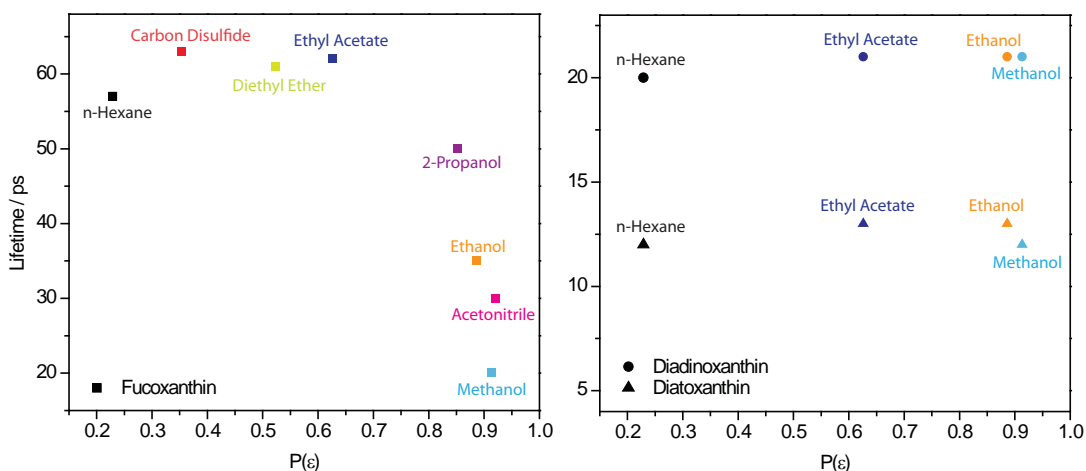


Figure 5.9: Lifetimes of the lowest excited state of fucoxanthin (\blacksquare), diadinoxanthin (\bullet), and diatoxanthin (\blacktriangle) plotted against the solvent polarity $P(\epsilon)$. In case of fucoxanthin the S_1 lifetime is almost constant up to a solvent polarity of $P(\epsilon) \approx 0.6$ and then decreases considerably with increasing solvent polarity. In contrast, the lifetimes obtained for the xanthophyll cycle pigments are almost constant.

up to a value of $P(\epsilon) \approx 0.6$ the S_1 lifetimes of fucoxanthin stay nearly constant and then decrease considerably with increasing solvent polarity. However, for acetonitrile the lifetime increases again though it has the highest solvent polarity. Like for the bandwidth, this can be explained with the fact that acetonitrile is a polar but a non-hydrogen bonding solvent. As mentioned before, the lifetime of the first excited state shows no solvent dependence for diadinoxanthin and diatoxanthin.

The observed changes of the dynamics of the excited states depending on the solvent polarity can be explained with the presence of the ICT state in carbonyl containing carotenoids. However, it can be assumed that in nonpolar solvents the ICT state is higher in energy than the $2A_g^-$ state. It could be close enough to be thermally populated after relaxation from the S_2 state to the S_1 state [88]. This would explain the observation of the weak contribution of the ICT excited state dynamics in solvents with low dielectric constants like in n-hexane (Figure 5.6 and 5.5). It is expected that the electron-withdrawing character of the carbonyl group stabilizes the charge transfer character, especially in polar solvents. Thus, the ICT ESA band increases with increasing solvent polarity.

The energy level diagram in Figure 5.10 describes the observed changes in the excited state dynamics in more detail. The potential energy surfaces and electronic transitions are shown for fucoxanthin in nonpolar and polar solvents, respectively. The model assumes a strong coupling between the $2A_g^-$ and ICT state leading to a distorted excited state potential energy surface with two solvent dependent minima. It is based on the one describing the excited state dynamics of peridinin proposed by Frank et al. [88]. With increasing solvent polarity the intensity of the $S_1 \rightarrow S_n$ band decreases accompanied by the raise of the $S_1 \rightarrow S_{n'}$ band. The presence of the ICT component shifts the minimum of the potential energy surface and leads to a redistribution of the excited state

Solvent	$P(\epsilon)$	Lifetime / ps		
		Fucoxanthin	Diadinoxanthin	Diatoxanthin
n-Hexane	0.229	57	20	12
Carbon Disulfide	0.354	63	–	–
Diethyl Ether	0.524	61	–	–
Ethyl Acetate	0.626	62	21	13
2-Propanol	0.852	50	–	–
Ethanol	0.886	36	21	13
Methanol	0.913	20	21	12
Acetonitrile	0.921	30	–	–

Table 5.3: Solvent dependence of the S_1 lifetime of isolated carotenoids. The values are sorted by the polarity factor $P(\epsilon)$.

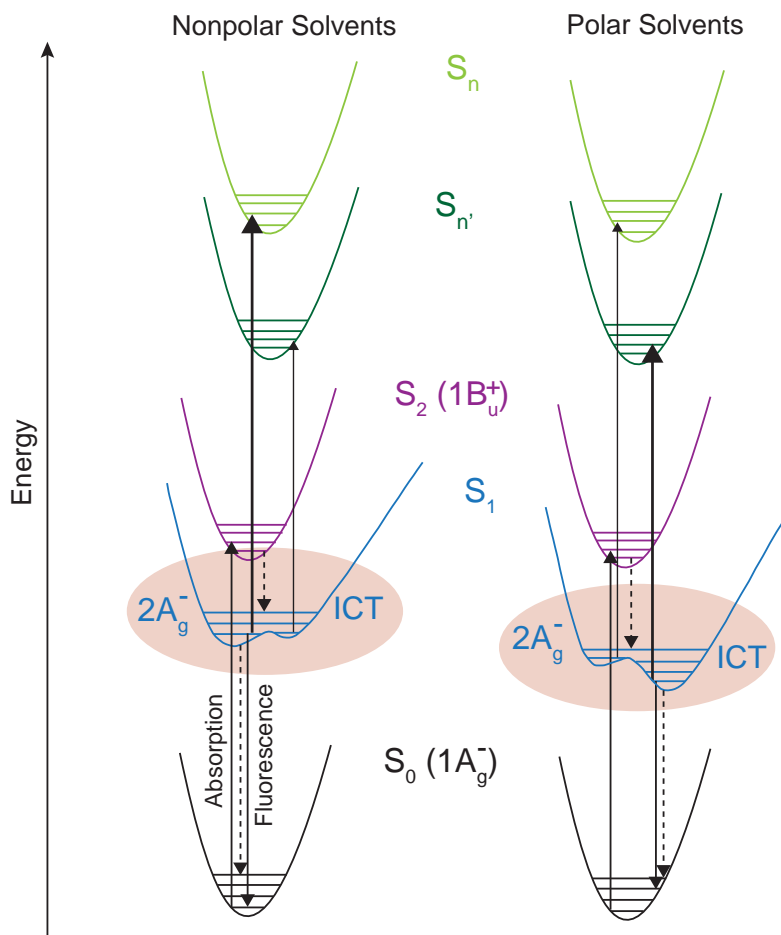


Figure 5.10: Potential energy surface scheme describing the solvent effects on the excited state dynamics of fucoxanthin. The potential energy surfaces on the left represent the dynamics in nonpolar solvents. On the right, the arrangement of the states in polar solvents is shown. In this model it is assumed that the $2A_g^-$ state and the ICT state are strongly coupled. The dashed lines represent internal conversion processes. The thickness of the arrows corresponds to the $S_1 \rightarrow S_n$ and $S_1 \rightarrow S_{n'}$ transition, respectively and reflects the intensity of the transition as obtained for fucoxanthin shown in Figure 5.6 and 5.5. The model is adopted from [88].

population between the ICT and the $2A_g^-$ state. This results in the solvent dependent excited state dynamics of fucoxanthin represented in Figure 5.5, where the decrease of the $2A_g^- \rightarrow S_n$ absorption band and concomitant increase of the $ICT \rightarrow S_{n'}$ absorption band is clearly visible. Furthermore, there is a blue shift of the $S_1 \rightarrow S_{n'}$ transition caused by the decrease of the potential energy minimum attributed to the ICT component relative to the $S_{n'}$ state [88]. This can explain the spectral development of the ICT ESA band depending on the solvent environment. In nonpolar solvent this ESA signal is strongest around $\lambda_{pr} = 650$ nm. With increasing solvent polarity the transient absorption band is broadened to shorter wavelengths. The decrease of the S_1 excited state lifetime in polar solvents can be explained with an enhanced internal conversion to the ground state due to the lower energy of the S_1/ICT state in polar solvents.

5.3 Fluorescence Lifetimes

The solvent dependence of the S_2 lifetime of the carotenoids was investigated by means of fluorescence upconversion measurements. To study the relaxation kinetics of the S_2 state to the S_1 state the S_2 fluorescence lifetimes were determined for β -carotene and fucoxanthin in polar and nonpolar solvents. The S_2 fluorescence lifetimes of diadinoxanthin and diatoxanthin were obtained only for ethanol solutions, since only very small amounts of these carotenoids were available.

For all solvents the cross correlation signal was measured in order to determine the time resolution of the experiment. This cross correlation signal was used in the data analysis to determine the fluorescence lifetime. The scattered excitation light was collected and overlapped with the gate pulse in the BBO crystal. The sum frequency of the two beams was recorded and the FWHM of this cross correlation signal is calculated assuming a Gaussian shape. It shows a solvent dependence due to the dispersion within the solvent with a FWHM varying from 125 fs to 210 fs. The measured cross correlation signals and two representing fit curves are displayed in Figure 5.11.

The carotenoids were excited at $\lambda_{exc} = 415$ nm and the fluorescence decays were determined at $\lambda_{pr} = 316$ nm corresponding to a fluorescence wavelength of $\lambda_{fl} = 510$ nm. The fluorescence transients were fitted with a single exponential decay and convoluted with the response function (cross correlation) using the Matlab program provided by Jörg Enderlein [233].

The measurements of β -carotene were mainly performed to characterize the setup, since values for the S_2 fluorescence lifetime are already published [89,241] and can be compared to the presented results. The fluorescence decay of β -carotene was measured in n-hexane, ethyl acetate, and ethanol and was found to depend on the solvent. The results and corresponding fit curves are shown in Figure 5.12 and the fluorescence lifetimes are summarized in table 5.4. The lifetime decreases with increasing solvent polarity from 220 fs in n-hexane and 195 fs in ethyl acetate to 138 fs in ethanol. The value found for β -carotene in ethanol was in good agreement with the one from Macpherson and Gillbro

5.3. Fluorescence Lifetimes

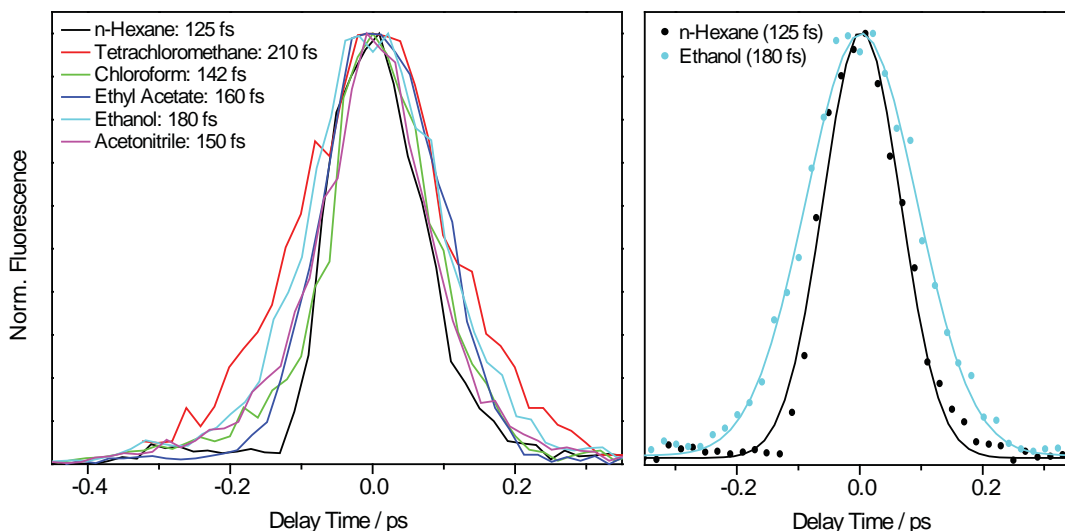


Figure 5.11: Solvent dependence of the cross correlation width. In the left panel the data for various solvents are depicted and the right panel shows two representative fit curves (solid lines) of the data (•) for n-hexane and ethanol.

(144 fs) [89]. However, the fluorescence lifetime obtained for n-hexane was slightly higher with 220 fs compared to 177 fs. The deviation could be due to differences of the applied excitation and/or detected fluorescence wavelength. Experiments with β -carotene in several other nonpolar and polar solvents by Macpherson and Gillbro indicated that both the polarity and polarizability of the solvents are correlated with the decay of the S_2 state [89]. According to their interpretation the decrease of the S_2 lifetime results from a distortion of the C_{2h} symmetry and a vibronic coupling of the two lowest excited singlet states. Furthermore, one has to consider a possible involvement of an intermediate

Solvent	β -Carotene	Fucoxanthin	Diadinoxanthin	Diatoxanthin
n-Hexane	220 (177)	166	–	–
Ethyl Acetate	195	166	–	–
Ethanol	138 (144)	128	158	181
Acetonitrile	–	121	–	–

Table 5.4: Fluorescence lifetimes in fs of β -carotene, fucoxanthin, diadinoxanthin, and diatoxanthin obtained from fluorescence upconversion experiments. The values in parentheses were published by Macpherson and Gillbro [89].

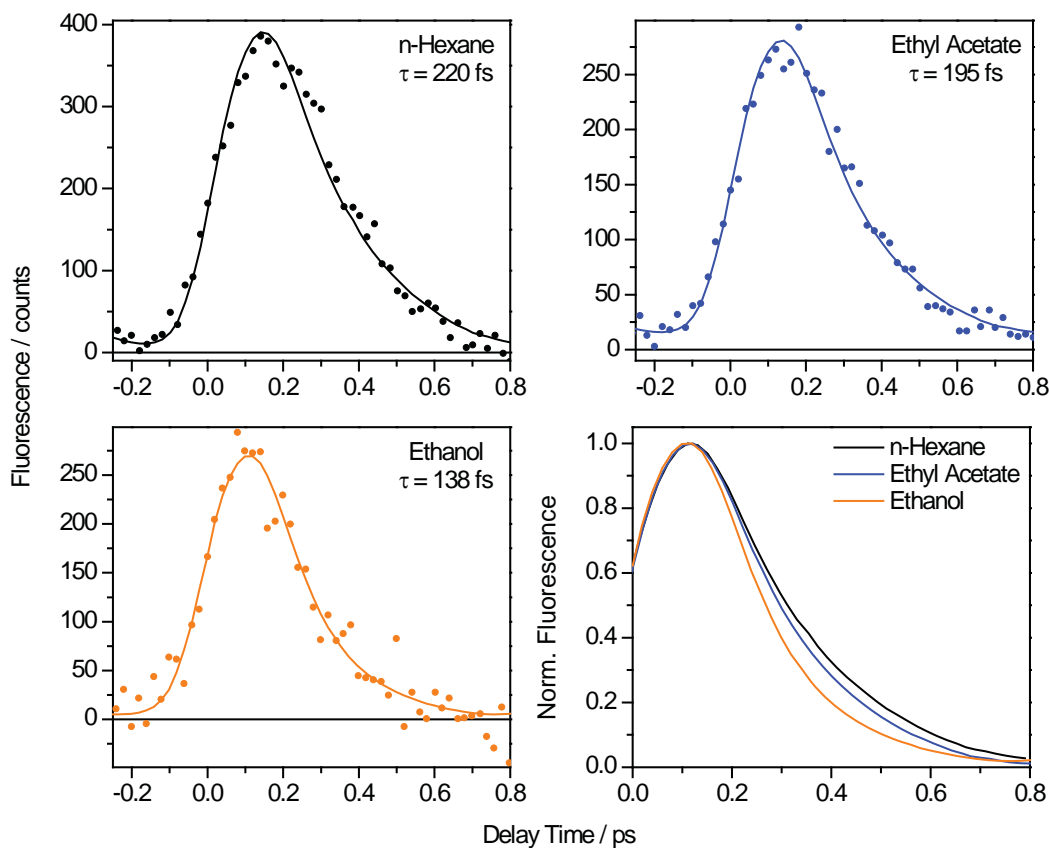


Figure 5.12: Upconversion measurements of β -carotene in n-hexane, ethyl acetate, and ethanol. The dots denote the measured signals and the solid lines represent the fit curves. In the lower right panel the fluorescence decays in the three solvents are compared.

dark state ($1B_u^-$) between the S_2 ($1B_u^+$) and S_1 ($2A_g^-$) states which can influence the relaxation dynamics [8].

The S_2 fluorescence lifetimes for fucoxanthin were determined in n-hexane, ethyl acetate, ethanol, and acetonitrile. The measured data and corresponding fit curves are depicted in Figure 5.13. The obtained lifetimes are collected and compared to the other carotenoids in table 5.4. Like for β -carotene the obtained lifetimes were longer in nonpolar solvents with $\tau = 166$ fs (n-hexane and ethyl acetate) and shorter in polar solvents with 128 fs for ethanol and 121 fs for acetonitrile. In case of the xanthophyll cycle pigments the fluorescence lifetimes in ethanol were longer compared to fucoxanthin and β -carotene in ethanol with $\tau = 158$ fs and $\tau = 181$ fs for diadinoxanthin and diatoxanthin, respectively (Figure 5.14). To further characterize the carotenoids con-

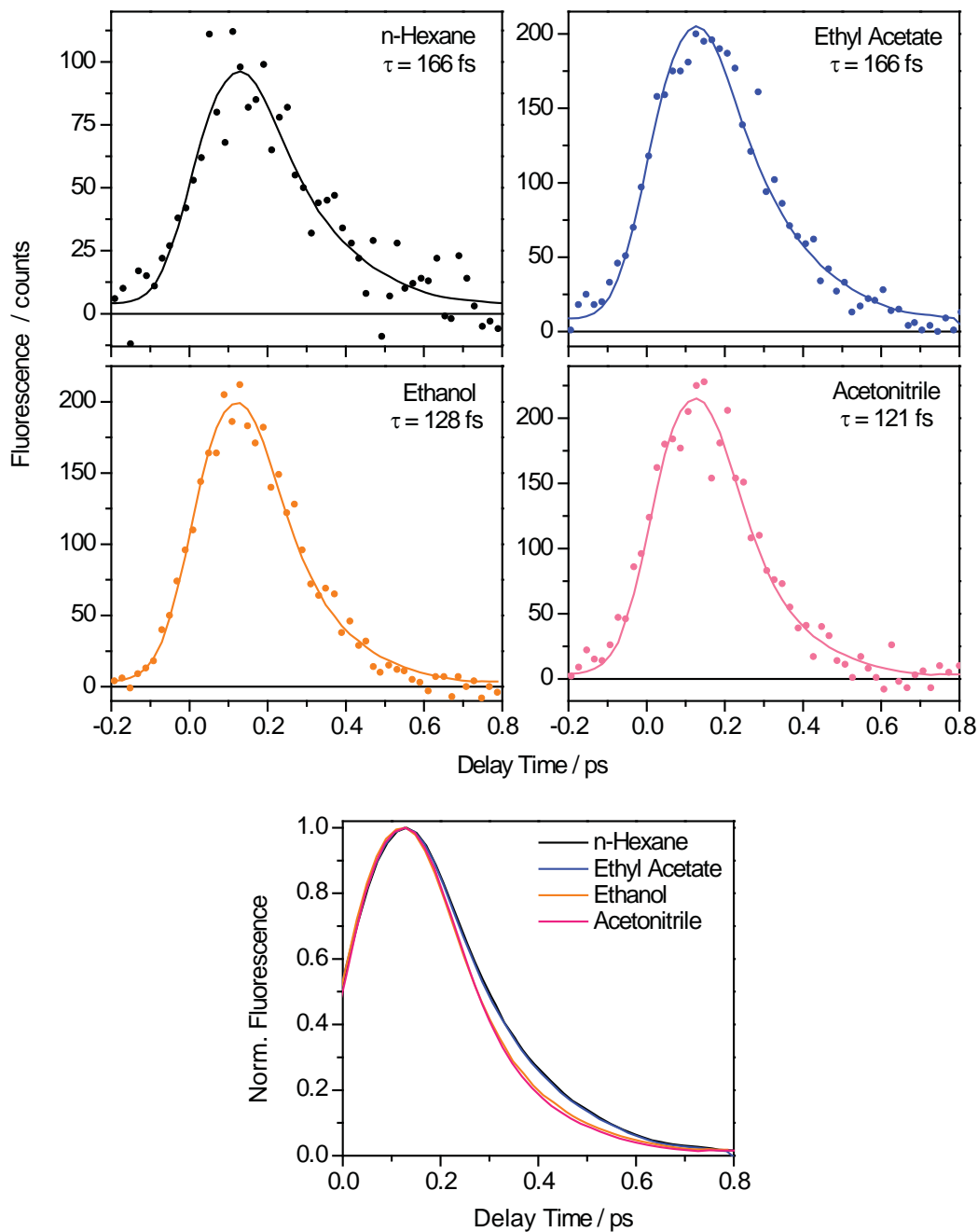


Figure 5.13: Upconversion measurements of fucoxanthin in various solvents. The dots denote the measured signals and the solid lines represent the fit curves. In the lowest panel the fluorescence decays in all applied solvents are compared. The low number of counts detected for fucoxanthin in n-hexane can be explained with poor solubility in this solvent.

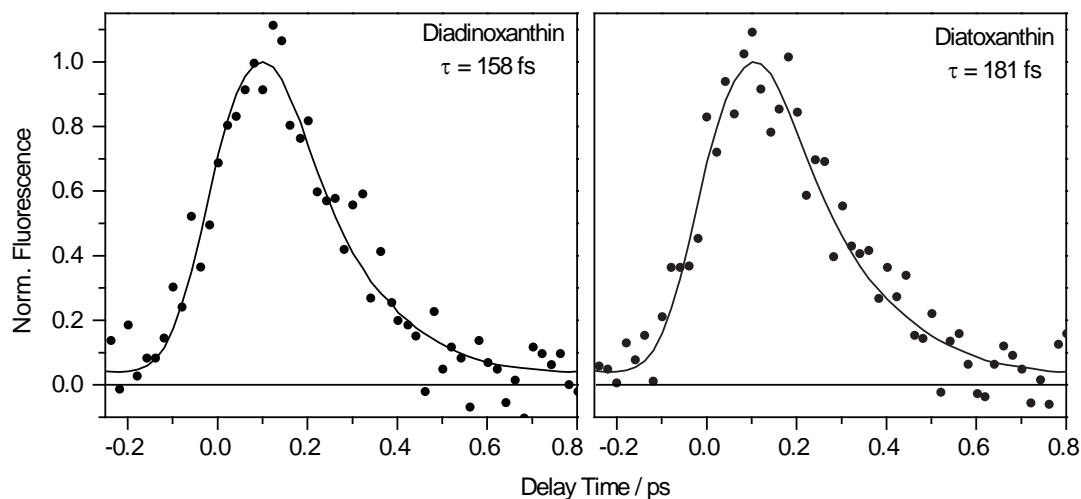


Figure 5.14: Upconversion measurements of diadinoxanthin (left) and diatoxanthin (right) in ethanol. The dots denote the measured signals and the solid lines represent the fit curves.

tained in FCPs additional experiments are necessary. For example the excitation and probing wavelength dependence of the S_2 fluorescence lifetime should be investigated in many different solvents and the results should be compared with experiments of related carotenoids. Furthermore, the S_1 fluorescence lifetimes should be studied. With the described Kerr shutter setup it should be possible to monitor the fluorescence behavior from the first and second excited singlet state simultaneously. From a multitude of previous experiments addressing the S_2 lifetime [5] and the presented results above it can be concluded that the lifetime of the S_2 state mainly depends on the solvent. Solvent effects can be explained with the S_2 - S_1 energy gap, which decreases with increasing solvent polarizability resulting in shorter S_2 lifetimes in solvents with higher refractive indices [89].

Chapter 6

Excitation Energy Transfer in FCPs

An ancestor of mine maintained, that if you eliminate the impossible, whatever remains, however improbable, must be the truth.

(Mr. Spock in *Star Trek VI: The Undiscovered Country*)

The ultrafast carotenoid excitation energy transfer to chlorophyll in fucoxanthin chlorophyll proteins (FCPs) was studied using the transient absorption technique in the visible and near infrared spectral region. Static fluorescence experiments were used to investigate the energy transfer efficiency. The influence of the oligomeric state and the growth conditions as well as the excitation wavelength dependence were examined. Polarized transient absorption spectroscopy was applied to gain further information concerning the pigment arrangement within the protein.

All presented results were obtained for FCP samples extracted and purified in the group of Prof. Claudia Büchel. As mentioned before, the FCP samples were diluted in a buffer containing 25 mM Tris at pH 7.4, 2 mM KCl, and 0.03 % β -DDM. The optical density was ≈ 0.9 at 671 nm in the 1 mm cuvette applied for all time resolved measurements. This corresponds to a Chl *a* concentration of ≈ 0.13 mg per 1 mL sample volume. All measurements were carried out at room temperature.

6.1 Steady State Characterization

For the steady state characterization of the FCPs absorption, emission and excitation spectra were recorded. The absorption spectrum (Figure 6.1) is dominated by the spectral features of Chl *a* and Chl *c*₂. The Soret and the Q_y band of Chl *a* are visible

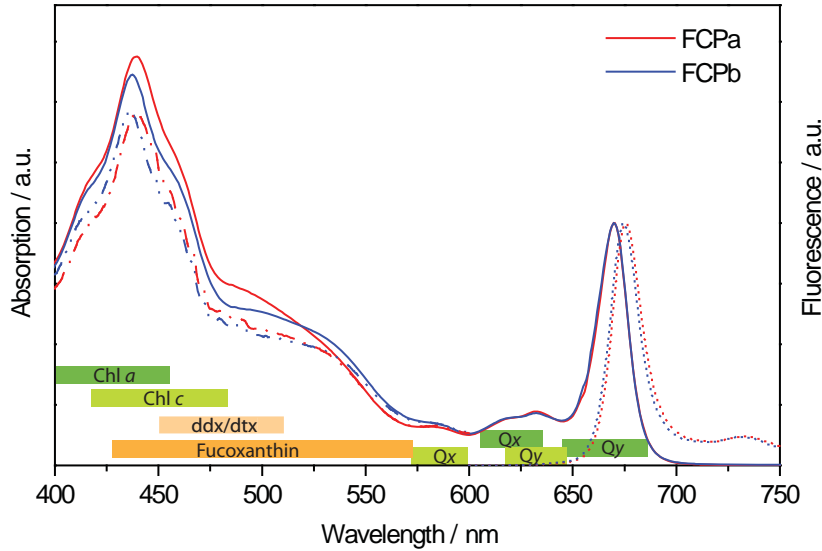


Figure 6.1: Steady state absorption (—), excitation (---), and emission (···) spectra of FCPa (red) and FCPb (blue). The excitation spectra were recorded at $\lambda_{\text{fluo}} = 675$ nm and the fluorescence was detected upon excitation at 500 nm.

at 440 nm and at 670 nm while the shoulder around 460 nm and the weak band at 635 nm belong to the Soret and the Q_y band of Chl c_2 . The absorption in the spectral region between 480 nm and 570 nm originates from the $S_0 \rightarrow S_2$ transition of the carotenoids, mainly fucoxanthin. The absorption spectra of the fucoxanthin molecules in FCPs are red shifted compared to isolated fucoxanthins in solution [135]. Furthermore, the four fucoxanthin molecules have different absorption maxima due to their specific environment within the protein. Based on results from Stark spectroscopy performed by Premvardhan et al. red absorbing fucoxanthins (fx_{red}) could be distinguished from blue absorbing fucoxanthin molecules (fx_{blue}) [42]. Due to the small amount of diadinoxanthin and diatoxanthin their contribution to the spectrum is very small and appears most probably around 500 nm [42].

The emission spectra were detected upon excitation at $\lambda_{\text{exc}} = 500$ nm. The Chl a fluorescence band peaks at 675 nm and is accompanied by a vibrational band located around 730 nm for both samples. To control if the FCPs are intact with regard to the excitation energy transfer to Chl a excitation spectra were recorded at the Chl a fluorescence maximum ($\lambda_{\text{fluo}} = 675$ nm) and compared to the absorption spectra (Figure 6.1). For wavelengths between 535 nm and 600 nm both spectra resemble each other, whereas at lower wavelengths the excitation spectrum shows lower intensities. In the carotenoid band the energy transfer efficiency of the carotenoids absorbing around 550 nm seems

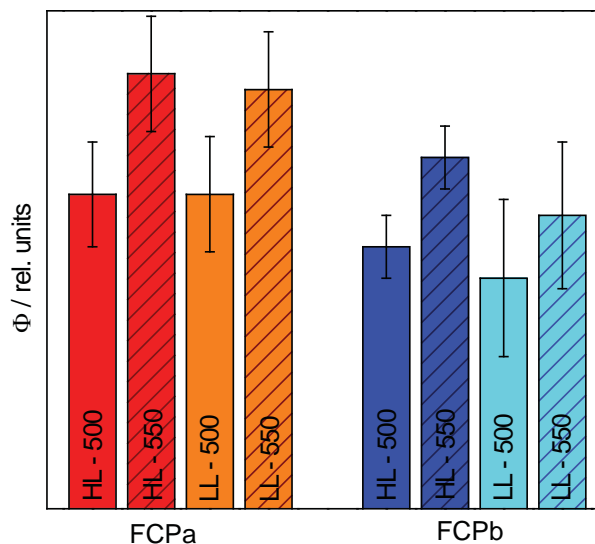


Figure 6.2: Fluorescence quantum yield of Chl *a* after excitation of the carotenoids at 500 nm and 550 nm of FCPa (red) and FCPb (blue) isolated from HL and LL cells.

to be higher compared to the ones absorbing around 500 nm. This may lead to the conclusion that diadinoxanthin and diatoxanthin are less or not involved in the excitation energy transfer and/or that one fucoxanthin absorbing in the blue region transfers energy poorly. Nevertheless, the close similarity of excitation and absorption spectra indicates that the energy transfer from Chl *c*₂ and the carotenoids to Chl *a* is the main pathway.

Fluorescence Quantum Yield

To further analyze the energy transfer efficiency from the carotenoids to Chl *a* the quantum yields of Chl *a* fluorescence after excitation of the carotenoids at 500 nm and 550 nm were determined for FCPa and FCPb isolated from cells grown under HL and LL conditions (Figure 6.2). The efficiencies were obtained by determining the Chl *a* fluorescence quantum yield after excitation of the S₂ state of the carotenoids. The emission spectra were recorded under identical conditions and corrected with the fluorimeter detection function. The fluorescence intensities were integrated and the respective absorption values of the reference and test samples with increasing concentrations were used to calculate the fluorescence quantum yield (see chapter 3.1). Because Chl *a* was not excited directly the obtained values represent the energy transfer efficiencies from the carotenoids to Chl *a* in the different FCP samples.

The complexes extracted from HL and LL cultures showed no significant differences

as the values are the same within the error margins. The most prominent changes due to varying light conditions during the growth were obtained for the deepoxidation ratio, which seems to have no significant influence on energy transfer efficiency. On the contrary, the Chl *a* fluorescence quantum yield varies when FCPb and FCPa samples as well as the different excitation wavelengths are compared. FCPa samples show a higher excitation energy transfer efficiency compared to FCPb samples. According to these results an increased quenching in the higher oligomers of the FCPb complexes can be assumed ("aggregation quenching") [242,243]. Regarding the excitation wavelength dependence higher fluorescence quantum yields are obtained after excitation of the red fucoxanthins at 550 nm. This is in accordance with the results from the excitation spectra and further confirms the assumption that a lower fraction of carotenoids transfers energy to Chl *a* upon excitation at 500 nm.

6.2 Fluorescence Lifetimes

All samples were characterized by means of TCSPC measurements. The Chl *a* fluorescence decay dynamics was investigated in order to observe whether the oligomeric state and the pigmentation has any influence on the fluorescence lifetime. As in the steady state fluorescence experiments the samples were excited in the carotenoid band at $\lambda_{\text{exc}} = 500$ nm and $\lambda_{\text{exc}} = 550$ nm, respectively. The single fluorescence photons were detected at $\lambda_{\text{fl}} = 675$ nm where the Chl *a* fluorescence has its maximum. The data and associated fit curves of the HL samples are displayed in Figure 6.3. HL and LL samples showed identical temporal behavior, thus the results for LL-FCPs are not shown.

There were nearly no variations found for the lifetimes of the different FCP samples. The two excitation wavelengths seem to have no significant influence on the Chl *a* fluorescence, since the obtained lifetimes are nearly identical. For the FCPb samples slightly ($\approx 10\%$) shorter lifetimes were observed compared to the FCPa samples. This provides further evidenced for an increased quenching in the higher oligomers of FCPb.

6.3 Transient Absorption Dynamics in FCPs

To analyze the transient absorption dynamics in FCPa and FCPb the samples isolated from HL and LL cells were excited at $\lambda_{\text{exc}} = 500$ nm and $\lambda_{\text{exc}} = 550$ nm, respectively. Excitation at $\lambda_{\text{exc}} = 550$ nm leads to the population of the S_2 state of red absorbing fucoxanthin molecules. Upon pumping at $\lambda_{\text{exc}} = 500$ nm blue absorbing fucoxanthins and probably also diadinoxanthin and diatoxanthin molecules are excited.

For a general band assignment the transient absorption data of HL-FCPa excited at 500 nm is displayed in a color coded 2D-plot in Figure 6.4. Region A shows the ground state bleach (GSB) of the carotenoids around 500 nm with an additional contribution of the chlorophylls GSB at lower probing wavelengths. In the spectral region between

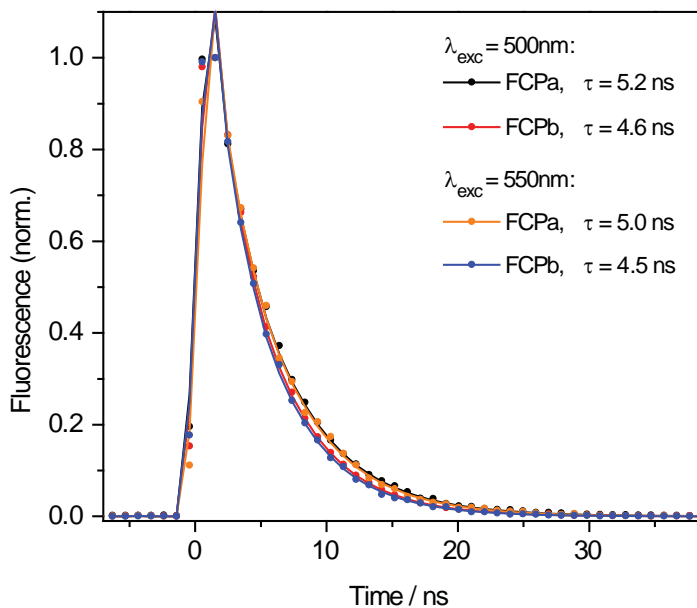


Figure 6.3: Chl *a* fluorescence lifetimes of HL-FCPs detected at $\lambda_{fl} = 675$ nm after excitation at $\lambda_{exc} = 500$ nm and $\lambda_{exc} = 550$ nm, respectively.

540 nm and 700 nm (region B) the broad ESA band originates from the fucoxanthin $S_1/ICT \rightarrow S_n$ transition. Transient signals from diadinoxanthin and diatoxanthin can not be distinguished from the fucoxanthin signals. The contributions from the xanthophyll cycle pigments is expected to be very weak due to their small amount in the investigated samples. The two regions labeled with C display the ESA of Chl *a* overlapping with signals of the fucoxanthins and dominating at later delay times. The stimulated emission (SE) of the Chl *a* Q_y state and the GSB of Chl *a* around $\lambda_{pr} = 670$ nm (region D) superimposes the ESA of the fucoxanthins and does not decay within the time window of the experiment as does the Chl *a* ESA (region C). In the NIR probing region two main spectral features are observed. Between 880 nm and 1090 nm the $S_2 \rightarrow S_N$ transition of the carotenoids is shown (region E). Due to the short lifetime of the second excited singlet state of fucoxanthin the signal decays within the time resolution of the experiment. The weak negative band at wavelengths above 950 nm (region F) can be attributed to the ICT SE of fucoxanthin, since this signal is not observed for carbonyl containing carotenoids in nonpolar solvents and carotenoids without a carbonyl group [105,244].

In order to get a more detailed description of the dynamics in Figure 6.5 kinetic traces for several probing wavelengths are depicted for FCPa and FCPb samples after

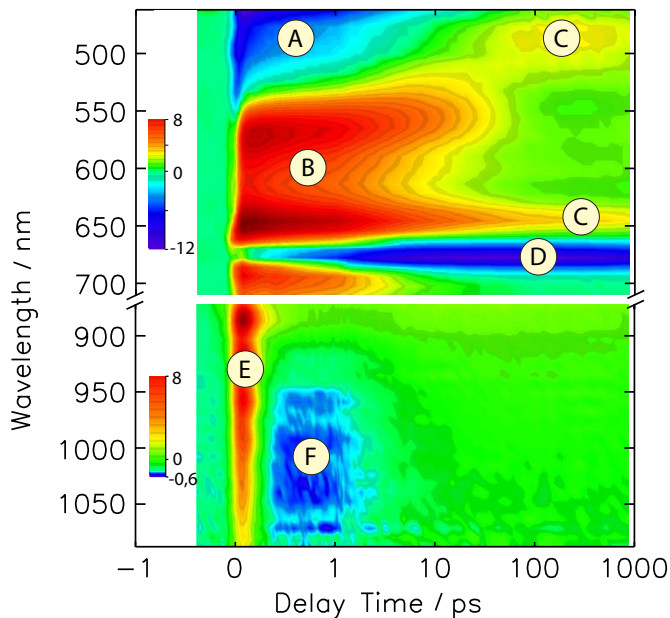


Figure 6.4: Transient absorption changes of HL-FCPa excited at 500 nm in the visible and NIR spectral region. The color code displays the absorbance change in units 10^{-3} and is different for the VIS and NIR probing region.

500 nm excitation. The curves were normalized for excitation energy and optical density at the respective excitation wavelength. At a probing wavelength of 486 nm at early delay times mainly the fucoxanthin bleach is visible and after a few picoseconds the ESA of Chl *a* dominates. At $\lambda_{\text{pr}} = 542$ nm the short negative signal at very early delay times corresponds to the SE of the S_2 state of the carotenoids. In this region the strong $S_1 \rightarrow S_n$ ESA of the carotenoids is rising and also Chl *a* shows weak ESA which extends to longer delay times. At $\lambda_{\text{pr}} = 646$ nm a strong ESA signal stemming from the ICT $\rightarrow S_n$ transition of the fucoxanthins again decays into a weaker Chl *a* ESA at later delay times. At this wavelengths also contributions of Chl *c*₂ are expected but no additional dynamics which could be attributed to the transient population of an excited Chl *c*₂ state are observed. The strong negative contribution at 678 nm originates from the Chl *a* GSB and SE and reflects the fast and efficient energy transfer from fucoxanthin to Chl *a*. Further to the red the dynamics are again dominated by the fucoxanthin ICT ESA with only a weak contribution of the bleach and SE of Chl *a*. In the NIR spectral region, at $\lambda_{\text{pr}} = 1000$ nm, a fast rise and decay of the $S_2 \rightarrow S_N$ transition appears at early delay times followed by a weak negative signal corresponding to the SE of the fucoxanthin ICT state. The weak positive signal at long delay times reflects an additional Chl *a* ESA band.

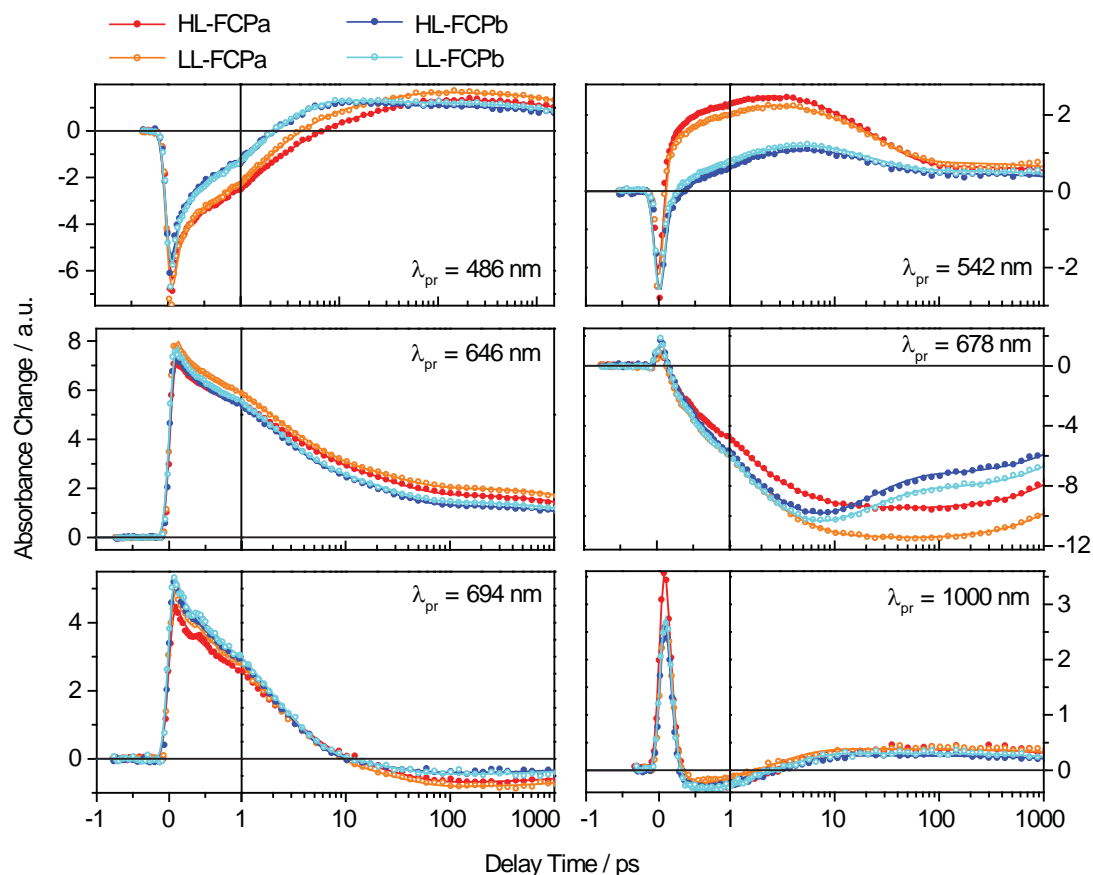


Figure 6.5: Individual kinetic traces of HL-FCPa (red), LL-FCPa (orange), HL-FCPb (blue), and LL-FCPb (cyan) after excitation at 500 nm at different probing wavelengths. Dots denote the measured data and lines the corresponding fit curves; both were normalized for optical density and excitation energy at the respective excitation wavelength. The time axis in these and following similar plots is linear up to 1 ps and logarithmic for longer delay times.

All data were analyzed with a global fitting procedure with either four or five time constants (summarized in table 6.1) depending on the excitation wavelength and the oligomeric state of the different FCPs. For all measurements the shortest time constant with values less than 150 fs lie within the time resolution of the experiment. Hence, the corresponding fit amplitudes for τ_1 are not plotted and will not be discussed in the following. However, it should be mentioned that this shortest time constant is also related to the short lived S_2 state of the carotenoids (see chapter 5.3). Due to the

difference signature remaining at the maximum observation time of the experiment one infinite time constant τ_{inf} is necessary to account for this.

6.3.1 Comparison of HL and LL Cultures

In a first step, data sets of HL and LL samples of both FCPa and FCPb after excitation at $\lambda_{\text{exc}} = 500$ nm as well as $\lambda_{\text{exc}} = 550$ nm were compared to investigate the influence of the modified pigment ratio (see Figure 2.11) on the excitation energy transfer. However, for these samples no significant differences were obtained as can be seen in the exemplary transients and decay associated spectra (DAS) depicted in Figure 6.5 and Figure 6.6, respectively. Slight alterations in the intensity of the signals are most likely due to minor changes in the probing white light occurring during the measurements.

The differences between FCPs extracted from HL and LL cultures are the polypeptide composition and the pigment ratio (see chapter 2.3.3). The most prominent effect upon varying the light conditions during the growth is the change in the deepoxidation ratio ($\text{dtx}/(\text{ddx}+\text{dtx})$), the amount of diatoxanthin increases considerably. According to that at least diatoxanthin does not seem to participate in the excitation energy transfer process, since no differences between the HL and LL samples are observed. It can be concluded that the deepoxidation ratio of diadinoxanthin to diatoxanthin has no significant influence on the dynamics of the energy transfer. The subsequent discussion therefore focuses on the analysis of the samples isolated from cultures grown under HL conditions.

6.3.2 Comparison of FCPa and FCPb

In contrast to the HL and LL samples the data sets obtained for FCPa and FCPb showed clear differences in the transient absorption spectra. The individual transients at selected probing wavelengths upon excitation at 500 nm and 550 nm are compared in Figure 6.7 and the corresponding fit amplitudes are shown in Figure 6.8. The differences between FCPa and FCPb obtained from the two excitation wavelengths are very similar.

In Figure 6.7 the kinetic traces at $\lambda_{\text{pr}} = 486$ nm show the GSB of the carotenoids at early delay times followed by a Chl *a* ESA after ≈ 3 ps. The comparison of FCPa and FCPb dynamics shows a faster recovery of the carotenoids GSB for FCPb. The rapid rise of the carotenoids ESA is visible around $\lambda_{\text{pr}} = 566$ nm and decays into a weaker ESA signal of Chl *a*. However, in case of FCPa after $\lambda_{\text{exc}} = 500$ nm the carotenoids ESA signal amplitude is considerably higher, while the Chl *a* ESA signal exhibits almost the same intensity for both samples. The differences are less pronounced after 550 nm excitation. The GSB and Q_y SE signal of Chl *a* at $\lambda_{\text{pr}} = 678$ nm increases until ≈ 10 ps, stays almost constant (in case of FCPa) and decays with a time constant beyond the observation time of the experiment. For the FCPb samples we observe not only a faster increase but also an immediate decay of this signal when compared to FCPa.

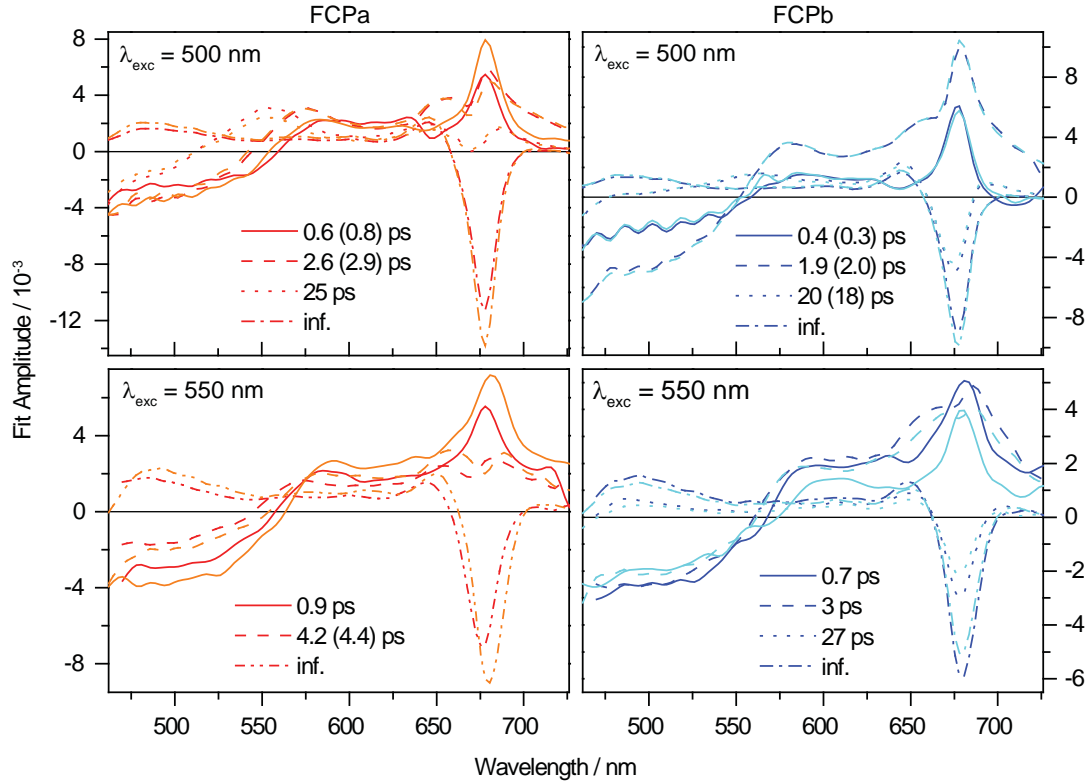


Figure 6.6: Decay associated spectra (DAS) of FCPa (left) and FCPb (right) isolated from HL (red/blue) and LL (orange/cyan) cells excited at $\lambda_{\text{exc}} = 500$ nm (top) and $\lambda_{\text{exc}} = 550$ nm (bottom). The time constants in parentheses correspond to the lifetimes of the LL cells and are only specified if they differ from the lifetimes obtained for the HL cells.

The decay associated spectra from the global fit analysis of HL-FCPa and HL-FCPb are depicted in Figure 6.8 and the corresponding lifetimes are summarized in table 6.1. After excitation at $\lambda_{\text{exc}} = 500$ nm five time constants were required to achieve an adequate fit for both samples. As mentioned before, the smallest decay time ($\tau_1 < 150$ fs) is in the range of the time resolution of the experiment and thus not shown. For τ_2 , τ_3 , and τ_{inf} the comparative analysis of FCPa and FCPb reveals a similar spectral shape as well as comparable values of the decay times. For the fit amplitudes belonging to τ_4 deviations are observed. In contrast to FCPb in FCPa the contribution of the ground state recovery of fucoxanthin is still visible around $\lambda_{\text{pr}} = 475$ nm and also the decay characteristics of the fucoxanthin ESA around $\lambda_{\text{pr}} = 560$ nm is more pronounced in FCPa. In case of FCPb for τ_4 the GSB/SE signal of Chl *a* dominates the DAS around $\lambda_{\text{pr}} = 675$ nm and only a small contribution of the decay of the fucoxanthin ESA is

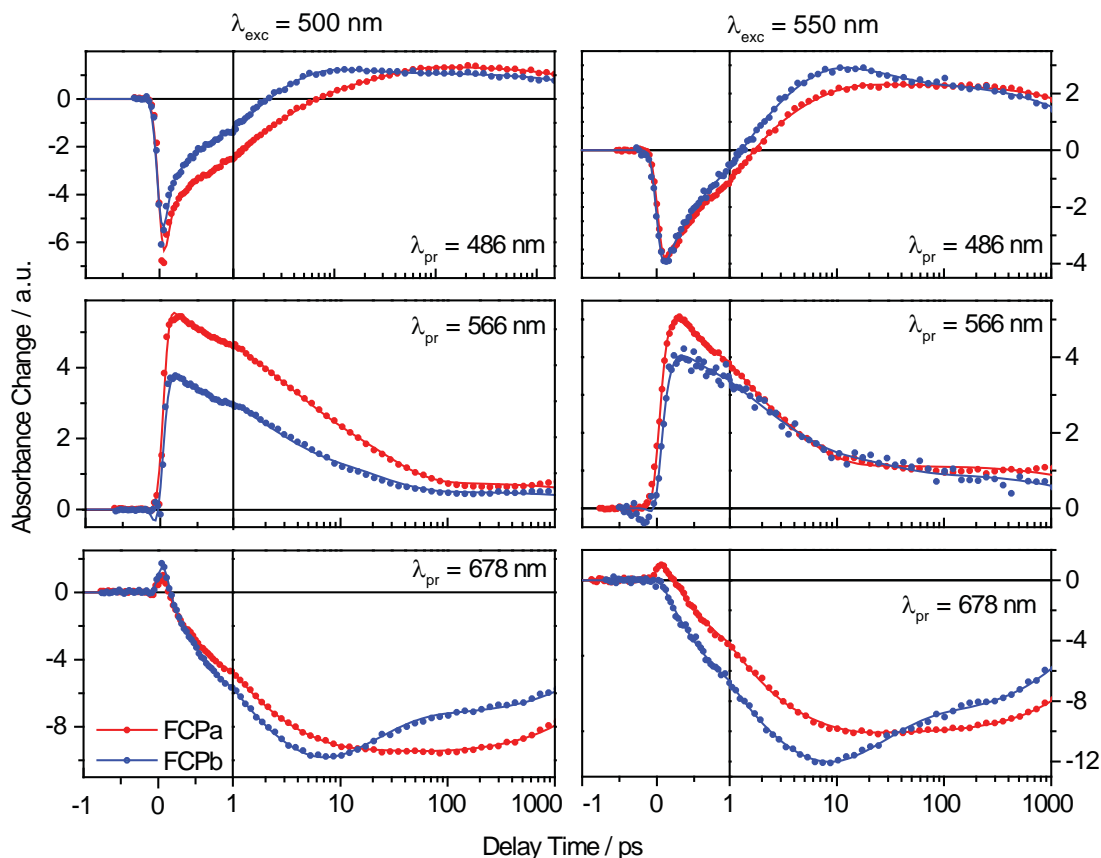


Figure 6.7: Individual transients of FCPa (red) and FCPb (blue) isolated from HL cells excited at $\lambda_{\text{exc}} = 500$ nm (left) and $\lambda_{\text{exc}} = 550$ nm (right). The data were normalized for optical density and excitation energy at the respective excitation wavelength.

visible at $\lambda_{\text{pr}} = 560$ nm. Upon $\lambda_{\text{exc}} = 550$ nm excitation of FCPb the fit amplitude associated with τ_4 shows no spectral contributions from the carotenoids but is similar to the fit amplitude obtained for τ_{inf} . For FCPa a global fit analysis with four time constants was sufficient, which will be discussed in detail in the following section.

The higher fucoxanthin ESA signal around $\lambda_{\text{pr}} = 560$ nm (Figure 6.7) could be explained with the higher total amount of diadinoxanthin and diatoxanthin in FCPa complexes. The growth conditions and accordingly the deepoxidation ratio showed no measurable influence on the excitation energy transfer. Thus, it is more likely that the amount of blue absorbing fucoxanthin molecules is higher in FCPa, because in FCPb the absorption is reduced around 490 nm and increased around 540 nm compared to FCPa (Figure 6.1). As mentioned before, HL-FCPa and LL-FCPa showed higher energy

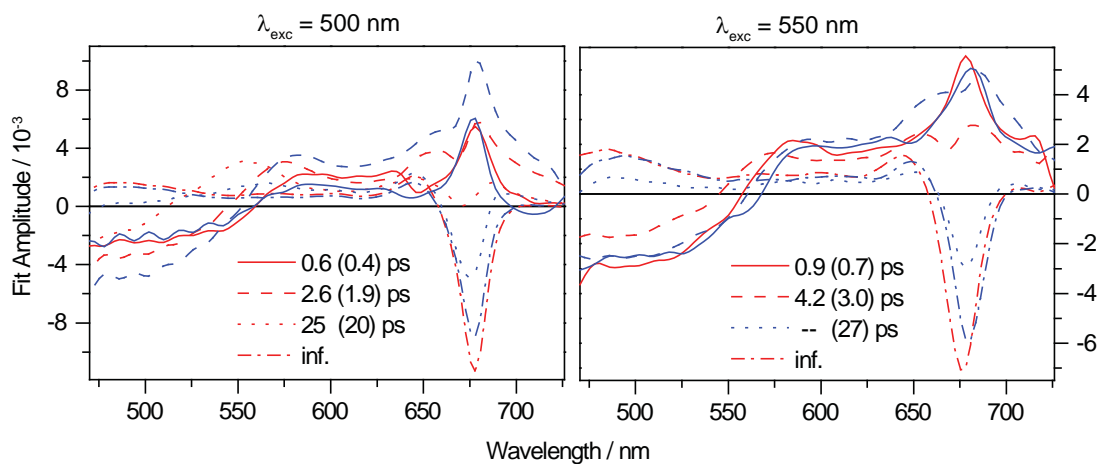


Figure 6.8: DAS of FCPa (red) and FCPb (blue) isolated from HL cells excited at 500 nm (left) and 550 nm (right). The time constants obtained for HL-FCPb are put in parentheses.

transfer efficiencies compared to FCPb complexes, thus it can be assumed that a part of the excitation energy is quenched in the higher oligomers of FCPb ("aggregation quenching") [242,243].

The transient absorption spectra recorded in the NIR spectral region were nearly identical for FCPa and FCPb (Figure 6.9). The ESA signal corresponding to the $S_2 \rightarrow S_N$ transition (Figure 6.5, $\lambda_{pr} = 1000$ nm) decays with a time constant $\tau_1 < 200$ fs for both samples. Also the ICT SE signal between $\lambda_{pr} = 950$ nm and $\lambda_{pr} = 1100$ nm (see Figure 6.9) shows a similar decay behavior for both oligomeric states. In the entire data set no evidence for a slow ICT channel was observed for fucoxanthin transferring

λ_{exc}	HL-FCPa		HL-FCPb	
	500 nm	550 nm	500 nm	550 nm
τ_2 / ps	0.6	0.9	0.4	0.7
τ_3 / ps	2.6	4.2	1.9	3.0
τ_4 / ps	25	–	20	27
τ_5 / ns	5.2	5.0	4.6	4.5

Table 6.1: Time constants obtained in a global fit analysis for HL-FCPa and HL-FCPb upon excitation at $\lambda_{exc} = 500$ nm and $\lambda_{exc} = 550$ nm, respectively.

energy to Chl *a*, since this negative signal decays within a few picoseconds [130].

6.3.3 Excitation Wavelength Dependence

The excitation of the different fucoxanthin molecules fx_{blue} and fx_{red} with $\lambda_{exc} = 500$ nm and $\lambda_{exc} = 550$ nm, respectively, results in noticeable differences in the transient absorption spectra. The differences were more pronounced in the FCPa data compared to the results obtained for FCPb. The 2D-plots in Figure 6.9 give an overview on the observed differences in the transient absorption spectra for HL-FCPa and HL-FCPb. In Figure 6.10 individual transients of FCPa and FCPb are compared and in Figure 6.11 transient spectra for different delay times for FCPa are depicted.

In the carotenoid GSB region (Figure 6.9, region A) around 500 nm and in the carotenoid ESA region (region B) mainly around $\lambda_{pr} = 560$ nm pronounced differences are observed. Upon excitation of fx_{red} at $\lambda_{exc} = 550$ nm the recovery of the ground state is faster compared to the excitation of fx_{blue} . Furthermore, the ESA around $\lambda_{pr} = 570$ nm exhibits a faster decay and is less pronounced after excitation of fx_{red} in case of FCPa. Here also the ESA of the fucoxanthins around $\lambda_{pr} = 640$ nm decays faster for $\lambda_{exc} = 550$ nm in comparison with $\lambda_{exc} = 500$ nm. The negative signal in region D belonging to the Chl *a* GSB and SE is similar for both excitation wavelengths. Probing in the NIR spectral region, the most pronounced differences are obtained for the $S_2 \rightarrow S_N$ ESA (Figure 6.9, region E). For $\lambda_{exc} = 550$ nm this ESA signal is restricted to wavelengths below 1000 nm. Upon excitation of the S_2 state of fx_{blue} molecules and probably also diadinoxanthin and diatoxanthin at $\lambda_{exc} = 500$ nm the ESA signal is clearly observed up to 1080 nm. The SE signal associated with the S_1/ICT state of fucoxanthin (region F) is slightly stronger in case of $\lambda_{exc} = 550$ nm in comparison with the data obtained for $\lambda_{exc} = 500$ nm.

The described differences are also nicely reflected in the individual decay curves depicted as examples in Figure 6.10. In the visible spectral region at $\lambda_{pr} = 486$ nm the GSB signal decays faster upon 550 nm excitation. This feature is more pronounced for FCPa. The ESA signal at $\lambda_{pr} = 566$ nm is more intense and exhibits a slower decay with $\lambda_{exc} = 550$ nm. The transients level off at different offsets associated to the ESA of Chl *a* for both excitation wavelengths. At $\lambda_{pr} = 1030$ nm the short lived ESA signal attributed to the $S_2 \rightarrow S_N$ is much stronger upon $\lambda_{exc} = 500$ nm.

The excitation wavelength dependence is also clearly observable in the transient absorption spectra of HL-FCPa depicted in Figure 6.11. Major differences are obtained in the spectrum for $\tau_D = 3$ ps, i.e. the remaining GSB for $\lambda_{pr} < 500$ nm and an additional ESA band around $\lambda_{pr} = 560$ nm. In the double difference spectrum ($\lambda_{exc} = 500$ nm minus $\lambda_{exc} = 550$ nm, inset Figure 6.11) for $\tau_D = 3$ ps these features are even more apparent. The transient spectra taken after $\tau_D = 25$ ps mainly consist of the Chl *a* contributions.

To obtain a satisfactory fit of the FCPa data for $\lambda_{exc} = 500$ nm a global fit analysis

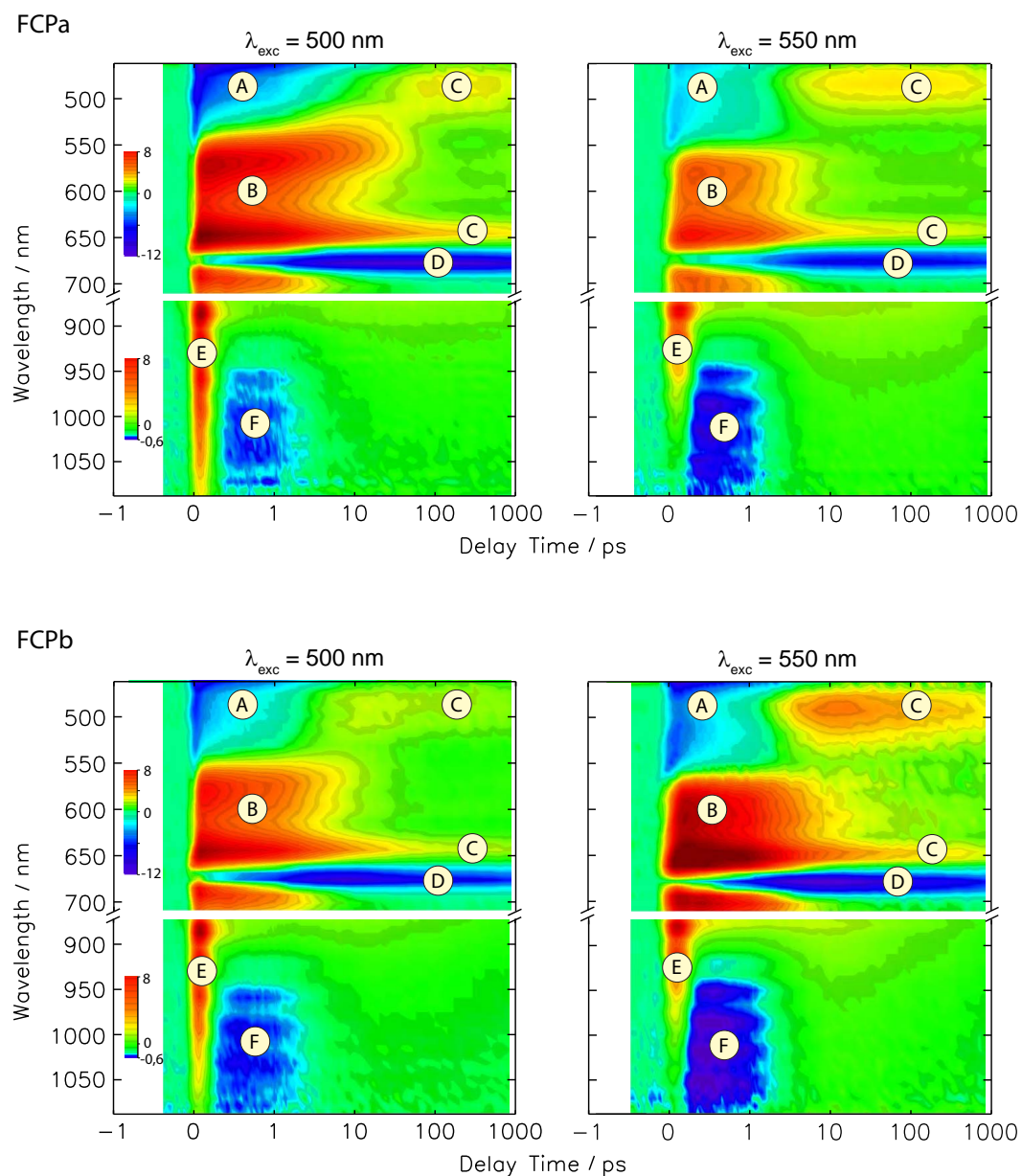


Figure 6.9: Transient absorption changes of HL-FCPa (top) and HL-FCPb (bottom) upon excitation of fx_{blue} ($\lambda_{exc} = 500$ nm) and fx_{red} ($\lambda_{exc} = 550$ nm) in the visible and NIR spectral region. The color code has different scales for the visible and NIR spectral region and displays the absorbance change in units 10^{-3} .

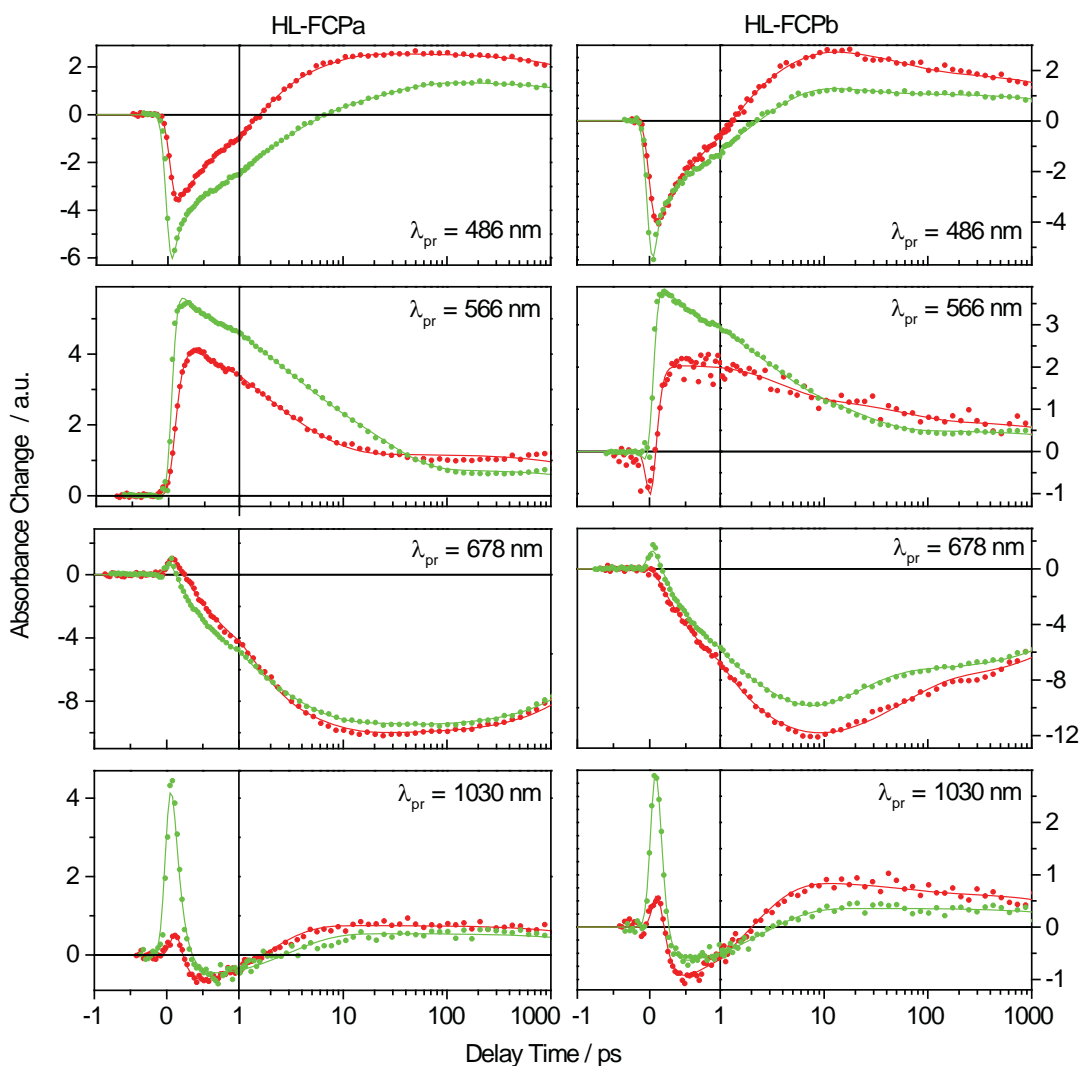


Figure 6.10: Individual transients at selected probing wavelengths for HL-FCPa (left) and HL-FCPb (right) after $\lambda_{\text{exc}} = 500$ nm (green) and $\lambda_{\text{exc}} = 550$ nm (red). The depicted curves were normalized for optical density and excitation energy.

with five time constants ($\tau_1 < 150$ fs, $\tau_2 = 0.6$ ps, $\tau_3 = 2.6$ ps, $\tau_4 = 25$ ps, and $\tau_5 = \text{infinite}$) was necessary. A comparable fit of the $\lambda_{\text{exc}} = 550$ nm data resulted in an insignificant fit amplitude of τ_4 . Thus, four time constants ($\tau_1 < 150$ fs, $\tau_2 = 0.9$ ps, $\tau_3 = 4.2$ ps, and $\tau_4 = \text{infinite}$) were sufficient for a good approximation of the data. The time constants are summarized in table 6.1. Around $\lambda_{\text{pr}} = 560$ nm the additional fit amplitude associated with $\tau_4 = 25$ ps for $\lambda_{\text{exc}} = 500$ nm clearly shows the spectral features of the $S_1/\text{ICT} \rightarrow S_n$

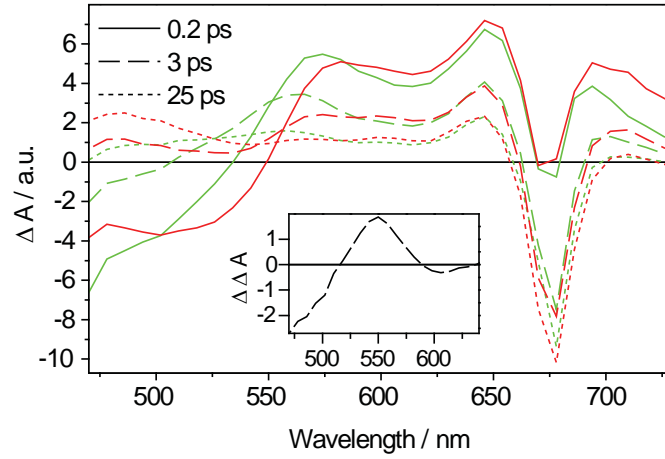


Figure 6.11: Transient absorption spectra of HL-FCPa at different delay times for $\lambda_{\text{exc}} = 500$ nm (green) and $\lambda_{\text{exc}} = 550$ nm (red). The difference $\lambda_{\text{exc}} = 500$ nm minus $\lambda_{\text{exc}} = 550$ nm calculated for the spectra recorded after 3 ps is shown in the inset.

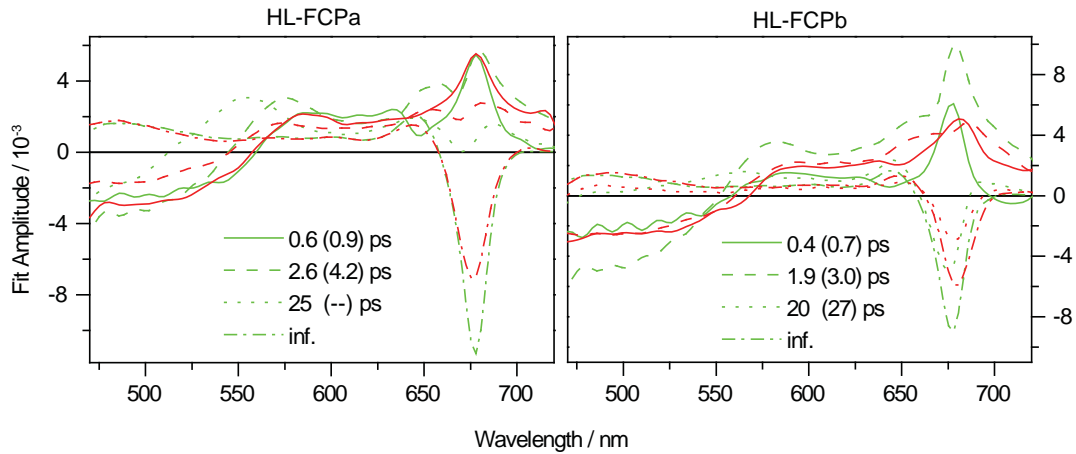


Figure 6.12: DAS of HL-FCPa (left) and HL-FCPb (right) excited at 500 nm (green) and 550 nm (red). The time constants obtained for $\lambda_{\text{exc}} = 550$ nm are put in parentheses.

transition of the fx_{blue} molecules (Figure 6.12, left panel).

In contrast, for the global fit analysis of the data obtained for FCPb five time constants were required for both excitation wavelengths ($\lambda_{\text{exc}} = 500$ nm: $\tau_1 < 150$ fs, $\tau_2 = 0.4$ ps, $\tau_3 = 2.0$ ps, $\tau_4 = 19$ ps, and $\tau_5 = \text{infinite}$; $\lambda_{\text{exc}} = 550$ nm: $\tau_1 < 150$ fs,

$\tau_2 = 0.7$ ps, $\tau_3 = 3.0$ ps, $\tau_4 = 27$ ps, and $\tau_5 = \text{infinite}$). The DAS corresponding to τ_2 , τ_3 , and τ_5 are similar, however, for τ_4 differences in the spectral shape are observed (Figure 6.12, right panel). The DAS of FCPb for $\lambda_{\text{exc}} = 550$ nm possesses only the spectral features of Chl *a* like the DAS for τ_{inf} . In the DAS obtained for $\lambda_{\text{exc}} = 500$ nm a contribution from the carotenoids around 560 nm is clearly visible though it is weaker compared to the DAS of FCPa for $\lambda_{\text{exc}} = 500$ nm (Figure 6.8).

Due to their specific microenvironment within the protein the fucoxanthin molecules obtain different spectral properties. As mentioned before, the $S_0 \rightarrow S_2$ absorption band is red shifted compared to fucoxanthin in solution. Furthermore, also the absorption maxima of the different fucoxanthins vary. Comparison of the transient absorption spectra in the NIR spectral region with regard to the two excitation wavelengths showed a stronger ICT SE signal in case of $\lambda_{\text{exc}} = 550$ nm for both FCPa and FCPb (Figure 6.10, $\lambda_{\text{pr}} = 1030$ nm). According to the results obtained for fucoxanthin in solution, it can be assumed that the red absorbing fucoxanthin molecules have a more polar protein environment compared to the blue absorbing fucoxanthins. Moreover, there is no evidence for a slow decaying ICT state, since the negative signal in the NIR spectral region attributed to the SE of the ICT state decays within 2-3 ps. The dynamics of this signal is similar for all samples and both excitation wavelengths.

6.3.4 Influence of Diadinoxanthin and Diatoxanthin on the Excitation Energy Transfer

To investigate the influence of the xanthophyll cycle pigments on the excitation energy transfer of the FCPs diadinoxanthin and diatoxanthin were removed from the samples. The isolated and purified protein complexes (FCPa) were prepared in the group of Prof. Büchel. In table 6.2 the amount of pigments contained in the investigated samples is listed normalized with respect to the Chl *a* content in HL-FCPa. Figure 6.13 shows the steady state absorption spectra of the FCPa samples normalized to the Q_y absorption maximum of Chl *a*. The spectra are very similar independent of the growth conditions and the amount of diadinoxanthin and diatoxanthin.

Sample	Chl c_2	Fucoxanthin	Diadinoxanthin	Diatoxanthin
LL-FCPa	0.33	1.06	0.02	0.01
HL-FCPa	0.30	1.00	0.03	0.03
LL-FCPa*	0.35	1.05	0	0
HL-FCPa*	0.33	1.02	0	0

Table 6.2: Pigment content in FCPa samples with and without (*) the xanthophyll cycle pigments.

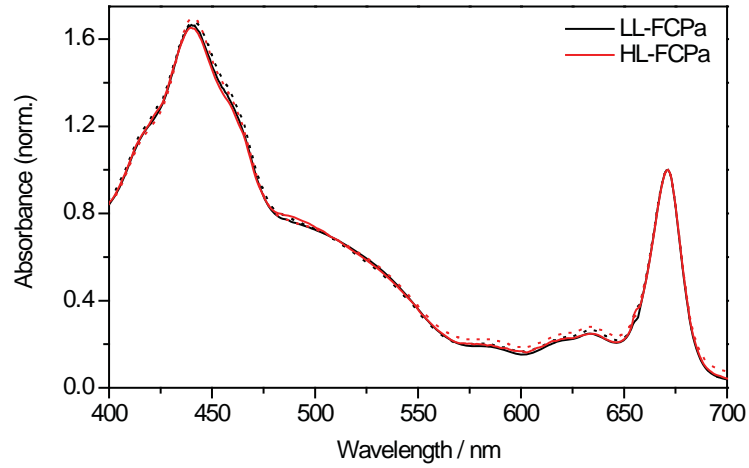


Figure 6.13: Steady state absorbance spectra of HL-FCPa (red) and LL-FCPa (black) with (—) and without (···) diadinoxanthin and diatoxanthin. The spectra were normalized to the Chl *a* Q_y absorption at 671 nm.

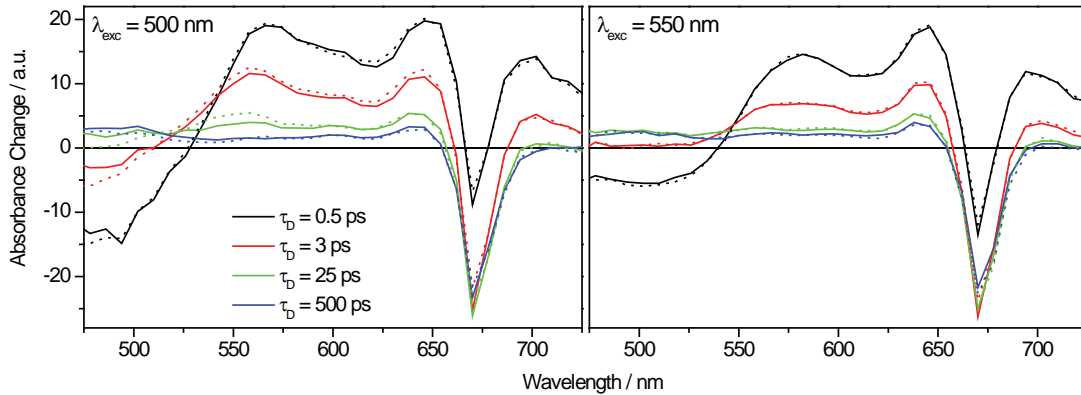


Figure 6.14: Transient absorbance spectra at different delay times τ_D of HL-FCPa excited at $\lambda_{exc} = 500$ nm (left) and $\lambda_{exc} = 550$ nm (right). The transient spectra are almost identical for both samples with (—) and without (···) the xanthophyll cycle pigments.

In Figure 6.14 transient absorbance spectra for different delay times τ_D obtained upon excitation at $\lambda_{exc} = 500$ nm (left panel) and $\lambda_{exc} = 550$ nm (right panel) are shown. All spectra at the various delay times are almost identical for both HL-FCPa samples independent of the xanthophyll cycle pigment content. If diadinoxanthin and diatoxanthin

had any influence on the excitation energy transfer one would expect differences at least for $\lambda_{\text{exc}} = 500$ nm where the xanthophyll cycle pigment should be excited. The results lead to the assumption that diadinoxanthin and diatoxanthin do not participate in the excitation energy transfer of the isolated FCP complexes. It could be also possible that they affect the dynamics too little to be observable with the resolution of the experiment. However, the differences obtained for the two excitation wavelengths seem not to stem from contributions of diadinoxanthin and diatoxanthin. Thus, the additional lifetime of 25 ps obtained for $\lambda_{\text{exc}} = 500$ nm can be attributed to a blue absorbing fucoxanthin molecule.

6.3.5 Excitation of Chl c_2

Chl c_2 was excited directly at $\lambda_{\text{exc}} = 630$ nm to investigate the energy transfer from Chl c_2 to Chl a in FCPs. The 2D spectra of the transient absorption experiments are shown in Figure 6.16 (top). Upon excitation of Chl c_2 one observes a transient spectrum of Chl a with the same spectral characteristics as obtained for large delay times for FCP complexes after excitation of the carotenoids. This is shown in the transient spectra taken at $\tau_D = 1$ ns for $\lambda_{\text{exc}} = 500$ nm, $\lambda_{\text{exc}} = 550$ nm, and $\lambda_{\text{exc}} = 630$ nm compared with $\tau_D = 0.5$ ps for $\lambda_{\text{exc}} = 630$ nm in Figure 6.15. The results indicate an extremely fast excitation energy transfer between the two chlorophyll species which could not be resolved in this experiment. Thus, it can be assumed that this energy transfer is complete within the first 150 fs.

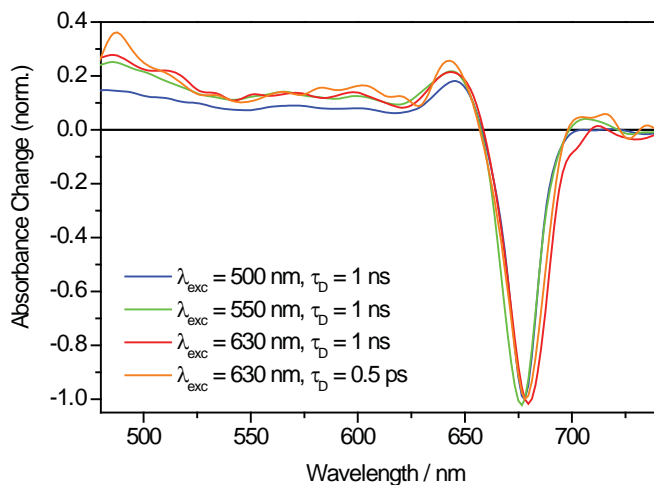


Figure 6.15: Comparison of the transient spectra recorded upon excitation of the red and blue absorbing fucoxanthins and Chl c_2 .

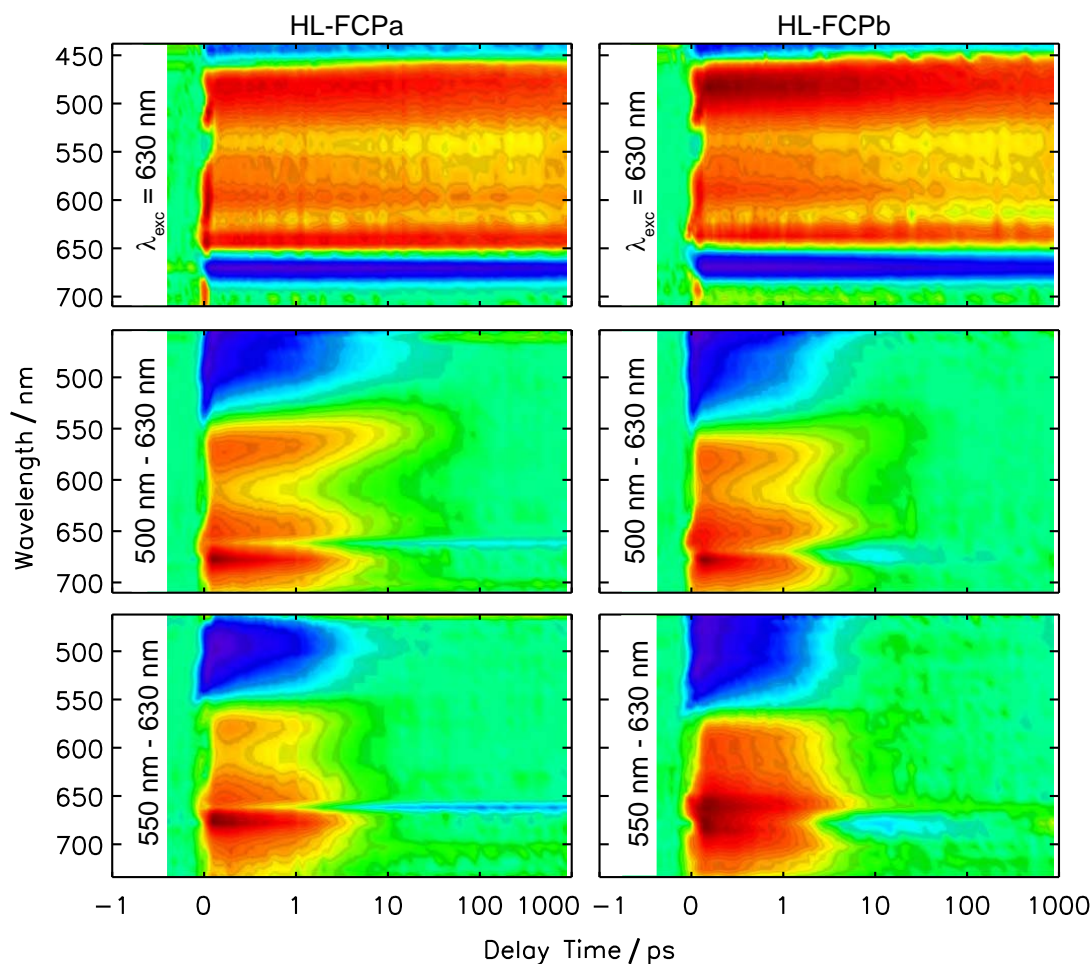


Figure 6.16: 2D-plots of the results obtained from Chl c_2 excitation at $\lambda_{\text{exc}} = 630$ nm (top) and calculated double difference spectra for HL-FCPa and HL-FCPb. The data obtained from $\lambda_{\text{exc}} = 630$ nm was subtracted from the data obtained from $\lambda_{\text{exc}} = 500$ nm (middle) and $\lambda_{\text{exc}} = 550$ nm (bottom), respectively. The double difference spectra show the transient carotenoids signals within the protein complexes.

The measurements were used to calculate a double difference spectrum of the spectra obtained for $\lambda_{\text{exc}} = 630$ nm minus $\lambda_{\text{exc}} = 500$ nm or $\lambda_{\text{exc}} = 550$ nm, respectively. The 2D-plots of the calculated differences are shown in Figure 6.16 for FCPa and FCPb. These double difference spectra reflect the transient absorption dynamics of fucoxanthin in FCP complexes. Both, the GSB and S_1 /ICT ESA are red shifted compared to fucoxanthin in solution (Figure 5.6, page 69). Additionally, the lifetime of the first excited state is considerably shorter due to the fast and efficient energy transfer to Chl a . As observed

for the transient spectra of FCPa and FCPb depicted in Figure 6.9 in case of the 500 nm – 630 nm double difference spectrum the S_1 excited state lifetime around $\lambda_{pr} = 550$ nm is longer compared to the 550 nm – 630 nm difference spectrum. As mentioned before, this effect is more pronounced in case of the FCPa samples.

6.3.6 Energy Transfer Model

In order to demonstrate the different energy transfer pathways for the two excitation wavelengths a model was designed for FCPa. With slight modifications the model might also be applied for FCPb due to the similarities in the transient absorption spectra. The model is based on analog schemes for LHC from *Amphidinium carterae* which contains peridinin [245] and for FCPs from *C. meneghiniana* obtained from former transient absorption experiments [130]. Based on the data obtained for the two excitation wavelengths the existence of at least two types of fucoxanthin molecules could be confirmed. Both, red and blue absorbing fucoxanthins are supposed to transfer their excitation energy very fast from the second excited singlet state to Chl *a* with lifetimes < 200 fs. After internal conversion to the first excited singlet state energy is transferred very ef-

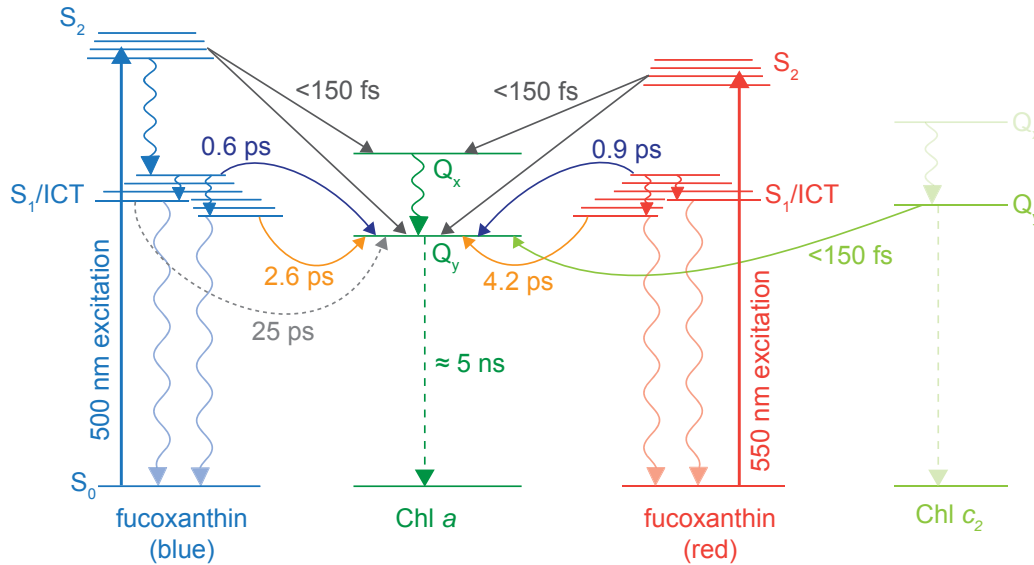


Figure 6.17: Schematic model describing the excitation energy transfer in HL-FCPa upon excitation of blue and red absorbing fucoxanthin molecules. The solid arrows depict the main energy transfer channels. The dashed arrow represents the Chl *a* fluorescence and the wavy arrows represent intramolecular decay processes. The dotted arrow denotes the slow transfer channel most probably from a blue absorbing fucoxanthin. An energy transfer channel from diadinoxanthin to Chl *a* cannot be excluded.

ficient from the vibrationally excited as well as relaxed S_1 /ICT state to Chl *a* resulting in two additional lifetimes (0.6/0.9 ps and 2.6/4.2 ps for HL-FCPa).

The results from the samples without diadinoxanthin and diatoxanthin showed no evidence for an energy transfer from diadinoxanthin and diatoxanthin. At least the energy transfer from diatoxanthin can be excluded, since it was found in former experiments that its energy lies below the energy of the Q_y state of Chl *a* [126]. In the experiments performed within the scope of this work neither changes in the deepoxidation ratio nor removing of the xanthophyll cycle pigments showed any influence on the investigated energy transfer processes. However, the energy transfer from diadinoxanthin could be very weak since it is contained only in substoichiometric amounts. The contribution to the measured absorption changes could be very weak and perhaps is not detectable with the resolution of the experiment. Hence, the 25 ps time constant found in the presented data can be attributed to the S_1 state of fucoxanthin. Furthermore, it can be concluded that the first excited singlet state of this specific fucoxanthin molecule has a very weak charge transfer character because the SE signal detected in the NIR spectral region decays within 2-3 ps. In contrast the signal corresponding to the $S_1 \rightarrow S_n$ transition has a lifetime of 25 ps.

6.4 Transient Anisotropy Measurements

To further investigate the energy transfer additional polarized transient absorption experiments were performed with HL-FCPa. As described in the previous section, the HL-FCPa samples were excited at 500 nm and 550 nm. Transient absorption spectra for different relative polarizations (parallel, magic angle, and perpendicular) of pump and probe pulses were recorded and analyzed. Therefore, the pump beam passes a zero-order half-wave plate that allows easy adjustment of its polarization with respect to the probe beam. To control the success of the measurements the parallel (ΔA_{\parallel}) and the perpendicular (ΔA_{\perp}) data were used to calculate the isotropic data ($\Delta A_{ma} = [\Delta A_{\parallel} + 2\Delta A_{\perp}]/3$). If the calculated isotropic data is in good agreement with the data obtained from magic angle polarization one can assume that the experiment worked. The time dependent anisotropy was calculated according to equation 3.6 (see chapter 3.1.1, page 25).

Figure 6.18 contains the experimental traces and the fitting curves for both excitation wavelengths. At $\lambda_{pr} = 486$ nm the GSB of the carotenoids followed by the Chl *a* ESA is visible and the kinetic trace at $\lambda_{pr} = 590$ nm shows the rise of the S_1 /ICT ESA of fucoxanthin decaying into the weak, long living ESA of Chl *a*. As expected, the measured decay curves have the highest values for parallel and the lowest values for perpendicular pump/probe polarization orientation. At longer delay times all kinetic traces decay to the same ΔA values. A global fit analysis of the data obtained from magic angle polarization resulted in the same time constants as obtained for the experiments presented in the previous section depicted in table 6.1. The obtained decay times were therefore kept constant for the analysis of the data from parallel and perpendicular

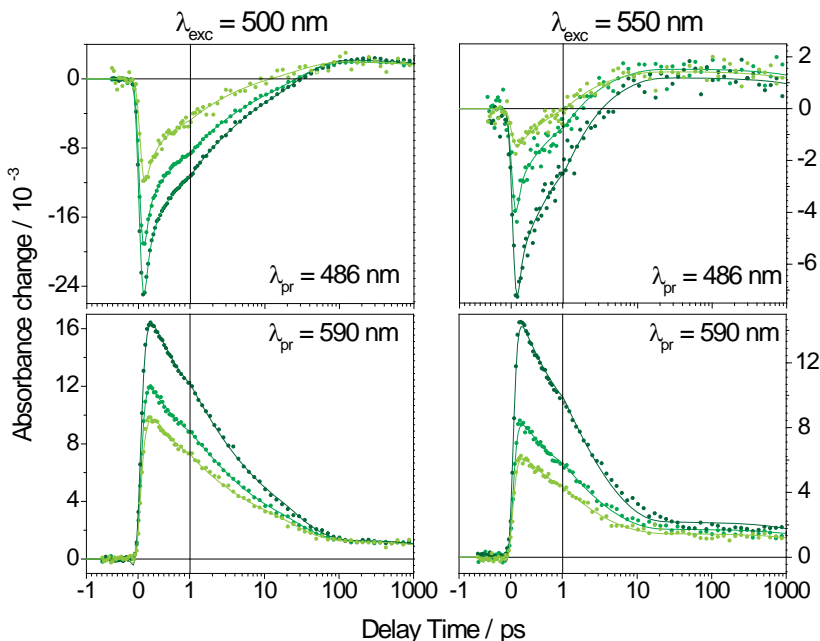


Figure 6.18: Anisotropy data (●) and fit curves (–) of HL-FCPa after $\lambda_{\text{exc}} = 500$ nm (left) and $\lambda_{\text{exc}} = 550$ nm (right). The plots demonstrate the quality of the fit with the same time constants for all three polarizations (parallel: dark green, magic angle: green, perpendicular: light green).

polarization. The plots in Figure 6.18 including the data and the respective fit curves demonstrate the quality of these fits.

For both excitation wavelengths the DAS are displayed in Figure 6.19. Just like the kinetic traces the fit amplitudes are lowest for perpendicular polarization, intermediate for magic angle polarization, and largest for parallel polarization. As mentioned before, the first time constant $\tau_1 < 150$ fs is below the time resolution of the experiment, thus the corresponding fit amplitude is not shown. Again, for τ_2 , τ_3 , and τ_5 the DAS are very similar for both excitation wavelengths. The DAS of $\tau_5 = \text{inf.}$ closely resemble each other. A significant fit amplitude corresponding to τ_4 was only obtained for $\lambda_{\text{exc}} = 500$ nm. For the $\lambda_{\text{exc}} = 550$ nm data again four time constants were sufficient for a satisfactory fit.

Besides the recovery of the GSB around $\lambda_{\text{pr}} = 500$ nm the DAS of $\tau_2 = 0.6/0.9$ ps shows the decay of two ESA bands with their maxima at $\lambda_{\text{pr}} = 585$ nm and $\lambda_{\text{pr}} = 680$ nm, respectively. These two maxima can be assigned to the fucoxanthin ESA of the S_1 state (585 nm) and of the ICT state (680 nm) referring to the two bands obtained in transient absorption measurements of fucoxanthin in polar solvents (see chapter 5.2). The

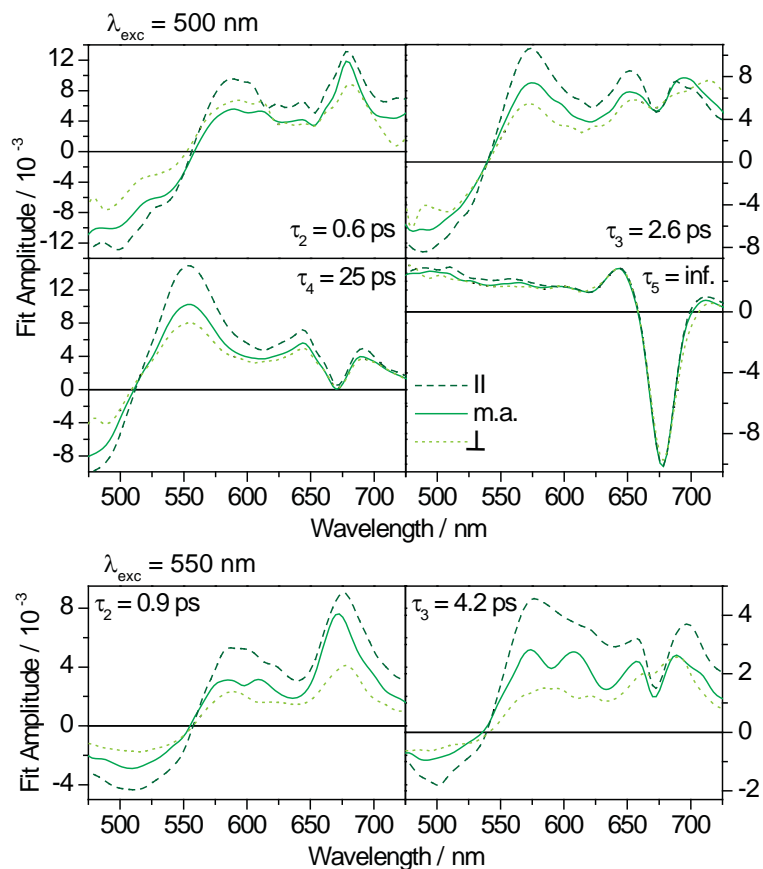


Figure 6.19: DAS for HL-FCPa upon excitation at $\lambda_{\text{exc}} = 500$ nm (top) and $\lambda_{\text{exc}} = 550$ nm (bottom) derived from the global fit analysis with fixed time constants for all polarizations. The amplitudes for τ_{inf} are similar for both excitation wavelengths and thus not shown for $\lambda_{\text{exc}} = 550$ nm. Again, for describing the dynamics upon $\lambda_{\text{exc}} = 550$ nm four time constants are sufficient, thus a respective amplitude for τ_4 does not exist.

maximum around $\lambda_{\text{pr}} = 585$ nm associated to the S_1 ESA of fucoxanthin is slightly blue-shifted in case of $\lambda_{\text{exc}} = 500$ nm. Around 675 nm the DAS for τ_3 contain a contribution of the GSB/SE decay of Chl *a* with the same magnitude for all polarizations. According to that the anisotropy vanishes after the energy transfer from the fucoxanthin molecules to Chl *a* as can be also concluded from the transient dynamics depicted in Figure 6.18. Upon $\lambda_{\text{exc}} = 500$ nm the DAS of $\tau_4 = 25$ ps mainly contains the spectral features of the decay of the $S_1/\text{ICT} \rightarrow S_n$ transition of the blue absorbing fucoxanthins shifted further to the blue with a maximum around $\lambda_{\text{pr}} = 550$ nm. The DAS of $\tau_5 = \text{inf}$ represents the difference spectrum at the maximum observation time of $\tau_{\text{D}} = 1.5$ ns. The DAS show an

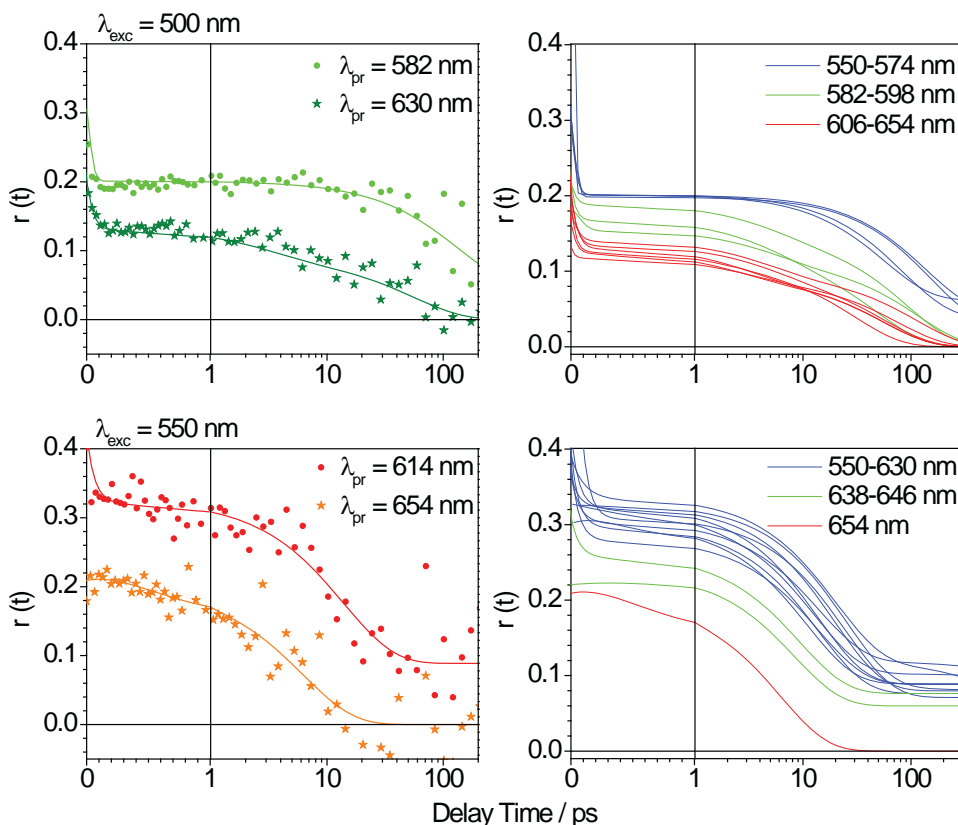


Figure 6.20: Left: Time dependent anisotropy decay $r(t)$ calculated from the parallel (ΔA_{\parallel}) and perpendicular (ΔA_{\perp}) signals for $\lambda_{\text{exc}} = 500$ nm (top) and $\lambda_{\text{exc}} = 550$ nm (bottom). The solid lines represent the fit curves of the calculated anisotropy values. Right: Fit curves for several probing wavelengths corresponding to the S_1 (blue) and the ICT (red) ESA signal. The time axis is restricted to delay times less than 300 ps.

identical shape for both excitations wavelengths displaying solely Chl *a* characteristics. The amplitudes are equal for all polarizations which is equivalent to an isotropic signal. It can be concluded that the initial anisotropy becomes zero after the energy transfer from fucoxanthin to Chl *a* is finished and probably most of the excitation energy is transferred to the Chl *a* molecules.

The analysis of the temporal behavior of the anisotropy was possible in the spectral region between 550 nm and 650 nm where only the S_1 /ICT ESA signal of fucoxanthin contributes. Figure 6.20 (left panel) contains the exemplary results at $\lambda_{\text{pr}} = 582$ nm and $\lambda_{\text{pr}} = 630$ nm for $\lambda_{\text{exc}} = 500$ nm (top) and at $\lambda_{\text{pr}} = 614$ nm and $\lambda_{\text{pr}} = 654$ nm for $\lambda_{\text{exc}} = 550$ nm (bottom). The data points represent the calculated anisotropy values from the parallel (ΔA_{\parallel}) and perpendicular (ΔA_{\perp}) signals at different delay times. The solid

lines in all four panels show the curves obtained from the fit analysis of the calculated time dependent anisotropy for different probe wavelengths.

At early delay times before the excitation energy transfer takes place high positive anisotropy values are expected. These initial anisotropy values are hard to determine due to the coherent artifact around delay time zero. Furthermore, the S_2 state of the fucoxanthins is excited which decays to the S_1 /ICT state or directly transfers its excitation energy to Chl *a* extremely fast with a time constant in the range of the time resolution of the experiment. Thus, the initial anisotropy values $r(t)$ decrease almost instantaneous within the first 100 fs to a constant value. These anisotropy values most probably reflect the transition dipole moments of the excited fucoxanthins in the S_1 /ICT state. Subsequently the anisotropy value again decays with faster dynamics obtained for $\lambda_{\text{exc}} = 550$ nm which is in accordance with the faster dynamics observed for the kinetics shown in the Figures 6.18 and 6.9 (page 93). The anisotropy values and the time dependent decays not only vary for the two excitation wavelengths but also depend on the probing wavelength. The right panels in Figure 6.20 show the anisotropy decays for the whole analyzed spectral region. Taking into account that the S_1 state of fucoxanthin absorbs in the blue region of the ESA band, whereas the ICT ESA signal is observed in the red part, different anisotropy values for the two states can be obtained. For $\lambda_{\text{exc}} = 500$ nm the anisotropy value decays from $r(t) = 0.20$ to an offset of $r(t) = 0.08$ after ≈ 100 ps in the spectral region between 550 nm and 574 nm which is associated with $S_1 \rightarrow S_n$ transition (Figure 6.20, blue curves). The anisotropy value for this spectral probing region is higher ($r(t) = 0.30$) upon excitation with $\lambda_{\text{exc}} = 550$ nm. However, it decays faster compared to the data obtained for $\lambda_{\text{exc}} = 500$ nm to approximately the same offset ($r(t) = 0.09$). After $\lambda_{\text{exc}} = 550$ nm the ESA band of fucoxanthin appears to be red shifted and is thus superimposed by the strong negative signal of Chl *a* around $\lambda_{\text{pr}} = 675$ nm. The anisotropy decay attributed to the ICT ESA of fucoxanthin (Figure 6.20, red curves) at $\lambda_{\text{pr}} = 654$ nm for $\lambda_{\text{exc}} = 550$ nm is again faster and drops from $r(1 \text{ ps}) = 0.17$ to $r(< 30 \text{ ps}) = 0$. Upon $\lambda_{\text{exc}} = 500$ nm the anisotropy value corresponding to the ICT ESA band ($\lambda_{\text{pr}} = 606\text{-}654$ nm) decays from $r(1 \text{ ps}) = 0.12$ to $r(> 300 \text{ ns}) = 0$. The green curves in Figure 6.20 (right panels, $\lambda_{\text{pr}} = 582\text{-}598$ nm and $\lambda_{\text{pr}} = 638\text{-}646$ nm) correspond to the spectral region between the S_1 and ICT ESA bands and can not be clearly assigned.

The instantaneous decay of the anisotropy value due to the internal conversion from the excited S_2 state to the S_1 /ICT state of fucoxanthin indicates that the S_1 /ICT transition dipole moment is oriented differently from the S_2 transition dipole moment. Assuming an initial anisotropy value of 0.4 the angles between the transition dipole moments can be calculated. For $\lambda_{\text{exc}} = 500$ nm the obtained anisotropy values correspond to averaged angles of 35° (S_1) and 43° (ICT) between the transition dipole moments. In case of $\lambda_{\text{exc}} = 550$ nm the calculated angles are slightly smaller with 24° (S_1) and 38° (ICT). In previous anisotropy studies by Andersson et al. [246,247] with other carotenoids in solution an angle of 23° was obtained between the S_2 and S_1 transition dipole moments. The investigation of the peridinin-chlorophyll protein (PCP) with polarized transient

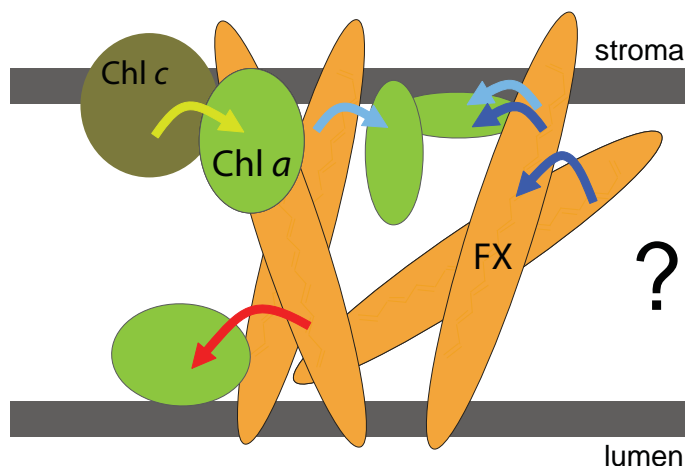


Figure 6.21: Simplified FCP model adopted from Figure 2.9 (page 16). The arrows denote possible energy transfer channels between the pigments contained in a monomer. The dark blue arrows represent the energy transfer from a fucoxanthin to Chl *a* via a second fucoxanthin molecule resulting in a slower transfer channel.

absorption spectroscopy by Krüger et al. [153] revealed an angle of 25° between the S_2 and S_1 transition dipole moments.

The dependence of the anisotropy value on the probing wavelengths in the S_1 /ICT ESA region indicates that the transition dipole moments of the S_1 state and the ICT state slightly differ. In addition, the anisotropy value varies with the excitation wavelength. The averaged angle of 24° obtained for $\lambda_{\text{exc}} = 550$ nm and attributed to the $S_1 \rightarrow S_n$ transition matches the findings for PCP and other carotenoids [153,246,247]. In case of $\lambda_{\text{exc}} = 500$ nm the mean angle is larger (35°), indicating that the determined anisotropy values are a mixture of the blue absorbing fucoxanthin molecules.

In LHCII the energy transfer from Chl *b* to Chl *a* is very fast with a time constant in the range of ≈ 250 fs [248–251]. Due to the results of the excitation of Chl c_2 one can assume that the energy transfer from Chl c_2 to Chl *a* in FCPs is equally fast. Thus, an ultrafast energy transfer from fucoxanthin via the Chl c_2 molecule could also be possible. Furthermore, an energy transfer between the S_1 /ICT states of different fucoxanthin molecules before the transfer to Chl *a* cannot be excluded. In theoretical studies of PCP Damjanović et al. found out that the $S_1 \rightarrow S_1$ energy transfer between two peridinin molecules is much slower compared to the energy transfer from the peridinin S_1 state to Chl *a* [252]. If we assume a similar kinetic situation for fucoxanthin in FCP, a $S_1 \rightarrow S_1$ excitation energy transfer between two blue absorbing fucoxanthin molecules preceding the $S_1 \rightarrow$ Chl *a* energy transfer could be responsible for the additional lifetime of 25 ps

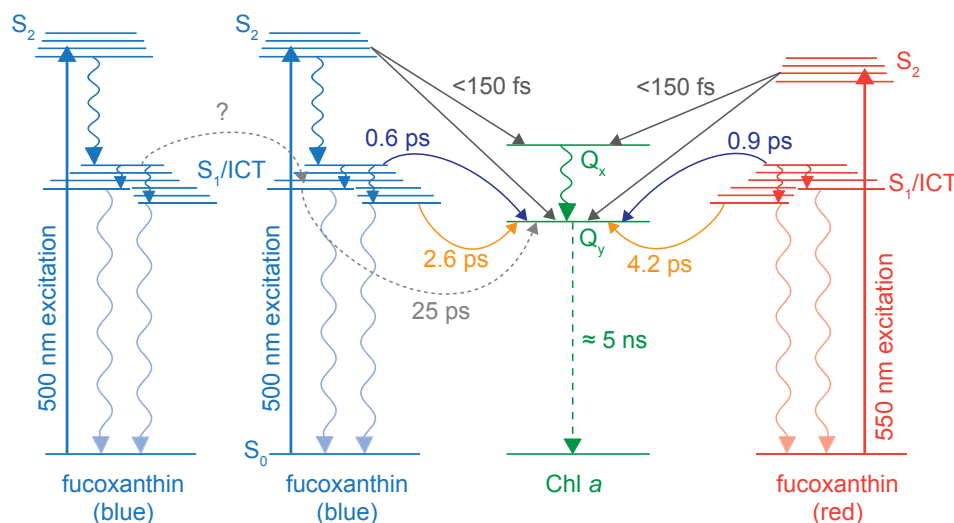


Figure 6.22: Modified schematic model describing the excitation energy transfer in HL-FCPa. In contrast to Figure 6.17 the energy transfer between two fucoxanthin molecules is considered based on the results from the anisotropy experiments. In this model the $\text{Chl } c_2 \rightarrow \text{Chl } a$ energy transfer is not included.

upon $\lambda_{\text{exc}} = 500 \text{ nm}$. This is in accordance with the dynamics observed for the intersected GSB/SE signal of $\text{Chl } a$ around $\lambda_{\text{pr}} = 675 \text{ nm}$ (Figure 6.10). Around $\tau_{\text{D}} = 25 \text{ ps}$ this signal already decreases for $\lambda_{\text{exc}} = 550 \text{ nm}$, whereas for $\lambda_{\text{exc}} = 500 \text{ nm}$ it slightly rises.

The FCP model is depicted in Figure 6.21 and the modified transfer scheme in Figure 6.22 can be used to summarize the presented results. Based on previous Stark spectroscopy measurements [42] and the presented results above, it can be assumed that the FCPs contain one red absorbing fucoxanthin molecule transferring the energy directly to one $\text{Chl } a$ molecule (red arrow). Two of the three remaining fx_{blue} molecules per FCP monomer seem to transfer the excitation energy directly to $\text{Chl } a$ and should therefore be located close to them (light blue arrows). At least one blue absorbing fucoxanthin molecule is probably not strongly associated with a $\text{Chl } a$ molecule and seems to transfer its excitation energy via a second fucoxanthin molecule to $\text{Chl } a$ (dark blue arrows). This is in agreement with the faster overall energy transfer rate in FCPa and which is also evident in the anisotropy decay for $\lambda_{\text{exc}} = 550 \text{ nm}$ and the slow transfer channel which is active in case of $\lambda_{\text{exc}} = 500 \text{ nm}$. $\text{Chl } c_2$ transfers its excitation energy very fast and efficient to $\text{Chl } a$ (yellow arrow).

Chapter 7

Coherent Effects

Life's a box of chocolates, Forrest. You never know what you're gonna get.

(Mrs. Gump in *Forrest Gump*)

In most of the transient absorption spectra measured within the scope of this work the ultrafast dynamics are superimposed by oscillations. These coherent contributions mainly appear in the red edge of the transient absorption spectra recorded in the visible spectral region corresponding to the S_1 /ICT ESA of fucoxanthin. The oscillations are reproducible and observed for different carotenoids in solution as well as FCP complexes. In the following chapter the coherent effects are analyzed and possible explanations are discussed.

Additional experiments were performed in order to investigate the influence of different parameters on the oscillatory features. The dependence on the excitation and probing wavelength as well as on the solvent environment was studied for fucoxanthin. For a better resolution of the oscillations the time resolution of the transient absorption measurements was optimized by means of the prism compressor in combination with the autocorrelator. Time resolutions down to 50-80 fs could be achieved depending on the probing wavelength.

7.1 Carotenoids in Solution

In Figure 7.1 the transient absorbance changes upon excitation at $\lambda_{\text{exc}} = 500$ nm of fucoxanthin in ethanol are displayed in a 2D-plot. The spectral region between 675-750 nm is enlarged from -0.2 ps to 1 ps in the right panel to demonstrate the oscillations which superimpose the excited state dynamics. In Figure 7.2 single transients at $\lambda_{\text{pr}} = 488$ nm

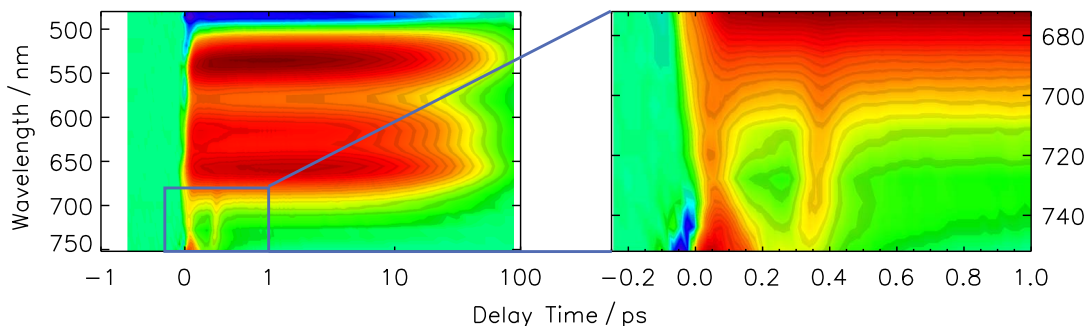


Figure 7.1: 2D-plot of the transient absorption spectra of fucoxanthin in ethanol focusing on the oscillations observed in the red edge of the S_1 /ICT ESA region.

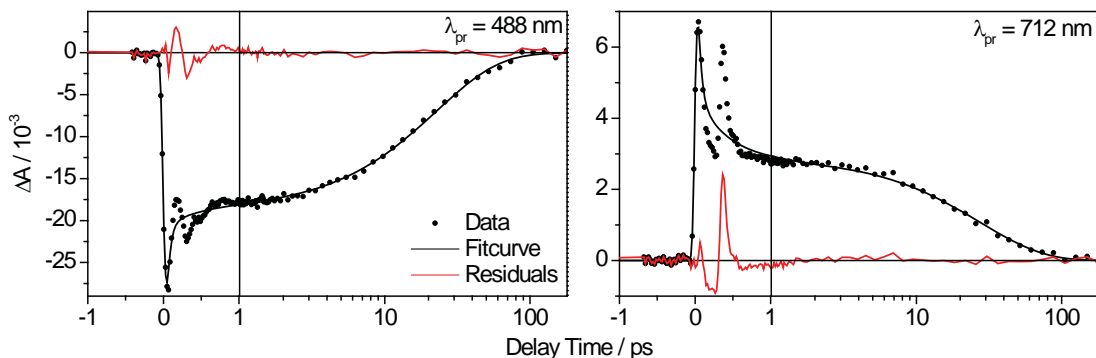


Figure 7.2: Individual transients of fucoxanthin in ethanol with coherent oscillations observed in the GSB ($\lambda_{pr} = 488$ nm) and ESA region ($\lambda_{pr} = 712$ nm). The data (dots) is fitted (black solid line) with a sum of exponentials in a global fit analysis. The fit curve is subtracted from the data to obtain the pure oscillations (red solid line).

and $\lambda_{pr} = 712$ nm for fucoxanthin in ethanol are depicted. Though in most cases the oscillations are observed between $\lambda_{pr} = 670 - 750$ nm in the red edge of the S_1 /ICT ESA region for a few samples also coherent effects are monitored in other spectral regions. In this case the oscillatory features superimpose the GSB signal of fucoxanthin at $\lambda_{pr} = 488$ nm.

The oscillatory features are analyzed by fitting of the data with a sum of exponential decays in a global fit analysis. Obviously, the oscillations superimposing the kinetics cannot be described by a simple combination of exponential decays. The fitting curves obtained either by a global analysis or by fitting of the single transients thus only account for the exponential kinetic components and do not describe the coherent contributions

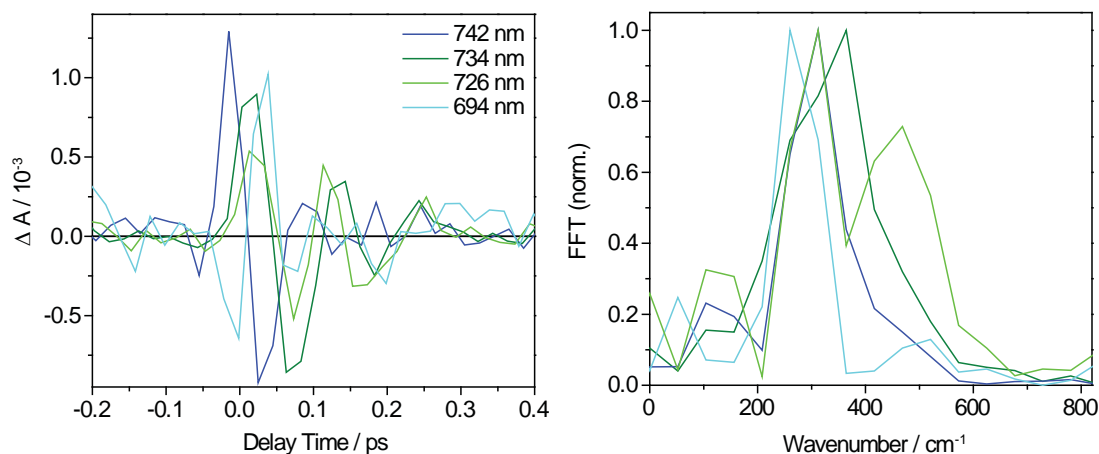


Figure 7.3: Coherent artifact obtained for pure ethanol between $\lambda_{pr} = 690 - 750$ nm (left). The solvent signal was analyzed by a Fourier transformation (right) like done for the residuals of the samples.

as shown in Figure 7.2. The fitting curves are subtracted from the original data. The residual curves contain the pure oscillations (Figure 7.2, red solid line). For further analysis the residuals were Fourier transformed. It has to be mentioned, that with this method it is not possible to separate the first oscillation from the coherent artifact and a potential ultrafast kinetic, since they all appear on the same time scale. The amplitude of the fast time constant may thus contain contributions of all of these three effects. Consequently the amplitude of the first oscillatory part would be underestimated in the residual plot leading to the unusual damping behaviour observed in most experiments.

To ensure that the observed oscillations are not due to contributions of the coherent artifact to the excited state dynamics, the signals observed for measurements with the pure solvent were analyzed just as the oscillatory features obtained for the samples. The coherent artifact was characterized in the spectral region where the oscillations are most pronounced in case of the dissolved carotenoids as well as the FCP complexes. The coherent artifact of ethanol is shown in Figure 7.3 (left panel) for different probing wavelengths and the corresponding FFT spectra are shown in the right panel. In case of pure ethanol for the frequency a mean value of ≈ 300 cm^{-1} was obtained corresponding to an oscillation period of ≈ 110 fs. The purpose of this analysis was just to compare the FFT spectra of both solvent and sample and were not done in order to determine a mode of ethanol. However, the obtained frequency of ≈ 300 cm^{-1} is comparable to values obtained in a comprehensive analysis of the coherent artifact by Kovalenko et al. [238]. In the cited publication different effects contributing to the coherent artifact are considered. The analysis of oscillations caused by impulsive stimulated Raman-

scattering resulted in a prominent mode at 367 cm^{-1} for pure chloroform [238]. Though the values are similar for ethanol comparable oscillatory features are not observed. The FFT spectra displayed in Figure 7.3 are only due to the coherent artifact itself and do not show a vibrational mode in ethanol.

Fucoxanthin

To further characterize the oscillations for a range of different conditions such as the excitation and probing wavelengths as well as the solvent environment, a large number of experiments with fucoxanthin were performed. The results for fucoxanthin dissolved in acetonitrile, ethanol, diethyl ether, and n-hexane are displayed in the left panel of Figure 7.4. The excitation wavelength was varied from $\lambda_{\text{exc}} = 480\text{ nm}$ to 500 nm and 520 nm . The oscillations show a very unusual damping behavior since they disappear already after two periods. They were more pronounced in polar solvents. In case of acetonitrile and diethyl ether the coherent effects are most prominent upon excitation at $\lambda_{\text{exc}} = 480\text{ nm}$. The second oscillation period is even higher than the first one. The transient absorption spectra recorded for fucoxanthin in ethanol seem not to have a significant excitation wavelength dependence. In principle, the residual curves show a very similar temporal behavior of the oscillatory features for all solvents and excitation wavelengths.

In Figure 7.5 the corresponding FFT spectra are depicted and compared for ethanol with varying excitation and probing wavelengths (upper panels) as well as for different solvents (lower panel). The obtained values for the frequencies and corresponding periods of oscillation are summarized in table 7.1. The frequency values of $\approx 100\text{ cm}^{-1}$ are significantly shorter compared to the values of $\approx 300\text{ cm}^{-1}$ obtained for the coherent artifact of pure ethanol depicted in Figure 7.3. Thus, the coherent artifact can be excluded as the origin of the coherent effects.

In case of fucoxanthin in ethanol the maximum of the FFT spectra is located around 95 cm^{-1} corresponding to an oscillation period of $\approx 350\text{ fs}$ upon excitation with $\lambda_{\text{exc}} = 500\text{ nm}$. The FFT spectra are very similar independent of the probing wavelengths. Nearly identical FFT spectra and oscillation periods are obtained for $\lambda_{\text{pr}} = 718\text{ nm}$ (Figure 7.5, right upper panel) and $\lambda_{\text{pr}} = 734\text{ nm}$ (data not shown). In contrast slightly different frequency values are obtained for the different excitation wavelengths. Though the FFT spectral width is similar the maxima shift to higher frequencies with increasing excitation wavelength.

For fucoxanthin in acetonitrile the frequencies of the oscillations were $\approx 100\text{ cm}^{-1}$ with a slightly shorter oscillation periods of $\approx 320\text{ fs}$ compared to ethanol. For acetonitrile the oscillation period is nearly constant independent of the probing and excitation wavelengths. With decreasing solvent polarity the period of oscillations seems to increase further, since for diethyl ether and n-hexane frequencies of $\approx 70\text{ cm}^{-1}$ ($\hat{=}$ 480 fs) and $\approx 80\text{ cm}^{-1}$ ($\hat{=}$ 420 fs) were obtained, respectively. This solvent dependence has to

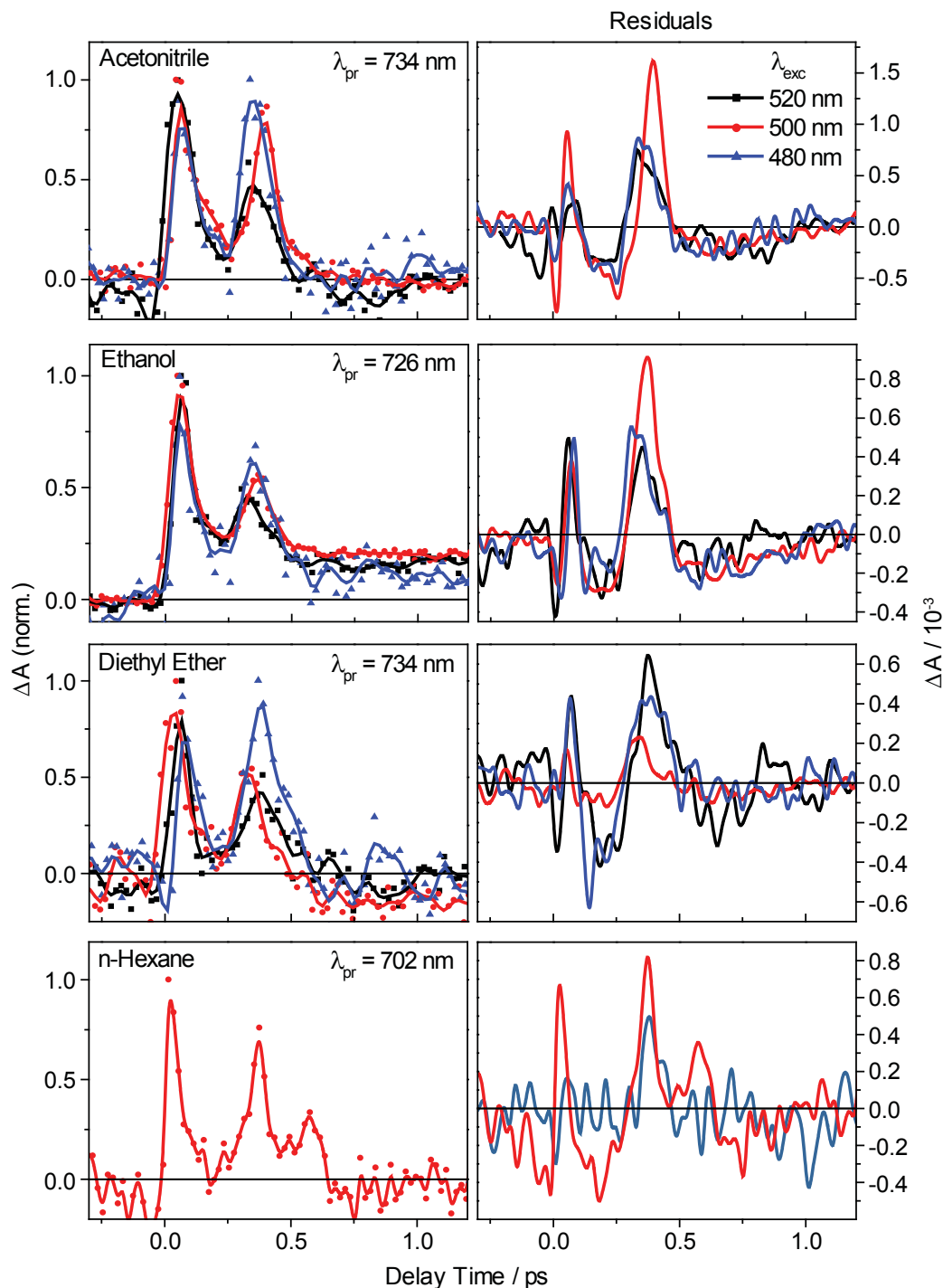


Figure 7.4: Oscillatory features in the transient absorbance data of fucoxanthin in acetonitrile, diethyl ether, ethanol, and n-hexane (left; symbols: data, line: smoothed curve; normalized) and corresponding residual curves (right; original data) for different excitation wavelengths.

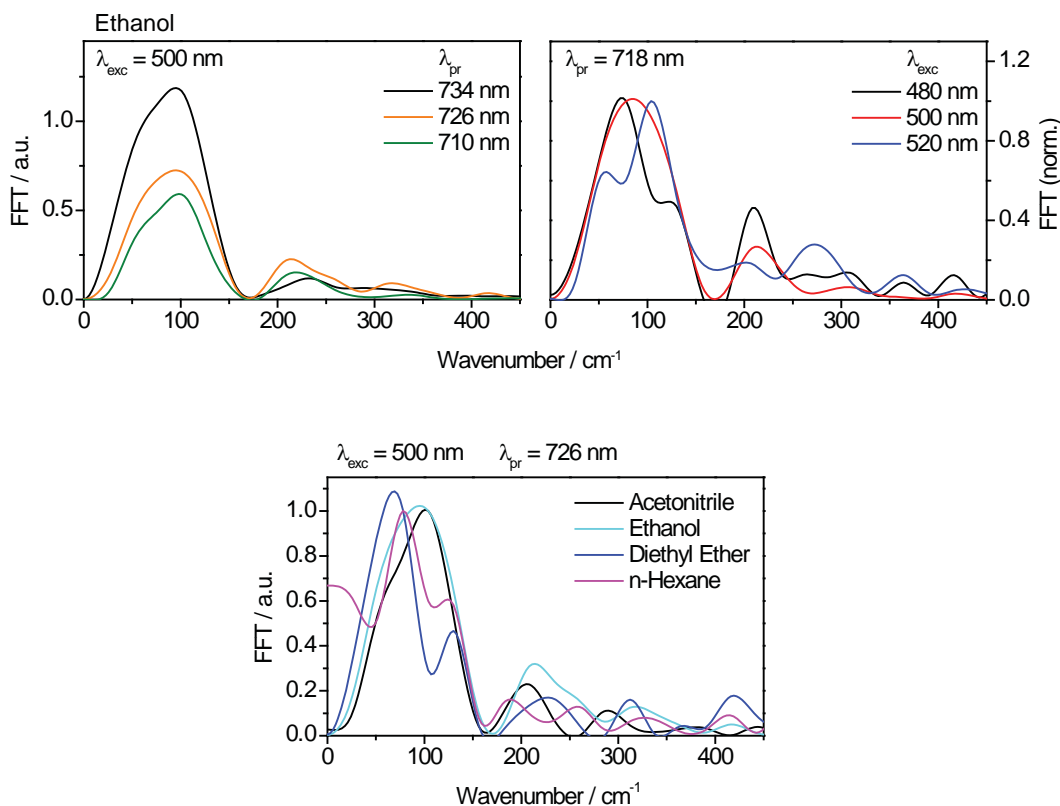


Figure 7.5: FFT spectra calculated for fucoxanthin in ethanol depending on the probing (left upper panel) and excitation wavelengths (right upper panel). In the lower panel FFT spectra of fucoxanthin in the different solvents are plotted. The curve for fucoxanthin in diethyl ether was obtained for $\lambda_{\text{pr}} = 734$ nm (see also table 7.1) instead of $\lambda_{\text{pr}} = 726$ nm as shown for the other solvents.

be characterized in more detail since the residue curves obtained for diethyl ether and n-hexane could hardly be analyzed. Due to the noisy residue curves it was not possible to obtain a distinct maximum in the FFT spectra with the two exceptions depicted in Figure 7.5 and given in table 7.1.

It has to be mentioned that the experimental parameters of the pump as well as the probe pulse seem to influence the strength of the coherent oscillations. By adjusting the excitation wavelengths with the NOPA and the pulse durations by means of the prism compressor the chirp of the pulse is also affected. In addition, the chirp of the white light is influenced by its adjustment. In the performed transient absorption measurements the wavelength and duration of the pump pulse as well as the stability of the probe light

were controlled, but the chirp of the pulses was not characterized. It was found that the strength of the modulations varied without varying the excitation wavelengths but by adjusting the prism compressor to improve the time resolution. First the oscillatory contributions seemed to increase with shorter excitation pulses. But with decreasing pulse duration the oscillations decreased again. Thus, it is assumed that the chirp also influences the coherent oscillations. Further investigations with a controlled chirp of the applied pulses will be necessary to clarify if the coherent features depend not only on excitation and probing wavelength but also on the chirp of the respective pulse.

β -Carotene

Similar coherent effects were obtained for β -carotene. In Figure 7.6 the results for β -carotene in acetonitrile are depicted. The individual transients depicted in the left upper panel are recorded in the NIR spectral region where the $S_2 \rightarrow S_N$ transition occurs. The oscillations were analyzed as for fucoxanthin. The residual curves and the calculated FFT spectra are similar for all probing wavelengths with only slight shifts of the maximum of the FFT spectra.

The obtained frequencies of about 180 cm^{-1} are higher compared to fucoxanthin in acetonitrile as well as the other solvents ($\approx 100 \text{ cm}^{-1}$). This corresponds to a faster oscillation period of $\approx 185 \text{ fs}$. The values obtained for β -carotene are comparable to the frequencies found for lutein by Ostroumov et al. [79]. In the cited publication coherent

	Acetonitrile			
	$\lambda_{\text{pr}} = 710 \text{ nm}$	$\lambda_{\text{pr}} = 718 \text{ nm}$	$\lambda_{\text{pr}} = 726 \text{ nm}$	$\lambda_{\text{pr}} = 734 \text{ nm}$
$\lambda_{\text{exc}} = 480 \text{ nm}$	–	105 (320)	–	–
$\lambda_{\text{exc}} = 500 \text{ nm}$	100 (330)	–	100 (320)	100 (320)
$\lambda_{\text{exc}} = 520 \text{ nm}$	–	105 (320)	–	105 (320)
	Ethanol			
$\lambda_{\text{exc}} = 480 \text{ nm}$	–	80 (420)	–	80 (420)
$\lambda_{\text{exc}} = 500 \text{ nm}$	95 (350)	95 (350)	95 (350)	95 (350)
$\lambda_{\text{exc}} = 520 \text{ nm}$	–	105 (320)	–	105 (320)
	Diethyl Ether			
$\lambda_{\text{exc}} = 480 \text{ nm}$	–	–	–	70 (480)
	n-Hexane			
$\lambda_{\text{exc}} = 500 \text{ nm}$	–	–	80 (420)	–

Table 7.1: Frequencies in cm^{-1} and corresponding periods of oscillation in fs (in parentheses) for fucoxanthin in different solvents. A dash means that the residue curve was too noisy to obtain a distinct maximum in the FFT spectra.

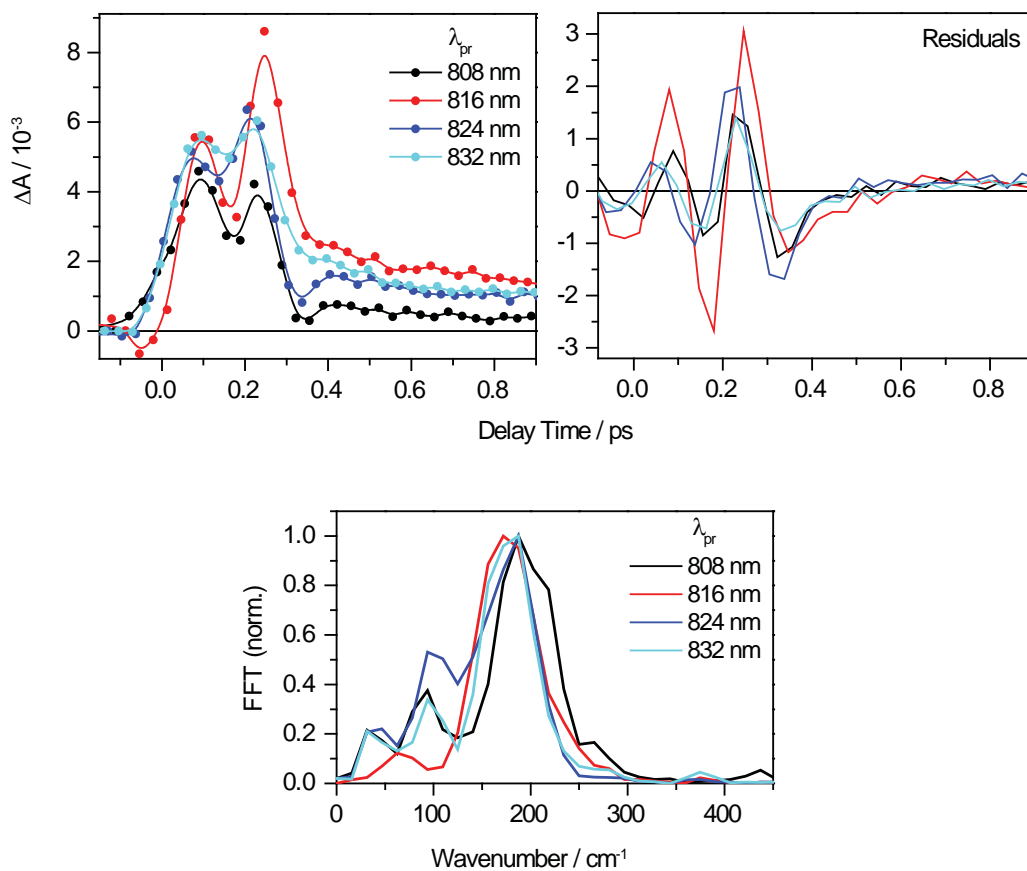


Figure 7.6: Oscillations in the transient absorption data of β -carotene in acetonitrile in the NIR probing region excited at $\lambda_{\text{exc}} = 500$ nm and corresponding residual curves (upper panels) as well as Fourier transformed spectra (lower panel).

effects occurring in the transient absorbance spectra of β -carotene and lutein in different solvents are discussed. The specified value for lutein in nonpolar solvents was 210 cm^{-1} corresponding to an oscillation period of 160 fs.

7.2 FCP Complexes

The unusual oscillations occur not only in the transient absorption spectra of the carotenoids in solution but also superimpose the ultrafast dynamics of the FCP complexes. In Figure 7.7 (upper panel) exemplary single transients at $\lambda_{\text{pr}} = 726$ nm are depicted. For both FCP complexes the oscillations are more pronounced upon excitation of the blue absorbing fucoxanthins with $\lambda_{\text{exc}} = 500$ nm. As for carotenoids in solution

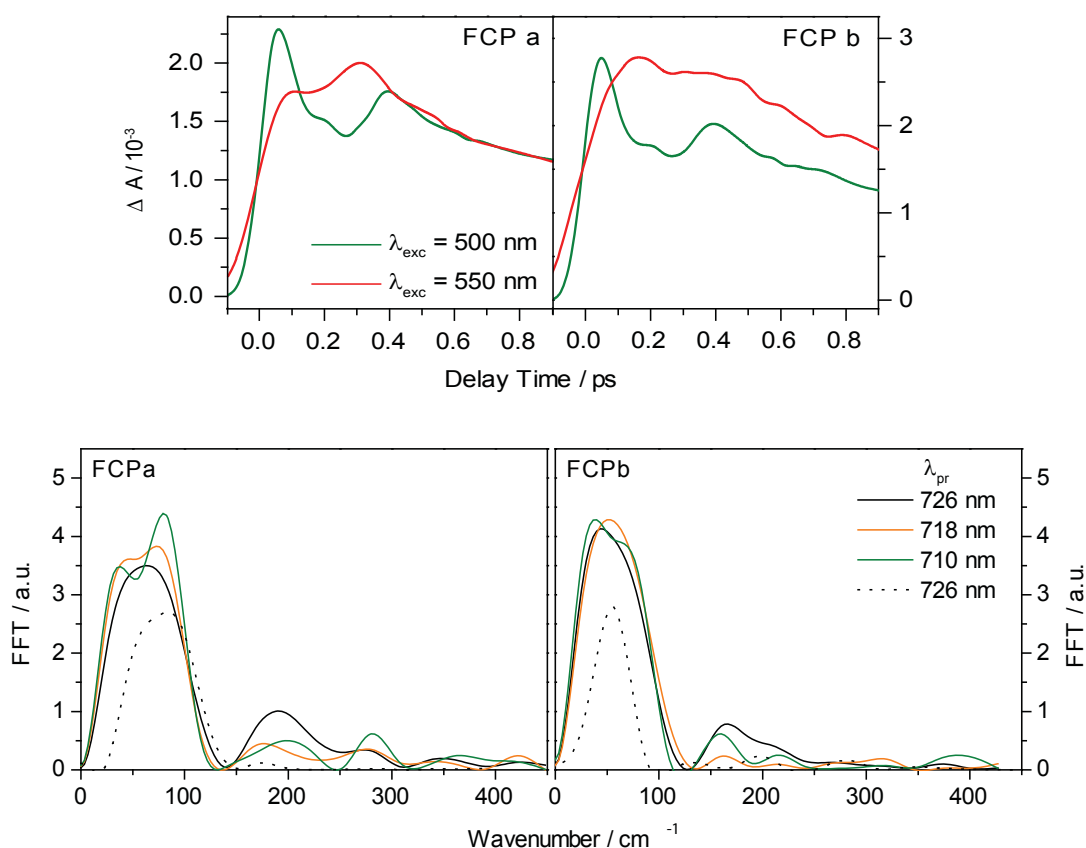


Figure 7.7: Oscillatory features in transient absorption data (top) of FCPa (left) and FCPb (right) after excitation with $\lambda_{\text{exc}} = 500$ nm (green) and $\lambda_{\text{exc}} = 550$ nm (red). The depicted individual kinetic traces were recorded at $\lambda_{\text{pr}} = 726$ nm. FFT spectra (bottom) calculated for $\lambda_{\text{exc}} = 500$ nm (solid lines) and $\lambda_{\text{exc}} = 550$ nm (dashed lines) compared for different probing wavelengths.

	FCPa	FCPb	Fucoxanthin
$\lambda_{\text{exc}} = 500 \text{ nm}$	60 (550)	45 (740)	≈ 100 (330)
$\lambda_{\text{exc}} = 550 \text{ nm}$	80 (420)	55 (610)	–

Table 7.2: Frequencies in cm^{-1} and corresponding periods of oscillation in fs (in parentheses) for FCPs and fucoxanthin in polar solvents.

the oscillations disappear already after two oscillation periods.

In the Fourier transformed spectra (Figure 7.7, lower panel) the maxima shifted to lower frequencies compared to fucoxanthin in solution. In table 7.2 the values for the frequencies and corresponding oscillation periods obtained for the FCP complexes are summarized. The frequency of $\approx 80 \text{ cm}^{-1}$ ($\approx 420 \text{ fs}$) for FCPa upon $\lambda_{\text{exc}} = 550 \text{ nm}$ is the only value comparable to the values for fucoxanthin in solution. The oscillation period for $\lambda_{\text{exc}} = 500 \text{ nm}$ was longer with $\approx 550 \text{ fs}$ (60 cm^{-1}). In case of FCPb the same trend was found with $\approx 610 \text{ fs}$ (55 cm^{-1}) for $\lambda_{\text{exc}} = 550 \text{ nm}$ and a longer period of $\approx 740 \text{ fs}$ (45 cm^{-1}) for $\lambda_{\text{exc}} = 500 \text{ nm}$.

In chapter 6.3.3 it was assumed that the red absorbing fucoxanthin molecules are located in a more polar protein environment compared to the blue absorbing fucoxanthins, since the ICT SE signal in the NIR spectral region was stronger for $\lambda_{\text{exc}} = 550 \text{ nm}$. This assumption is further confirmed by the results obtained from the analysis of the coherent effects in the FCP complexes. For both FCPs the frequencies obtained for the excitation of the blue absorbing fucoxanthins ($\lambda_{\text{exc}} = 500 \text{ nm}$) were smaller compared to the case when red absorbing fucoxanthin molecules are excited (see table 7.1). In case of fucoxanthin in solution for nonpolar solvents the frequencies were lower ($70/80 \text{ cm}^{-1}$) compared to a polar solvent environment ($\approx 100 \text{ cm}^{-1}$). Thus, the results from the analysis of the coherent effects are an additional evidence for a more polar protein environment of the red absorbing fucoxanthins.

7.3 The Origin of the Coherent Effects

Similar coherent effects were described before for β -carotene and lutein in different solvents [79,253]. Lustres et al. reported on amplitude modulations of transient absorption spectra at early delay times. The oscillations were observed for β -carotene in tetrahydrofuran (THF) after excitation at $\lambda_{\text{exc}} = 520 \text{ nm}$ and were most pronounced in the range between 400 and 500 nm corresponding to the GSB signal. They determined a constant oscillation period of $\approx 350 \text{ fs}$. According to the authors interpretation the origin of the oscillations is an electronic coupling between initially populated adiabatic states. In case of β -carotene this would refer to the vibronic coupling between the quasi-degenerated

vibronic states of the S_2 and the 'dark' S_1 state. Additional dark excited states were not included in this interpretation [253].

Ostroumov et al. investigated the ultrafast transient absorption dynamics of β -carotene and lutein with respect to the highly damped oscillatory features [79]. The oscillations showed a strong dependence on the excitation wavelength and the solvent and were more pronounced in case of lutein than in β -carotene. The coherent effects were observed in the probing region between 600 and 700 nm, where the S_1 ESA absorption and the S_2 SE emission contribute to the transient signal. Vibrational coherences in the ground state were excluded as cause for the coherent effects due to the oscillation period of 160 fs. Vibrational coherences typically have much higher frequencies ($> 1000 \text{ cm}^{-1}$), larger dephasing times, and occur in other wavelength regions [81]. Coherent excitation of strongly coupled excited states resulting in electronic quantum beats were assumed to be the origin of the oscillations [79]. The authors excluded the coupling between the S_2 and the S_1 state being the reason for the coherent features. The high frequency of the oscillations requires a strong coupling which is not possible for the S_2 and the S_1 state due to the large energy gap of $\approx 7000 \text{ cm}^{-1}$. It is thus supposed that another electronic dark state – namely the $1B_u^-$ state – located closer to the S_2 state is responsible for the oscillations. According to the authors interpretation this further confirms the existence of this dark state and its involvement in the internal conversion processes [79].

According to the results and their interpretation a model scheme concerning the excited state dynamics of lutein in diethyl ether was proposed [79]. The schemes depicted in Figure 7.8 are adopted from this model to visualize the explanation of the coherent effects. Due to the coherent excitation of the coupled electronic states $1B_u^-$ and $1B_u^+$ wavepacket motions between the two states are possible. This electronic quantum beat is supposed to be responsible for the observed oscillations. The unusual damping behavior results from the very short lifetime of the S_2 excited state since after internal conversion to the S_1 state the coupling of the two higher excited states is abolished.

Though the quantum beats are a reasonable explanation for the oscillatory feature and their unusual damping behavior observed in this work there is one drawback in the assumptions. The decay of the S_2 state to the S_1 state is ultrafast with lifetimes between 100 fs and 300 fs [5]. However, for fucoxanthin and β -carotene the period of oscillation is longer than the S_2 lifetime with values > 300 fs. Thus, it has to be assumed that the lifetime of the S_2 state is extended due to its repopulation from the $1B_u^+$ state. However, this can not explain the observations in the NIR spectral region where the $S_2 \rightarrow S_N$ transition occurs. Here the oscillations were not observed or very weak except for β -carotene.

Another possible explanation for the coherent oscillations is based on two-dimensional correlation spectroscopy of β -carotene performed by Christensson et al. [254]. This double-quantum two-dimensional spectroscopy (2Q-2D) was applied to selectively probe a state above the S_2 state populated by an additional $S_2 \rightarrow S_{N2}$ transition [254]. The corresponding ESA signal is supposed to appear in the visible spectral

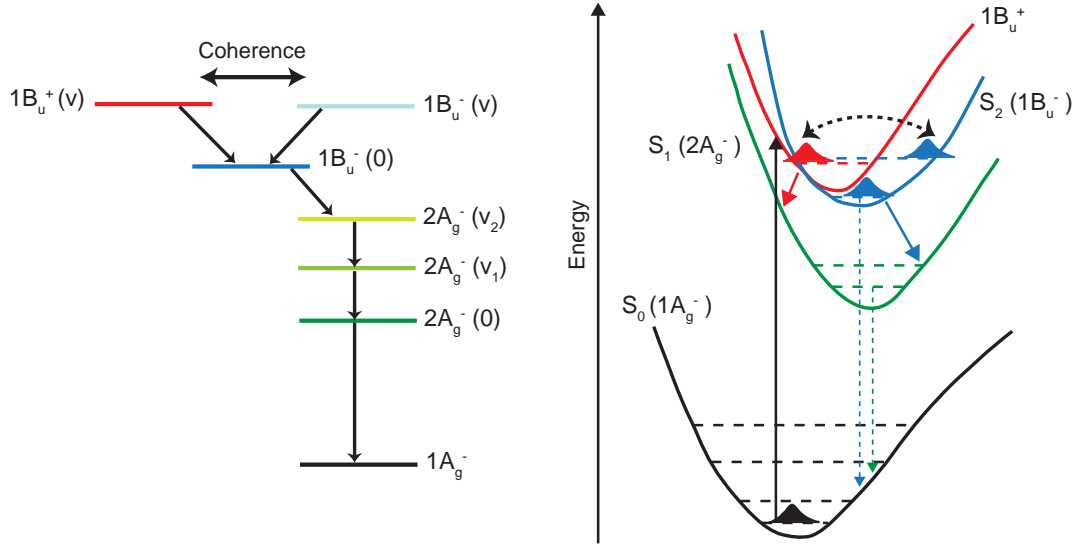


Figure 7.8: Excited state dynamics of carotenoids including the dark $1B_u^+$ state. The model assumes a strong coupling between the $1B_u^-$ and $1B_u^+$ state, which is responsible for the coherent effects in the transient absorption dynamics of carotenoids. The model was adopted from Ostroumov et al. [79] where it was published to explain the dynamics of lutein in diethyl ether.

region. In transient absorption spectra the ESA signal observed in the NIR spectral range can clearly be assigned to the $S_2 \rightarrow S_N$ transition since it is not superimposed by any other transient dynamics. Such an assignment would not be possible for a similar ESA corresponding to a $S_2 \rightarrow S_{N2}$ transition due to the overlapping signals with the GSB, the $S_2 \rightarrow S_0$ SE, and the $S_1/ICT \rightarrow S_n$ ESA. In contrast, the 2Q-2D experiment is insensitive to GSB and SE signals, hence a characterization of the ESA of the S_2 state is possible without disturbing negative contributions. The characterization of this additional ESA ($S_2 \rightarrow S_{N2}$) in the visible spectral region by 2Q-2D spectroscopy revealed that this pathway has to be considered in ultrafast excited state dynamics of carotenoids since it modulates the transient dynamics at early delay times.

In addition, Christensson et al. calculated transient absorption signals taking the $S_2 \rightarrow S_{N2}$ transition into account [254]. These transients showed a modulation similar to the highly damped oscillations observed in the transient absorption data presented above and described for β -carotene and lutein [79, 253]. Based on the calculations an effective oscillation period of ≈ 120 fs was determined. The modulations showed an excitation as well as a probing wavelength dependence. They were most pronounced

upon pumping close to the first peak of the absorption spectrum with $\lambda_{\text{exc}} = 476$ nm and were hardly observed for $\lambda_{\text{exc}} = 500$ nm. In case of $\lambda_{\text{pr}} = 615$ nm the modulations were stronger compared to $\lambda_{\text{pr}} = 580$ nm. Only for a combination of $\lambda_{\text{exc}} = 476$ nm and $\lambda_{\text{pr}} = 615$ nm the rise of the SE and $S_2 \rightarrow S_{N2}$ ESA are sufficiently different resulting in significant modulations of the transients [254]. According to the authors interpretation the different excitation wavelengths vary the nuclear modes of the S_2 state and thus alter the shape and amplitude of the spectra as well as the temporal behavior of the dynamics. Pumping in the red edge of the absorption spectra without excess vibrational energy results in a faster rise of the SE signal as well as a faster decay of the $S_2 \rightarrow S_{N2}$ ESA signal and a concomitant decrease of the $S_2 \rightarrow S_{N2}$ ESA amplitude. The dependence on the probing wavelength is much more complicated making the analysis of the coherent features very difficult. Thus, further 1Q-2D and 2Q-2D experiments have to be performed to complete the information concerning the modulation of transient absorption spectra [254]. However, an additional $S_2 \rightarrow S_{N2}$ transition which appears in the visible spectral region can explain the experimentally observed coherent oscillations without the inclusion of additional dark electronic states located close to the second excited singlet state. It can also explain the strong excitation and probing wavelength dependence of the oscillations and the varying strengths of the coherent effects in similar transient absorption experiments.

Nevertheless, it has to be mentioned that the modulation of the excited state dynamics was also obtained for β -carotene in the $S_2 \rightarrow S_N$ ESA region in the NIR spectral region (Figure 7.6) as well as for fucoxanthin in the GSB region (Figure 7.2). It could be assumed that the $S_2 \rightarrow S_{N2}$ ESA is very broad. It is also possible that the coherent effects are the result of a combination of excited state dynamics not observable with transient absorption spectroscopy. Both considered causes could contribute to the coherent effects and have a different impact depending on the carotenoid structure and its environment.

Chapter 8

Concluding Remarks

Luke, you're going to find that many of the truths we cling to depend greatly on our own point of view.

(Ben 'Obi-Wan' Kenobi in *Star Wars VI: Return of the Jedi*)

The aim of this thesis was to elucidate the excitation energy transfer in the fucoxanthin-chlorophyll proteins isolated from the diatom *Cyclotella meneghiniana* in detail and to clarify the role of the different pigments contained. Because the protein complexes possess several different pigments, complicated energy transfer processes upon photoexcitation are expected. Thus, in a first step the excited state dynamics of the free pigments were studied by means of time-resolved absorption and fluorescence techniques combined with steady state absorption spectroscopy.

The FCP complexes possess three different carotenoid species. Besides the main light-harvesting carotenoid fucoxanthin the xanthophyll cycle pigments diadinoxanthin and diatoxanthin are found. Diadinoxanthin can be deepoxidised to the photoprotective diatoxanthin under high light conditions. This so called diadinoxanthin cycle is comparable to the violaxanthin (xanthophyll) cycle and the increase of the diatoxanthin content is associated with the nonphotochemical quenching process in diatoms. In case of diadinoxanthin and diatoxanthin, changing the solvent polarity showed no significant effects on the absorption spectrum and its vibronic structure and the excited state dynamics were hardly influenced. The transient absorption spectra of both carotenoids showed a ground state bleach and a strong $S_1 \rightarrow S_n$ excited state absorption. For diatoxanthin faster kinetics were observed than for diadinoxanthin.

In contrast to the substoichiometric amount of the xanthophyll cycle pigments, fucoxanthin is contained in a rather unusual carotenoid-to-chlorophyll ratio of about one. A carbonyl group conjugated with the π -electron system of the carbon chain is responsi-

ble for the solvent dependence observed in the absorption spectrum and excited state dynamics of fucoxanthin. The spectral broadening and accompanied vanishing vibrational structure of its absorption spectrum can be explained with a broad distribution of isomers further enhanced by the charge transfer character of the ground state. In polar solvents the charge transfer character is stronger and protic solvents can further stabilize it by forming a hydrogen bond to the carbonyl oxygen. Also the excited state dynamics of fucoxanthin differs from those of carotenoids lacking the carbonyl group and show unique features. These include a strong S_1 lifetime dependence on the solvent polarity, an additional broad excited state absorption band red shifted compared to the S_1 excited state absorption, and the appearance of a stimulated emission band in the near-infrared spectral region. All these effects can be explained by an intramolecular charge transfer (ICT) state. The occurrence of the described features depends on the solvent since the charge transfer state is stabilized in a polar environment. For the S_1 and the ICT state distinct excited state lifetimes could not be obtained, leading to the conclusion that these states are coupled.

Despite its rather short excited state lifetimes of less than 200 fs (S_2) and 30 – 60 ps (S_1), fucoxanthin acts as a very efficient energy donor in the FCP complexes. The ultra-fast energy transfer dynamics of the isolated proteins FCPa and FCPb were investigated in a comprehensive study using static fluorescence spectroscopy as well as transient absorption in the visible and near infrared spectral region complemented with polarized transient absorption spectroscopy. The experiments focused on the dependence of the energy transfer on the growth conditions, the oligomeric state, as well as the excitation wavelength.

Neither the energy transfer efficiencies determined by fluorescence measurements nor the excitation energy transfer were influenced significantly by changing the light conditions during the growth, which yields an altered amount of the xanthophyll cycle pigments. Additional experiments with FCP complexes devoid of diadinoxanthin and diatoxanthin were performed but no significant dynamic changes were observed. Therefore, it can be concluded that the contribution of the xanthophyll cycle pigments to the energy transfer is not significant. The altered oligomerization state of both antenna systems results in a more efficient energy transfer for FCPa, which is also reflected in the different Chl *a* fluorescence quantum yields. Thus, an increased quenching in the higher oligomers of FCPb can be assumed. Chl-Chl excitation energy transfer was addressed by the excitation of Chl *c*₂ at 630 nm. The results indicated an extremely fast excitation energy transfer between the two chlorophyll species which seems to be complete in less than 150 fs.

The observed dynamics change drastically for two different excitation wavelengths $\lambda_{\text{exc}} = 500$ nm and $\lambda_{\text{exc}} = 550$ nm, which both lead to the population of the S_2 excited state of individual carotenoids. With the excitation at the two wavelengths it was possible to confirm the existence of two fucoxanthin species, namely blue and red absorbing fucoxanthin molecules. Most likely, the differing absorption maxima result from distinct microenvironments within the protein. For FCPa an additional slow time constant of

25 ps was found after excitation at 500 nm. It can be assigned to either the intrinsic lifetime of blue absorbing fucoxanthin molecules or an additional slow energy transfer channel. By means of polarized transient absorption spectroscopy applied to the trimeric FCPa different transition dipole moments for the S_1 and the ICT state of fucoxanthin could be identified. Furthermore, distinct transition dipole moments for the first excited state were obtained depending on the excitation wavelength.

Based on the presented studies a detailed model explaining the excitation energy transfer pathways could be developed and the pigment arrangement in FCPa could be further characterized. It can be assumed that the protein contains one red absorbing fucoxanthin molecule that transfers the energy directly to one Chl *a* molecule. Two of the three remaining fucoxanthins which absorb around 500 nm transfer their excitation energy also directly to Chl *a* molecules and should therefore be associated with the chlorophylls. In agreement with the faster overall transfer rate which is also evident in the anisotropy data in case of 550 nm excitation, upon excitation at 500 nm one slow transfer channel is active. It can be attributed to a blue absorbing fucoxanthin not strongly associated with a Chl *a* molecule. Most likely excitation energy transfer takes place between the S_1 /ICT states of two different fucoxanthin molecules before the energy is transferred to Chl *a*. The rapid energy transfer from Chl c_2 to Chl *a* indicates that one Chl *a* is located very close to the Chl c_2 molecule.

Additional transient absorption experiments with an improved time resolution were performed to investigate the oscillations observed in various datasets. These coherent effects superimposed the kinetics of isolated carotenoids as well as FCP complexes within the first 500 fs. The oscillations showed a very unusual damping behavior and vanished already after two oscillation periods. In case of fucoxanthin, the solvent environment as well as the excitation wavelengths had an influence on the oscillations. The frequencies of the oscillations were 70-100 cm^{-1} for fucoxanthin in solvents with varying polarity and 50-80 cm^{-1} for the FCPs at both excitation wavelengths. These results could further confirm the assumption that the red absorbing fucoxanthin molecules are located in a more polar environment within the protein compared to the blue absorbing fucoxanthins. To clarify the origin of the oscillations in more detail, further experiments with a controlled chirp of the applied pulses and comparison between different carotenoids in various solvents are required. This approach promises to give further insight in the excited state dynamics and to answer the question whether dark states are involved. Right now, the coherent excitation of the strongly coupled excited states $1B_u^+$ (S_2) and $1B_u^-$ resulting in electronic quantum beats and the existence of an additional short lived excited state absorption ($S_2 \rightarrow S_{N2}$) in the visible spectral region are the most reasonable explanations for the occurrence of the coherent effects in the transient absorption spectra of carotenoids.

Chapter 9

Zusammenfassung

Ziel der vorliegenden Arbeit war die detaillierte Untersuchung des ultraschnellen Energietransfers (50 fs – 100 ps) in Fucoxanthin-Chlorophyll-Proteinen (FCPs), die aus Kieselalgen isoliert wurden. Um die Rolle der enthaltenen Carotinoide beim Energietransfer in den Lichtsammelkomplexen zu untersuchen, wurden sowohl die isolierten Pigmente als auch die Proteinkomplexe mittels zeitaufgelöster optischer Spektroskopie untersucht. Hierbei lagen die Schwerpunkte auf den lichtinduzierten Dynamiken der Carotinoide in verschiedenen Lösungsmitteln sowie den Energietransfer-Reaktionen innerhalb der Proteine in Abhängigkeit ihrer Pigmentierung, Oligomerisierung und der Anregungswellenlänge.

Photosynthese und Diatomeen

Die Natur hat zur Nutzung des Sonnenlichts als Energiequelle ein erstaunlich effizientes System entwickelt: die photosynthetischen Komplexe. Organismen, die zur oxygenen Photosynthese befähigt sind, sind perfekt an ihre Umgebung angepasst und haben eine Vielzahl so genannter Lichtsammelkomplexe entwickelt, welche das Sonnenlicht aufnehmen und die Energie dann an die Reaktionszentren weiterleiten. Gerade in der heutigen Zeit ist es besonders wichtig, diese hoch effektiven Prozesse zur Energieumwandlung im Detail zu verstehen. Die Nutzung des Sonnenlichts als saubere und unbegrenzte Energiequelle ist von großer Wichtigkeit für die weltweite Energieversorgung. Daher beschäftigt sich die aktuelle Forschung mit der Entwicklung künstlicher, photosynthetischer Prozesse, die eine effiziente photochemische Umwandlung der Sonnenenergie ermöglichen.

Aufgrund ihrer Sessilität müssen Pflanzen über besondere Strategien verfügen, die es ihnen ermöglichen auf Veränderungen in ihrer Umwelt zu reagieren. Schwankungen in der Intensität des einfallenden Sonnenlichts stellen dabei eine besondere Herausforderung dar. Bei geringer Sonneneinstrahlung muss die zur Verfügung stehende Sonnenenergie vollständig genutzt werden, jedoch kann eine erhöhte Einstrahlung schnell zur Schädigung

gung des Photosyntheseapparates führen. Daher müssen photosynthetische Organismen über Mechanismen verfügen, die auf unterschiedlich starke Lichteinstrahlung reagieren und überschüssige Energie abführen können, ohne dass eine Schädigung auftritt. Carotinoide spielen eine besondere Rolle sowohl bei der Absorption des Sonnenlichts als auch für den Schutz des Photosyntheseapparates. Sie sind, nach den Chlorophyllen, die auf der Erde am häufigsten vorkommenden Pigmente. Es gibt eine Vielzahl an Carotinoiden mit unterschiedlichsten Strukturen und biologischen Funktionen. Sie fungieren als akzessorische Pigmente im Photosyntheseapparat, da sie die so genannte "Grünlücke" im Absorptionsspektrum der Chlorophylle verringern und somit die Absorption einer größeren Menge an Sonnenlicht ermöglichen. Neben ihren farbgebenden Eigenschaften haben Carotinoide auch strukturbildende Funktionen in Proteinen und Membranen. Durch ihre Fähigkeit Triplett-Zustände der Chlorophylle abzufangen und so der Bildung des gefährlichen Singulett-Sauerstoffs vorzubeugen, besitzen Carotinoide außerdem eine wichtige Schutzfunktion. Sie sind nicht nur in Pflanzen sondern auch in Tieren und im menschlichen Organismus wirksame Antioxidantien, die verschiedenen Krebserkrankungen und anderen Krankheiten wie Arteriosklerose und Makuladegeneration vorbeugen können. Um den Zusammenhang zwischen Struktur und Funktion zu verstehen, sind Kenntnisse der Anordnung und der Dynamik der angeregten Zustände der Carotinoide entscheidend. Bis heute werden die Eigenschaften der elektronisch angeregten Zustände diskutiert, da sie sehr kompliziert sind. Umstritten sind zum Beispiel die Funktion der Radikalkationen von Carotinoiden während des Schutzmechanismus oder die Rolle dunkler elektronischer Zustände bei der Relaxation in den Grundzustand.

In den globalen, biochemischen Zyklen des Kohlenstoffs, Stickstoffs, Phosphors und Siliziums spielen Kieselalgen (Diatomeen) eine Hauptrolle, weshalb sie von großer ökologischer Bedeutung sind. Es handelt sich um einzellige, eukaryotische Algen eingebettet in einer Hülle aus Siliziumdioxid. Man vermutet, dass über 100.000 verschiedene Arten existieren, von denen bis heute etwa 6.000 klassifiziert sind. Obwohl ihre Lichtsammelkomplexe den Komplexen höherer Pflanzen (LHCII) ähneln, enthalten sie andere Pigmente in einer ungewöhnlichen Zusammensetzung. Wie in jedem photosynthetischen Komplex ist Chlorophyll *a* enthalten, jedoch ist Chlorophyll *b* gegen Chlorophyll *c*₂ ausgetauscht, welches keinen Phytolrest besitzt. Neben dem wichtigsten akzessorischen Pigment Fucoxanthin findet man Diadinoxanthin und Diatoxanthin in substöchiometrischen Mengen. Unter starkem Lichteinfall wird Diadinoxanthin zu Diatoxanthin deepoxidiert, ein Prozess vergleichbar mit dem Violaxanthin- bzw. Xanthophyll-Zyklus höherer Pflanzen. Normalerweise befinden sich in Lichtsammelkomplexen deutlich mehr Chlorophylle als Carotinoide. Fucoxanthin ist dagegen in einem ungewöhnlich hohen Carotinoid-zu-Chlorophyll Verhältnis von etwa eins enthalten, wobei vier Fucoxanthin-Moleküle in einem Monomer eingelagert sind. Es besitzt eine Carbonylgruppe, welche mit dem π -Elektronensystem der Kohlenstoffkette konjugiert ist. Die Rolle der Carotinoide beim Energietransfer und die Dynamiken in den Lichtsammelkomplexen wurden anhand von zwei verschiedenen FCPs untersucht, die in der Arbeitsgruppe von Prof. Claudia Büchel aus der Kieselalge *Cyclotella meneghiniana* isoliert wurden. Die beiden

FCPs unterscheiden sich durch ihren Oligomerisierungszustand: FCPa ist ein Trimer, FCPb ein höheres Oligomer.

Methoden

Moderne Laserspektroskopie ermöglicht die Untersuchung photophysikalischer und photochemischer Prozesse auf verschiedenen Zeitskalen. Insbesondere die optische Spektroskopie mit Zeitauflösungen im Femtosekundenbereich erlaubt die Aufklärung elektronischer Strukturen, die Beobachtung verschiedener Zerfallspfade und Konformationsdynamiken innerhalb biologischer Moleküle und größerer Systeme wie zum Beispiel Proteinen. So können unter anderem der Elektronentransfer in den photosynthetischen Reaktionszentren oder Energietransfer-Reaktionen in Lichtsammelkomplexen untersucht werden. Hierzu wurden im Rahmen der vorliegenden Arbeit eine Vielzahl an Experimenten durchgeführt. Zudem wurde die bereits vorhandene Anlage zur Messung transienter Absorptionsspektren um zwei Anlagen für zeitaufgelöste Fluoreszenzspektroskopie, die Fluoreszenz-Aufkonvertierung und den Kerr-Schalter, erweitert. Die Messung transienter Absorptionsspektren im Femto- bis Nanosekundenbereich beruht auf dem Anreg-Abtast-Prinzip, bei welchem der Abtastpuls mit Hilfe einer Verzögerungsstrecke gegenüber dem Anregepuls zeitlich verzögert wird. Die Zeitauflösung wird maßgeblich durch die Dauer der verwendeten Pulse bestimmt, weshalb entsprechend kurze Pulse von etwa 100 fs benötigt werden. Diese Methode ermöglicht die Aufnahme spektral breitbandiger Absorptionsspektren, welche sich aus mehreren Beiträgen wie dem Grundzustandsbleichen, der Absorption angeregter Zustände, der stimulierten Emission und unter Umständen auch Produktbanden zusammensetzen. Oft überlagern diese verschiedenen Beiträge, was die Analyse und Interpretation der Daten deutlich erschwert. Daher kann es sehr hilfreich sein, transiente Absorptionsmessungen durch zeitaufgelöste Fluoreszenzspektren zu ergänzen, da diese die direkte Beobachtung einzelner, elektronisch angeregter Zustände ohne zusätzliche überlagernde Beiträge erlauben. Dabei ermöglicht die Fluoreszenz-Aufkonvertierung die Aufnahme einzelner Transienten im sichtbaren und nahinfraroten Spektralbereich basierend auf der Summenfrequenzerzeugung in einem nichtlinearen Kristall. Die von Ute Förster konzipierte Anlage kombiniert die Fluoreszenzaufkonvertierung mit der Methode des zeitkorrelierten Einzelphotonenzählens und deckt somit einen Zeitbereich von Femto- bis Millisekunden ab, in dem Fluoreszenzlebensdauern ohne größere apparative Veränderungen bestimmt werden können. Dagegen ermöglicht der Kerr-Schalter das gleichzeitige Detektieren ganzer Fluoreszenzspektren im sichtbaren Spektralbereich, aus diesem Grund wurde ein entsprechendes Experiment zusätzlich zur Fluoreszenz-Aufkonvertierung aufgebaut. Die Messmethode basiert auf dem Kerr-Effekt, der in einem isotropen Medium durch einen kurzen so genannten Schaltimpuls induziert wird und ebenfalls Zeitauflösungen bis zu mehreren zehn Femtosekunden ermöglicht.

Isolierte Carotinoide

Hauptgegenstand der vorliegenden Arbeit war die detaillierte Aufklärung der Energietransfer-Reaktionen in FCPs aus der Kieselalge *Cyclotella meneghiniana*. Nach Photoanregung erwartet man komplizierte Prozesse, da in den Proteinkomplexen verschiedene Pigmente enthalten sind. Daher wurden zunächst die Lösungsmiteleinflüsse auf die Dynamiken der isolierten Carotinoide mittels statischer und zeitaufgelöster spektroskopischer Methoden untersucht.

Die Absorptionsspektren von Carotinoiden weisen eine breite Absorptionsbande im sichtbaren Spektralbereich zwischen 350 nm und 550 nm auf. Die Bande kann dem Übergang aus dem Grundzustand in den zweiten elektronisch angeregten Zustand (S_2) zugeordnet werden, da der Übergang in den ersten angeregten Zustand (S_1) symmetrieverboten ist. Es handelt sich um eine Bande mit meist ausgeprägter vibronischer Struktur, die abhängig von der Struktur des jeweiligen Carotinoids und dem Lösungsmittel ist. Im Falle von Diadinoxanthin und Diatoxanthin hatten Änderungen der Lösungsmittelpolarität nahezu keinen Einfluss auf die Absorptionsspektren und ihre vibronische Struktur. Im Gegensatz dazu wurde das Absorptionsspektrum von Fucoxanthin mit steigender Lösungsmittelpolarität spektral breiter und die vibronische Struktur ging verloren. Dies kann mit dem Auftreten mehrerer Isomere und einem zusätzlichen Ladungstransferzustand, welcher mit dem Grundzustand gekoppelt ist, erklärt werden. In polaren Lösungsmitteln ist der Ladungstransferzustand stärker ausgeprägt als in unpolaren. Protische Lösungsmittel können ihn noch zusätzlich stabilisieren, da sie eine Wasserstoffbrückenbindung zum Carbonyl-Sauerstoff ausbilden können.

Auch die zeitaufgelösten Absorptionsspektren von Diadinoxanthin und Diatoxanthin blieben unverändert trotz unterschiedlicher Polaritäten der verwendeten Lösungsmittel. Für beide Carotinoide können zwei Banden unterschieden werden, von denen die negative dem Grundzustandsbleichen und die positive der Absorption des ersten angeregten Zustands zugeordnet werden kann. Die S_1 -Zerfallsdynamiken von Diatoxanthin mit einer Zeitkonstante von 13 ps waren etwas schneller als die des Diadinoxanthins (21 ps). Die Dynamik des Fucoxanthins veränderte sich erheblich in den unterschiedlichen Lösungsmitteln, was es von Carotinoiden ohne konjugierte Carbonylgruppe unterscheidet. Neben einer starken Abhängigkeit der Lebensdauer des S_1 -Zustands kann man eine zusätzliche, positive transiente Absorptionsbande rotverschoben zur S_1 -Absorption und eine stimulierte Emissionsbande im nahinfraroten Spektralbereich beobachten. Diese Effekte können mit einem intramolekularen Ladungstransferzustand (ICT) erklärt werden, welcher in polaren und vor allem protischen Lösungsmitteln stabilisiert wird. Für diesen Ladungstransferzustand und den S_1 -Zustand wurden die gleichen Lebensdauern bestimmt, woraus man schließen kann, dass beide Zustände miteinander gekoppelt sind. Die Lebensdauern nehmen von etwa 60 ps in unpolaren Lösungsmitteln ab auf 20 ps im protischen Methanol. Die zusätzliche transiente Absorptionsbande wie auch die stimulierte Emissionsbande werden mit zunehmender Lösungsmittelpolarität immer stärker und können daher dem Ladungstransferzustand zugeordnet werden.

Fucoxanthin-Chlorophyll-Proteine

Die ultraschnellen Transferdynamiken der beiden Oligomere FCPa und FCPb wurden mit Hilfe von statischer Absorptions- und Fluoreszenzspektroskopie und transientser Absorption im sichtbaren und nahinfraroten Spektralbereich eingehend untersucht. Hierbei standen die Abhängigkeit der Dynamiken von der Pigmentierung und des oligomeren Zustands der FCPs sowie der Einfluss der Anregungswellenlänge im Vordergrund. Aufgrund der räumlichen Nähe zu den Chlorophyll-Molekülen innerhalb der Lichtsammelkomplexe ist Fucoxanthin, trotz der sehr kurzen Lebensdauern der angeregten Zustände, ein sehr effektiver Energiedonor. Mit Hilfe von Fluoreszenzmessungen wurde die Effizienz dieses Energietransfers in den verschiedenen Proben untersucht.

Aufgrund der verschiedenen Pigmente innerhalb der Protein-Komplexe erhält man ein transientes Absorptionsspektrum, in welchem sich die Beiträge der Carotinoide und Chlorophylle überlagern. Das erschwert die Analyse der Dynamik, weshalb eine genaue Bandenzuordnung sehr wichtig ist. Am blauen Ende des sichtbaren Spektralbereichs für Wellenlängen < 500 nm ist das Grundzustandsbleichen der Carotinoide sichtbar. Nach einigen Pikosekunden klingt das Signal ab und wird von der Absorption des angeregten Chlorophylls überlagert. Der spektrale Bereich zwischen 520 nm und 715 nm zeigt eine breite, positive Absorptionsbande mit zwei Maxima, die dem ersten angeregten Zustand (um 575 nm) und dem gekoppelten Ladungstransferzustand (um 650 nm) des Fucoxanthins zugeordnet werden können. Beide Banden zerfallen innerhalb einiger Pikosekunden. Die ICT-Bande weist einen tiefen negativen Einschnitt um 675 nm auf, der aufgrund der Überlagerung mit dem Grundzustandsbleichen und der stimulierten Emission des Chlorophylls entsteht. Zudem ist eine weitere Absorptionsbande des angeregten Chlorophylls um 640 nm sichtbar. Die Chlorophyllbanden zerfallen langsam mit Lebensdauern größer als die maximale Beobachtungszeit des Experiments (1.5 ns). Im nahinfraroten Spektralbereich sind lediglich zwei Beiträge zu beobachten, die dem Fucoxanthin zugeordnet werden können: zum einen die sehr kurzlebige, breitbandige Absorption des zweiten angeregten Zustands zwischen 850 nm und 1100 nm, zum anderen die stimulierte Emission des Ladungstransferzustands (950 nm und 1100 nm) mit Zerfallszeiten von wenigen Pikosekunden.

Weder die Transferdynamiken noch die Effizienz des Energietransfers wurden durch unterschiedliche Gehalte der Pigmente Diadinoxanthin und Diatoxanthin beeinflusst. Dies wurde anhand von Proben überprüft, die aus Zellen stammten, die entweder bei starkem oder schwachem Lichteinfall angezogen wurden. Zusätzliche Experimente mit Proben ohne Diadinoxanthin und Diatoxanthin zeigten ebenfalls keine veränderte Dynamik, weshalb ein Beitrag der Xanthophyll-Zyklus-Pigmente zum Energietransfer weitestgehend ausgeschlossen werden kann. Der Vergleich der beiden Komplexe FCPa und FCPb, die sich durch den Oligomerisierungszustand unterscheiden, zeigte einen effizienteren Energietransfer im trimeren FCPa, was wiederum auf ein erhöhtes Quenchen im höher oligomeren FCPb schließen lässt. Der Energietransfer zwischen den beiden Chlorophyllen Chl *a* und Chl *c*₂ wurde durch Anregung von Chl *c*₂ bei 630 nm unter-

sucht. Die Ergebnisse bestätigen einen extrem schnellen Energietransfer zwischen Chl c_2 und Chl a , der in weniger als 150 fs abgeschlossen ist.

Die untersuchten Dynamiken ändern sich deutlich nach der Anregung der Carotinoide mit zwei verschiedenen Wellenlängen (500 nm und 550 nm). Beide Wellenlängen führen zu der Besetzung des zweiten elektronisch angeregten Zustands (S_2) individueller Fucoxanthin-Moleküle. So konnte die Existenz zweier Fucoxanthinspezies bestätigt werden, nämlich die in der Literatur bekannten blau- und rot-absorbierenden Fucoxanthine. Die unterschiedlichen Absorptionsmaxima resultieren höchstwahrscheinlich aus den verschiedenen Umgebungen der einzelnen Fucoxanthin-Moleküle innerhalb des Proteins. In einer globalen Fitanalyse wurden die Zerfallszeiten bestimmt, die hier exemplarisch für FCPa angegeben werden. Dabei konnten die Daten, die nach 550 nm Anregung aufgenommen wurden, mit vier Zeitkonstanten zufriedenstellend angepasst werden. $\tau_1 < 150$ fs liegt unterhalb der Zeitaufösung des Experiments, kann jedoch der Lebensdauer des zweiten angeregten Zustands der Carotinoide zugeordnet werden. $\tau_2 = 0.9$ ps und $\tau_3 = 4.2$ ps entsprechen der Schwingungsrelaxation und dem Zerfall des ersten angeregten Zustands des Fucoxanthins. τ_∞ berücksichtigt die Chlorophyllsignale, welche über die maximale Beobachtungszeit hinaus bestehen bleiben. Neben ähnlichen Zerfallskonstanten ($\tau_1 < 150$ fs, $\tau_2 = 0.6$ ps, $\tau_3 = 2.6$ ps, $\tau_\infty = \text{unendlich}$) war für die Anregung bei 500 nm eine weitere Zerfallskonstante $\tau_4 = 25$ ps für die Anpassung der Daten nötig. Diese zusätzliche Zeitkonstante kann der intrinsischen Lebensdauer eines blau-absorbierenden Fucoxanthins oder einem langsameren Energietransferpfad zugeordnet werden. Zur genaueren Charakterisierung wurde FCPa zusätzlich in polarisationsabhängigen transienten Absorptionsexperimenten untersucht. Für den ersten angeregten Zustand und den zugehörigen Ladungstransferzustand wurden unterschiedliche Übergangsdipolmomente gefunden. Des Weiteren ergaben sich unterschiedliche Übergangsdipolmomente für die beiden Anregungswellenlängen.

Basierend auf den in der Arbeit vorgestellten Ergebnissen konnte ein detailliertes Modell zur Erklärung der Energietransfer-Reaktionen in FCPs aufgestellt werden und die Anordnung der Pigmente vor allem in FCPa genauer charakterisiert werden. Dabei kann angenommen werden, dass ein rot-absorbierendes Fucoxanthin die absorbierte Energie effizient und direkt an ein Chl a -Molekül weitergibt. Zwei der drei verbleibenden Fucoxanthine mit einem Absorptionsmaximum um 500 nm scheinen ebenso ihre Anregungsenergie direkt an Chl a zu transferieren. In Übereinstimmung mit der schnelleren Transferrate nach Anregung bei 550 nm, die auch in den Anisotropiedaten gefunden wurde, ist nach Anregung bei 500 nm ein zusätzlicher, langsamerer Transferpfad (25 ps) aktiv. Dieser kann demnach einem blau-absorbierenden Fucoxanthin zugeordnet werden, welches weniger stark mit den Chl a -Molekülen assoziiert ist als die anderen Fucoxanthine. Dabei findet vor der Weiterleitung zu Chl a wahrscheinlich ein Energietransfer zwischen den ersten angeregten Zuständen zweier unterschiedlicher Fucoxanthine statt. Der schnelle Transfer von Chl c_2 zu Chl a impliziert, dass eines der Chl a -Moleküle in unmittelbarer Nähe zum Chl c_2 lokalisiert ist.

Kohärente Effekte

Zusätzliche zeitaufgelöste Absorptionsexperimente mit verbesserter Zeitauflösung wurden durchgeführt um die oszillatorischen Effekte, die in den meisten Daten zu sehen waren, näher zu untersuchen. Diese kohärenten Effekte überlagern die Dynamiken sowohl der isolierten Carotinoide als auch der FCPs innerhalb der ersten 500 fs. Die Oszillationen zeigten ein ungewöhnliches Dämpfungsverhalten, da sie schon nach zwei Oszillationsperioden verschwinden. Außerdem weisen sie eine Abhängigkeit von der Anregungswellenlänge und im Falle von Fucoxanthin auch vom Lösungsmittel auf. In Abhängigkeit der Polarität des Lösungsmittels ergaben sich für Fucoxanthin Frequenzen zwischen 70-100 cm^{-1} . Für die FCPs variierte die Frequenz zwischen 50-80 cm^{-1} in Abhängigkeit von der Anregungswellenlänge. Diese Ergebnisse bestätigten die Annahme, dass sich das rot-absorbierende Fucoxanthin in einer polareren Umgebung als das blau-absorbierende Fucoxanthin befindet. Um den Ursprung der Oszillation noch genauer aufzuklären sind weitere Experimente mit einem kontrollierten Chirp der verwendeten Pulse und Vergleiche zwischen verschiedenen Carotinoiden in unterschiedlichen Lösungsmitteln notwendig. Weiterführende Ergebnisse sollten helfen, die Dynamiken und vor allem die Beteiligung so genannter "dunkler Zustände" noch besser zu verstehen. Zum jetzigen Zeitpunkt sind die in der Literatur diskutierte kohärente Anregung der stark gekoppelten, angeregten Zustände $1B_u^+$ (S_2) und $1B_u^-$, welche zu elektronischen Quantumbeats führt, oder auch eine zusätzliche, extrem kurzlebige Absorption aus dem S_2 -Zustand in einen S_{N2} -Zustand im sichtbaren Spektralbereich plausible Erklärungen für das Auftreten der kohärenten Effekte in transienten Absorptionsspektren von Carotinoiden.

Bibliography

- [1] G. Renger. *Photosynthese in: Biophysik*. Springer, 2nd edition, 1982.
- [2] P. Sitte, E. Weiler, J. Kadereit, A. Bresinsky and C. Körner. *Strasburger - Lehrbuch der Botanik*. Spektrum Akademischer Verlag, 35th edition, 2002.
- [3] V. Balzani, A. Credi and M. Venturi. *Photochemical conversion of solar energy*. ChemSusChem 1: 26–58, 2008.
- [4] G. Britton, S. Liaaen-Jensen and H. Pfander, eds. *Carotenoids, Volume 4: Natural Functions*. Birkhäuser Verlag, 2008.
- [5] T. Polívka and V. Sundström. *Ultrafast dynamics of carotenoid excited states - From solution to natural and artificial systems*. Chem. Rev. 104: 2021–2071, 2004.
- [6] N. Holt, D. Zigmantas, L. Valkunas, X. Li, K. Niyogi and G. Fleming. *Carotenoid cation formation and the regulation of photosynthetic light harvesting*. Science 307: 433–436, 2005.
- [7] S. Amarie, K. Arefe, J. H. Starcke, A. Dreuw and J. Wachtveitl. *Identification of an Additional Low-Lying Excited State of Carotenoid Radical Cations*. J. Phys. Chem. B 112: 14011–14017, 2008.
- [8] T. Polívka and V. Sundström. *Dark excited states of carotenoids: Consensus and controversy*. Chem. Phys. Lett. 477: 1–11, 2009.
- [9] L. Medlin and I. Kaczmarska. *Evolution of the diatoms: V. Morphological and cytological support for the major clades and a taxonomic revision*. Phycologia 43: 245–270, 2004.
- [10] S. Adl, A. Simpson, M. Farmer, R. Andersen, O. Anderson, J. Barta, S. Bowser, G. Brugerolle, R. Fensome, S. Fredericq and et al. *The new higher level classification of eukaryotes with emphasis on the taxonomy of protists*. J. Eukaryot. Microbiol. 52: 399–451, 2005.
- [11] C. Wilhelm, C. Büchel, J. Fisahn, R. Goss, T. Jakob, J. LaRoche, J. Lavaud, M. Lohr, U. Riebesell, K. Stehfest, K. Valentin and P. G. Kroth. *The regulation*

- of carbon and nutrient assimilation in diatoms is significantly different from green algae.* Protist 157: 91–124, 2006.
- [12] A. Beer, K. Gundermann, J. Beckmann and C. Büchel. *Subunit composition and pigmentation of fucoxanthin-chlorophyll proteins in diatoms: Evidence for a subunit involved in diadinoxanthin and diatoxanthin binding.* Biochemistry 45: 13046–13053, 2006.
- [13] A. Zewail. *Femtochemistry: Atomic-scale dynamics of the chemical bond.* J. Phys. Chem. A 104: 5660–5694, 2000.
- [14] W. Zinth and J. Wachtveitl. *The first picoseconds in bacterial photosynthesis - Ultrafast electron transfer for the efficient conversion of light energy.* ChemPhysChem 6: 871–880, 2005.
- [15] J. Wachtveitl and W. Zinth. *Electron transfer in photosynthetic reaction centers in: Chlorophylls and bacteriochlorophylls: Biochemistry, biophysics, functions and applications.* Springer, 2006.
- [16] D. Hess. *Pflanzenphysiologie: Grundlagen von Stoffwechsel und Entwicklung der Pflanzen.* Ulmer, Stuttgart, 1999.
- [17] A. Telfer, A. Pascal and A. Gall. *Carotenoids in Photosynthesis in: Carotenoids, Volume 4: Natural Functions.* Birkhäuser Verlag, 2008.
- [18] P. Jordan, P. Fromme, H. Witt, O. Klukas, W. Saenger and N. Krauss. *Three-dimensional structure of cyanobacterial photosystem I at 2.5 angstrom resolution.* Nature 411: 909–917, 2001.
- [19] A. Zouni, H. Witt, J. Kern, P. Fromme, N. Krauss, W. Saenger and P. Orth. *Crystal structure of photosystem II from Synechococcus elongatus at 3.8 angstrom resolution.* Nature 409: 739–743, 2001.
- [20] N. Kamiya and J. Shen. *Crystal structure of oxygen-evolving photosystem II from Thermosynechococcus vulcanus at 3.7-angstrom resolution.* Proc. Natl. Acad. Sci. U.S.A. 100: 98–103, 2003.
- [21] K. Ferreira, T. Iverson, K. Maghlaoui, J. Barber and S. Iwata. *Architecture of the photosynthetic oxygen-evolving center.* Science 303: 1831–1838, 2004.
- [22] P. Fromme and I. Grotjohann. *Photosynthetic Protein Complexes: A Structural Approach.* WILEY-VCH Verlag, Weinheim, 2008.
- [23] R. van Grondelle and V. Novoderezhkin. *Energy transfer in photosynthesis: experimental insights and quantitative models.* Phys. Chem. Chem. Phys. 8: 793–807, 2006.

- [24] G. McDermott, S. Prince, A. Freer, A. Hawthornthwaitelawless, M. Papiz, R. Cogdell and N. Isaacs. *Crystal-structure of an integral membrane light-harvesting complex from photosynthetic bacteria*. Nature 374: 517–521, 1995.
- [25] J. Koepke, X. Hu, C. Muenke, K. Schulten and H. Michel. *The crystal structure of the light-harvesting complex II (B800-850) from Rhodospirillum rubrum*. Structure 4: 581–597, 1996.
- [26] M. Papiz, S. Prince, T. Howard, R. Cogdell and N. Isaacs. *The structure and thermal motion of the B800-850 LH2 complex from Rps. acidophila at 2.0 Å over-circle resolution and 100 K: New structural features and functionally relevant motions*. J. Mol. Biol. 326: 1523–1538, 2003.
- [27] S. Scheuring, J. Seguin, S. Marco, D. Levy, B. Robert and J. Rigaud. *Nanodissection and high-resolution imaging of the Rhodospirillum rubrum photosynthetic core complex in native membranes by AFM*. Proc. Natl. Acad. Sci. U.S.A. 100: 1690–1693, 2003.
- [28] A. Roszak, T. Howard, J. Southall, A. Gardiner, C. Law, N. Isaacs and R. Cogdell. *Crystal structure of the RC-LH1 core complex from Rhodospirillum rubrum*. Science 302: 1969–1972, 2003.
- [29] W. Kühlbrandt, D. Wang and Y. Fujiyoshi. *Atomic model of plant light-harvesting complex by electron crystallography*. Nature 367: 614–621, 1994.
- [30] Z. Liu, H. Yan, K. Wang, T. Kuang, J. Zhang, L. Gui, X. An and W. Chang. *Crystal structure of spinach major light-harvesting complex at 2.72 angstrom resolution*. Nature 428: 287–292, 2004.
- [31] R. Standfuss, A. van Scheltinga, M. Lamborghini and W. Kühlbrandt. *Mechanisms of photoprotection and nonphotochemical quenching in pea light-harvesting complex at 2.5 Å resolution*. Embo J. 24: 919–928, 2005.
- [32] R. J. Cogdell, A. Gall and J. Köhler. *The architecture and function of the light-harvesting apparatus of purple bacteria: from single molecules to in vivo membranes*. Q. Rev. Biophys. 39: 227–324, 2006.
- [33] A. Ben-Shem, F. Frolov and N. Nelson. *Crystal structure of plant photosystem I*. Nature 426: 630–635, 2003.
- [34] J. Nield, O. Kruse, J. Ruprecht, P. da Fonseca, C. Büchel and J. Barber. *Three-dimensional structure of Chlamydomonas reinhardtii and Synechococcus elongatus photosystem II complexes allows for comparison of their oxygen-evolving complex organization*. J. Biol. Chem. 275: 27940–27946, 2000.
- [35] R. Harrer. *Associations between light-harvesting complexes and Photosystem II from Marchantia polymorpha L. determined by two- and three-dimensional electron microscopy*. Photosynth. Res. 75: 249–258, 2003.

- [36] J. Nield and J. Barber. *Refinement of the structural model for the Photosystem II supercomplex of higher plants*. Biochim. Biophys. Acta - Bioenerg. 1757: 353–361, 2006.
- [37] P. Horton, A. Ruban and R. Walters. *Regulation of light harvesting in green plants*. Annu. Rev. Plant Physiol. Plant Molec. Biol. 47: 655–684, 1996.
- [38] A. Pascal, Z. Liu, K. Broess, B. van Oort, H. van Amerongen, C. Wang, P. Horton, B. Robert, W. Chang and A. Ruban. *Molecular basis of photoprotection and control of photosynthetic light-harvesting*. Nature 436: 134–137, 2005.
- [39] A. Nilsson, D. Stys, T. Drakenberg, M. Spangfort, S. Forsen and J. Allen. *Phosphorylation controls the three-dimensional structure of plant light harvesting complex II*. J. Biol. Chem. 272: 18350–18357, 1997.
- [40] N. Adir. *Elucidation of the molecular structures of components of the phycobilisome: reconstructing a giant*. Photosynth. Res. 85: 15–32, 2005.
- [41] A. Hoff and J. Amesz. *Visible Absorption Spectroscopy of Chlorophylls in: Chlorophylls*. CRC Press, 1991.
- [42] L. Premvardhan, D. J. Sandberg, H. Fey, R. R. Birge, C. Büchel and R. van Grondelle. *The charge-transfer properties of the S-2 state of fucoxanthin in solution and in fucoxanthin chlorophyll-a/c(2) protein (FCP) based on Stark spectroscopy and molecular-orbital theory*. J. Phys. Chem. B 112: 11838–11853, 2008.
- [43] L. Thomas, J. Kim and T. Cotton. *Comparative-study of resonance Raman and surface-enhanced resonance Raman chlorophyll-a spectra using Soret and red excitation*. J. Am. Chem. Soc. 112: 9378–9386, 1990.
- [44] C. Weiss. *Pi-electron structure and absorption spectra of chlorophylls in solution*. J. Mol. Spectrosc. 44: 37–80, 1972.
- [45] D. Sundholm. *Comparison of the electronic excitation spectra of chlorophyll a and pheophytin a calculated at density functional theory level*. Chem. Phys. Lett. 317: 545–552, 2000.
- [46] G. Kaiser. *Emissions- und Anregungsspektroskopie am photosynthetisierenden Bakterium Rhodospseudomonas sphaeroides bei tiefen Temperaturen*. Hochschul-Verlag - Freiburg, 1981.
- [47] D. Siefermann-Harms. *The light-harvesting and protective functions of carotenoids in photosynthetic membranes*. Physiol. Plant. 69: 561–568, 1987.
- [48] B. Demmig-Adams, A. Gilmore and W. Adams. *Carotenoids .3. In vivo functions of carotenoids in higher plants*. FASEB J. 10: 403–412, 1996.

-
- [49] H. Dutton, W. Manning and B. Duggar. *Chlorophyll fluorescence and energy transfer in the diatom Nitzschia closteriumi*. J. Phys. Chem. 47: 308–313, 1943.
- [50] H. Frank and R. Cogdell. *Carotenoids in photosynthesis*. Photochem. Photobiol. 63: 257–264, 1996.
- [51] Y. Wang, L. Mao and X. Hu. *Insight into the structural role of carotenoids in the Photosystem I: A quantum chemical analysis*. Biophys. J. 86: 3097–3111, 2004.
- [52] R. Edge, D. McGarvey and T. Truscott. *The carotenoids as anti-oxidants - a review*. J. Photochem. Photobiol. B-Biol. 41: 189–200, 1997.
- [53] R. Peto, R. Doll, J. Buckley and M. Sporn. *Can dietary beta-carotene materially reduce human cancer rates?* Nature 290: 201–208, 1981.
- [54] E. Greenberg, J. Baron, T. Stukel, M. Stevens, J. Mandel, S. Spencer, P. Elias, N. Lowe, D. Nierenberg, G. Bayrd, J. Vance, D. Freeman, W. Clendenning and T. Kwan. *A clinical-trial of beta-carotene to prevent basal-cell and squamous-cell cancers of the skin*. N. Engl. J. Med. 323: 789–795, 1990.
- [55] J. Landrum and R. Bone. *Lutein, zeaxanthin, and the macular pigment*. Arch. Biochem. Biophys. 385: 28–40, 2001.
- [56] J. Dwyer, M. Navab, K. Dwyer, K. Hassan, P. Sun, A. Shircore, S. Hama-Levy, G. Hough, X. Wang, T. Drake, C. Merz and A. Fogelman. *Oxygenated carotenoid lutein and progression of early atherosclerosis - The Los Angeles Atherosclerosis Study*. Circulation 103: 2922–2927, 2001.
- [57] J. Olson and N. Krinsky. *The colorful, fascinating world of the carotenoids: Important physiologic modulators - Introduction*. FASEB J. 9: 1547–1550, 1995.
- [58] K. Schulten and M. Karplus. *Origin of a low-lying forbidden transition in polyenes and related molecules*. Chem. Phys. Lett. 14: 305–309, 1972.
- [59] H. Frank and R. Christensen. *Excited Electronic States, Photochemistry and Photophysics of Carotenoids in: Carotenoids, Volume 4: Natural Functions*. Birkhäuser Verlag, 2008.
- [60] H. Frank. *Spectroscopic studies of the low-lying singlet excited electronic states and photochemical properties of carotenoids*. Arch. Biochem. Biophys. 385: 53–60, 2001.
- [61] R. Pariser. *Theory of the electronic spectra and structure of the polyacenes and of alternant hydrocarbons*. J. Chem. Phys. 24: 250–268, 1956.
- [62] P. Callis, T. Scott and A. Albrecht. *Perturbation selection-rules for multiphoton electronic spectroscopy of neutral alternant hydrocarbons*. J. Chem. Phys. 78: 16–22, 1983.

- [63] W. Menke. *Über den Zustand der Carotinoide in den Plastiden*. Naturwissenschaften 28: 31, 1940.
- [64] J. Kirk. *Thermal-dissociation of fucoxanthin-protein binding in pigment complexes from chloroplasts of Hormosira (Phaeophyta)*. Plant Sci. Lett. 9: 373–380, 1977.
- [65] B. Hudson and B. Kohler. *Low-lying weak transition in polyene alpha,omega-diphenyloctatetraene*. Chem. Phys. Lett. 14: 299–304, 1972.
- [66] P. Tavan and K. Schulten. *The low-lying electronic excitations in long polyenes - a PPP-MRD-CL study*. J. Chem. Phys. 85: 6602–6609, 1986.
- [67] P. Tavan and K. Schulten. *Electronic excitations in finite and infinite polyenes*. Phys. Rev. B 36: 4337–4358, 1987.
- [68] M. Wasielewski and L. Kispert. *Direct measurement of the lowest excited singlet-state lifetime of all-trans-beta-carotene and related carotenoids*. Chem. Phys. Lett. 128: 238–243, 1986.
- [69] Y. Koyama, M. Kuki, P. Andersson and T. Gillbro. *Singlet excited states and the light-harvesting function of carotenoids in bacterial photosynthesis*. Photochem. Photobiol. 63: 243–256, 1996.
- [70] C. Gradinaru, J. Kennis, E. Papagiannakis, I. van Stokkum, R. Cogdell, G. Fleming, R. Niederman and R. van Grondelle. *An unusual pathway of excitation energy deactivation in carotenoids: Singlet-to-triplet conversion on an ultrafast timescale in a photosynthetic antenna*. Proc. Natl. Acad. Sci. U. S. A. 98: 2364–2369, 2001.
- [71] K. Furuichi, T. Sashima and Y. Koyama. *The first detection of the $3A(g)(-)$ state in carotenoids using resonance-Raman excitation profiles*. Chem. Phys. Lett. 356: 547–555, 2002.
- [72] M. Kleinschmidt, C. M. Marian, M. Waletzke and S. Grimme. *Parallel multireference configuration interaction calculations on mini-beta-carotenes and beta-carotene*. J. Chem. Phys. 130, 2009.
- [73] C. M. Marian and N. Gilka. *Performance of the density functional theory/multireference configuration interaction method on electronic excitation of extended pi-systems*. J. Chem. Theory Comput. 4: 1501–1515, 2008.
- [74] D. Kosumi, M. Fujiwara, R. Fujii, R. J. Cogdell, H. Hashimoto and M. Yoshizawa. *The dependence of the ultrafast relaxation kinetics of the S-2 and S-1 states in beta-carotene homologs and lycopene on conjugation length studied by femtosecond time-resolved absorption and Kerr-gate fluorescence spectroscopies*. J. Chem. Phys. 130: 214506, 2009.

- [75] D. Kosumi, K. Yanagi, R. Fujii, H. Hashimoto and M. Yoshizawa. *Conjugation length dependence of relaxation kinetics in beta-carotene homologs probed by femtosecond Kerr-gate fluorescence spectroscopy*. Chem. Phys. Lett. 425: 66–70, 2006.
- [76] Y. Koyama, F. Rondonuwu, R. Fujii and Y. Watanabe. *Light-harvesting function of carotenoids in photo-synthesis: The roles of the newly found $1(1)B(u)(-)$ state*. Biopolymers 74: 2–18, 2004.
- [77] J. A. Davis, L. V. Dao, M. T. Do, P. Hannaford, K. A. Nugent and H. M. Quiney. *Noninterferometric two-dimensional fourier-transform spectroscopy of multilevel systems*. Phys. Rev. Lett. 100, 2008.
- [78] T. Miki, Y. Kakitani, Y. Koyama and H. Nagae. *Stimulated emission from the $1B(u)(-)(0)$ level and the $1B(u)(+)(0)+1B(u)(-)$ (1 and 2) diabatic levels upon excitation to the $1B(u)(+)(0)$ level in neurosporene and spheroidene*. Chem. Phys. Lett. 457: 222–226, 2008.
- [79] E. Ostroumov, M. G. Müller, C. M. Marian, M. Kleinschmidt and A. R. Holzwarth. *Electronic Coherence Provides a Direct Proof for Energy-Level Crossing in Photoexcited Lutein and beta-Carotene*. Phys. Rev. Lett. 103: 108302, 2009.
- [80] N. Christensson, T. Polívka, A. Yartsev and T. Pullerits. *Photon echo spectroscopy reveals structure-dynamics relationships in carotenoids*. Phys. Rev. B 79: 245118, 2009.
- [81] J. Hauer, T. Buckup and M. Motzkus. *Quantum control spectroscopy of vibrational modes: Comparison of control scenarios for ground and excited states in beta-carotene*. Chem. Phys. 350: 220–229, 2008.
- [82] J. Hauer, T. Buckup and M. Motzkus. *Pump-degenerate four wave mixing as a technique for analyzing structural and electronic evolution: Multidimensional time-resolved dynamics near a conical intersection*. J. Phys. Chem. A 111: 10517–10529, 2007.
- [83] T. Buckup, J. Savolainen, W. Wohlleben, J. L. Herek, H. Hashimoto, R. R. B. Correia and M. Motzkus. *Pump-probe and pump-deplete-probe spectroscopies on carotenoids with $N=9-15$ conjugated bonds*. J. Chem. Phys. 125: 194505, 2006.
- [84] D. Niedzwiedzki, J. F. Kosciielecki, H. Cong, J. O. Sullivan, G. N. Gibson, R. R. Birge and H. A. Frank. *Ultrafast dynamics and excited state spectra of open-chain carotenoids at room and low temperatures*. J. Phys. Chem. B 111: 5984–5998, 2007.
- [85] H. Frank, R. Desamero, V. Chynwat, R. Gebhard, I. van der Hoef, F. Jansen, J. Lugtenburg, D. Gosztola and M. Wasielewski. *Spectroscopic properties of spheroidene analogs having different extents of pi-electron conjugation*. J. Phys. Chem. A 101: 149–157, 1997.

- [86] P. Andersson, S. Bachilo, R. Chen and T. Gillbro. *Solvent and temperature effects on dual fluorescence in a series of carotenes - energy-gap dependence of the internal-conversion rate*. J. Phys. Chem. 99: 16199–16209, 1995.
- [87] H. Frank, J. Josue, J. Bautista, I. van der Hoef, F. Jansen, J. Lugtenburg, G. Wiederrecht and R. Christensen. *Spectroscopic and photochemical properties of open-chain carotenoids*. J. Phys. Chem. B 106: 2083–2092, 2002.
- [88] H. Frank, J. Bautista, J. Josue, Z. Pendon, R. Hiller, F. Sharples, D. Gosztola and M. Wasielewski. *Effect of the solvent environment on the spectroscopic properties and dynamics of the lowest excited states of carotenoids*. J. Phys. Chem. B 104: 4569–4577, 2000.
- [89] A. Macpherson and T. Gillbro. *Solvent dependence of the ultrafast S-2-S-1 internal conversion rate of beta-carotene*. J. Phys. Chem. A 102: 5049–5058, 1998.
- [90] R. Christensen, M. Goyette, L. Gallagher, J. Duncan, B. DeCoster, J. Lugtenburg, F. Jansen and I. van der Hoef. *S-1 and S-2 states of apo- and diapocarotenes*. J. Phys. Chem. A 103: 2399–2407, 1999.
- [91] V. Chynwat and H. Frank. *The application of the energy-gap law to the S-1 energies and dynamics of carotenoids*. Chem. Phys. 194: 237–244, 1995.
- [92] T. Polívka, J. Herek, D. Zigmantas, H. Akerlund and V. Sundström. *Direct observation of the (forbidden) S-1 state in carotenoids*. Proc. Natl. Acad. Sci. U. S. A. 96: 4914–4917, 1999.
- [93] H. Billsten, D. Zigmantas, V. Sundström and T. Polívka. *Dynamics of vibrational relaxation in the S-1 state of carotenoids having 11 conjugated C=C bonds*. Chem. Phys. Lett. 355: 465–470, 2002.
- [94] M. Ricci, S. Bradforth, R. Jimenez and G. Fleming. *Internal conversion and energy transfer dynamics of spheroidene in solution and in the LH-1 and LH-2 light-harvesting complexes*. Chem. Phys. Lett. 259: 381–390, 1996.
- [95] S. Akimoto, I. Yamazaki, S. Takaichi and M. Mimuro. *Excitation relaxation of carotenoids within the S-2 state probed by the femtosecond fluorescence up-conversion method*. Chem. Phys. Lett. 313: 63–68, 1999.
- [96] S. Akimoto, I. Yamazaki, T. Sakawa and M. Mimuro. *Temperature effects on excitation relaxation dynamics of the carotenoid beta-carotene and its analogue beta-apo-8 '-carotenal, probed by femtosecond fluorescence spectroscopy*. J. Phys. Chem. A 106: 2237–2243, 2002.
- [97] T. Förster. *Zwischenmolekulare Energiewanderung und Fluoreszenz*. Ann. Physik 2: 55–75, 1948.

- [98] D. Dexter. *A theory of sensitized luminescence in solids*. J. Chem. Phys. 21: 836–850, 1953.
- [99] J. Bautista, R. Connors, B. Raju, R. Hiller, F. Sharples, D. Gosztola, M. Wasielewski and H. Frank. *Excited state properties of peridinin: Observation of a solvent dependence of the lowest excited singlet state lifetime and spectral behavior unique among carotenoids*. J. Phys. Chem. B 103: 8751–8758, 1999.
- [100] D. Zigmantas, R. Hiller, F. Sharples, H. Frank, V. Sundström and T. Polívka. *Effect of a conjugated carbonyl group on the photophysical properties of carotenoids*. Phys. Chem. Chem. Phys. 6: 3009–3016, 2004.
- [101] D. Zigmantas, R. Hiller, A. Yartsev, V. Sundström and T. Polívka. *Dynamics of excited states of the carotenoid peridinin in polar solvents: Dependence on excitation wavelength, viscosity, and temperature*. J. Phys. Chem. B 107: 5339–5348, 2003.
- [102] S. Shima, R. Ilagan, N. Gillespie, B. Sommer, R. Hiller, F. Sharples, H. Frank and R. Birge. *Two-photon and fluorescence spectroscopy and the effect of environment on the photochemical properties of peridinin in solution and in the peridinin-chlorophyll-protein from Amphidinium carterae*. J. Phys. Chem. A 107: 8052–8066, 2003.
- [103] M. Mimuro, U. Nagashima, S. Takaichi, Y. Nishimura, I. Yamazaki and T. Katoh. *Molecular-structure and optical-properties of carotenoids for the in vivo energy-transfer function in the algal photosynthetic pigment system*. Biochim. Biophys. Acta 1098: 271–274, 1992.
- [104] M. Mimuro, Y. Nishimura, S. Takaichi, Y. Yamano, M. Ito, S. Nagaoka, I. Yamazaki, T. Katoh and U. Nagashima. *The effect of molecular-structure on the relaxation process of carotenoids containing a carbonyl group*. Chem. Phys. Lett. 213: 576–580, 1993.
- [105] D. Zigmantas, T. Polívka, R. Hiller, A. Yartsev and V. Sundström. *Spectroscopic and dynamic properties of the peridinin lowest singlet excited states*. J. Phys. Chem. A 105: 10296–10306, 2001.
- [106] H. Vaswani, C. Hsu, M. Head-Gordon and G. Fleming. *Quantum chemical evidence for an intramolecular charge-transfer state in the carotenoid peridinin of peridinin-chlorophyll-protein*. J. Phys. Chem. B 107: 7940–7946, 2003.
- [107] M. M. Enriquez, M. Fuciman, A. M. LaFountain, N. L. Wagner, R. R. Birge and H. A. Frank. *The Intramolecular Charge Transfer State in Carbonyl-Containing Polyenes and Carotenoids*. J. Phys. Chem. B 114: 12416–12426, 2010.

- [108] E. Papagiannakis, D. Larsen, I. van Stokkum, M. Vengris, R. Hiller and R. van Grondelle. *Resolving the excited state equilibrium of peridinin in solution*. *Biochemistry* 43: 15303–15309, 2004.
- [109] E. Papagiannakis, M. Vengris, D. Larsen, I. van Stokkum, R. Hiller and R. van Grondelle. *Use of ultrafast dispersed pump-dump-probe and pump-repump-probe spectroscopies to explore the light-induced dynamics of peridinin in solution*. *J. Phys. Chem. B* 110: 512–521, 2006.
- [110] D. Kosumi, T. Kusumoto, R. Fujii, M. Sugisaki, Y. Iinuma, N. Oka, Y. Takaesu, T. Taira, M. Iha, H. A. Frank and H. Hashimoto. *One- and two-photon pump-probe optical spectroscopic measurements reveal the S-1 and intramolecular charge transfer states are distinct in fucoxanthin*. *Chem. Phys. Lett.* 483: 95–100, 2009.
- [111] P. Linden, J. Zimmermann, T. Brixner, N. Holt, H. Vaswani, R. Hiller and G. Fleming. *Transient absorption study of peridinin and peridinin-chlorophyll a-protein after two-photon excitation*. *J. Phys. Chem. B* 108: 10340–10345, 2004.
- [112] N. Adir, H. Zer, S. Shochat and I. Ohad. *Photoinhibition - a historical perspective*. *Photosynth. Res.* 76: 343–370, 2003.
- [113] M. Havaux, F. Eymery, S. Porfirova, P. Rey and P. Dormann. *Vitamin E protects against photoinhibition and photooxidative stress in Arabidopsis thaliana*. *Plant Cell* 17: 3451–3469, 2005.
- [114] E. Peterman, F. Dukker, R. van Grondelle and H. van Amerongen. *Chlorophyll a and carotenoid triplet states in light-harvesting complex II of higher plants*. *Biophys. J.* 69: 2670–2678, 1995.
- [115] K. Maxwell and G. Johnson. *Chlorophyll fluorescence - a practical guide*. *J. Exp. Bot.* 51: 659–668, 2000.
- [116] B. Demmig-Adams and W. Adams. *The role of xanthophyll cycle carotenoids in the protection of photosynthesis*. *Trends Plant Sci.* 1: 21–26, 1996.
- [117] A. Ruban, J. Lavaud, B. Rousseau, G. Guglielmi, P. Horton and A. Etienne. *The super-excess energy dissipation in diatom algae: comparative analysis with higher plants*. *Photosynth. Res.* 82: 165–175, 2004.
- [118] S. Amarie, J. Standfuss, T. Barros, W. Kühlbrandt, A. Dreuw and J. Wachtveitl. *Carotenoid radical cations as a probe for the molecular mechanism of nonphotochemical quenching in oxygenic photosynthesis*. *J. Phys. Chem. B* 111: 3481–3487, 2007.
- [119] R. Goss, E. A. Pinto, C. Wilhelm and M. Richter. *The importance of a highly active and Delta pH-regulated diatoxanthin epoxidase for the regulation of the PSII antenna function in diadinoxanthin cycle containing algae*. *J. Plant Physiol.* 163: 1008–1021, 2006.

- [120] I. Grouneva, T. Jakob, C. Wilhelm and R. Goss. *Influence of ascorbate and pH on the activity of the diatom xanthophyll cycle-enzyme diadinoxanthin de-epoxidase*. *Physiol. Plant.* 126: 205–211, 2006.
- [121] I. Grouneva, T. Jakob, C. Wilhelm and R. Goss. *A new multicomponent NPQ mechanism in the diatom Cyclotella meneghiniana*. *Plant Cell Physiol.* 49: 1217–1225, 2008.
- [122] B. Green and D. Durnford. *The chlorophyll-carotenoid proteins of oxygenic photosynthesis*. *Annu. Rev. Plant Physiol. Plant Molec. Biol.* 47: 685–714, 1996.
- [123] D. Bhaya and A. Grossman. *Characterization of gene clusters encoding the fucoxanthin chlorophyll proteins of the diatom Phaeodactylum tricorutum*. *Nucleic Acids Res.* 21: 4458–4466, 1993.
- [124] M. Eppard and E. Rhiel. *The genes encoding light-harvesting subunits of Cyclotella cryptica (Bacillariophyceae) constitute a complex and heterogeneous family*. *Mol. Gen. Genet.* 260: 335–345, 1998.
- [125] C. Büchel. *Fucoxanthin-chlorophyll proteins in diatoms: 18 and 19 kDa subunits assemble into different oligomeric states*. *Biochemistry* 42: 13027–13034, 2003.
- [126] H. Frank, A. Cua, V. Chynwat, A. Young, D. Gosztola and M. Wasielewski. *The lifetimes and energies of the first excited singlet states of diadinoxanthin and diatoxanthin: The role of these molecules in excess energy dissipation in algae*. *Biochim. Biophys. Acta - Bioenerg.* 1277: 243–252, 1996.
- [127] D. Durnford, R. Aebersold and B. Green. *The fucoxanthin-chlorophyll proteins from a chromophyte alga are part of a large multigene family: Structural and evolutionary relationships to other light harvesting antennae*. *Mol. Gen. Genet.* 253: 377–386, 1996.
- [128] T. Owens and E. Wold. *Light-harvesting function in the diatom Phaeodactylum tricorutum. 1. Isolation and characterization of pigment-protein complexes*. *Plant Physiol.* 80: 732–738, 1986.
- [129] C. Berkaloff, L. Caron and B. Rousseau. *Subunit organization of PSI particles from brown-algae and diatoms - polypeptide and pigment analysis*. *Photosynth. Res.* 23: 181–193, 1990.
- [130] E. Papagiannakis, I. van Stokkum, H. Fey, C. Büchel and R. van Grondelle. *Spectroscopic characterization of the excitation energy transfer in the fucoxanthin-chlorophyll protein of diatoms*. *Photosynth. Res.* 86: 241–250, 2005.
- [131] B. Green and E. Pichersky. *Hypothesis for the evolution of three-helix Chl a/b and Chl a/c light-harvesting antenna proteins from two-helix and four-helix ancestors*. *Photosynth. Res.* 39: 149–162, 1994.

- [132] M. Lohr and C. Wilhelm. *Algae displaying the diadinoxanthin cycle also possess the violaxanthin cycle*. Proc. Natl. Acad. Sci. U.S.A. 96: 8784–8789, 1999.
- [133] A. Ruban, P. Lee, M. Wentworth, A. Young and P. Horton. *Determination of the stoichiometry and strength of binding of xanthophylls to the photosystem II light harvesting complexes*. J. Biol. Chem. 274: 10458–10465, 1999.
- [134] J. Lavaud, B. Rousseau and A. Etienne. *Enrichment of the light-harvesting complex in diadinoxanthin and implications for the nonphotochemical fluorescence quenching in diatoms*. Biochemistry 42: 5802–5808, 2003.
- [135] A. Pascal, L. Caron, B. Rousseau, K. Lapouge, J. Duval and B. Robert. *Resonance Raman spectroscopy of a light-harvesting protein from the brown alga *Laminaria saccharina**. Biochemistry 37: 2450–2457, 1998.
- [136] L. Premvardhan, B. Robert, A. Beer and C. Büchel. *Pigment organization in fucoxanthin chlorophyll *a/c*(2) proteins (FCP) based on resonance Raman spectroscopy and sequence analysis*. Biochim. Biophys. Acta - Bioenerg. 1797: 1647–1656, 2010.
- [137] M. Eppard and E. Rhiel. *Investigations on gene copy number, introns and chromosomal arrangement of genes encoding the fucoxanthin chlorophyll *a/c*-binding proteins of the centric diatom *Cyclotella cryptica**. Protist 151: 27–39, 2000.
- [138] T. Veith, J. Brauns, W. Weisheit, M. Mittag and C. Büchel. *Identification of a specific fucoxanthin-chlorophyll protein in the light harvesting complex of photosystem I in the diatom *Cyclotella meneghiniana**. Biochim. Biophys. Acta - Bioenerg. 1787: 905–912, 2009.
- [139] Y. Miloslavina, I. Grouneva, P. H. Lambrev, B. Lepetit, R. Goss, C. Wilhelm and A. R. Holzwarth. *Ultrafast fluorescence study on the location and mechanism of non-photochemical quenching in diatoms*. Biochim. Biophys. Acta - Bioenerg. 1787: 1189–1197, 2009.
- [140] A. Oeltjen, W. Krumbein and E. Rhiel. *Investigations on transcript sizes, steady state mRNA concentrations and diurnal expression of genes encoding fucoxanthin chlorophyll *a/c* light harvesting polypeptides in the centric diatom *Cyclotella cryptica**. Plant Biol. 4: 250–257, 2002.
- [141] K. Gundermann and C. Büchel. *The fluorescence yield of the trimeric fucoxanthin-chlorophyll-protein FCPa in the diatom *Cyclotella meneghiniana* is dependent on the amount of bound diatoxanthin*. Photosynth. Res. 95: 229–235, 2008.
- [142] C. Büchel and C. Wilhelm. *Isolation and characterization of a photosystem I-associated antenna (LHC-I) and a photosystem I-core complex from the chlorophyll-*c*-containing alga *Pleurochloris meiringensis* (Xanthophyceae)*. J. Photochem. Photobiol. B-Biol. 20: 87–93, 1993.

-
- [143] P. Atkins and J. de Paula. *Physical Chemistry*. Oxford University Press, 8th edition, 2006.
- [144] H. Haken and H. Wolf. *Molekülphysik und Quantenchemie - Einführung in die experimentellen und theoretischen Grundlagen*. Springer Berlin Heidelberg New York, 5th edition, 2006.
- [145] M. Hesse, H. Meier and B. Zeeh. *Spektroskopische Methoden in der organischen Chemie*. Georg Thieme Verlag KG Stuttgart, 7th edition, 2005.
- [146] M. Kasha. *Characterization of electronic transitions in complex molecules*. Farad. Disc. pp. 14–19, 1950.
- [147] I. van Stokkum, D. Larsen and R. van Grondelle. *Global and target analysis of time-resolved spectra*. Biochim. Biophys. Acta - Bioenerg. 1657: 82–104, 2004.
- [148] S. E. Braslavsky. *Glossary of terms used in Photochemistry 3(rd) Edition (IUPAC Recommendations 2006)*. Pure Appl. Chem. 79: 293–465, 2007.
- [149] J. Lakowicz. *Principles of Fluorescence Spectroscopy*. Springer, 3rd edition, 2006.
- [150] F. Kleima, E. Hofmann, B. Gobets, I. van Stokkum, R. van Grondelle, K. Diederichs and H. van Amerongen. *Förster excitation energy transfer in peridinin-chlorophyll-a-protein*. Biophys. J. 78: 344–353, 2000.
- [151] J. Kennis, B. Gobets, I. van Stokkum, J. Dekker, R. van Grondelle and G. Fleming. *Light harvesting by chlorophylls and carotenoids in the photosystem I core complex of Synechococcus elongatus: A fluorescence upconversion study*. J. Phys. Chem. B 105: 4485–4494, 2001.
- [152] T. Tomi, Y. Shibata, Y. Ikeda, S. Taniguchi, C. Haik, N. Mataga, K. Shimada and S. Itoh. *Energy and electron transfer in the photosynthetic reaction center complex of Acidiphilium rubrum containing Zn-bacteriochlorophyll a studied by femtosecond up-conversion spectroscopy*. Biochim. Biophys. Acta - Bioenerg. 1767: 22–30, 2007.
- [153] B. Krueger, S. Lampoura, I. van Stokkum, E. Papagiannakis, J. Salverda, C. Gradinaru, D. Rutkauskas, R. Hiller and R. van Grondelle. *Energy transfer in the peridinin chlorophyll-a protein of Amphidinium carterae studied by polarized transient absorption and target analysis*. Biophys. J. 80: 2843–2855, 2001.
- [154] D. Jonas, M. Lang, Y. Nagasawa, T. Joo and G. Fleming. *Pump-probe polarization anisotropy study of femtosecond energy transfer within the photosynthetic reaction center of Rhodospirillum rubrum R26*. J. Phys. Chem. 100: 12660–12673, 1996.
- [155] S. Wawilow. *The fluorescence yield of dyestuff solutions*. Z. Phys. 22: 266–272, 1924.

- [156] R. Kubin and A. Fletcher. *Fluorescence quantum yields of some rhodamine dyes*. J. Lumines. 27: 455–462, 1982.
- [157] J. Demas and G. Crosby. *Measurement of photoluminescence quantum yields - Review*. J. Phys. Chem. 75: 991–1024, 1971.
- [158] C. Parker and W. Rees. *Correction of fluorescence spectra and measurement of fluorescence quantum efficiency*. Analyst 85: 587–600, 1960.
- [159] A. Williams, S. Winfield and J. Miller. *Relative fluorescence quantum yields using a computer-controlled luminescence spectrometer*. Analyst 108: 1067–1071, 1983.
- [160] R. Norrish and G. Porter. *Chemical reactions produced by very high light intensities*. Nature 164: 658, 1949.
- [161] R. Norrish. *Kinetics and analysis of very fast chemical reactions*. Science 149: 1470–1482, 1965.
- [162] L. Bollinger and G. Thomas. *Measurement of time dependence of scintillation intensity by a delayed-coincidence method*. Rev. Sci. Instrum. 32: 1044, 1961.
- [163] R. Boyd. *Nonlinear Optics*. Elsevier, 3rd edition, 2008.
- [164] W. Demtröder. *Laserspektroskopie*. Springer, 5th edition, 2007.
- [165] J. Eichler and H. Eichler. *Laser - Bauformen, Strahlführung, Anwendungen*. Springer, 7th edition, 2010.
- [166] D. Meschede. *Optik, Licht und Laser*. Vieweg + Teubner, 3rd edition, 2008.
- [167] H. Eichler, A. Fleischer, J. Kross, M. Krystek, H. Lang, H. Niedrig, H. Rauch, G. Schmahl, H. Schoenebeck, E. Sedlmayr, H. Weber and K. Weber. *Lehrbuch der Experimentalphysik: Optik*, volume 3. Walter de Gruyter, 9th edition, 1993.
- [168] A. DeMaria, D. Stetser and W. Glenn. *Ultrashort light pulses*. Science 156: 1557–1568, 1967.
- [169] P. French. *The generation of ultrashort laser-pulses*. Rep. Prog. Phys. 58: 169–262, 1995.
- [170] R. Paschotta. *Encyclopedia of Laser Physics and Technology*. Wiley VCH Verlag GmbH, 2008.
- [171] M. Fermann, M. Andrejco, Y. Silberberg and M. Stock. *Passive-mode locking by using nonlinear polarization evolution in a polarization-maintaining erbium-doped fiber*. Opt. Lett. 18: 894–896, 1993.
- [172] E. Ippen, L. Liu and H. Haus. *Self-starting condition for additive-pulse mode-locked lasers*. Opt. Lett. 15: 183–185, 1990.

-
- [173] G. Steinmeyer, D. Sutter, L. Gallmann, N. Matuschek and U. Keller. *Frontiers in ultrashort pulse generation: Pushing the limits in linear and nonlinear optics*. Science 286: 1507–1512, 1999.
- [174] T. Brabec, C. Spielmann, P. Curley and F. Krausz. *Kerr lens mode-locking*. Opt. Lett. 17: 1292–1294, 1992.
- [175] S. Chen and J. Wang. *Self-starting issues of passive self-focusing mode-locking*. Opt. Lett. 16: 1689–1691, 1991.
- [176] D. Strickland and G. Mourou. *Compression of amplified chirped optical pulses*. Opt. Commun. 56: 219–221, 1985.
- [177] G. Vaillancourt, T. Norris, J. Coe, P. Bado and G. Mourou. *Operation of a 1-kHz pulse-pumped Ti-sapphire regenerative amplifier*. Opt. Lett. 15: 317–319, 1990.
- [178] I. Kozma, P. Baum, U. Schmidhammer, S. Lochbrunner and E. Riedle. *Compact autocorrelator for the online measurement of tunable 10 femtosecond pulses*. Rev. Sci. Instrum. 75: 2323–2327, 2004.
- [179] G. Cerullo, M. Nisoli and S. De Silvestri. *Generation of 11 fs pulses tunable across the visible by optical parametric amplification*. Appl. Phys. Lett. 71: 3616–3618, 1997.
- [180] G. Cerullo and S. De Silvestri. *Ultrafast optical parametric amplifiers*. Rev. Sci. Instrum. 74: 1–18, 2003.
- [181] R. Huber, H. Satzger, W. Zinth and J. Wachtveitl. *Noncollinear optical parametric amplifiers with output parameters improved by the application of a white light continuum generated in CaF₂*. Opt. Commun. 194: 443–448, 2001.
- [182] J. Piel, M. Beutler and E. Riedle. *20-50-fs pulses tunable across the near infrared from a blue-pumped noncollinear parametric amplifier*. Opt. Lett. 25: 180–182, 2000.
- [183] T. Wilhelm, J. Piel and E. Riedle. *Sub-20-fs pulses tunable across the visible from a blue-pumped single-pass noncollinear parametric converter*. Opt. Lett. 22: 1494–1496, 1997.
- [184] R. Alfano and S. Shapiro. *Observation of self-phase modulation and small-scale filaments in crystals and glasses*. Phys. Rev. Lett. 24: 592–594, 1970.
- [185] R. Alfano and S. Shapiro. *Emission in region 4000 to 7000 Å via 4-photon coupling in glass*. Phys. Rev. Lett. 24: 584–578, 1970.
- [186] R. Fork, C. Shank, C. Hirlimann, R. Yen and W. Tomlinson. *Femtosecond white-light continuum pulses*. Opt. Lett. 8: 1–3, 1983.

- [187] A. Gaeta. *Catastrophic collapse of ultrashort pulses*. Phys. Rev. Lett. 84: 3582–3585, 2000.
- [188] M. Kolesik, G. Katona, J. Moloney and E. Wright. *Theory and simulation of supercontinuum generation in transparent bulk media*. Appl. Phys. B-Lasers Opt. 77: 185–195, 2003.
- [189] M. Kolesik, G. Katona, J. Moloney and E. Wright. *Physical factors limiting the spectral extent and band gap dependence of supercontinuum generation*. Phys. Rev. Lett. 91: 043905, 2003.
- [190] H. Dachraoui, C. Oberer, M. Michelswirth and U. Heinzmann. *Direct time-domain observation of laser pulse filaments in transparent media*. Phys. Rev. A 82: 043820, 2010.
- [191] A. Brodeur and S. Chin. *Band-gap dependence of the ultrafast white-light continuum*. Phys. Rev. Lett. 80: 4406–4409, 1998.
- [192] A. Brodeur and S. Chin. *Ultrafast white-light continuum generation and self-focusing in transparent condensed media*. J. Opt. Soc. Am. B-Opt. Phys. 16: 637–650, 1999.
- [193] W. Ware, S. Lee, G. Brant and P. Chow. *Nanosecond time-resolved emission spectroscopy - spectral shifts due to solvent-excited solute relaxation*. J. Chem. Phys. 54: 4729–4737, 1971.
- [194] J. Karolczak, D. Komar, J. Kubicki, T. Wrozowa, K. Dobek, B. Ciesielska and A. Maciejewski. *The measurements of picosecond fluorescence lifetimes with high accuracy and subpicosecond precision*. Chem. Phys. Lett. 344: 154–164, 2001.
- [195] W. Becker, A. Bergmann, M. Hink, K. Konig, K. Benndorf and C. Biskup. *Fluorescence lifetime imaging by time-correlated single-photon counting*. Microsc. Res. Tech. 63: 58–66, 2004.
- [196] G. Porter, E. Reid and C. Tredwell. *Time resolved fluorescence in the picosecond region*. Chem. Phys. Lett. 29: 469–472, 1974.
- [197] G. Beddard, T. Doust and G. Porter. *Picosecond fluorescence depolarization measured by frequency-conversion*. Chem. Phys. 61: 17–23, 1981.
- [198] M. Kahlow, W. Jarzeba, T. Dubruil and P. Barbara. *Ultrafast emission-spectroscopy in the ultraviolet by time-gated upconversion*. Rev. Sci. Instrum. 59: 1098–1109, 1988.
- [199] H. Mahr and M. Hirsch. *Optical up-conversion light gate with picosecond resolution*. Opt. Commun. 13: 96–99, 1975.

-
- [200] M. Glasbeek and H. Zhang. *Femtosecond studies of solvation and intramolecular configurational dynamics of fluorophores in liquid solution*. Chem. Rev. 104: 1929–1954, 2004.
- [201] R. Schanz, S. Kovalenko, V. Kharlanov and N. Ernsting. *Broad-band fluorescence upconversion for femtosecond spectroscopy*. Appl. Phys. Lett. 79: 566–568, 2001.
- [202] S. Kovalenko, R. Schanz, T. Senyushkina and N. Ernsting. *Femtosecond spectroscopy of p-dimethylaminocyanostilbene in solution - no evidence for dual fluorescence*. Phys. Chem. Chem. Phys. 4: 703–707, 2002.
- [203] L. Zhao, J. Lustres, V. Farztdinov and N. Ernsting. *Femtosecond fluorescence spectroscopy by upconversion with tilted gate pulses*. Phys. Chem. Chem. Phys. 7: 1716–1725, 2005.
- [204] J. Takeda, K. Nakajima, S. Kurita, S. Tomimoto, S. Saito and T. Suemoto. *Time-resolved luminescence spectroscopy by the optical Kerr-gate method applicable to ultrafast relaxation processes*. Phys. Rev. B 62: 10083–10087, 2000.
- [205] S. Kinoshita, H. Ozawa, Y. Kanematsu, I. Tanaka, N. Sugimoto and S. Fujiwara. *Efficient optical Kerr shutter for femtosecond time-resolved luminescence spectroscopy*. Rev. Sci. Instrum. 71: 3317–3322, 2000.
- [206] S. Arzhantsev and M. Maroncelli. *Design and characterization of a femtosecond fluorescence spectrometer based on optical Kerr gating*. Appl. Spectrosc. 59: 206–220, 2005.
- [207] L. Yan, J. Yue, J. Si and X. Hou. *Influence of self-diffraction effect on femtosecond pump-probe optical Kerr measurements*. Opt. Express 16: 12069–12074, 2008.
- [208] B. Schmidt. *Femtosekunden-Fluoreszenzspektroskopie photoisomerisierender Molekuele*. Ph.D. thesis, Ludwig-Maximilians-University, München, 2004.
- [209] N. Sugimoto, S. Ito, S. Fujiwara, T. Suzuki, H. Kanbara and K. Hirao. *Femtosecond and terahertz optical Kerr shutter switching in glass containing high concentration of Bi₂O₃*. Opt. Commun. 161: 47–50, 1999.
- [210] J. Aber, M. Newstein and B. Garetz. *Femtosecond optical Kerr effect measurements in silicate glasses*. J. Opt. Soc. Am. B-Opt. Phys. 17: 120–127, 2000.
- [211] R. Fujii, K. Onaka, M. Kuki, Y. Koyama and Y. Watanabe. *The 2A(g)(-) energies of all-trans-neurosporene and spheroidene as determined by fluorescence spectroscopy*. Chem. Phys. Lett. 288: 847–853, 1998.
- [212] H. Frank, J. Bautista, J. Josue and A. Young. *Mechanism of nonphotochemical quenching in green plants: Energies of the lowest excited singlet states of violaxanthin and zeaxanthin*. Biochemistry 39: 2831–2837, 2000.

- [213] Spectra-Physics. *Manual: Millennia Pro s-Series - Diode-pumped, CW visible laser systems.*
- [214] Spectra-Physics. *Manual: Empower - Intracavity-doubled, diode-pumped Nd:YLF laser systems.*
- [215] Spectra-Physics. *Manual: Tsunami - Mode-locked Ti:sapphire laser.*
- [216] Spectra-Physics. *Manual: Spitfire Pro - Ti:sapphire regenerative amplifier systems.*
- [217] B. Heinz. *Alte Photoreaktionen in neuem Licht - Ultraschnelle Spektroskopie an Fulgimiden und photolabilen Schutzgruppen.* Ph.D. thesis, Ludwig-Maximilians-University, München, 2008.
- [218] Princeton-Instruments. *Data sheet: Acton Standard Series of Monochromators and Spectrographs.*
- [219] Princeton-Instruments. *Data sheet: Spec-10:400.*
- [220] P. Trojanowski. *Aufbau einer breitbandigen fs-zeitaufgeloesten Fluoreszenzapparatur zur Charakterisierung von photoschaltbaren Systemen.* Master's thesis, Goethe University Frankfurt, 2009.
- [221] M. Roth. *Aufbau eines nichtkollinear gepumpten optisch parametrischen Verstaerkers.* Master's thesis, Friedrich-Schiller-University, Jena, 2000.
- [222] H. Studzinski. *Aufbau und Charakterisierung eines nichtkollinear optisch-parametrischen Verstaerkers.* Master's thesis, Christian-Albrechts-University, Kiel, 2002.
- [223] M. Lenz. *Kurzzeitspektroskopische Untersuchungen photoinduzierter Ladungstransferreaktionen.* Ph.D. thesis, Goethe University Frankfurt, 2005.
- [224] U. Förster. *Untersuchung der Konformation und Dynamik von RNA mit Hilfe fluoreszierender Farbstoffmoleküle.* Ph.D. thesis, Goethe University, Frankfurt am Main, 2010.
- [225] A. Dharmadhikari, F. Rajgara and D. Mathur. *Systematic study of highly efficient white light generation in transparent materials using intense femtosecond laser pulses.* Appl. Phys. B-Lasers Opt. 80: 61–66, 2005.
- [226] R. Kaindl, M. Wurm, K. Reimann, P. Hamm, A. Weiner and M. Woerner. *Generation, shaping, and characterization of intense femtosecond pulses tunable from 3 to 20 μ m.* J. Opt. Soc. Am. B-Opt. Phys. 17: 2086–2094, 2000.
- [227] P. Hamm, R. Kaindl and J. Stenger. *Noise suppression in femtosecond mid-infrared light sources.* Opt. Lett. 25: 1798–1800, 2000.

-
- [228] R. Fork, O. Martinez and J. Gordon. *Negative dispersion using pairs of prisms*. Opt. Lett. 9: 150–152, 1984.
- [229] J. Kafka and T. Baer. *Prism-pair dispersive delay-lines in optical pulse compression*. Opt. Lett. 12: 401–403, 1987.
- [230] F. J. Duarte. *Generalized multiple-prism dispersion theory for laser pulse compression: higher order phase derivatives*. Appl. Phys. B-Lasers Opt. 96: 809–814, 2009.
- [231] U. Förster, N. Gildenhoff, C. Grünewald, J. W. Engels and J. Wachtveitl. *Photophysics of 1-ethynylpyrene-modified RNA base adenine*. J. Lumines. 129: 1454–1458, 2009.
- [232] T. Pancur. *Untersuchung der Isomerisierungsdynamik von Azobenzolen und der strahlungslosen Desaktivierung von Nukleobasen mit Hilfe der Femtosekunden-Fluoreszenzspektroskopie*. Ph.D. thesis, Christian-Albrechts-University, Kiel, 2004.
- [233] J. Enderlein and R. Erdmann. *Fast fitting of multi-exponential decay curves*. Opt. Commun. 134: 371–378, 1997.
- [234] Clark-Inc. *Manual: Clark-MRX CPA 2001 Laser System*.
- [235] S. Amarie. *Photo-protective function of carotenoids in photosynthesis*. Ph.D. thesis, Goethe University Frankfurt, 2008.
- [236] A. Dobryakov, S. Kovalenko and N. Ernsting. *Electronic and vibrational coherence effects in broadband transient absorption spectroscopy with chirped supercontinuum probing*. J. Chem. Phys. 119: 988–1002, 2003.
- [237] A. Dobryakov, S. Kovalenko and N. Ernsting. *Coherent and sequential contributions to femtosecond transient absorption spectra of a rhodamine dye in solution*. J. Chem. Phys. 123: 044502, 2005.
- [238] S. Kovalenko, A. Dobryakov, J. Ruthmann and N. Ernsting. *Femtosecond spectroscopy of condensed phases with chirped supercontinuum probing*. Phys. Rev. A 59: 2369–2384, 1999.
- [239] M. Lorenc, M. Ziolk, R. Naskrecki, J. Karolczak, J. Kubicki and A. Maciejewski. *Artifacts in femtosecond transient absorption spectroscopy*. Appl. Phys. B-Lasers Opt. 74: 19–27, 2002.
- [240] R. Christensen and B. Kohler. *Low resolution optical spectroscopy of retinyl polyenes - low-lying electronic levels and spectral broadness*. Photochem. Photobiol. 18: 293–301, 1973.

- [241] M. Mimuro, S. Akimoto, S. Takaichi and I. Yamazaki. *Effect of molecular structures and solvents on the excited state dynamics of the S-2 state of carotenoids analyzed by the femtosecond up-conversion method*. J. Am. Chem. Soc. 119: 1452–1453, 1997.
- [242] I. Szabo, E. Bergantino and G. Giacometti. *Light and oxygenic photosynthesis: energy dissipation as a protection mechanism against photo-oxidation*. EMBO Rep. 6: 629–634, 2005.
- [243] A. V. Ruban, R. Berera, C. Illoaia, I. H. M. van Stokkum, J. T. M. Kennis, A. A. Pascal, H. van Amerongen, B. Robert, P. Horton and R. van Grondelle. *Identification of a mechanism of photoprotective energy dissipation in higher plants*. Nature 450: 575–578, 2007.
- [244] E. Papagiannakis, I. van Stokkum, R. van Grondelle, R. Niederman, D. Zigmantas, V. Sundström and T. Polívka. *A near-infrared transient absorption study of the excited-state dynamics of the carotenoid spirilloxanthin in solution and in the LH1 complex of Rhodospirillum rubrum*. J. Phys. Chem. B 107: 11216–11223, 2003.
- [245] T. Polívka, I. H. M. van Stokkum, D. Zigmantas, R. van Grondelle, V. Sundström and R. G. Hiller. *Energy transfer in the major intrinsic light-harvesting complex from Amphidinium carterae*. Biochemistry 45: 8516–8526, 2006.
- [246] P. Andersson and T. Gillbro. *Photophysics and dynamics of the lowest excited singlet-state in long substituted polyenes with implications to the very long-chain limit*. J. Chem. Phys. 103: 2509–2519, 1995.
- [247] P. Andersson, R. Cogdell and T. Gillbro. *Femtosecond dynamics of carotenoid-to-bacteriochlorophyll a energy transfer in the light-harvesting antenna complexes from the purple bacterium Chromatium purpuratum*. Chem. Phys. 210: 195–217, 1996.
- [248] T. Bittner, K. Irrgang, G. Renger and M. Wasielewski. *Ultrafast excitation-energy transfer and exciton-exciton annihilation processes in isolated light-harvesting complexes of photosystem-II (LHC-II) from spinach*. J. Phys. Chem. 98: 11821–11826, 1994.
- [249] F. Kleima, C. Gradinaru, F. Calkoen, I. van Stokkum, R. van Grondelle and H. van Amerongen. *Energy transfer in LHCII monomers at 77K studied by sub-picosecond transient absorption spectroscopy*. Biochemistry 36: 15262–15268, 1997.
- [250] M. A. Palacios, J. Standfuss, M. Vengris, B. F. van Oort, I. H. M. van Stokkum, W. Kühlbrandt, H. van Amerongen and R. van Grondelle. *A comparison of the three isoforms of the light-harvesting complex II using transient absorption and time-resolved fluorescence measurements*. Photosynth. Res. 88: 269–285, 2006.

-
- [251] J. Pieper, M. Raetsep, K.-D. Irrgang and A. Freiberg. *Chromophore-Chromophore and Chromophore-Protein Interactions in Monomeric Light-Harvesting Complex II of Green Plants Studied by Spectral Hole Burning and Fluorescence Line Narrowing*. J. Phys. Chem. B 113: 10870–10880, 2009.
- [252] A. Damjanovic, T. Ritz and K. Schulten. *Excitation transfer in the peridinin-chlorophyll-protein of Amphidinium carterae*. Biophys. J. 79: 1695–1705, 2000.
- [253] J. L. P. Lustres, A. L. Dobryakov, A. Holzwarth and M. Veiga. *S₂ -> S₁ internal conversion in beta-carotene: Strong vibronic coupling from amplitude oscillations of transient absorption bands*. Angew. Chem.-Int. Edit. 46: 3758–3761, 2007.
- [254] N. Christensson, P. Chabera, R. G. Hiller, T. Pullerits and T. Polívka. *Four-wave-mixing spectroscopy of peridinin in solution and in the peridinin-chlorophyll-a protein*. Chem. Phys. 373: 15–22, 2010.

Publikationen

N. Gildenhoff, J. Herz, K. Gundermann, C. Büchel and J. Wachtveitl; *The excitation energy transfer in the trimeric fucoxanthin-chlorophyll protein from Cyclotella meneghiniana analyzed by polarized transient absorption spectroscopy*; Chemical Physics (**2010**) 373, 104-109

N. Gildenhoff, S. Amarie, K. Gundermann, A. Beer, C. Büchel, and J. Wachtveitl; *Oligomerization and pigmentation dependent excitation energy transfer in fucoxanthin-chlorophyll proteins*; Biochimica et Biophysica Acta – Bioenergetics (**2010**) 1797, 543-549

S. Amarie, U. Förster, N. Gildenhoff, A. Dreuw and J. Wachtveitl; *Excited state dynamics of the astaxanthin radical cation*; Chemical Physics (**2010**) 373, 8-14

U. Förster, N. Gildenhoff, C. Grünewald, J.W. Engels, and J. Wachtveitl; *Photophysics of 1-ethynylpyrene modified RNA base adenine*; Journal of Luminescence (**2009**) 129, 1454-1458

Publizierte Konferenzbeiträge

N. Gildenhoff, K. Gundermann, C. Büchel and J. Wachtveitl; *Coherent effects in the carbonyl containing carotenoid fucoxanthin* in: Ultrafast Phenomena XVII, (M. Chergui, D.M. Jonas, E. Riedle, R.W. Schoenlein, A.J. Taylor eds.), 361-363, Springer, Berlin/Heidelberg/New York, **2011**

N. Gildenhoff, S. Amarie, A. Beer, K. Gundermann, C. Büchel and J. Wachtveitl; *Light Harvesting, Energy Transfer and Photoprotection in the Fucoxanthin-Chlorophyll Proteins of Cyclotella meneghiniana*; in: Ultrafast Phenomena XVI, (P. Corkum, S. De Silvestri, K.A. Nelson E. Riedle, R.W. Schoenlein eds.), 577-579, Springer, Berlin/Heidelberg/New York, **2009**

Danksagung

It's Dr. Evil, I didn't spend six years in Evil Medical School to be called "Mister", thank you very much.

(Dr. Evil in *Austin Powers: International Man of Mystery*)

Abschließend möchte ich all den Menschen danken, die mich auf dem Weg hierher begleitet und unterstützt haben.

Meinem Doktorvater **Prof. Josef Wachtveitl** danke ich für die Betreuung in den letzten Jahren. Vielen dank für Deine unermüdliche Unterstützung, Deine Hilfe bei Fragen und Problemen, für das interessante Thema und für das entgegenbrachte Vertrauen. Dank Deiner Motivation und Deinem Engagement hat mir die Zeit meiner Doktorarbeit sehr viel Spaß gemacht, vor allem auch, weil ich die Chance hatte so viel Neues zu lernen.

Prof. Claudia Büchel und ihren Mitarbeiterinnen **Dr. Anja Beer** und **Kathi Gundermann** danke ich sehr für die fruchtbare Zusammenarbeit, die Bereitstellung der vielen unterschiedlichen FCP-Proben in immer ausreichenden Mengen, die Extraktion der Pigmente und die stete Diskussionsbereitschaft.

Einen besonderen Dank möchte ich **Dr. Ute Förster** aussprechen. Du bist, wenn man das so sagen darf, meine Doktormama. Von Dir habe ich so viel gelernt und Du hast mir mit viel Geduld alles erklärt. Ohne Dich hätte ich meinen Weg durch den Spiegelwald wohl kaum gefunden! An die Zeit mit Dir im Labor und im Büro werde ich immer gerne zurückdenken.

Weiterhin geht mein Dank an **Dr. Karsten Neumann**, der mir von Anfang an mit Rat und Tat zur Seite stand. Wann immer es ein Problem gab, konnte man sich auf Dich verlassen. Außerdem hast Du mir das Lötten beigebracht, hattest immer ein offenes Ohr und aufmunternde Worte für mich. Bleibt mir nur noch zu sagen: Wenn's gut werden soll, muss es der Knilch machen!

Zu großem Dank verpflichtet bin ich auch **Dr. Mirka-Kristin Verhoefen**. Danke für Deine große Unterstützung, vor allem auch bei den "schriftlichen Arbeiten", und die vielen Diskussionen und Gespräche, sowohl wissenschaftlicher als auch privater Natur... Tausend Dank!

Ein herzliches Dankeschön geht auch an **Heike Staudt**, die mir immer freundschaftlich zur Seite stand. Vielen Dank für die vielen offenen Gespräche und für Deine Hilfe bei der Bedienung von Clark und Selma.

Ein großer Dank gilt **Ernst Winter** und den **Mitarbeitern der Feinmechanik-Werkstätten** unter der Leitung von **Herrn Jäger** vor allem für ihre zuverlässigen und exakten Arbeiten und Sonderanfertigungen, ohne die der Aufbau der Anlagen wohl

kaum möglich gewesen wäre.

Frau Grönitz, Frau Lill und **Frau von Sulecki** möchte ich für ihre Hilfe bei allen administrativen Dingen danken. Außerdem danke ich den "**Lektoren**" Dr. Mirka-Kristin Verhoefen, Dr. Markus Braun, Julia Herz, Andreas Meßmer und Ute Förster. Ein großes Dankeschön gilt **Birgitt und Ernst von Wisberg** für ihre Druckbereitschaft!

Allen Mitarbeitern der **Arbeitsgruppe Wachtveitl** danke ich für das besonders angenehme und freundschaftliche Arbeitsklima und für ihre Hilfs- und Diskussionsbereitschaft. **Dr. Sergiu Amarie** danke ich für die Unterstützung bei den ersten FCP-Messungen, die nützlichen Diskussionen und die Hilfe beim Suchen des Überlapps, wenn Selma mal wieder zickte. Auch **Lars Dworak** danke ich für die Hilfe bei der Justage an der transienten Absorptionsanlage. **Dr. Lisa Lorenz** danke ich vor allem für die Einführung in das Programm IDL und für ihre stete Hilfsbereitschaft. **Peter Trojanowski** - meinem ehemaligen Diplomand und nun "Alt-Welpen" - danke ich für seine Geduld mit mir und dem Kerr-Schalter. Pass auf Deine Augen auf, Kleiner! Auch **Andreas Meßmer** möchte ich für seine Hilfsbereitschaft, die vielen Ratschläge im Labor und das stets offene Ohr danken. **Julia Herz** möchte ich ein großes Dankeschön für die Zusammenarbeit bei den Anisotropiemessungen aussprechen. Ich bin froh, dass ich Dich während Deiner Bachelor-Arbeit betreuen durfte und umso glücklicher darüber, dass sich daraus eine tolle Freundschaft entwickelt hat.

Für die wunderbare Atmosphäre im Aromalabor, die verrücktesten Gespräche und Diskussionen und das angenehme Arbeitsklima möchte ich mich bei allen aktuellen und ehemaligen Mitarbeitern der Arbeitsgruppen Wachtveitl, Dreuw und Stock bedanken. Auch allen Mitarbeitern der Arbeitskreise Mäntele und Bredenbeck möchte ich für das kollegiale und schöne Miteinander danken. Ohne Anspruch auf Vollständigkeit möchte ich hier einige Namen nennen: Karsten, Martin, Thomas, Victor, Sergiu, Peter P., Ute, Mirka, Heike, Lisa, Lars, Julia, Frank, Peter T., Jörg, Markus, Elena, Chavdar, Radhan, Rainer, Maja, Andreas D., Jan-Hendrik, Jürgen, Michael, Philipp, Stefan, Dirk, Carsten, Gabi, Georg, Andreas M., Eliza-Beth... und alle, die ich vergessen habe.

Schließlich danke ich meiner ganzen Familie und all meinen Freunden. Danke für eure Geduld, eure Aufmunterungen und die schöne Zeit mit euch! Ein besonderer Dank gilt meinem Ehemann **Gerrit Scheich**, der mich all die Jahre begleitet und unterstützt hat. Dank Dir hatte ich immer ein warmes Essen, egal wie spät es Abends wurde, eine Schulter zum Anlehnen und die tollsten Urlaube zur Erholung. Ohne Dich hätte ich wohl kaum durchgehalten! Meinen Schwestern im Blute und im Geiste, **Jana Nill** und **Nicole Kreß**, möchte ich ebenfalls mein herzlichstes Dankeschön aussprechen. Ich bin so froh, dass ich mich immer auf euch verlassen kann und ihr mich immer so erfolgreich ablenken könnt. Ihr seid die beste Schwester und die beste Freundin, die man sich wünschen kann! Zu guter letzt geht der größte Dank an meine Eltern **Conny und Uwe**. Euer Stolz war immer eine besondere Stütze für mich und es ist das größte Glück, euch beide als Eltern zu haben.

Curriculum Vitae

PERSÖNLICHE DATEN

Name	Nina Gildenhoff
Geburtsdatum	02. März 1981
Geburtsort	Offenbach am Main
Staatsangehörigkeit	deutsch
Familienstand	verheiratet

SCHULAUSBILDUNG

08/1987 bis 07/1991	Johannes-Kepler-Grundschule, Hainburg
08/1991 bis 07/2000	Einhardschule (gymnasialer Zweig), Seligenstadt
Schulabschluss	Abitur 2000

UNIVERSITÄRER WERDEGANG

10/2000 bis 05/2006	Studium für das Lehramt an Gymnasien mit den Fächern Chemie und Biologie an der Johann Wolfgang Goethe-Universität Frankfurt
Studienabschluss	1. Staatsexamen für das Lehramt an Gymnasien, Thema der Wissenschaftlichen Hausarbeit: <i>Isolation von Myxoxanthophyll und seinen Derivaten und ihre Bedeutung beim Schutz vor Photooxidation</i>
seit 06/2006	Promotion an der Johann Wolfgang Goethe-Universität im Institut für Physikalische und Theoretische Chemie bei Prof. Dr. J. Wachtveitl, Thema: <i>Time-Resolved Spectroscopic Analysis of Fucoxanthin-Chlorophyll Proteins and Isolated Carotenoids</i>

AKADEMISCHE LEHRER

T. Allert, H.J. Bader, F. Borsch, J. Engels, J. Feierabend, L. Fink, S. Gholami, W. Gnatzy, M. Göbel, A. Gold, J. Hammerl, H.P. Klein, W. Münzinger, H.D. Osiewacz, P. Pickel, M. Piepenbring, R. Prinzing, J. Richter, G. Sandmann, H. Schwalbe, A. Starzinski-Powitz, B. Streit, M. Tatur, J. Wachtveitl, M. Wagner, W. Wiltschko, C. Winter, H. Zimmermann, G. Zizka